The University of Sheffield

Investigating quantified biomarkers of skin barrier function & anti-inflammatory skin treatment using optical coherence tomography

Student: Mengqiu Duan
Registration number: 200296841
Supervisor: Prof. Stephen Matcher

A thesis submitted in partial fulfilment of the requirements for a PhD degree in Electrical and Electronic Engineering at the Department of Electrical and Electronic Engineering

April 2025

Abstract

Optical coherence tomography (OCT) is a novel, non-invasive tomographic imaging technique which generates cross-sectional images of the tissue with a resolution of a few micrometres. With a penetration depth of a few millimetres that matches the skin thickness, OCT has also been applied in dermatology to identify skin layers, components and assess cutaneous disease progressions. In this research, with a clinical focus of atopic dermatitis (AD), novel OCT systems are used to investigate quantified biomarkers of skin barrier function & anti-inflammatory skin treatment for AD.

Part 1: Atopic dermatitis (AD) is a chronic inflammatory disease which is associated with an impaired skin barrier. Conventional near infrared OCT systems typically have an axial resolution of ~10μm, thus can image skin layers such as epidermis and dermis. However, the top layer of skin which contains information on skin barrier function, stratum corneum (SC) at non-load-bearing skin sites with a typical thickness of 10-30μm cannot be visualized using standard near infrared OCT system. In this research, a novel visible-light OCT system with an axial resolution of ~1μm is used on 15 human subjects' dorsal hands to investigate their skin barrier function. Two skin barrier biomarkers: SC thickness and SC reflectance (reveals SC hydration information) are quantified using visible-light OCT system along with their seasonal, hydrational, age and gender variations.

Part 2: Atopic dermatitis (AD) is normally treated with topical corticosteroids (TCS) for anti-inflammatory purposes; however, this treatment is often associated with adverse side-effects such as skin atrophy. Crisaborole is a non-steroidal phosphodiesterase 4 (PDE4) inhibitor that has been regulated by FDA in 2016 to treat AD patients over the age of 2 years old. An extension OCT system, polarization sensitive OCT is used on 37 AD patients to investigate how their skin responds to these two treatments.

Acknowledgement

在读博士的四个春秋里，于无数个安静的夜晚，我思考着，人生这道题，怎么选都会有遗憾。活着，就要逢山开路，遇水架桥，更不要去美化那条没走过的路。

During the four years of my PhD studies, on countless quiet nights, I thought about the question of life, no matter what choice you make, there are always regrets. To live, you must open roads across mountains and build bridges when encountering water, let alone beautify the road that has not been travelled.

我很庆幸我选择了这条路，我遇见了认真负责的教授，我遇见了对科研十分固执的同事，我遇见了相互支持的同学们，他们教会了我沉静待事，善良待人，无惧困难，拥抱未知。

I am very glad that I chose this path. I met a responsible and kind professor, Prof. Stephen Matcher. I met a colleague who is resilient, and sometimes stubborn in pursuing answers in scientific research, Dr Dmitry Revin. I met lovely and smart people who always support each other, Doctors-soon-to-be – Yuan Rui and Frances SW Hooper.

我感谢他们的善意，我感谢自己的坚持，我更感谢家庭带给我的支持。用一句我最喜欢的诗词来结尾，两岸猿声啼不住，轻舟已过万重山。

I am grateful for their support, kindness, and countless happy moments. I am also grateful for the resilience of myself, as well as the support coming from my family and loved ones. To end with one of my favourite poems, while on cliffs of the Yangtze Gorges, gibbons ceaselessly cry, ten thousand folds of mountains, my skiff has slipped them by!

Published work

Journal articles

1. **Duan, M. Q.**, Byers, R. A., Danby, S. G., Sahib, S., Amy, C. H. A., Zang, C., … Matcher, S. J. (2023). Potential application of PS-OCT in the safety assessment of non-steroidal topical creams for atopic dermatitis treatment. Biomedical Optics Express, 14(8), 4126–4136. https://doi.org/10.1364/BOE.494464

2. Revin, D. G., Byers, R. A., **Duan, M. Q**., Li, W., & Matcher, S. J. (2023). Visible-light optical coherence tomography platform for the characterization of the skin barrier. Biomedical Optics Express, 14(8), 3914–3923. https://doi.org/10.1364/BOE.494356

3. Danby, S. G., Matcher, S., Byers, R., Taylor, R., Sahib, S., Andrew, P., Brown, K., Kay, L., Wright, C., Pinnock, A., Chittock, J., **Duan, M**., Cha, A., Adiri, R., Zang, C., Werth, J., & Cork, M. J. (2024). Novel biophysical skin biomarkers discriminate topical anti-inflammatory treatments based on their potential for local adverse effects. JEADV Clinical Practice. https://doi.org/10.1002/jvc2.540

Conference proceeding paper

1. **Mengqiu Duan**, Robert Byers, Simon G. Danby, Rosie N. Taylor, Amy Cha, Roni Adiri, Chuanbo Zang, John Werth, Michael J. Cork, and Stephen J. Matcher "The potential application of PS-OCT in the safety assessment of non-steroidal topical creams for atopic dermatitis treatment", Proc. SPIE PC12352, Photonics in Dermatology and Plastic Surgery 2023, PC123520F (17 March 2023); https://doi.org/10.1117/12.2647545

2. Dmitry G. Revin, Robert A. Byers, **Meng Q. Duan**, Wei Li, and Stephen J. Matcher "Visible-light optical coherence tomography platform for the development of novel atopic dermatitis treatment", Proc. SPIE 12352, Photonics in Dermatology and Plastic Surgery 2023, 123520B (14 March 2023); https://doi.org/10.1117/12.2647563

3. A Head-to-Head Comparison of Two Topical Anti-inflammatory Treatments, Crisaborole and Betamethasone Valerate, Reveals Marked Differences in Their Effects on the Microstructure of the Skin. Simon G. Danby, Stephen Matcher, Robert Byers, Rosie Taylor, Sura Sahib, Paul Andrew, Kirsty Brown, Linda Kay, Carl Wright, Abi Pinnock, John Chittock, **Mengqiu Duan**, Amy Cha, Roni Adiri, Chuanbo Zang, John Werth and Michael J. Cork Presented at the 25th World Congress of Dermatology; Suntec City, Singapore; July 3-8, 2023. https://sheffielddermatologyresearch.com/posters

4. A randomized controlled phase 2 trial comparing the effects of crisaborole 2% ointment to betamethasone valerate 0.1% cream on skin structure in participants with atopic dermatitis Simon G. Danby, Stephen Matcher, Robert Byers, Rosie Taylor, Sura Sahib, Paul Andrew, Kirsty Brown, Linda Kay, Carl Wright, Abi Pinnock, John Chittock, **Mengqiu Duan**, Amy Cha, Roni Adiri, Chuanbo Zang, John Werth and Michael J. Cork Presented at the International Society of Atopic Dermatitis (ISAD) Hybrid Congress; Montréal, Canada; October 7-19, 2022. https://sheffielddermatologyresearch.com/posters

Table of contents

Table of Contents

Contents

List of figures

Part 1. Investigating quantified skin barrier biomarkers using visible-light optical coherence tomography

1. Introduction

1.1 Skin (epidermis, dermis and hypodermis)

As the largest organ in the human body, skin serves as a protector against external mechanical stimuli, adverse microbes and abrasion while maintaining some of the most imperative physiological functions like insulation; temperature regulation; sensation and evaporation. Being the interface between the internal and external milieus, its mechanical and biochemical properties are indubitably influenced by extrinsic factors such as UV exposure, ambient air quality, temperature and moisture levels. Structure-wise, skin is multi-layer built with epidermis, dermis, and hypodermis. The epidermis is the outermost layer, and it is subdivided into another 4-5 layers. From surface to bottom, epidermis consists of stratum cornuem; stratum lucidum (only presented in palmar area); stratum granulosum; stratum spinosum and stratum basale. The primary cells found in the epidermis are keratinocytes, which account for 90%-95% of the epidermal cells, the ones found in the stratum basale refer to epidermal stem cells, they undergo a proliferation process where they move upwards to the skin surface and become enucleated. During such a process, keratinocytes shape into a more organised alignment and secret keratin proteins and lipids into the extracellular matrix. At the end stage of proliferation, keratinocytes become flattened enucleated cells called corneocytes and eventually are shed off, i.e., desquamation. Other cells found in the epidermis include Merkel cells, melanocytes and Langerhans cells which are predominantly found in stratum basale and stratum spinosum, they are primarily responsible for tactile sensation, UV protection and phagocytosis respectively. As there is no blood supply found in the epidermis and the nourishment of this layer is ensured by oxygen diffusion from the ambient air.

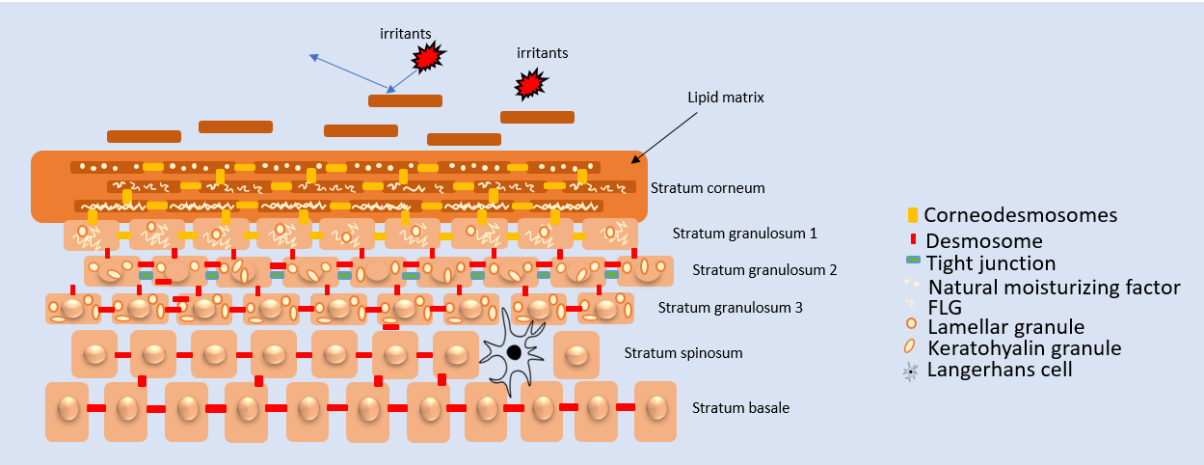

Figure 1. Schematic illustration of a healthy epidermis with key components.

Noticing, the SC is widely acknowledged as the skin barrier, i.e., the outermost layer of the epidermis, which functions as a defensive role against external stimuli, and it prevents loss of moisture from the underlying aqueous habitat. The anucleated corneocytes and the extracellular lipid matrix in the SC together construct as a 'brick and mortar' structure, as the proteinaceous envelope of the corneocytes is cornified and it binds tightly to the lipid matrix ensuring this layer is selectively permeable to external microbes, whereas within the corneocytes there are humectants, or called natural moisturising factors (NMF), which are molecules that bind water molecules to maintain skin hydration. The lipid content in the extracellular matrix primarily consists of ceramides, cholesterol and free fatty acid, its' molecular organisation and composition are crucially important for the barrier efficiency of the SC, a highly ordered lipid lamellae arrangement and a balanced lipid composition effectively retain moisture in the SC. The layer below the epidermis is the dermis and is composed of papillary dermis and reticular dermis. The main components found in the dermis are collagen and elastin fibres, thus protecting the body by acting as a buffer to external stress and strain. Mechanical and thermal receptors are also discovered in the dermis, along with hair follicles, sweat glands and blood vessels. The papillary region of the dermis resembles a finger-like structure, namely dermal papillae or papillae, it is formed of loosely packed collagen fibre and is connected with the epidermis via rete ridges, i.e., epithelia extension of the epidermis. The lower part of the dermis is called reticular dermis, composed of densely packed collagen and elastin fibres. The reticular dermis is much thicker than the papillary dermis, based on its composition, it provides mechanical support of the skin and ensures its' elasticity. The layer below the epidermis and the dermis is called hypodermis, often referred to as the subcutaneous layer. Larger blood vessels and lymphatic vessels are found here, and namely, it is the main site of the skin to store adipocytes, i.e., cells composed of fat to store energy.

1.2 Atopic Dermatitis

Atopic dermatitis, conventionally known as AD, is a chronic inflammatory disease featured by pruritus, i.e., a continuous, intense itch; erythematous lesion; and an increased transepidermal water loss (TEWL) which have a cutaneous manifestation of dry and cracked skin. The severity of the AD symptoms may vary depending on the IgE levels, i.e., an antibody indicating hyper-reactivity of the immune system. Mildly AD symptoms can be treated with emollient regimen as well as topical corticosteroids, severe AD would require immune-suppression medications such as cyclosporine and

Mycophenolic acid which commonly are used for organ transplant. The prevalence of AD in developed countries has increased for the past 3 decades and now affects up to 10-20% of the population [1]. It is often reported, patients with AD tend to have a poor quality of life due to constant sleep deprivation and anxiety induced by the continuing pruritus.

Genetically speaking, it has been recognized that IgE-mediated antigen production is thought to be a major event during the development of AD, and a few gene loci have been proposed to have a linkage with the production and an increase in IgE levels. However, genetic influence can't solely explain the aetiology of AD as the prevalence of AD has increased dramatically for the past few decades, environmental factors are then stated as another branch of contributors for the development of AD [1]. With a significant raise in the personal wash product sales and personal washing water figures, it is stated that such behaviour of increased usage of detergent, soap and hard water directly damages one's skin barrier; on top of this, thermal regulations within households provide a better living zone for house mites, and this also attributes to a breakdown of skin barrier. Thus, a defect skin barrier, specifically, a dysfunctional SC is considered as a hallmark of, and tend to promote, AD. Therefore, it is widely acknowledged that the pathogenesis of AD is thought to be a combination of a defect skin barrier and an enhanced type 2 immune response.

As mentioned, a healthy skin barrier, denoted as SC onwards, resembles a 'brick and mortar' structure, where the corneocytes represent the brick, and mortar indicates the lipid matrix. This concept of the 'brick and mortar' SC model has been popular, but recent studies proposed a dynamic model in which the alignment of corneocytes and the lipid organisation constructs a strong skin barrier [2]. Figure 1 shows an illustration of a healthy epidermis with its' skin barrier against external irritants such as allergens and microbes. The keratinocytes residue in the basale layer systematically proliferate and differentiate into enucleated corneocytes as they move towards to the surface, this desquamation process is regulated by a balanced protein lipid ratio, the corneocytes at the upper layers are thus organised vertically and are embedded in a well-arranged extracellular lipid matrix. For AD patients, the proliferation rate and protease activity in the epidermis are abnormally high, and it has also been found that the lipid arrangement and composition for AD patients both express irregularities. A key protein called filaggrin in the epidermis plays a vital role in the facilitation of barrier function, gene encoded

filaggrin (FLG) within the corneocytes assembles the keratin filaments together to form a scaffold, other structural proteins thus aggregate together on the scaffold and later structure into the insoluble cornified envelope by cross-linking. It is reported that AD patients' FLG mutates and loses its function which can lead to an irregular corneocytes morphology and its' natural moisture factors (NMFs) concentration, however, the link between FLG mutation and AD cutaneous manifestation is not always observed as some subjects who carry FLG mutation show no obvious AD skin symptoms [2]. Shown in Figure 1, corneocytes to corneocytes linkage and adhesion are ensured by tight junctions (TJs) and desmosomes/corneodesmosomes. TJs consist of transmembrane protein which firmly inserts into the phospholipid bilayer, they govern the passage of molecules between cells and regulate barrier permeability and it has been observed that a function breakdown of TJs exists in AD patients. Corneodesmosomes, modified from desmosomes, is an adhesive protein complex which encases the corneocytes and equips the SC with tensile strength against external mechanical stress, AD patients have been reported to have a loosely packed corneocytes resulting from a weak corneodesmosomes binding and a degraded corneodesmosomes function. Having describe above, see Figure 2, AD patients tend to have an impaired skin barrier which is featured by a loosely packed lipid matrix; an unbalanced surface pH; abnormal shedding; a weakened corneodesmosomes; a leaking tight junction and a hyper-transepidermal water loss (TEWL) rate, thus, makes the skin to be hyper-sensitive to external allergens and irritants [2].

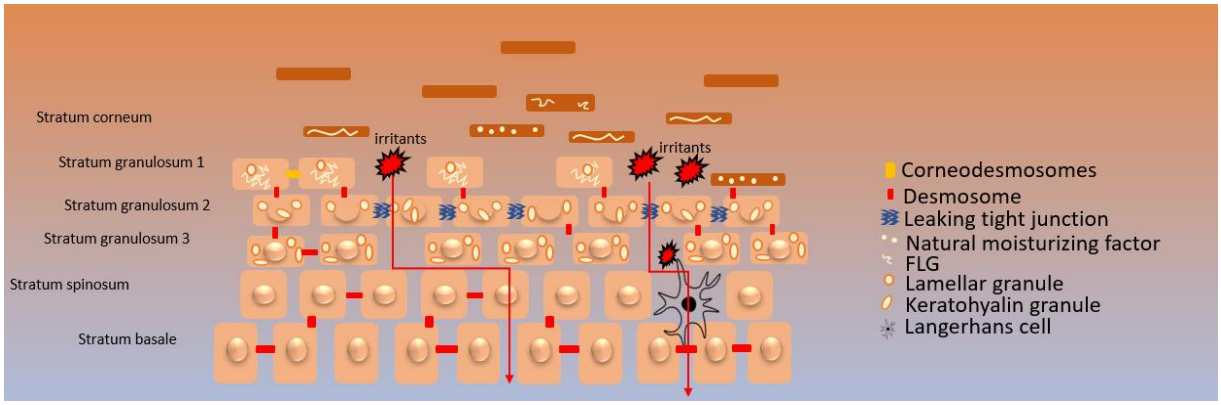

Figure 2. Schematic illustration of an AD dysfunctional epidermis with key components.

1.3 Optical Coherence Tomography (OCT)

Optical coherence tomography (OCT), often referred to as an optical biopsy, is a non-invasive tomographic imaging technique that is applied in medical fields with a few micrometres' resolution. The history of OCT dates to the 1970s and 1980s, where James G. Fujimoto, David Huang and Eric A.

Swanson acquired the first sets of images of OCT on the human retina in vivo [3]. Soon after, the clinical OCT prototype was used to image 5000 patients' eyes with diabetic retinopathy, age-related macular degeneration and glaucoma, henceforward, ophthalmology became the largest clinical application of OCT [4]. Typically, a near-infrared (NIR) OCT system is capable of imaging stratified tissues with a penetration depth of 1.5mm-2mm, skin, with a typical thickness of a few millimetres and a layered structure, is particularly suitable for OCT imaging. Ever since, apart from the second largest clinical application of intravascular OCT in cardiology, OCT has been applied in dermatology to delineate superficial layers of skin, identify eccrine sweat glands, and observe skin condition [5].

As a well-established, non-invasive imaging technique, OCT's principle is based on interferometry. Light from a light source such as a super luminescent diode (SLD) is split by a beam splitter and projected onto the reference mirror and the sample. The reference beam and the sample beam will be reflected back from the sample and mirror, two beams interfere when their optic paths match within a coherent length, and the interference is detected by a detector. For the past 3 decades, OCT went through a series of technological enhancements which improved its imaging speed, resolution, optical source, as well as imaging contrast. At the same time, functional extensions of OCT were also developed for various clinical interests. Optical coherence tomography angiography (OCTA) refers to a branch of OCT where it is used to generate vascular images based on motion contrast of the red blood cells without the need of using contrast agents. Polarisation sensitive optical coherence tomography (PS-OCT) is another functional extension of OCT, where the polarisation of light is detected in addition to the signal intensity. This added knowledge on light polarisation states grants PS-OCT the ability to differentiate anisotropic tissue like muscles, ligaments, tendon and fibrous tissue from other tissue. Other functional extension of OCT such as optical coherence elastography (OCE) has been popular due to its' role of assessing the elasticity of biological tissues, Doppler OCT can return the flow velocity of biological tissue and spectroscopic OCT which offers molecular contrast of tissue has also been developed [6].

2.0 Objectives

The main objective of this part of research is to investigate quantified skin barrier biomarkers for Atopic dermatitis via the use of optical coherence tomography. As mentioned, AD patients often have an impaired skin barrier/stratum corneum, thus, stratum corneum biomarkers such as its thickness and hydration are valuable for the diagnosis of the disease or when assessing the effectiveness and side-effects of the treatment.

Optical coherence tomography (OCT) is a novel, non-invasive tomographic imaging tool which has been applied in many clinical fields due to its advantages in spatial resolution of ~10 microns. Conventional OCT systems are only able to study the part of skin which matches its' resolution, epidermis, and dermis for example. The outermost layer of skin, SC at non-palmar skin is often neglected due to its' ultra-thin layer nature. In this research, an advanced OCT system (Visible light OCT) with a spatial resolution of ~ 1 micron has been used to study SC on 15 healthy human subjects, with an improved resolution, SC thickness and hydration for 15 subjects are quantified, along with its hydrational, seasonal, age, gender variations.

As there is a lack of the quantitative data on human SC thickness measurement in vivo, the finding of this research will offer valuable baseline data along with its seasonal change, as well as under various hydration states. These findings will add knowledge to the broad field of skin barrier research, also, for those who have a clinical interest in the diagnosis, treatment for atopic dermatitis, contact dermatitis, and psoriasis. Non-clinically, the finding of this research will interest companies which work on products that are in direct contact with skin, for example, personal wash products, shaving equipment, cosmetics, artificial skin.

3.0 Literature review

3.1 Stratum corneum properties/biomarkers

3.11 stratum corneum properties

It is recognised that a breakdown of the skin barrier, i.e., lower part of the stratum corneum (SC) is a key event during the development of Atopic dermatitis (AD), thus, to investigate the aetiology, disease progression, as well as treatment evaluation, probing the biomechanical properties of SC is essential in AD research. Some of the popular aspects of SC properties are the lipid composition, transepidermal water loss (TEWL), hydration, surface pH, thickness and corneodesmosome cohesions [7]. The lipids in the extracellular matrix are arranged in a lamellar form, they are usually well organised laterally and are orthorhombically (lipid lamellae are stacked in a form where 3 unequal lamellae lengths are perpendicular to each other. It is reported that in healthy human SC, the lipids are arranged in an orthorhombically style, and for diseased skin such as lamellar ichthyosis, the amount of free fatty acid (FFA) is significantly lower than healthy skin and the lipid arrangements are structured less orthorhombically [8]. Another prevalent angle to assess SC barrier function is to look at the transepidermal water loss (TEWL) rate, i.e., the flux of water evaporating from the underlying layers to the ambient environment. When there is an increase in the TEWL value, SC gets very dry and peeling may occur, thus leading to an impaired SC due to abnormal shedding. However, this measurement is an indirect way to evaluate the SC barrier function, as in, the value that TEWL gives only contains information in a singular direction, it only yields the water flux evaporating from the surface to the ambient environment, not the other way around. Moreover, it does not include any depth-profile information which makes this evaluation limited [9]. In contrast to the water that is diffusing out of the SC, that water that is preserved in the skin can also be used to grade the barrier function. The water molecule in SC mainly reside in the corneocytes and it is bounded to the keratin inside of the corneocytes which makes this part of water not influenced by the external factors, however, another fraction of water is bounded to the lipids and the natural moisturising factor (NMF) which makes them sensitive to external environment. Function-wise, mentioned before, the water content in SC is responsible for enzymatic functions during normal cutaneous shedding, if this value drops below a critical point, the enzymatic process becomes abnormal, which can lead to an aggregation of corneocytes on the skin surface, thus makes the skin flaky, dry and rough [10]. The thickness of SC can be used as an indicator of desquamation rate, it also has a correlation with epidermal permeability,

TEWL rates as well as surface pH. It can be used as an indicator to evaluate the side effects of topical treatment for AD skin, Zhang et. al reported that, by applying emulsifier on isolated porcine skin, SC thickness was reduced due to lipid removal [11]. The surface pH of human skin are known to be acidic (5.4-5.9) [12], and it is linked with the barrier function due to its' role of maintaining normal desquamation rate, AD patients have been discovered to have an elevated surface pH and studies have been carried out to correlate the effect of water hardness on surface pH in relation of AD epidemiology [13].

In this literature review chapter, SC hydration and SC thickness are the two main SC biomarkers reviewed, SC hydration measurements obtained by optic sensing and electric sensing are illustrated, in vivo SC thickness measurements obtained using various modality are investigated mainly, some ex vivo results are also reported.

3.12 Stratum corneum hydration (optic sensing and electric sensing)

As xerosis is a typical symptom of Atopic dermatitis (AD), skin hydration is thus often assessed as one of the biomarkers for AD. Commonly, optical sensing and electrical sensing methods are used to measure the moisture content of skin, and the sub-layer of the skin, the stratum corneum (SC), is the one of the frequently assessed layers due to its nature of barrier function. SC is composed of corneocytes embedded in an extracellular lipid matrix, and this lamellar lipid matrix along with its hydrophilic components such as natural moisturising factors (NMFs) together construct an effective boundary for water retention and holding, it is also recognized that a balanced water concentration in SC regulates the normal desquamation of the corneocytes. Generally, some of the key factors which can induce alterations in SC hydration are perspiration, as in water evaporating from the skin surface, which can be measured with transepidermal water loss (TEWL); overall body water content which is frequently estimated from body mass; and water-holding capacity which can be measured via optic sensing or electric sensing [14].

One of the most utilised optic sensing methods in skin molecular mapping is called confocal Raman microscopy (CRM) or confocal Raman spectroscopy (CRS). The physical principle of such methods is based on inelastic scattering of light, where, when the molecules of the sample tissue are being illuminated with a monochromatic light source, a defined amount of energy from the photon is

transferred to the sample tissue molecule and excites the molecules, when the excited molecule vibrates, the corresponding scattered light typically has a wavelength that is longer than the incident light source. The resulting Raman shift, as in the energy difference between the incident laser source and the scattered light is expressed in a Raman shift spectrum. Classically, two regions of the Raman spectrum are used for molecular analysis of the substance, the fingerprint region, i.e., low wavenumber region (400-2000cm^{-1}) and high wavenumber region (2000-4000cm^{-1}). The fingerprint region is enriched with biomedical information of the tissue such as protein, lipid, DNA and blood and the analysis of this region has been applied extensively in biomedical fields, however, high wavenumber regions not only contain important information about the molecular vibrations of the components, but it also provides valuable signals related to water molecules [15]. In the spirit of this, Caspers et. al calculated the water concentration profile of the SC at volar arm of 6 healthy subjects using CRM, where, the water concentration is obtained from the water to protein intensity ratio at Raman bands of 3350 to 3550cm^{-1} (Raman signal intensity of water due to OH^- stretching vibrations) and 2910 to 2965cm^{-1} (Raman signal intensity of protein due to CH_3^- stretching vibrations). Their results showed that at the skin surface, the water concentration is about 30% and increased to roughly 65% at a depth of 15μm at volar arm, by assuming the junction between SC and stratum granulosum is located at the high end of the steep water concentration gradient of the Raman spectrum, an estimation of SC thickness was made to be 15μm [16]. Using the same Raman spectral band characterization, Crowther et. al reported a SC water profile at volar forearm for 14 healthy subjects to be 20 - 30% at skin surface and increased to 60 - 70% in a sigmoidal curve at a depth of ~15μm. Based on such a method, an estimation of SC thickness at cheek, volar forearm and leg for 9 subjects were stated to be 12.8 ± 0.9μm, 18.0 ± 3.9μm and 22.0 ± 6.9μm respectively [17]. From the aspect of skin ageing, ChunSik et. al compared the hydrogen bound water molecule types in SC for 11 healthy subjects, where they were categorised into an ‘older group’ and a ‘younger group’, their ratio of area under curve (AUCs) of 3450cm^{-1} and 3250cm^{-1} in the Raman spectra was used to entail the hydrogen bond water molecules across their volar forearm SC. Their results showed that the older group had a higher ratio of hydrogen bound water molecules at 10-30% of SC depth, meaning there are more water molecules that are bonded with surrounding molecules such as NMF, keratin and intra-cellular lipids, hence there are less ‘free water molecule’, such a finding may result in a clinical view of ‘dry skin’. Using the same principle that Casper et. al reported, a thickness estimation of 21 ± 2.3μm and 19 ± 1.3μm was reported for older and younger subject groups [18]. The

utilisation of CRM in assessing SC hydration is also often associated with moisturisers. Commonly found in cosmetic products, humectants are often contained to promote moisturised skin and potentially reverse the signs of aged or dried skin, its principle is thought to be when penetrated SC, it traps the water molecule within the epidermis as it moves upwards from lower layers. Emollients and occlusive agents are also often included in these products to smooth skin and generate an artificial barrier to reduce transepidermal water loss, however, undesired effects such as inflammation or metabolism altering may come with these chemicals. Thus, an understanding of how SC hydrates under application of these agents may help to develop a better moisturiser formulation. Wang et. al used CRM to investigate the mechanism of SC hydration via using deuterium oxide ((D_2O) as a probe to differentiate endogenous water (H_2O) from exogenous deuterium oxide (D_2O). In their study, relative endogenous water OH content was calculated using the method of Casper et. al, the exogenous deuterium oxide OD content was obtained by integrating area ratio of OD stretch band (2400-2700cm^{-1}) and protein CH stretch band (2910-2965cm^{-1}). On the volar forearm of two healthy subjects, occlusive deuterium oxide patch was placed for 30 minutes for arm sites with glycerin application and without, CRM measurements were taken in vivo at a time interval of 5 minutes for 30 minutes. Their results showed that glycerin promotes the penetration of water (deuterium oxide) and allows water to retain in the skin for a longer period when compared with control sites [19].

The electric sensing method that has been frequently used when measuring the SC hydration is called Corneometry, since it was introduced in 1980s, it has been applied in dermatology and became the most used device when investigating skin hydration due to the world-wide commercialisation of a device called Corneometer (Courage & Khazaka Electronic GmBH, Koln, Germany). This device itself is a hand-held probe which measures the dielectric properties of SC, as the dielectric properties of SC changes when its' hydration level changes, i.e., higher water content leads to a higher dielectric constant, by sending a weak AC current to the dielectric medium, here the SC, the measured impedance is used to calculate the SC hydration, and the result is expressed in an arbitrary-unit number between 0-120. Some of the main advantages of the Corneometer which promote its' fast spread of usage in research include prompt measurement (1s) and minimum contact which allow continuous repetitive measurement. However, the results given by the device are sensitive to contact pressure hence it requires an experienced operator. To investigate the gender influence on skin physiology,

Luebberding et. al measured SC hydration for 300 Caucasian subjects with no skin disease or other physical disorder with cutaneous manifestation using Corneometer, the measurements were taken at anatomical sites of forehead, cheek, neck, volar forearm and dorsal hand, and the results showed that the lowest reading was found at dorsal hand for both gender, while the highest reading was found at check for women and neck for men, and with one anatomical site exception at dorsal hand, men's SC hydration reading was reported to be significantly higher than women. As the subjects were evenly distributed into different age groups, it was reported that for men, SC hydration progressively decreases with increasing age, and results show opposite trend for women [20]. A similar study with a large sample size, Lee at al. recruited 397 female subjects with no cutaneous pathology from Southeast Asian (Indonesian, Vietnamese and Singaporean) and to investigate the influence of ethnicity on skin biophysical parameters and measured their SC hydration using Corneometer. Readings were taken at anatomical sites of forehead and cheek, and results showed that for all three ethnicity groups, SC hydration readings at the forehead are significantly higher than the readings taken at the cheek. And regarding to ethnic differences, Vietnamese subjects SC hydration is significantly higher than both Indonesian and Singaporean subjects, where no significant difference was found between Indonesian subjects and Singaporean subjects [21]. Seasonal influence on skin hydration was investigated by Nam et. al, where 89 Korean female subjects completed a study where their skin hydration was recorded using Corneometer throughout 13 months from April 2007 to April 2008. Readings were taken at anatomical sites of the forehead, under the eye, cheek, Crow's feet, inner forearm and face, results showed that at Crow's feet, SC hydration showed highest reading, and it was significantly higher when compared with forearm and cheek readings. And seasonal effect on SC hydration readings was observed, there was an increasing trend from April to September for all most of the anatomical sites, and the SC started to decrease from September to December before it started to rise from December to next April [22]. Song et. al performed a similar study to investigate the seasonal influence on skin biophysical parameters on 100 male subjects, where Corneometer readings were taken at the anatomical sites of forehead, cheek and forearm during summer and winter season. The results of this study reported at all three skin sites, SC hydration measured by Corneometer during summer was significantly higher than that measured in winter [23]. Apart from taking measurements on healthy subjects, Corneometer has also been used on patients with cutaneous disease where xerosis is a typical symptom, for the relevance of this research, take AD as an example, Firooz et. al measured SC

hydration using Corneometer on 30 healthy and AD Iranian subjects and reported that AD subjects' SC hydration is significantly lower than that of those healthy subjects at anatomical sites of palm and dorsal hand [24]. Similarly, Sator et. al recruited 24 Caucasian patients with AD and 24 Caucasian healthy subjects with equal gender ratio to investigate their SC hydration using Corneometer, and their results reported that at three anatomical skin sites of dorsal hand, forehead and suprasternal notch, Corneometer readings of AD subjects are significantly lower than of those healthy subjects at all skin sites. Moreover, a negative correlation was found between age and SC hydration for male AD subjects at dorsal hand indicating the older male AD subjects get, the drier their skin [25]. Grinich et. al used Corneometer and measured SC hydration for 50 AD subjects with lesional and nonlesional skin at their forearm and reported SC hydration for AD patients regardless of lesion presence, their SC hydration is still lower than of those healthy ones [26].

To summarise, Corneometer remain as a powerful tool when assessing SC hydration, literatures on the utilisation of Corneometer still show up-trending scale, in addition, when new skin hydration modalities have been developed, Corneometer still holds its' validation position in research. When used on human subjects, a systematic review done by Samdi et. al reported a comprehensive Corneometer readings on health subjects with different gender, anatomical sites and age. They concluded some generally accepted observations, that SC hydration generally decreases with age, and different results have been stated regarding the gender influences, moreover, intra-variation of the results have been confirmed by the Corneometer results taken at different anatomical skin sites [27].

3.13 Stratum corneum thickness

Stratum corneum (SC) thickness is an important biomarker which indicates the barrier function of SC, a defective skin barrier may reflect as a dry, flaky, cracked, thinned or thickened SC, and it is often associated with epidermal hyperproliferation and impaired differentiation, which are classic symptoms for skin conditions such as psoriasis or AD. SC structures also undergo changes in response to treatment for skin disease such as AD, as a swollen or hydrated SC in response to moisturiser demonstrates the effectiveness of the treatment. In addition, clinically, SC thickness is also an important parameter for transdermal drug delivery research as skin remain as a popular route for pharmaceutical administrations over oral administration and hypodermic injection, hence, when assessing the uptake

and penetration of small pharmaceuticals administration, SC thickness is often used in the modelling and design of the drug delivery system [28]. In skin cancer, SC thickness has been used to explore its relationship with Basal cell carcinoma (BCC) and knowledge of SC thickness can be used to assess the effect of topical photodynamic therapy for skin tumours [29]. In skin disease where SC becomes significantly thicker than healthy skins such as congenital ichthyosis, SC thickness can be used to assess the disease severity [30]. It was also found that SC thickness of subjects with vitiligo at lesional sites is significantly higher than non-lesion skin sites [31]. For AD patients, SC is reported to be thinner than of those healthy subjects with fewer layers of corneocytes, and frequent soap washing can induce a reduction in the cell layers in SC [32]. Non-clinically, SC thickness was used to assess the effectiveness of commercial shavers in relation to SC thickness removal [33]. The thickness of SC was mainly measured by tape-stripping or biopsy methods ex vivo before the development of in vivo imaging modalities such as confocal raman microscopy (CRM) / confocal raman spectroscopy (CRS) and OCT, to date, CRM and OCT remain the most used imaging system to quantify SC thickness in vivo, the principles of CRM and OCT were illustrated previously, briefly recall, an estimation of SC thickness can be derived from the water concentration profile of CRM, i.e., by detecting the boundary of SC and stratum granulosum (SG). OCT provides tomographic images of the skin where, when the axial resolution is sufficient to delineate SC at non-palmer skin sites, SC thickness can be calculated.

Liu et. al used CRS to assess the effect of various PEGylated emulsifiers on SC as research has stated that adverse effects in relation to a reduced SC thickness has been shown with the application of long PEG-chained emulsifiers. Isolated porcine ear SC was used and an averaged SC thickness of 13.7μm ± 2.5 μm was reported [34]. Comparable study was done by Mahrhauser et. al, where isolated porcine ear SC was used, and an average SC thickness of 11.1μm ± 1.5μm was reported [35]. Choe et. al used CRM on 6 human subjects' forearms and, by detecting the water profile boundary between SC and SG, an average thickness of 19.8μm was reported [36]. Crowther et. al measured SC thickness of 9 human subjects' cheek, forearm and leg using CRS and reported results of 12.8μm ± 0.9μm, 18.0μm ± 3.9μm and 22.0μm ± 6.9μm respectively, such results were compared with OCT measurements of 11.1μm ± 1.8μm, 10.4μm ± 0.9μm and 13.7μm ±1.4μm, although the actual values of both measurement method showed significant differences, the trend of decreasing across three body sites coherently matched, suggesting human SC thickness measurement obtained by CRS in vivo is comparable to OCT [37].

Egawa et. al used CRS to acquire SC thickness across cheek, upper arm, forearm, dorsal hand and the palm for 15 human subjects and reported a thickness of 16.8μm ±2.8μm, 21.8μm ±3.6μm, 22.6μm ±4.3μm, 29.3μm ±6.8μm and 173.0μm ±36.9μm respectively. An interesting finding of this research was that by increasing the hydration level using water-soaked cotton wool on subjects' forearms, the corresponding SC thickness increased by a factor of 2 after 90 seconds of water exposure [38]. Bohling et. al also reported using CRS on 18 human subjects' volar forearm, lower leg and cheek, an average SC thickness of 19μm, 22μm and 13μm was reported for these anatomical sites [39]. Their results were compared with Zhen et. al, where cell layers of SC for 301 human subjects at anatomical skin areas of face, scalp, neck, trunk, genital, extremities and acral region were counted ex vivo, and Bohling et. al's results matched with Zhen et. al's results on facial area's SC thicknesses are the lowest compared to other skin sites. Interestingly, Zhen et. al reported for male subjects, there is a decreasing trend of SC thickness with increasing age, and no significant differences were found between the SC thickness for two genders [40]. The influence of age in SC thickness is stated to be more pronounced when comparing infants with adults, as infants' skin have a higher keratinocytes proliferation and desquamation rates which could result in a SC with smaller corneocytes and thus become thinner [41]. Stamatas et. al used CRM to compare SC thickness between infants and adults and reported that infants' SC thickness is roughly 30% thinner than adults with values of 15μm and 25μm respectively [42].

Apart from using CRS/CRM, OCT has also been used to quantify human SC thickness in vivo for body sites with thick SC. Liu et. al used a conventional NIR OCT system (1300nm) on human subjects' finger-pad and palm, where they reported a result of 160μm - 600μm and 130μm - 270μm respectively [43]. Maiti et. al also used a NIR OCT system to quantify the epidermal thickness and roughness at 21 anatomical skin sites for 12 human subjects at both relaxed and overextended positions, due to the limited axial resolution of 5μm of the OCT system, SC thickness was only quantifiable at load bearing skin sites such as foot, heel and fingertip. Their results reported an averaged SC thickness at foot, fingertip and heel being 601μm, 295μm and 311μm respectively, and at an overextended state, a significant reduction in the SC thickness was shown at most of the anatomical skin sites. It was reported that male subjects had a significantly higher SC thickness at the skin site of heel, and female subjects' epidermal thickness is significantly higher in ear canal [44]. Kato et. al used a 1300 nm NIR OCT system

on 20 human subjects' fingertips and acquired an average SC thickness of 480μm [45]. Fruhstorfer et. al measured 87 healthy subjects (41 female, 46 male) and 18 subjects with diabetes using a 1300 nm NIR OCT system and reported that healthy female subjects had significant thinner SC at fingertips than male subjects, and there were no significant differences between the healthy subjects and subjects with diabetes [46]. Non-palmer skin sites' SC thickness has been quantified using Line-confocal OCT (newly developed system that combines reflectance confocal microscopy and Time-domain OCT), Shazli et. al used line-confocal OCT (LC-OCT) on 8 subjects to measure their facial SC thickness after hydradermabrasion (an exfoliative cosmetic procedure for skin rejuvenation) and reported a decrease in SC thickness after treatment and an increase in two weeks of follow-up [47]. Bonnier et. al also used LC-OCT on 100 healthy Caucasian female subjects and quantified their SC thickness at three skin sites on their facial area. Reported, there is a 7.6% increase in the SC thickness from younger age group to older age group (13.2μm ± 0.8μm - 14.2μm ± 1.0μm) at the upper part of facial skin; comparable results were detected at lower part of their facial skin (13.1μm ± 0.4μm - 13.9μm ± 1.3μm); and at the middle part (cheekbone), no age related difference was found [48]. A smaller population study done by Monnier et. al measured SC thickness across forehead, nose, check, chest, back, forearm and back of hand on 29 healthy subjects using LC-OCT and reported a SC thickness of 11.6μm ± 1.7μm, 10.4μm ± 1.4μm, 9.0μm ± 1.1μm, 9.1μm ± 1.2μm, 9.5μm ± 1.3μm, 12.7μm ± 3.2μm and 29.5μm ± 5.7μm respectively [49]. Chaeuvel-Picard et. al also measured SC thickness using LC-OCT on 8 healthy female subjects across seven body sites and reported dorsal part of the hand had highest SC thickness (24.1μm ± 4.6μm) compared to the rest of body sites (forehand – 11.7μm ± 2.1μm; nose – 12.6μm ± 2.8μm; cheek - 10.0μm ± 1.3μm; chest - 29.5μm ± 5.7μm; back – 12.3μm ± 2.1μm; dorsal forearm – 15.2μm ± 3.9μm) [50].

Briefly mentioned, tape stripping has been used frequently to quantify SC thickness, although, due to its' invasive nature, it is not dominantly applied anymore, for reference purposes, results obtained by tape stripping still pose as valuable information. Tsang et. al tape stripped 6 human subjects' volar forearm and reported a SC thickness of 9.3μm ± 2.5μm [51]. Similarly, Russell et. al obtained an average value of 10μm - 20μm for 31 anatomical skin sites of 18 volunteers [52]. Ex-vivo measurements of SC thickness done by autopsy or biopsy studies also pose good reference data, Fairley et. al compared SC thickness at abdomen of infants, children and adult and reported an average SC

thickness of 35.4μm ± 11.3μm, 28.8μm ± 10.6μm and 35.4μm ± 6.4μm respectively, and there were no significant differences found between these age groups [53]. Sandby-Moller obtained biopsy from 71 healthy subjects' forearm, shoulder and buttock and measured the SC thickness using light microscopy, it was reported that SC thickness at these three body sites is significantly different from each other and actual values reported were 18.3μm ± 4.9μm, 11.0μm ± 2.2μm and 14.9μm ± 3.4μm respectively. It was also found that SC thickness negatively correlates with years of smoking, and no significant difference was detected when discriminating subjects into different age and gender groups [54].

Having described above, it has been observed that most of the human SC thickness at non-load bearing skin sites in vivo measurements are quantified using CRM/CRS, some measurements at skin sites with a significantly thicker SC are obtained using OCT, tape stripping has also been applied to quantify SC thickness. Popular skin sites of measurements are the hand region, forearm, facial area and flexures, and many studies have been carried out to assess the effect of moisturising cream on SC thickness as changes on SC thickness is often associated with adverse effects of topical treatments. It is reviewed that at load-bearing skin sites such as the heel, palm, fingertips have a significantly thicker SC, flexure areas such as inner forearm and back of the leg has a significantly thinner SC, and some studies have stated that some of the facial area such as the eyelid, cheek, eye-bad has the thinnest SC. Apart from the intra- and inter-variations of the results, it also has been reported that SC thickness varies with different hydration states. The fact of the vast majority of the SC thickness are taken by CRM/CRS over OCT can be explained by the low axial resolution of standard NIR OCT system, as most of the NIR OCT system developed for the past few decades had a typical axial resolution of ~ 7.5μm – 10μm, and SC thickness at non-load bearing skin sites are reported to be within ~10μm – 30μm, sometimes even few microns. The VIS-OCT system developed by the author's group, has demonstrated an axial resolution of ~ 1μm in air, thus revealing great potential in SC thickness quantification.

3.2 Optical coherence tomography

3.21 OCT overview

Optical coherence tomography (OCT), often referred to as an optic equivalent of ultrasound imaging, is a non-invasive tomographic imaging technique that is often applied in medical fields with few micrometres' spatial resolution [55]. As OCT is capable of imaging tissue with a penetration depth of

1.5-2mm, skin, as the largest organ in the human body, is particularly suitable for OCT imaging. Since the 1990s, OCT has been applied in dermatology to delineate superficial skin layers such as epidermal and dermal layer, identify eccrine sweat glands units and observe skin condition.

As a relatively new, well-established, non-invasive medical imaging system, OCT was primarily reported by D.Huang et. al to image retina layers, and its principle is based on interferometer, see figure 3. Low coherent light (E_{in}) from a light source (SuperLuminescent Diode) is emitted, such a light beam is split by a beam splitter and projected onto the reference arm (E_r) and the sample arm (E_s); the light signal at the reference arm (E_r) is reflected from a reference mirror; the light signal at the sample arm (E_s) is back-scattered from the sample; two beams will interfere when their optic path matches within a coherent length, and such interference is detected by a photo detector [56]. Since it was developed, there are two generations of OCT systems: Time-domain OCT (TD-OCT), which is characterised by a movable reference mirror to match the layered sample; Fourier-domain OCT (FD-OCT), which is characterised by a fixed reference mirror, and involves using fast fourier transform in their calculation. In Fourier-domain OCT, Spectral-domain OCT and swept-source OCT systems are developed to have better system performance. Hence, for the past 3 decades, OCT went through a series of technological enhancements which improved its imaging speed, resolution, optic source, as well as contrast [57,58].

In this chapter, mathematical principles of OCT generations (TD-OCT and FD-OCT) are explained, some practical aspects of OCT system features such as axial and lateral resolution are also discussed, along with common functional extension of OCT systems.

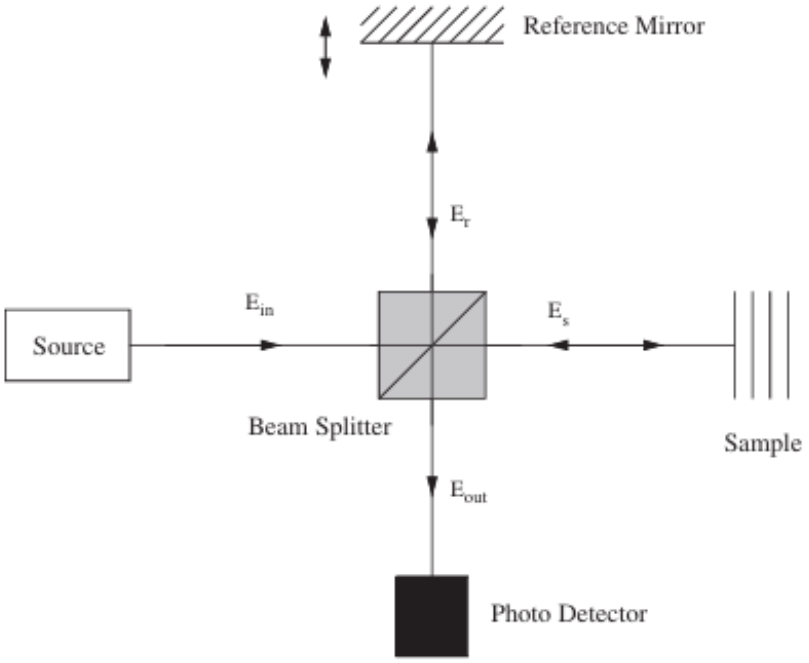

Figure 3. Schematic illustration of a Michelson interferometer [56].

3.22 OCT mathematical representations

As OCT involves using the electric field of the light source, mathematical formula of an electric field $E(w,t)$ shall be expressed by:

$$E(w,t) = s(w)exp[-i(wt+kz)] \quad \textbf{(1)}$$

$s(w)$ is the spectrum amplitude of the electric field, w and t is the frequency and time variation, and the terms k and z in the exponential part of this equation stands for wavenumber and distance of the phase accumulated in the interferometer. As the input phase is arbitrary, only the relative output phase between two optic paths is measured, the phase term can be 'neglected' in this field equation. Hence, the field component in input, output, reference arm and sample arm in the interferometer can be denoted by $Ein, Eout, Er, Es$. The reference mirror in the interferometer is assumed to be ideal, and the reference arm and sample arm intensity transmittance in the beam splitter is denoted by Tr and Ts, where, $Tr + Ts = 1$. The sample has a frequency domain response function $H(w)$ which describes its structure, hence, the optic fields component are described by:

$$Ein(w,t) = s(w)exp[-iwt] \quad \textbf{(2)}$$

$$Er(w,t,\Delta z) = (TrTs)^{1/2}Ein(w,t)exp[-i\phi(\Delta z)] \quad \textbf{(3)}$$

$$Es(w,t) = (TrTs)^{1/2}Ein(w,t)H(w) \quad \textbf{(4)}$$

$$Eout(w,t,\Delta z) = Er(w,t) + Es(w,t,\Delta z) \quad \textbf{(5)}$$

where $\phi(\Delta z)$ is the phase accumulated in the reference mirror and:

$$\Delta z = \Delta tc/n(air) \quad (6)$$

$$\phi(\Delta z) = (2wn(air)\Delta z)/c \quad (7)$$

Δt is the optic time of flight difference, c corresponds to speed of light in vacuum state and $n(air)$ represents the refractive index of air, hence, these equations also assume that the interferometer is operating in air. Optical detectors are square-law intensity detectors which detects the intensity, and this is proportional to a time average over the electric field multiplied by its complex conjugate:

$$I(w,\Delta z) = \lim_{T\to\infty} 1/2T \int_{-T}^{T} Eout(w,t,\Delta z)E*_{out}(w,t,\Delta z)\, dt \quad (8)$$

Rewrite equation (8) by combining equation (5) to:

$$I(w,\Delta z) = \langle EsE*_s \rangle + \langle ErE*_r \rangle + 2\acute{R}\{\langle EsE*_r \rangle\} \quad (9)$$

The first two terms in equation (9) can be seen as 'self-interference', and the third term in this equation is the real term ($\acute{R}$) of the 'cross interference'. Combine with equation (2) and (4), this is rewritten as:

$$I(w,\Delta z) = TrTS(w)|H(w)|^2 + TrTsS(w) + 2TrTs\acute{R}\{S(w)H(w)exp[-i\phi(\Delta z)]\} \quad (10)$$

$H(w)$ is the sample response function, and it is used to describe the sample structure in z direction:

$$H(w) = \int_{-\infty}^{\infty} r(w,t)exp[i2n(w,z)wz/c]dz \quad (11)$$

$r(w,t)$ is the back-scattered coefficient of the sample, and $n(w,t)$ is the refractive index that is dependent on the frequency and depth, and the exponential term, again, represents the phase accumulated by the multiple layers of the sample. As shown in equation (10), the structure information obtained from the interferometer is expressed in both time and frequency domains, that corresponds to the main two generations of OCT systems, Time-domain and Frequency-domain. The details are described in chapters below [56].

3.23 Time-domain OCT system

During the early stage of the OCT development, Time domain (TD-OCT) was mainly used across various fields, where the reference mirror in the interferometer is movable to match the coherent length of the reflections from the samples. In TD-OCT, equation (10) can be rewritten as a function of path length of reference displacement by integrating the source spectrum, by assuming the beam splitter is ideal, where the beams are split 50:50, each axial scan in TD-OCT is written as:

$$I(\Delta z) = T_0 + \acute{R}\{T(\Delta z)\} \quad (12)$$

As T0 only has self-interferences, $T(\Delta z)$ contains cross-interferences information:

$$T(\Delta z) = 1/2 \int_{-\infty}^{\infty} H(w)S(w)cos\{\phi(\Delta z)\}dw \quad (13)$$

A layered sample with N layers, while assume negligible dispersions can be written as:

$$H = \sum_{j=1}^{N} r_j \, exp[\{i2w/c \sum_{m=1}^{j} n_m z_m\}] \quad (14)$$

where, z_m is the thickness of the layer m, with corresponding refractive index n_m and, r_j is the layer reflectivity, by assuming incident light is perpendicular to each layer, the reflectance can by compute as:

$$r_j = n_{j+1} - n_j / n_{j+1} + n_j \quad (15)$$

3.24 Fourier-domain OCT system

In modern days, Fourier domain OCT (FD-OCT), are used more extensively, within the sector of FD-OCT, further division exists based on whether the system is spectrometer based or swept source based. If the system is spectrometer based, the interference signal is diffracted based on its direction by diffraction grating and then detected by a single dimensional charged coupled device, 1D-CCD. If the system is swept source based, like TD-OCT, the interference signal is detected by a single channel photoreceiver, except, the broadband low coherent light source is replaced by a swept source laser. The reason behind the frequent replacement of FD-OCT over TD-OCT is, unlike TD-OCT, the reference mirror of FD-OCT is fixed, the detected interference intensity signal is reconstructed into depth-resolved axial scans using Fourier transform, which equips FD-OCT with a much higher acquisition rate. Additionally, the sensitivity of FD-OCT is significantly higher [59].

Same as TD-OCT's mathematical equations, FD-OCT's principle is based on equation (10), since the reference mirror is fixed in FD-OCT, Δz becomes 0, while using the same assumption that beam splitter splits the incident light into 50:50 ratio, the detected spectrum is written as:

$$I(w) = 1/4 \, S(w) \, \{H(w) + 1\}^2 \quad (16)$$

Using Fourier transform, the depth resolved spectrum can be convert into a time domain interference signal pattern:

$$I(t) = FT\{I(w)\} \quad (17)$$

Where FT denotes the Fourier transform, and in a real system, the output spectrum $I(w)$ consists of N discrete points that correspond to an intensity measurement on a detector in an array, therefore, using

Fast Fourier transform on a computer, Fourier transform of the output can be achieved. The result of this Fourier transform is composed of N/2 discrete steps in time $\Delta\mathcal{T}$ where:

$$\Delta\mathcal{T} = 2\pi/\Delta\Omega \quad \textbf{(18)}$$

And the detected spectrum is approximated by:

$$\Delta\Omega = 2\pi c\Delta\lambda/\lambda^2 \textbf{ (19)}$$

Combine equation (18) and (19), and both sides multiply an average refractive index n_{ave} and divide c, and the maximum depth z_{max}can be written as:

$$z_{max} = (1/4n_{ave})({\lambda_0}^2/\Delta\lambda)N \textbf{ (20)}$$

If the FD-OCT system is spectrometer based, the system uses a spectrometer to detect the signal by diffractive gating, here, the signal current is detected as a function of the wavenumber, by using a Fourier transform, the sample reflectivity profile $\sqrt{R_R R_{Sn}}$ can be estimated, see below equation for an A-scan:

$$I_D(z) = \frac{\rho}{8}[\gamma(z)[R_R + R_{S1} + R_{S2} + \cdots] + \frac{\rho}{4}\sum_{n=1}^{N}\sqrt{R_R R_{sn}}[(\gamma[2(z_R - z_{Sn})] + (\gamma[-2(z_R - z_{Sn})]] + \frac{\rho}{4}\sum_{n\neq m=1}^{N}\sqrt{R_{Sn}R_{sm}}[(\gamma[2(z_{Sn} - z_{Sm})] + (\gamma[-2(z_{Sn} - z_{Sm})]] \textbf{ (21)}$$

In equation (21), r_R is the electric field reflectivity, and the square of that is the power reflectivity R_R, It is assumed that the reference beam travels via air and the distance between the beam splitter and the reference mirror is written as Z_R. Z_s is the path variable between the sample and the beam splitter, here $\gamma(z)$ is the inverse Fourier transform of a normalised Gaussian function $S(k)$ and it is written as:

$$\gamma(z) = e^{-(z)^2\triangle k^2} \quad \textbf{(22)}$$

$$S(k) = \frac{1}{\Delta k'\sqrt{\pi}}e^{-[\frac{k-k0}{\triangle k'}]^2} \quad \textbf{(23)}$$

, here k_0 is the centre wavenumber of the light source and Δk is its' spectral bandwidth, coherence function $\gamma(z)$ corresponds to the half-width spectrum at its maximum 1/e, see figure 4 below for an example of FD-OCT A-scan, and B-scans are constructed of multiple A-scans in the depth direction.

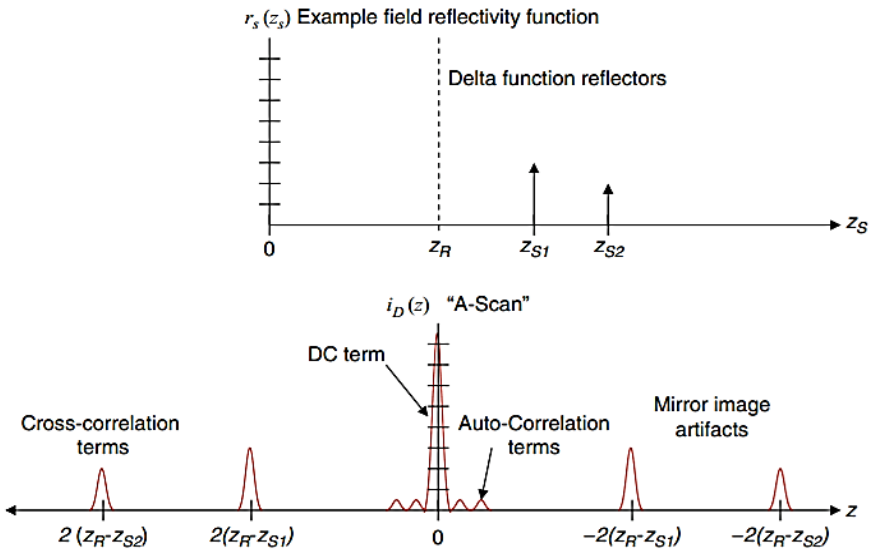

Figure 4. Example A-scan of Fourier-Domain OCT.

As shown in figure 4, the sample reflectivity profile is embedded in the cross-correlation term, and such term is Hermitian symmetrical, hence it leads to a complex conjugate artefact, i.e., the original function is equal to imaginary complex part with opposite sign. Hence, in practice, only the positive half-space is used in generating A-scans. The auto-correlation term also creates artefact in signal generating, using the adjacent signal's coherent length, such artefacts can be deduced. The SC term usually has a large artefact amplitude in signals which can be eliminated by subtracting the reference signal. Swept source OCT, i.e., SS-OCT's signal is detected like TD-OCT with a single-channel detector, with a controlled narrowband light source with a specific wavenumber, the signal processing resembles SD-OCT, where the reflectivity profile is calculated by using inverse Fourier transform on the cross-correlation terms [60].

3.24 Axial, lateral resolution and sensitivity of OCT systems

The axial (depth) resolution is an essential feature of OCT systems, and in the OCT community, it is generally defined by the coherent length of the source. The coherent length of the source is commonly defined by the full width at half maximum (FWHM) of the source self-coherence function multiplied by the speed of light, where the source self-coherence function is the inverse Fourier transform of the intensity spectrum of the source. The source spectrum intensity is assumed to be Gaussian, and it is defined by:

$$w = \Delta w/2\sqrt{In2} \qquad \textbf{(24)}$$

Where, Δw is the FWHM and the Fourier transform of this Gaussian spectrum yields a temporal pulse and the envelop is also Gaussian:

$$A(t) = exp[-1/4t^2w] \quad \textbf{(25)}$$

The FWHM of this pulse is the coherence time t_c where:

$$t_c = (1/\Delta v) * (4ln(2)/\pi) \quad \textbf{(26)}$$

Δv is the frequency spectral width and is related to the equivalent wavelength by:

$$\frac{dv}{d\lambda} \approx \frac{\Delta v}{\Delta \lambda} = -c/\lambda^2 \quad \textbf{(27)}$$

Therefore, the axial resolution is defined by:

$$\Delta z \approx I_c = \frac{2lnln\,(2)}{\pi}\frac{\lambda_0^2}{\Delta\lambda} \approx 0.44\frac{\lambda_0^2}{\Delta\lambda} \quad \textbf{(28)}$$

, where I_c is the coherence length of the light source, λ_0 is the centre wavelength of the light source and $\Delta\lambda$ is the spectral bandwidth. Using this definition, for a typical super continuum diode (SLD) with a center wavelength of 820 nm and 20 nm FWHM would have a theoretical axial resolution of 15μm. Note here, SLDs are commonly used as the light source of OCT systems as their intensity spectrum are generally Gaussian, they are also relatively inexpensive with a broad spectra of 10-70 nm FWHM within the center wavelength range of 675 nm - 1550 nm.

The lateral resolution of OCT is independent from its' axial resolution, and it is defined by:

$$\Delta x = 1.22(\lambda/2NA_{obj}) \quad \textbf{(29)}$$

Where NA_{obj} is the lens objectives, and the field depth Z of this objective is defined by:

$$Z = 2(\lambda n/{NA_{obj}}^2) \quad \textbf{(30)}$$

Where n is the refractive index of the tissue, and in general, a finer lateral resolution can be achieved with optic design, however, a trade-off of the penetration depth is sacrificed [56].

The sensitivity of OCT systems, is defined by the ratio of signal power generated using a perfectly placed mirror to the noise of the system:

$$SNR_p = {i_s}^2/{i_n}^2 \quad \textbf{(31)}$$

Where ${i_s}^2$ is the signal current generated by the interference at the photo detector, and can be rewritten as:

$$i_s = (\eta q_e/\hbar\omega_0) * P \quad \textbf{(32)}$$

where η is the quantum efficient of the detector, q_e is the electron charge, the Planck's constant corresponds to $\hbar$, ω_0 is the angular frequency of the source and the source power spectral density is integrated into P. There are three main noises in OCT systems: shot noise, arise from the light field interacts with the electrons in the detector and it is expressed as:

$$i_{shot\ noise} = \sqrt{2q_e i_{dc} B} \quad \textbf{(33)}$$

The photodetector current is denoted as i_{dc}, and B is the measured bandwidth as a function of acquisition time t ($B = 1/2t$). The second type of noise is called optical intensity noise, which arises from the constitute frequencies of source spectrum beating with each other, and it is described by:

$$i_{optic\ intensity\ noise} = i_{dc}\sqrt{\frac{B}{2\pi\Delta w}} \quad \textbf{(34)}$$

The third type of noise is the thermal noise, which arises from the initial resistance by the photocurrent in the receiver electronics, this noise generated by the amplification process can be expressed by:

$$i_{thermal\ noise} = \sqrt{\frac{4kTB}{R_{eff}}} \quad \textbf{(35)}$$

where k is the Boltzmann's constant and T is the absolute temperature. These three noise sums up the total noise, the noise current is written as:

$$i_n{}^2 = i_{shot\ noise}{}^2 + i_{optic\ intensity\ noise}{}^2 + i_{thermal\ noise}{}^2 \quad \textbf{(36)}$$

Often, when imaging a tissue which is highly scattered, the system can be designed to neglect the optic intensity noise and the thermal noise, this is done by arranging the optic field of the reference arm to be much bigger than the sample arm. Hence, the noise of the system can be considered to be equal to the shot noise, where:

$$SNR_p = \eta P/B\hbar\omega_0 \quad \textbf{(37)}$$

And the signal to noise ratio expresses in dB:

$$SNR_i = 10log_{10}(\sqrt{SNR_p}) \quad \textbf{(38)}\ [56]$$

3.25 OCT functional extensions

Apart from technological enhancement of OCT from Time-domain to Fourier-domain, functional extensions of OCT were also developed for clinical interests. Optical coherence tomography angiography, i.e., OCTA, refers to a branch of OCT where it is used to generate a vascular image based on motion contrast of the red blood cells without the need of a contrast agent. Since its introduction in

2006, OCTA has successively replaced and reduced the conventional use of fluorescein angiography and indocyanine green angiography, due to its' advantages of probing vascular perfusion without contrast medium and can be performed repeatedly, OCTA has been very appealing to medical fields where vascular imaging is needed [61]. R.A.Byers et. al carried-out research where OCTA was used to evaluate the microvascular morphology of murine skin after few tumour transplants, such evaluation is beneficial for cancer studies as abnormal vascular function and morphology are key events during tumour growth. By quantifying vessel parameters such as density, diameter and tortuosity, significant differences were found between the control group and the sample group, as well as sample groups' cancer type. Such findings affirmed OCTA's advantages of probing tissue's vascularity non-invasively, and potentials for longitudinal studies [62]. Ophthalmology is one of the most applied clinical areas for OCT, OCTA thus is also utilised to assess ocular state such as sclera inflammation. S.C.Hau et. al obtained OCTA scans for patients with episcleritis and scleritis, by imaging the vascular density of the tested sites, differentiation between the control group and diseased group was observed, furthermore, it was also possible to map out the vascular network at various anatomic site in sclera [63].

Polarisation sensitive OCT, as in PS-OCT, is also an extension of OCT, and it has gained significant attention due to its ability to differentiate anisotropic tissues such as ligaments, muscles and tendon. Its principle is based on, in addition to optic signal intensity, polarisation state of light is detected. This extension of OCT not only inherits the benefits of standard OCT of being non-invasive, fast at 3D imaging, easily integrated with catheter, it also measures tissue's phase retardance, or phase delay, diattenuation and depolarization. Since its introduction, PS-OCT has been successfully applied in dermatology, to image striae distensae, i.e., stretch marks. Lin W.C. et. al performed a study on imaging stretch marks via PS-OCT, their results showed that skin sites withs striae ditensae had a higher tissue birefringence than the controlled group [64]. D.C. Adams used PS-OCT in assessing the disease progression of systemic sclerosis via the optic axis and optic axis entropy. In such a study, degree of polarisation (DOP), phase retardance, optic axis (OA) and optic axis entropy were measured at subjects' forearms to assess the depth dependence of such a method. Later, OA scans for murine skin were obtained, results showed that a significant difference was found in the collagen network shown in OA images between the fibrotic and controlled group, which ascertained PS-OCT's ability in imaging cutaneous tissue fibre's architecture [65].

Another functional extension of OCT is called OCT elastography or OCE (Optical coherence elastography). This functional extension of OCT has also been popular due to its role of assessing elasticity of biological tissues. In clinical practice, one way of evaluating tissue elasticity is via elastography, i.e., when probing mechanical features of the tissue in a macro-scale, elastography techniques such as ultra-sonography or MRI based magnetic resonance elastography can provide scans which contain elasticity information about the tissue. These approaches tend to have a resolution of millimetre-scaled which can offer information of the human body from parts of tissue to whole body range. In a cellular scale of nanoscale, atomic force microscopy is used to acquire knowledge on how the cells react to external force which reveals insights on the cellular mechanics. Between the range of cells and organs, optical elastography is introduced as it can scan tissue with a micro-scaled resolution, which reveals potential values for in vivo diagnosis of several clinical fields. OCE's principle is based on an introduction of a load onto the sample and measuring deformation responses, typical loading mechanisms embedded in OCE can be generalised into compression, harmonic and transient while still, dominated by compression [66]. J.M.Schmitt has applied compressive force onto skin and skin model to assess their elasticity, under applied stress, strain of deformation was detected using speckle tracking, and the results of such a study shows that compressive OCE can be used to quantify micro-deformation of biological tissue [67]. More comprehensively, K.M. Kennedy et. al has used an OCE system with compression force on excised breast tissue as well as silicone phantoms to quantify the elasticity of the target sample. Elasticity parameters were determined by the stress-strain response and their results successfully showed that such a method can be used to differentiate malignant breast tissue from benign ones [68].

Other functional extensions of OCT including Doppler OCT (DOCT), which is a functional extension of OCT that is closely related to OCTA, while OCTA can offer valuable information on the vasculature structure of tissue, quantitative information on blood flow, or blood flood velocity is not directly gathered. DOCT typically records duplicate scans at the same position with a time delay. By extracting the phase difference of the signal, it grants the system ability to detect blood flow velocity of the tissue [69]. In dermatology, DOCT has been successfully applied to detect vascular abnormalities in patients with Port-Wine Stains (PWS) and haemangiomas, A.Latrive et. al used OCT and DOCT to image the lesional

skin on 5 patients with haemangiomas and PWS. Compared to normal skin, OCT scans of PWS and haemangiomas detected large dark cavities in the dermis, to distinguish these large dark cavities from other static cutaneous structure such as sebaceous glands, DOCT scans of patients with PWS and haemangiomas showed signals of moving particles, thus indicating those big cavities are abnormally large blood vessels [70]. Based on PS-OCT, MM-OCT, as in, Magnetomotive OCT is introduced, where, during MM-OCT scanning, tissue or cells are labelled with nano-magnetic particles such as SPION, i.e., superparamagnetic iron oxide, widely used in MRI. With an induced magnetic altering field, these cells or tissues are 'moved', neighbouring tissue or cells are therefore 'moved' which induce a displacement that can be detected as a phase shift with PS-OCT [60].

Apart from the mentioned functional extensions of OCT, the functional extension of OCT which particularly needs to be highlighted in this chapter is called visible-light OCT, i.e., VIS-OCT system. Previously mentioned, to quantify stratum corneum biomarkers such as its' thickness and hydration in vivo is the primary goal for this part of research, this is due to its' deterministic role in assessing skin barrier function. Listed in the literature chapters, a decent amount of efforts have been devoted into quantifying stratum corneum thickness and hydration in vivo using other means such as confocal raman microscopy and Corneometer, however, sub-surface information where in vivo validation of the measurements is rarely presented. While OCT can provide subsurface information of skin in vivo, most studies have used conventional OCT system to measure stratum corneum thickness at load bearing skin sites with a thickened stratum corneum, hence, there is a paucity of baseline data for non-load bearing stratum corneum thickness. OCT's ability in imaging stratified skin thickness is determined by its spatial resolution, and described earlier, the axial resolution which determines the stratum corneum thickness, also being the focused resolution for this part of research, is independent of the numerical aperture, and is defined by:

$$\Delta z \approx I_c = \frac{2ln\ln(2)}{\pi}\frac{\lambda_0^2}{\Delta\lambda} \approx 0.44\frac{\lambda_0^2}{\Delta\lambda} \quad [74] \qquad \textbf{(39)}$$

, where I_c is the coherence length of the light source, λ_0 is the centre wavelength of the light source and $\Delta\lambda$ is the spectral bandwidth. As the axial resolution is an inverse function of the spectral bandwidth, by changing the light source from narrow bandwidth to a broader bandwidth, a finer axial resolution can be achieved; in addition, by shortening the centre wavelength from near infrared to visible light visible light, finer axial resolution can also be obtained.

Reported, the axial resolution with a near-infrared light source with a centre wavelength ranging from 900 nm to 1300 nm is 1.2 μm to 7.5 μm. By switching the light source from near infrared to visible light with a centre wavelength from 400 nm *to 700* nm, an axial resolution of 0.8 μm to 1.4 μm can be achieved [71]. As ophthalmology remains as the most applied field for OCT, VIS-OCT, as a burgeoning extension of OCT, has been utilised to image retina in mouse and human subjects [72,73]. In dermatology, the author's group has developed a Fourier domain visible – light OCT system to image the human stratum corneum in vivo, a detailed system configuration is explained in later chapters.

In this chapter, skin barrier properties are reviewed with a special focus on stratum corneum hydration and thickness. In vivo/ex vivo quantifications of these parameter using the state-of-art techniques such as confocal Raman microscopy (CRM), optical coherence tomography (OCT) and Corneometry are listed. Human stratum corneum thickness in vivo has been stated in literature to fall within the range of 10-30μm, with water incubation, in can increase up to 2-3 folds. The system that has been used in this research, optical coherence tomography (OCT), has been reviewed with its' principle, mathematical representation and functional extensions. In later chapter, a recent innovation of the OCT system, visible-light OCT will be introduced with its system configuration, along with experiment design and post processing.

References

[1]. S. Weidinger, L. A. Beck, T. Bieber, K. Kabashima, and A. D. Irvine, “Atopic dermatitis,” Nature reviews. Disease primers, vol. 4, no. 1, pp. 1–1, 2018, doi: 10.1038/s41572-018-0001-z.

[2]. M. J. Cork et al., “Epidermal Barrier Dysfunction in Atopic Dermatitis,” Journal of investigative dermatology, vol. 129, no. 8, pp. 1892–1908, 2009, doi: 10.1038/jid.2009.133.

[3]. E. A. Swanson et al., “In vivo retinal imaging by optical coherence tomography,” Optics letters, vol. 18, no. 21, pp. 1864–1866, 1993, doi: 10.1364/OL.18.001864.

[4]. J. G. Fujimoto, E. A. Swanson, and D. Huang, “Optical Coherence Tomography - History, Evolution, and Future Prospects: 2023 Lasker-DeBakey Clinical Medical Research Award,” JAMA : the journal of the American Medical Association, vol. 330, no. 15, pp. 1427–1428, 2023, doi: 10.1001/jama.2023.16942.

[5]. B. Wan et al., “Applications and future directions for optical coherence tomography in dermatology,” British journal of dermatology (1951), vol. 184, no. 6, pp. 1014–1022, 2021, doi: 10.1111/bjd.19553.

[6]. B. Baumann, “Polarization sensitive optical coherence tomography: A review of technology and applications,” Applied sciences, vol. 7, no. 5, p. 474, 2017, doi: 10.3390/app7050474.

[7]. J. Schleusener, A. Salazar, J. von Hagen, J. Lademann, and M. E. Darvin, “Retaining skin barrier function properties of the stratum corneum with components of the natural moisturizing factor—a randomized, placebo-controlled double-blind in vivo study,” Molecules (Basel, Switzerland), vol. 26, no. 6, p. 1649, 2021, doi: 10.3390/molecules26061649.

[8].T. Berkers, D. Visscher, G. S. Gooris, and J. A. Bouwstra, “Degree of skin barrier disruption affects lipid organization in regenerated stratum corneum,” Acta dermato-venereologica, vol. 98, no. 4, pp. 421–427, 2018, doi: 10.2340/00015555-2865.

[9]. M. Akdeniz, S. Gabriel, A. Lichterfeld-Kottner, U. Blume-Peytavi, and J. Kottner, “Transepidermal water loss in healthy adults: a systematic review and meta-analysis update,” British journal of dermatology (1951), vol. 179, no. 5, pp. 1049–1055, 2018, doi: 10.1111/bjd.17025.

[10]. Verdier-Sévrain S, Bonté F. Skin hydration: a review on its molecular mechanisms. J Cosmet Dermatol. 2007 Jun;6(2):75-82. doi: 10.1111/j.1473-2165.2007.00300.x. PMID: 17524122.

[11]. Z. Zhang and D. J. Lunter, “Confocal Raman microspectroscopy as an alternative to differential scanning calorimetry to detect the impact of emulsifiers and formulations on stratum corneum lipid conformation,” European journal of pharmaceutical sciences, vol. 121, pp. 1–8, 2018, doi: 10.1016/j.ejps.2018.05.013.

[12]. Braun-Falco O, Korting HC. Der normale pH-Wert der menschlichen Haut [Normal pH value of human skin]. Hautarzt. 1986 Mar;37(3):126-9. German. PMID: 3700100.

[13]. Z. K. Jabbar-Lopez et. al, “The effect of water hardness on atopic eczema, skin barrier function: A systematic review, meta-analysis,” Clinical and experimental allergy, vol. 51, no. 3, pp. 430–451, 2021, doi: 10.1111/cea.13797.

[14]. I. M. Gidado, M. Qassem, I. F. Triantis, and P. A. Kyriacou, “Review of Advances in the Measurement of Skin Hydration Based on Sensing of Optical and Electrical Tissue Properties,” Sensors (Basel, Switzerland), vol. 22, no. 19, p. 7151, 2022, doi: 10.3390/s22197151.

[15]. C. Ruini et. al, “In vivo examination of healthy human skin after short-time treatment with moisturizers using confocal Raman spectroscopy and optical coherence tomography: Preliminary observations,” Skin research and technology, vol. 28, no. 1, pp. 119–132, 2022, doi: 10.1111/srt.13101.

[16]. P. J. Caspers, H. A. Bruining, G. J. Puppels, G. W. Lucassen, and E. A. Carter, “In Vivo Confocal Raman Microspectroscopy of the Skin: Noninvasive Determination of Molecular Concentration Profiles,” Journal of investigative dermatology, vol. 116, no. 3, pp. 434–442, 2001, doi: 10.1046/j.1523-1747.2001.01258.x.

[17]. J. M. Crowther et. al, “Measuring the effects of topical moisturizers on changes in SC thickness, water gradients and hydration in vivo,” British journal of dermatology (1951), vol. 159, no. 3, pp. 567–577, 2008, doi: 10.1111/j.1365-2133.2008.08703.x.

[18]. C. Choe, J. Schleusener, J. Lademann, and M. E. Darvin, “Age related depth profiles of human SC barrier-related molecular parameters by confocal Raman microscopy in vivo,” Mechanisms of ageing and development, vol. 172, pp. 6–12, 2018, doi: 10.1016/j.mad.2017.08.011.

[19]. H. Wang et. al, “Novel confocal Raman microscopy method to investigate hydration mechanisms in human skin,” Skin research and technology, vol. 25, no. 5, pp. 653–661, 2019, doi: 10.1111/srt.12698.

[20]. S. Luebberding, N. Krueger, and M. Kerscher, “Skin physiology in men and women: in vivo evaluation of 300 people including TEWL, SC hydration, sebum content and skin surface pH,” International journal of cosmetic science, vol. 35, no. 5, pp. 477–483, 2013, doi: 10.1111/ics.12068.

[21]. M. R. Lee et. al, “Comparison of the skin biophysical parameters of Southeast Asia females: forehead-cheek and ethnic groups,” Journal of the European Academy of Dermatology and Venereology, vol. 27, no. 12, pp. 1521–1526, 2013, doi: 10.1111/jdv.12042.

[22]. G. W. Nam, J. H. Baek, J. S. Koh, and J.-K. Hwang, “The seasonal variation in skin hydration, sebum, scaliness, brightness and elasticity in Korean females,” Skin research and technology, vol. 21, no. 1, pp. 1–8, 2015, doi: 10.1111/srt.12145.
[23]. E. J. Song et. al, “A study on seasonal variation of skin parameters in Korean males,” International journal of cosmetic science, vol. 37, no. 1, pp. 92–97, 2015, doi: 10.1111/ics.12174.
[24]. A. Firooz et. al, “Comparison of hydration, sebum and pH values in clinically normal skin of patients with atopic dermatitis and healthy controls,” Clinical and experimental dermatology, vol. 32, no. 3, pp. 321–322, 2007, doi: 10.1111/j.1365-2230.2007.02364.x.
[25]. P.-G. Sator, J. B. Schmidt, and H. Hönigsmann, “Comparison of epidermal hydration and skin surface lipids in healthy individuals and in patients with atopic dermatitis,” Journal of the American Academy of Dermatology, vol. 48, no. 3, pp. 352–358, 2003, doi: 10.1067/mjd.2003.105.
[26]. E. E. Grinich, C. Topham, D. Haynes, J. Chung, E. Latour, and E. L. Simpson, “Validation of a novel patient-operated device for measuring skin barrier function in atopic dermatitis,” Skin research and technology, vol. 27, no. 5, pp. 824–830, 2021, doi: 10.1111/srt.13027.
[27]. A. Samadi et. al, “Stratum corneum hydration in healthy adult humans according to the skin area, age and sex: a systematic review and meta-analysis,” Journal of the European Academy of Dermatology and Venereology, vol. 36, no. 10, pp. 1713–1721, 2022, doi: 10.1111/jdv.18297.
[28]. M. Gelker, C. C. Müller-Goymann, and W. Viöl, “Permeabilization of human stratum corneum and full-thickness skin samples by a direct dielectric barrier discharge,” Clinical plasma medicine, vol. 9, pp. 34–40, 2018, doi: 10.1016/j.cpme.2018.02.001.
[29]. O. A. Foss, P. Mjønes, S. Fismen, and E. Christensen, “Is There a Relationship between the Stratum Corneum Thickness and That of the Viable Parts of Tumour Cells in Basal Cell Carcinoma?,” Journal of Skin Cancer, vol. 2016, pp. 6146091–5, 2016, doi: 10.1155/2016/6146091.
[30]. Y. Tomita, M. Akiyama, and H. Shimizu, “Stratum corneum hydration and flexibility are useful parameters to indicate clinical severity of congenital ichthyosis,” Experimental dermatology, vol. 14, no. 8, pp. 619–624, 2005, doi: 10.1111/j.0906-6705.2005.00341.x.
[31]. L. Huang, W. Sun, Z. Ye, Y. Liu, K. He, and S. Li, “Changes in epidermal thickness and their correlation with clinical characteristics in patients with vitiligo,” Archives of Dermatological Research, vol. 316, no. 8, p. 519, 2024, doi: 10.1007/s00403-024-03265-w.
[32]. M. I. White, D. M. Jenkinson, and D. H. Lloyd, “The effect of washing on the thickness of the stratum corneum in normal and atopic individuals,” British journal of dermatology (1951), vol. 116, no. 4, pp. 525–530, 1987, doi: 10.1111/j.1365-2133.1987.tb05873.x.
[33]. F. M. W. Rodijk, G. Zanelli, M. Geerligs, P. E. J. van Erp, and M. Peppelman, “The influence of different shavers on the skin quantified by non-invasive reflectance confocal microscopy,” Skin research and technology, vol. 22, no. 3, pp. 311–317, 2016, doi: 10.1111/srt.12263.
[34]. Y. Liu and D. J. Lunter, “Optimal configuration of confocal Raman spectroscopy for precisely determining stratum corneum thickness: Evaluation of the effects of polyoxyethylene stearyl ethers on skin,” International journal of pharmaceutics, vol. 597, pp. 120308–120308, 2021, doi: 10.1016/j.ijpharm.2021.120308.
[35]. D.-S. Mahrhauser et. al, “Assessment of Raman spectroscopy as a fast and non-invasive method for total stratum corneum thickness determination of pig skin,” International journal of pharmaceutics, vol. 495, no. 1, pp. 482–484, 2015, doi: 10.1016/j.ijpharm.2015.09.018.
[36]. C. Choe, J. Lademann, and M. E. Darvin, “Lipid organization and stratum corneum thickness determined in vivo in human skin analyzing lipid-keratin peak (2820-3030 cm−1) using confocal Raman microscopy,” Journal of Raman spectroscopy, vol. 47, no. 11, pp. 1327–1331, 2016, doi: 10.1002/jrs.4975.
[37]. J. M. Crowther et. al, “Measuring the effects of topical moisturizers on changes in stratum corneum thickness, water gradients and hydration in vivo,” British journal of dermatology (1951), vol. 159, no. 3, pp. 567–577, 2008, doi: 10.1111/j.1365-2133.2008.08703.x.
[38]. M. Egawa, T. Hirao, and M. Takahashi, “In vivo estimation of stratum corneum thickness from water concentration profiles obtained with raman spectroscopy,” Acta dermato-venereologica, vol. 87, no. 1, pp. 4–8, 2007, doi: 10.2340/00015555-0183.
[39]. A. Böhling, S. Bielfeldt, A. Himmelmann, M. Keskin, and K.-P. Wilhelm, “Comparison of the stratum corneum thickness measured in vivo with confocal Raman spectroscopy and confocal reflectance microscopy,” Skin research and technology, vol. 20, no. 1, pp. 50–57, 2014, doi: 10.1111/srt.12082.
[40]. Z. Ya-Xian, T. Suetake, and H. Tagami, “Number of cell layers of the stratum corneum in normal skin relationship to the anatomical location an the body, age, sex and physical parameters,” Archives of Dermatological Research, vol. 291, no. 10, pp. 555–559, 1999, doi: 10.1007/s004030050453.
[41]. G. N. Stamatas et. al, “A predictive self-organizing multicellular computational model of infant skin permeability to topically applied substances,” 2021.

[42]. “Assessment of infant stratum corneum composition and thickness with Raman spectroscopy,” Journal of the American Academy of Dermatology, vol. 66, no. 4, pp. AB35–AB35, 2012, doi: 10.1016/j.jaad.2011.11.155.
[43]. X. Liu, D. Gad, Z. Lu, R. Lewis, M. J. Carre, and S. J. Matcher, “The contributions of skin structural properties to the friction of human finger-pads,” 2015.
[44]. R. Maiti, M. Duan, S. G. Danby, R. Lewis, S. J. Matcher, and M. J. Carré, “Morphological parametric mapping of 21 skin sites throughout the body using optical coherence tomography,” Journal of the mechanical behavior of biomedical materials, vol. 102, pp. 103501–103501, 2020, doi: 10.1016/j.jmbbm.2019.103501.
[45]. K. Kato et. al, “Analysis of sweating by optical coherence tomography in patients with palmoplantar hyperhidrosis,” Journal of dermatology, vol. 48, no. 3, pp. 334–343, 2021, doi: 10.1111/1346-8138.15694.
[46]. H. Fruhstorfer, U. Abel, C.-D. Garthe, and A. Knüttel, “Thickness of the stratum corneum of the volar fingertips,” Clinical anatomy (New York, N.Y.), vol. 13, no. 6, pp. 429–433, 2000, doi: 10.1002/1098-2353(2000)13:6<429::AID-CA6>3.0.CO;2-5.
[47]. S. Razi, T. M. Truong, S. Khan, B. Sanabria, and B. Rao, “Hydradermabrasion through the lens of Line-Field Confocal Optical Coherence Tomography,” Skin research and technology, vol. 30, no. 4, pp. e13684-n/a, 2024, doi: 10.1111/srt.13684.
[48]. F. Bonnier et. al, “Line-field confocal optical coherence tomography coupled with artificial intelligence algorithms to identify quantitative biomarkers of facial skin ageing,” Scientific reports, vol. 13, no. 1, pp. 13881–13881, 2023, doi: 10.1038/s41598-023-40340-0.
[49]. J. Monnier et. al, “In vivo characterization of healthy human skin with a novel, non-invasive imaging technique: line-field confocal optical coherence tomography,” Journal of the European Academy of Dermatology and Venereology, vol. 34, no. 12, pp. 2914–2921, 2020, doi: 10.1111/jdv.16857.
[50]. J. Chauvel-Picard et. al, “Line-field confocal optical coherence tomography as a tool for three-dimensional in vivo quantification of healthy epidermis: A pilot study,” Journal of biophotonics, vol. 15, no. 2, pp. e202100236-n/a, 2022, doi: 10.1002/jbio.202100236.
[51]. M. Tsang and R. H. Guy, “Effect of Aqueous Cream BP on human stratum corneum in vivo,” British journal of dermatology (1951), vol. 163, no. 5, pp. 954–958, 2010, doi: 10.1111/j.1365-2133.2010.09954.x.
[52]. L. M. Russell, S. Wiedersberg, and M. Begoña Delgado-Charro, “The determination of stratum corneum thickness An alternative approach,” European journal of pharmaceutics and biopharmaceutics, vol. 69, no. 3, pp. 861–870, 2008, doi: 10.1016/j.ejpb.2008.02.002.
[53]. J. A. Fairley and J. E. Rasmussen, “Comparison of stratum corneum thickness in children and adults,” Journal of the American Academy of Dermatology, vol. 8, no. 5, pp. 652–654, 1983, doi: 10.1016/S0190-9622(83)70074-5.
[54]. J. Sandby-Møller, T. Poulsen, and H. C. Wulf, “Epidermal Thickness at Different Body Sites: Relationship to Age, Gender, Pigmentation, Blood Content, Skin Type and Smoking Habits,” Acta dermato-venereologica, vol. 83, no. 6, pp. 410–413, 2003, doi: 10.1080/00015550310015419.
[55]. D. Huang et. al, “Optical Coherence Tomography,” Science (American Association for the Advancement of Science), vol. 254, no. 5035, pp. 1178–1181, 1991, doi: 10.1126/science.1957169.
[56]. P.Tomlins et. al, “Theory, developments and applications of optical coherence tomography” Journal of Physics D: Applied Physics, Volume 38, Number 15. DOI 10.1088/0022-3727/38/15/002
[57]. B. Baumann, “Polarization sensitive optical coherence tomography: A review of technology and applications,” Applied sciences, vol. 7, no. 5, p. 474, doi: 10.3390/app7050474.
[58]. J. Welzel, E. Lankenau, R. Birngruber, and R. Engelhardt, “Optical coherence tomography of the human skin,” Journal of the American Academy of Dermatology, vol. 37, no. 6, pp. 958–963, 1997, doi: 10.1016/S0190-9622(97)70072-0.
[59]. W. Drexler, M. Liu, A. Kumar, T. Kamali, A. Unterhuber, and R. A. Leitgeb, “Optical coherence tomography today: speed, contrast, and multimodality,” Journal of biomedical optics, vol. 19, no. 7, pp. 071412–071412, 2014, doi: 10.1117/1.JBO.19.7.071412.
[60]. W.Li (2020), Development of Magnetomotive Optical Coherence Tomography and Polarization-Sensitive Optical Coherence Tomography for clinical Applications. PhD thesis. University of Sheffield.
[61]. A. Haas, D. Ahmed, M. Stattin, A. Graf, K. Krepler, and S. Ansari-Shahrezaei, “Comparison of macular neovascularization lesion size by the use of Spectral-Domain Optical Coherence Tomography Angiography and Swept-Source Optical Coherence Tomography Angiography versus Indocyanine Green Angiography,” Acta ophthalmologica (Oxford, England), vol. 99, no. 2, pp. e260–e266, 2021, doi: 10.1111/aos.14572.
[62]. R. A. Byers, M. Fisher, N. J. Brown, G. M. Tozer, and S. J. Matcher, “Vascular patterning of subcutaneous mouse fibrosarcomas expressing individual VEGF isoforms can be differentiated using angiographic optical coherence tomography,” 2017.

[63]. S. C. Hau, K. Devarajan, and M. Ang, “Anterior Segment Optical Coherence Tomography Angiography and Optical Coherence Tomography in the Evaluation of Episcleritis and Scleritis,” Ocular immunology and inflammation, vol. 29, no. 2, pp. 362–369, 2021, doi: 10.1080/09273948.2019.1682617.
[64]. W. C. Lin, R. A. Byers, W. Li, S. G. Danby, M. J. Cork, and S. J. Matcher, “Imaging striae distensae : a comparison between PS-OCT and digital dermoscopy,” 2021.
[65]. D. C. Adams et. al, “Assessing the progression of systemic sclerosis by monitoring the tissue optic axis using PS-OCT,” Scientific reports, vol. 10, no. 1, p. 2561, 2020, doi: 10.1038/s41598-020-59330-7.
[66]. B. F. Kennedy, P. Wijesinghe, and D. D. Sampson, “The emergence of optical elastography in biomedicine,” Nature photonics, vol. 11, no. 4, pp. 215–221, 2017, doi: 10.1038/nphoton.2017.6.
[67]. J. Schmitt, “OCT elastography: imaging microscopic deformation and strain of tissue,” Optics express, vol. 3, no. 6, pp. 199–211, 1998, doi: 10.1364/OE.3.000199.
[68]. K. M. Kennedy et. al, “Quantitative micro-elastography: imaging of tissue elasticity using compression optical coherence elastography,” Scientific reports, vol. 5, no. 1, pp. 15538–15538, 2015, doi: 10.1038/srep15538.
[69]. S. Desissaire et. al, “Analysis of longitudinal sections of retinal vessels using Doppler OCT,” Biomedical optics express, vol. 11, no. 4, pp. 1772–1789, 2020, doi: 10.1364/BOE.385938.
[70]. A. Latrive, L. R. C. Teixeira, A. S. L. Gomes, and D. M. Zezell, “Characterization of skin Port-Wine Stain and Hemangioma vascular lesions using Doppler OCT,” Skin research and technology, vol. 22, no. 2, pp. 223–229, 2016, doi: 10.1111/srt.12253.
[71]. X. Shu, L. Beckmann, and H. F. Zhang, “Visible-light optical coherence tomography: a review,” Journal of biomedical optics, vol. 22, no. 12, pp. 121707–121707, 2017, doi: 10.1117/1.JBO.22.12.121707.
[72]. J. Wang et. al, “A dual-channel visible light optical coherence tomography system enables wide-field, full-range, and shot-noise limited human retinal imaging,” Communications engineering, vol. 3, no. 1, pp. 21–13, 2024, doi: 10.1038/s44172-024-00167-7.
[73]. P. Chauhan, A. M. Kho, P. FitzGerald, B. Shibata, and V. J. Srinivasan, “Subcellular Comparison of Visible-Light Optical Coherence Tomography and Electron Microscopy in the Mouse Outer Retina,” Investigative ophthalmology & visual science, vol. 63, no. 9, pp. 10–10, 2022, doi: 10.1167/iovs.63.9.10.
[74]. D. G. Revin, R. A. Byers, M. Q. Duan, W. Li, and S. J. Matcher, “Visible-light optical coherence tomography platform for the characterization of the skin barrier,” Biomedical optics express, vol. 14, no. 8, pp. 3914–3923, 2023, doi: 10.1364/BOE.494356.

4.0 Experiment

4.1 Materials and methods

In total, 15 human subjects (10 males, 5 females) aged between 21-60 with Fitzpatrick skin type 1-4 (a numerical classification for human skin colour based on skin's response to exposure to UV light. Scale examples: 1 - pale white skin, blue/green eyes, blond/red hair, always burn on UV exposure; 2 - fair skin, blue eyes; burns easily and tan slightly on UV exposure; 3 - darker white skin, tan after initial burn on UV exposure; 4 - light brown skin, burns minimally, tans easily on UV exposure) were recruited for this study; the subjects claimed no skin conditions which involves medical treatment; this study was approved by the ethics committee of the department of Electronic and Electrical Engineering at the University of Sheffield, UK (Reference Number 050061); informed consent along with risk assessment (RA); standard operation procedure (SOP) and participant information sheet were obtained and provided.

The experiment took place in a lab where the air temperature was kept at 20-21°C and the relative humidity was maintained at ~35%. During the experiment, subjects' hands were immersed in a bucket of tap water for 40 minutes (hydrating phase). Initial temperature of the water was around 30°C and it steadily increased to about 35°C as the subject's hand warmed it up. After 40 minutes of immersing, the subjects took out their hands and dried it using disposable towels, and the hands were left to spontaneously dehydrate for 40 minutes (dehydrating phase).

During the hydrating and dehydrating phase, at every 5 minutes of interval (after drying it using a disposable towel), visible light OCT (VIS-OCT) B-scans of the subjects' dorsal hand were collected (8mm x 0.85mm corresponds to 1600 x 1024 pixels), and the SC hydration were measured by a Corneometer ® CM 825 (Courage + Khazaka electronic GmbH) for comparison. The experiment took place in 2023, where 11 out of 15 subjects completed the experiment in spring-summer season (March – April 2023); and 12 out of 15 subjects completed the experiment in autumn-winter season (October – December 2023); and 8 subjects completed the experiment in both seasons. Corneometer® CM 825 (Courage + Khazaka electronic GmbH) measurements were only obtained during autumn-winter season as it was not available in spring-summer season.

4.2 Visible-light OCT system

The VIS-OCT system used in this experiment has been assembled using commercially available components, and figure 5 shows the system configuration of the VIS-OCT system.

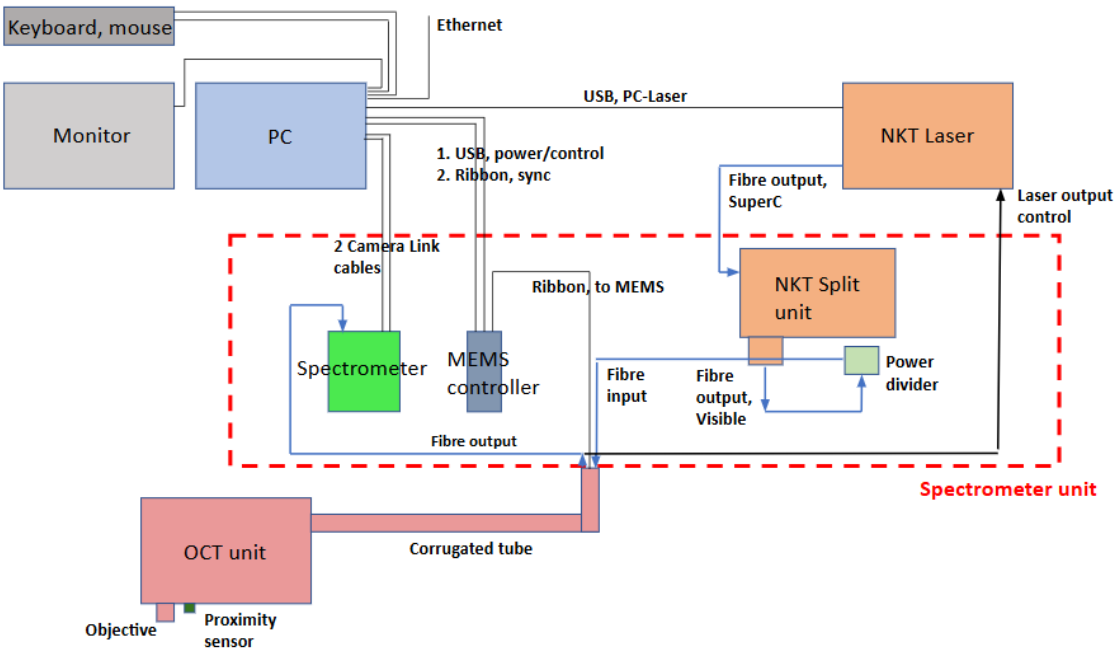

Figure 5. System configuration of the VIS-OCT system

As shown in figure 5, the supercontinuum laser source of this system is from NKT Photonics (model: SuperK EXTREME EXU-6), the wavelength range of this laser is between ~400-2000 nm with a maximum output power of 5 W and a repetition rate of 78 MHz. The near infrared part of the laser (>~900 nm) emitted from the laser source is blocked by the SuperK Split unit, and the remaining output power is reduced by a partially reflecting optical plate, two bandpass filters then further crop the emission spectrum to its' targeted visible light range (~450-720 nm). In addition, to adjust the emitted spectrum to be closer to a Gaussian shape, an additional filter from Thorlabs Inc. (model: FGB37-A) is applied. The emitted laser spectrum is directed into a Michelson interferometer via a single mode fibre from Corning Inc. (model: RGB400), and this fibre is further coupled into a reflective collimator from Thorlabs Inc. (model: RC04APC-P01) to offer a ~2.5 mm diameter free space laser beam within the interferometer. As shown in figure 6 (left), the free space bulk optics Michelson interferometer was built using optical components from Thorlabs Inc. A cube beam splitter separates the incident light into a reference arm and a sample arm with a 70:30 ratio. In the reference arm, the beam power relative to the sample arm is controlled by a 1 mm thick neutral density reflective fused silica wedged filter. At the sample arm, the incident light beam is reflected by an intermediate mirror at an angle of ~22 degrees

onto a microelectromechanical mirror (MEMS) scanner from Mirrorcle Technologies Inc, to provide area scanning. The MEMS mirror's diameter is 4.6 mm, it contains a low pass filter with a cutoff frequency of 120 Hz to ensure the mirror can't be excited at its' resonant frequency (364 Hz). The light reflected from the MEMS mirror is then focused onto the tissue sample by a telecentric lens with a focal length of 39 mm from Thorlabs Inc. (model: LSM03-VIS). The maximum field of view (FOV) of this system is 8mm x 8mm and the overall light attenuation is adjusted to have an output power of ~1 mW. The light beam that gets backscattered from the sample arm and the light beam reflected from the reference arm interferes at the beam splitter, the interfered beam is then coupled into a single mode fibre is from Thorlabs Inc. (model: SM450) and then directed towards a spectrometer from Wasatch Photonics (model: Cobra VIS), the spectral resolution of this spectrometer is ~0.1 nm. A 492-698 nm complementary metal oxide semiconductor (CMOS) 2048-pixel line array camera from Octoplus (model: Teledyne e2V) is attached to the spectrometer to detect the laser spectrum, and spectral data were collected by a frame grabber from Teledyne DALSA, Inc. (model: Xtium-CL MX4) which is synchronised with MEMS's movement. The system operation is controlled by a software package written in MATLAB, and the OCT images of the backscattered intensity are displayed on a dB scale. As shown in figure 6 (right), the bulk optics interferometer components are made attached to a 6 mm acrylic plate and enclosed in an acrylic box (310 mm x 240 mm x 85mm) which weighed ~*3.3 kg,* at the side where the objective lens is placed, a proximity sensor is mounted for safety measures, as in, the laser is only switched on when the sensor senses an object. Along with the spectrometer unit and laser source, the whole system was designed to be trolly mounted available for clinical application.

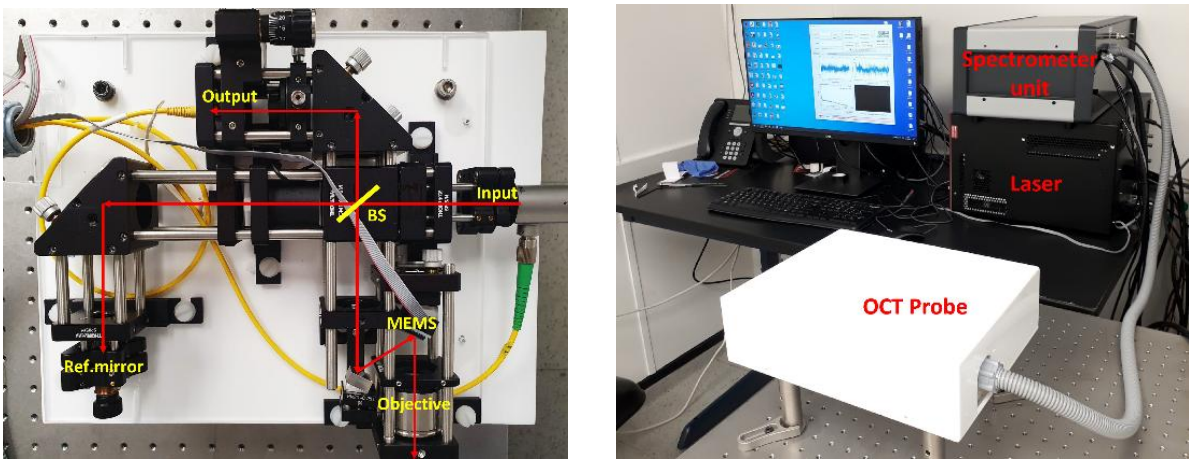

Figure 6. VIS-OCT system components. left - Free space bulk optics Michelson interferometer. BS – beam splitter; Ref.mirror – reference mirror; right) VIS-OCT system main components overview. The laser unit is from NKT Photonics (model: SuperK EXTREME EXU-6); right - the spectrometer is Wasatch Photonics (model: Cobra

VIS), and this unit contains the CMOS camera and MEMS controller; the Michelson interferometer is enclosed in an acrylic box (OCT Probe); and the whole system is controlled by a PC with a MATLAB software [1].

The shape of the laser light spectrum projected onto the sample is close to a Gaussian shape, and the centre wavelength of the spectrum λ_0 is 585 nm with a full width half maximum (FWHM) of 95 nm. The axial resolution of this system was estimated to be 1.56 μm in air using Fourier transform of the resampled spectral fringes from zero optical path difference (OPD), i.e., the mirror is placed at the sample arm at a depth of ~167 nm away from the objective lens. The resampling table calculated from this mirror depth was used to obtain OCT images. The measured axial resolution was 1.58μm in air, which was very comparable to the estimation, by assuming the refractive index of the stratum corneum to be 1.55, the axial resolution in tissue was estimated to be ~1 μm. The axial resolution can be further improved with a wider spectrum or a numerical approach, however, the stratum corneum at non-palmer skin sites has a typical thickness of few micrometres to 50 micrometres, hence, the current axial resolution is sufficient to obtain a good visualisation of the stratum corneum in vivo. The lateral resolution of this VIS-OCT system was estimated to be ~7 μm in air, using a US Air Force 1951 resolution test target, such a resolution was very comparable of the theoretical lateral resolution calculated from $\Delta x = 1.22(\lambda/2NA_{obj})$[2]. The maximum imaging depth in air is ~0.85 mm in air which corresponds to ~0.6 mm in tissue, and one pixel in an A-scan corresponds to ~0.53 μm in tissue. The sensitivity of the system when measured from a mirror at the sample arm positioned close to zero OPD, was estimated as ~75 dB. One B-scan contains 1600 A-scans that are obtained at ~39 Hz [1].

4.3 Visible-light OCT scan processing

4.31 Finding the skin surface and stratum corneum/stratum granulosum (SC/SG) junction

Figure 7 shows a typical B-scan of a subject's dorsal hand before hydration taken by the VIS-OCT system. The B-scan size is 1600 pixels x 1024 pixels (8 mm x 0.85 mm). The SC in the scans is defined as a hypoechogenic band that is just below the bright 'entrance signal'. As shown in figure, apart from the SC, other skin components such as blood vessels; epidermal/dermal junction; epidermis and dermis are also visually clear to locate. For most subjects, the B-scans were segmented automatically using an algorithm developed in MATLAB. However, for some subjects with atypical stratum corneum B-scans, manual segmentation was used, explained later. The processing steps of the B-scan

segmentation is straightforward, firstly, the algorithm/researcher finds the skin surface, secondly, it/he/she finds the SC/SG junction. Using the locations of the skin surface and the SC/SG junction, a SC thickness calculation and a SC reflectance (average brightness) were defined. The entrance signal, which we define as the skin surface, is a result of the Fresnel reflection at the air/tissue interface. It is found by moving a 5-pixel averaging window over the A-scan and locating the peak position in this smoothed A-scan. In figure 8, The red curve shows this peak position for each A-scan; and, by visual inspection, the curve needs smoothing, hence it was smoothed using a 25-order 1D median filter (MATLAB *medfilt1* function), the smoothed curve or skin surface is plotted as the blue curve in figure 9. The smoothing function is very useful when hairs or other components are captured by the segmentation. For each subject, manual segmentations are visually inspected on the spot; for automatic segmentation using the algorithms, visual inspections are performed after processing the volumetric scans.

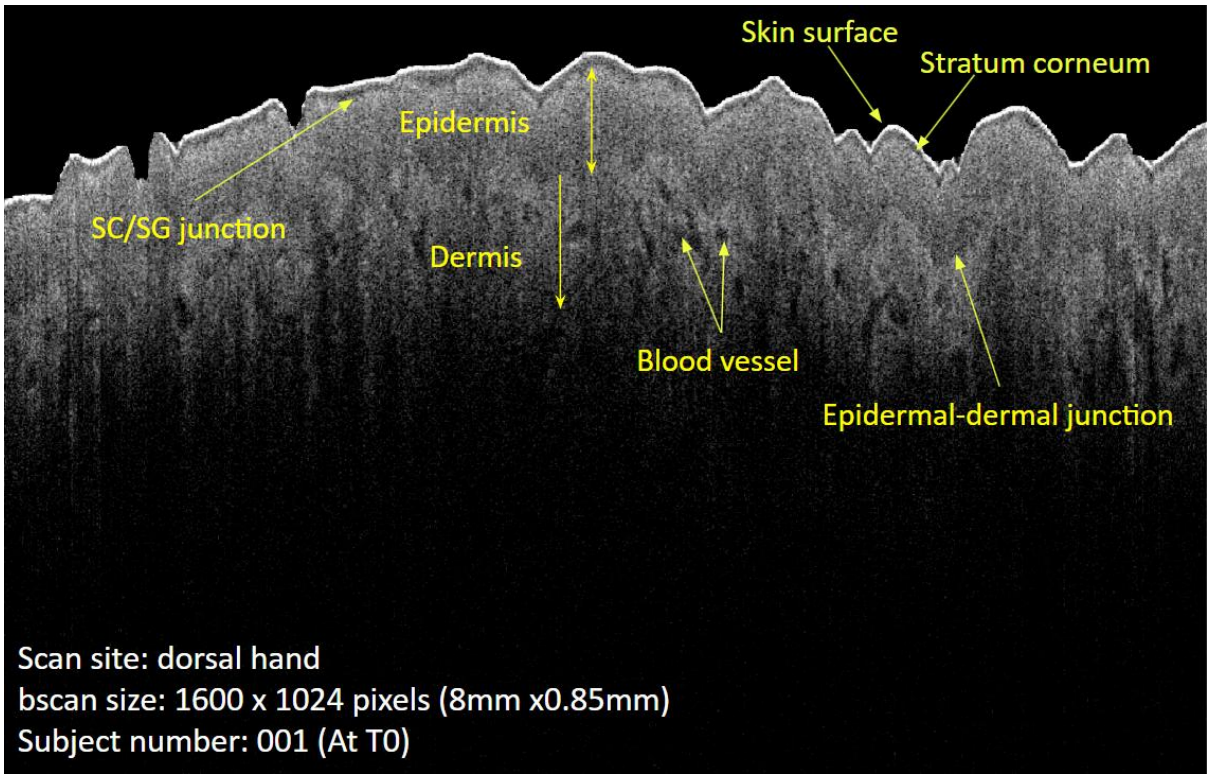

Figure 7. A typical B-scan of the subject's dorsal hand before hydration (T0). SC/SG: stratum corneum/stratum granulosum junction

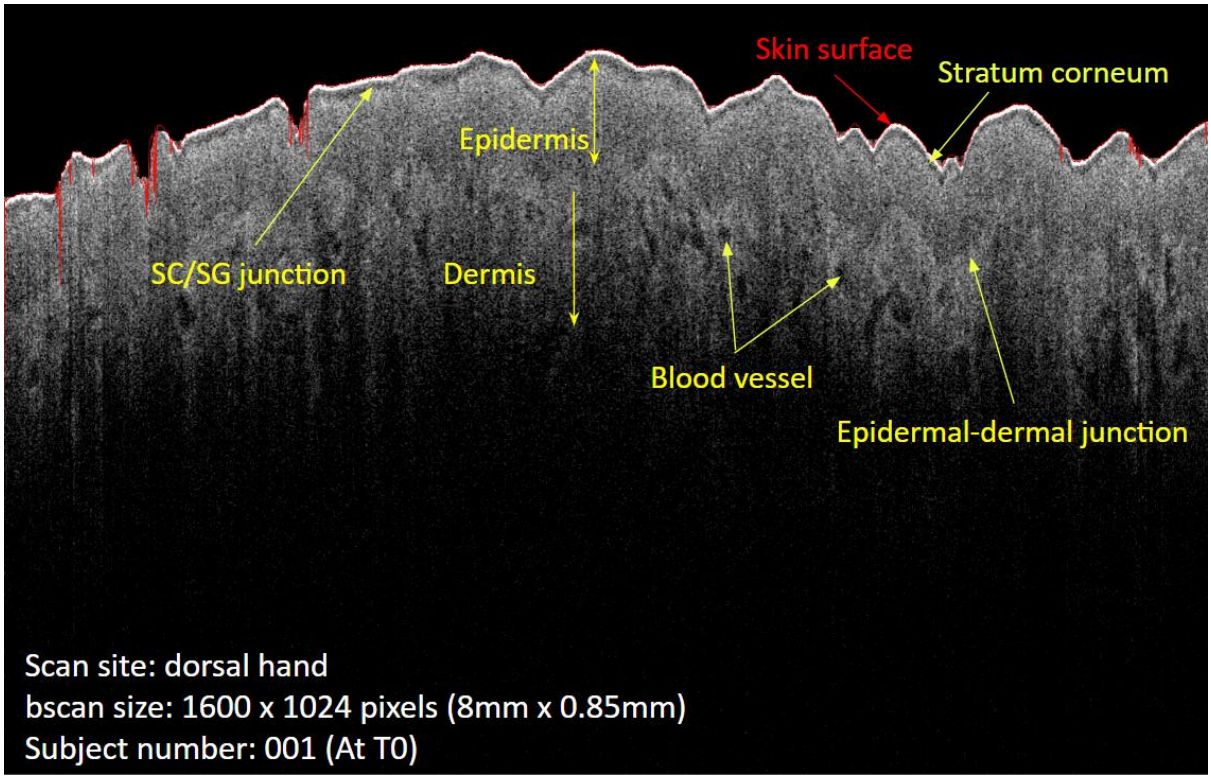

Figure 8. A typical B-scan of the subject's dorsal hand before hydration (T0) with skin surface (pre smoothed) detected. SC/SG: stratum corneum/stratum granulosum junction

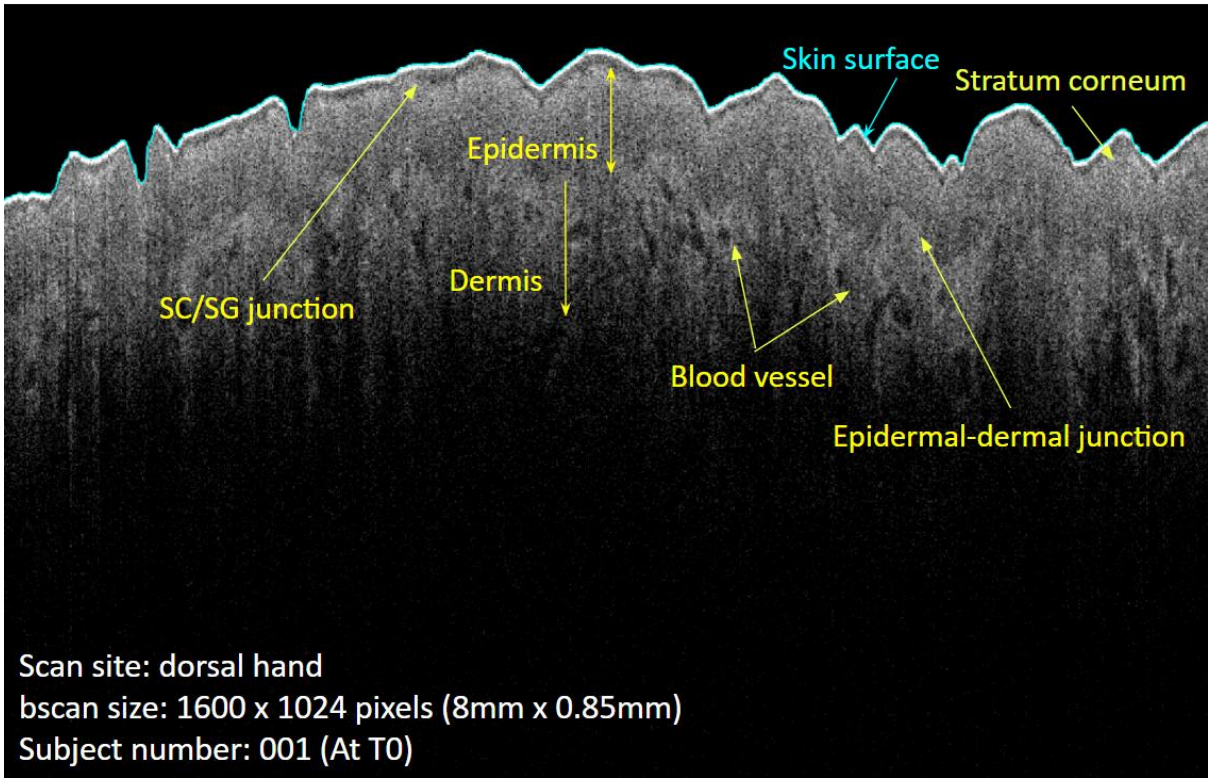

Figure 9. A typical B-scan of the subject's dorsal hand before hydration (T0) with skin surface (smoothed) detected. SC/SG: stratum corneum/stratum granulosum junction

To find the SC/SG junction, the smoothed A-scan (using the 5-pixel window) is searched for the position that maximise the ratio between the reflectance at the surface and the reflectance at that position, where the range being restricted to run from pixel 20 to pixel 30, this is based on the empirical knowledge of manual segmentations, for most subjects, the SC/SG junction is located between such a range. The SC/SG junction profile is plotted as the yellow curve in figure 10, using the same median filter that has been applied to smooth the skin surface, the smoothed SC/SG junction profile is plotted as the green curve, shown in figure 11. For each subject, 10 B-scans were obtained at each time interval (every 5 minutes), the hypoechogenic band representing the SC changes its brightness and evolves into a hyperechogenic band after hydration in water, shown in figure 12, and it returns to its hypoechogenic state after drying in lab. During the hydration and dehydration phase, the brightness/reflectance of the SC changes gradually and at certain time points there is thus not enough contrast to detect the SC/SG junction. For that reason, the SC thickness calculation was only done at 3 distinct times: before hydration, after hydration in water for 40 minutes and after drying in the lab for 40 minutes.

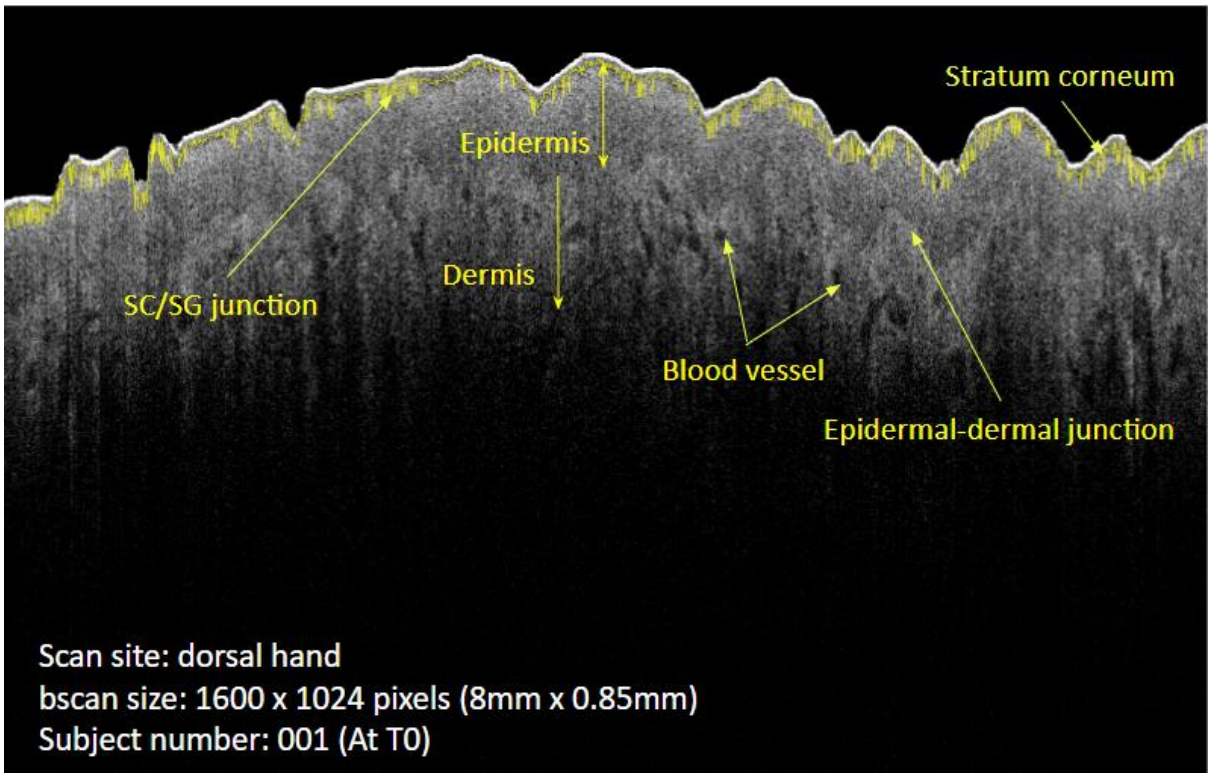

Figure 10. A typical B-scan of the subject's dorsal hand before hydration (T0) with SC/SG junction (pre smoothed) detected. SC/SG: stratum corneum/stratum granulosum junction

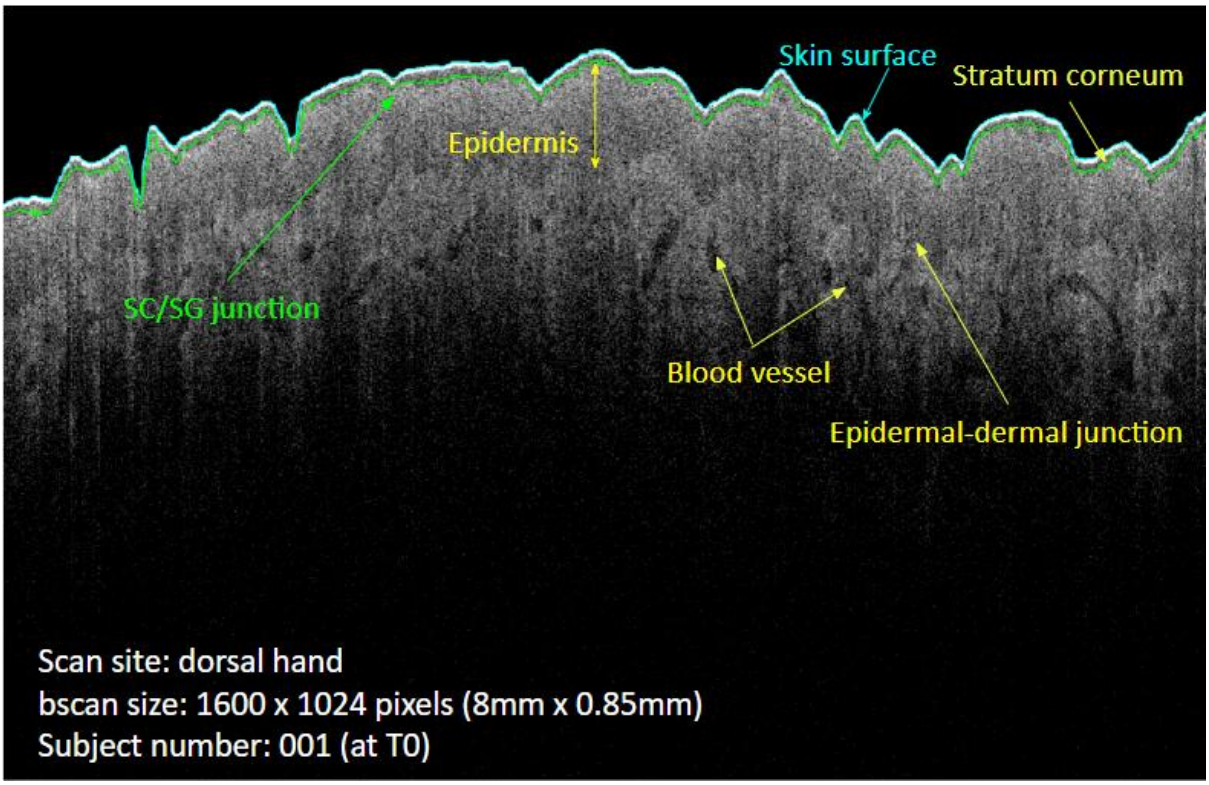

Figure 11. A typical B-scan of the subject's dorsal hand before hydration (T0) with skin surface (smoothed) and SC/SG junction (smoothed) detected. SC/SG: stratum corneum/stratum granulosum junction

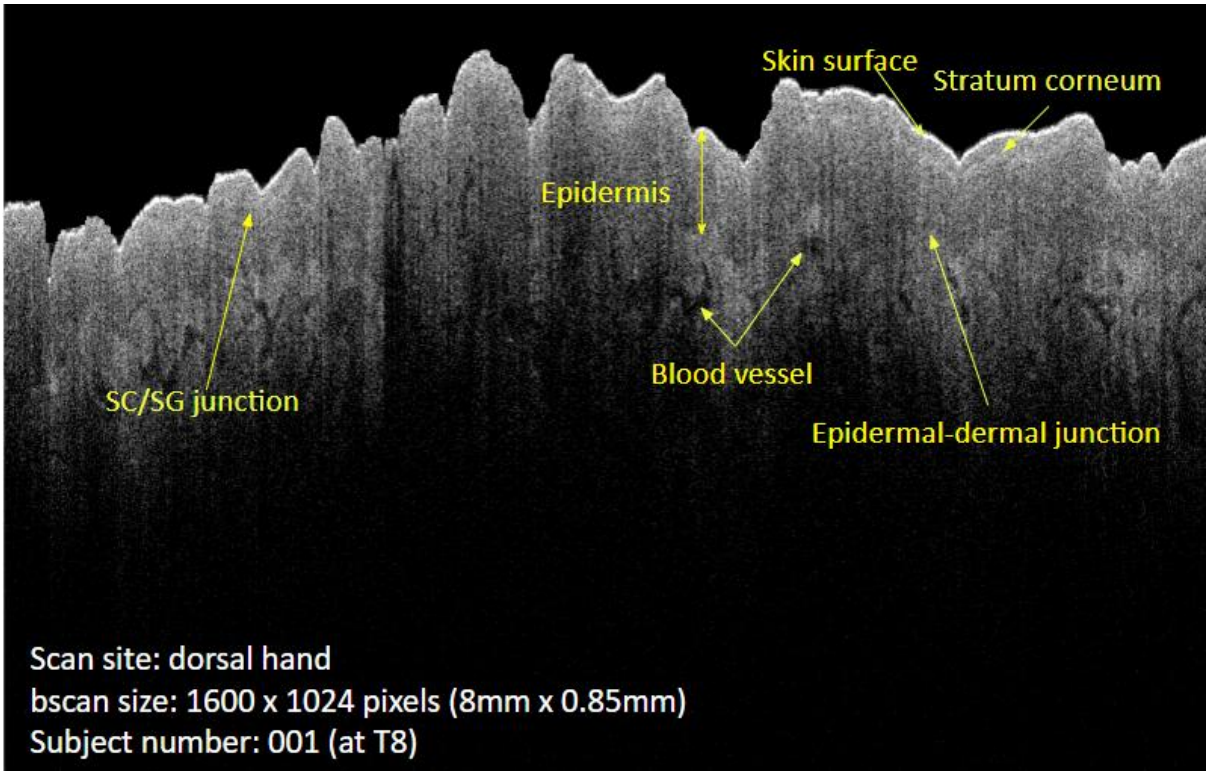

Figure 12. A typical B-scan of the subject's dorsal hand after hydration in water for 40 minutes (T8). SC/SG: stratum corneum/stratum granulosum junction

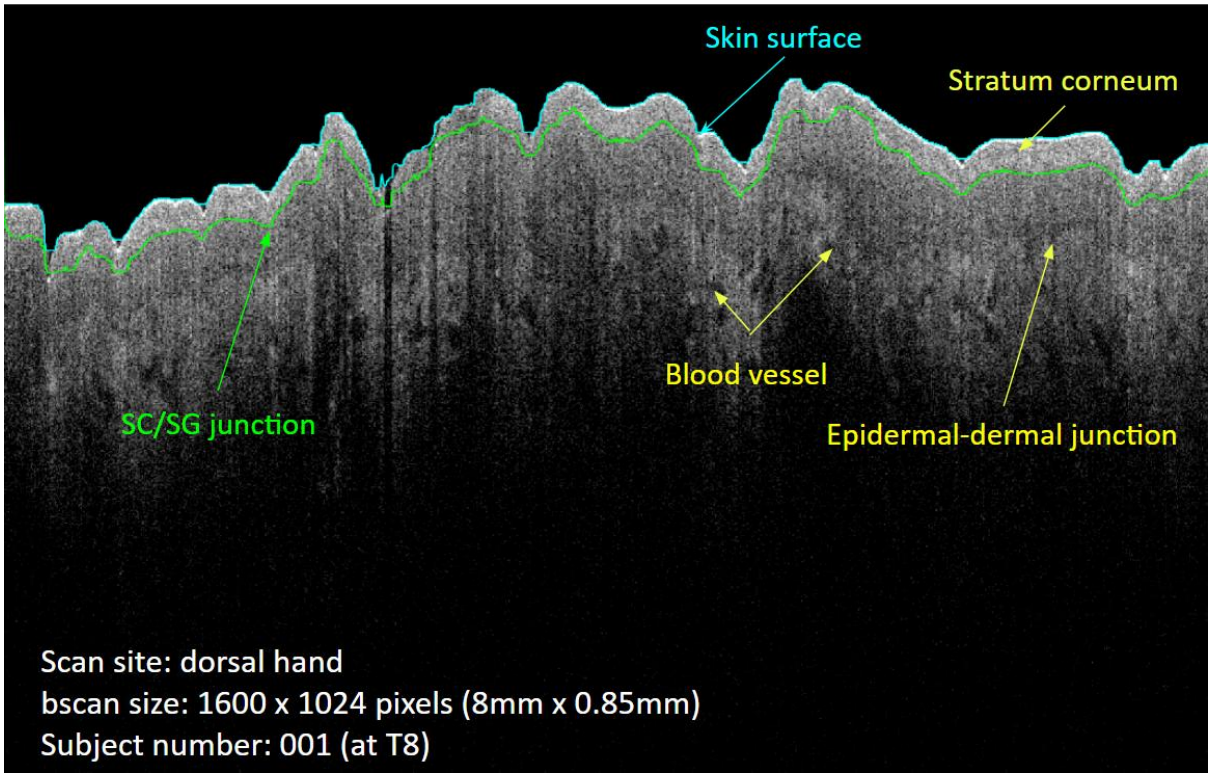

Figure 13. A typical B-scan of the subject's dorsal hand after hydration in water for 40 minutes (T8) with skin surface (smoothed) and SC/SG junction (smoothed) detected. SC/SG: stratum corneum/stratum granulosum junction

The SC/SG junction of the B-scans after hydration in water for 40 minutes was calculated using similar detection algorithm described earlier, however, it is now done by searching for the maximum ratio between the peak reflectance, in a 5-pixel window immediately below, but excluding the surface, and the reflectance in a searched range of 50-60 pixels below the skin surface, see figure 12 and 13 for a undetected and detected example. Figure 14 shows an atypical B-scan of a subject's dorsal hand taken by the VIS-OCT system before hydration. As shown in the graph, the skin surface of this B-scan is very clear to locate, hence the skin surface can be detected using the automated algorithm described earlier. However, the SC/SG junction of this B-scan is not relatively evenly distributed, in addition, the contrast of such an area is rather blurry at some locations, thus, the algorithm cannot make an accurate detection. In such cases, the SC/SG junction is detected manually. It is done by using an embedded APP in MATLAB and *ImageLabeler,* where the researcher manually clicks points on the B-scan where he/she thinks the location of the SC/SG junctions. The 'points' of the skin surface and junction position are defined by a coordinate (x,y) corresponding to the horizontal and vertical location in the B-scan, then, using MATLAB command *interp1,* a vector consists of 1600 points (corresponding to 1600 pixels in the horizontal direction) is created for skin surface and the junction, these vector are the defined location 'curve' shown in figure 15. As shown, the manual detection of the SC/SG junction is not perfect,

however, it is a relatively accurate approximation. Shown in figure 16, the same approach is used at the time point of after hydration in water for 40 minutes, the algorithm determines the location of the skin surface, manual detection is used to find the SC/SG junction.

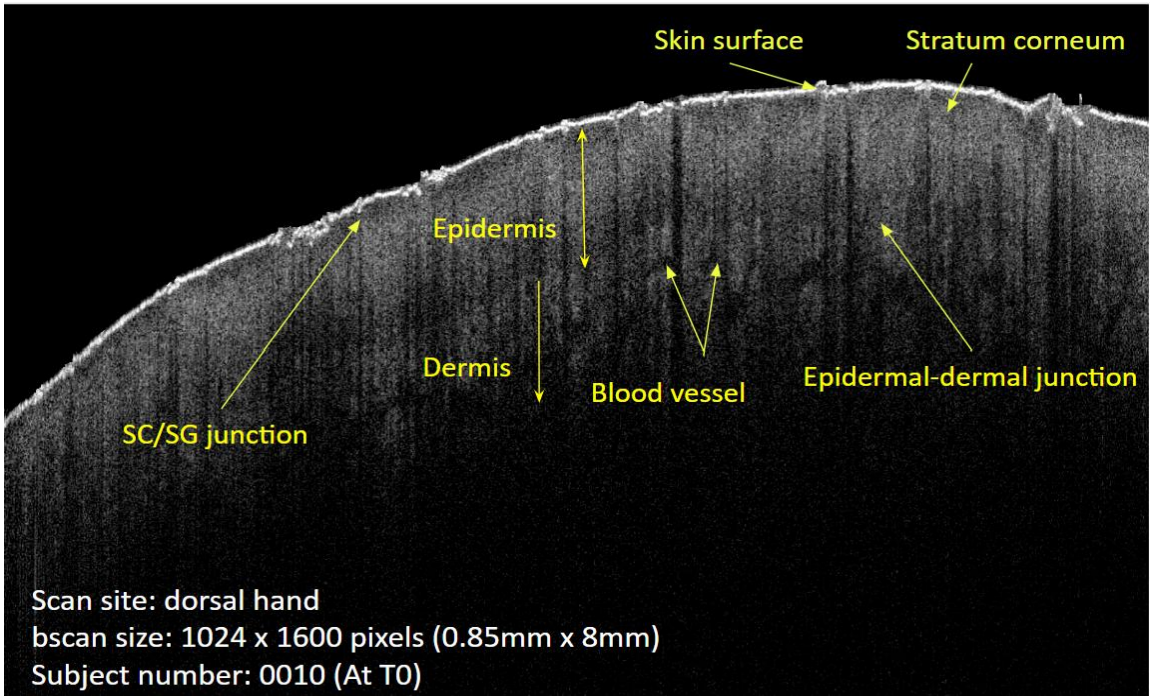

Figure 14. An atypical B-scan of the subject's dorsal hand before hydration (T0). SC/SG: stratum corneum/stratum granulosum junction

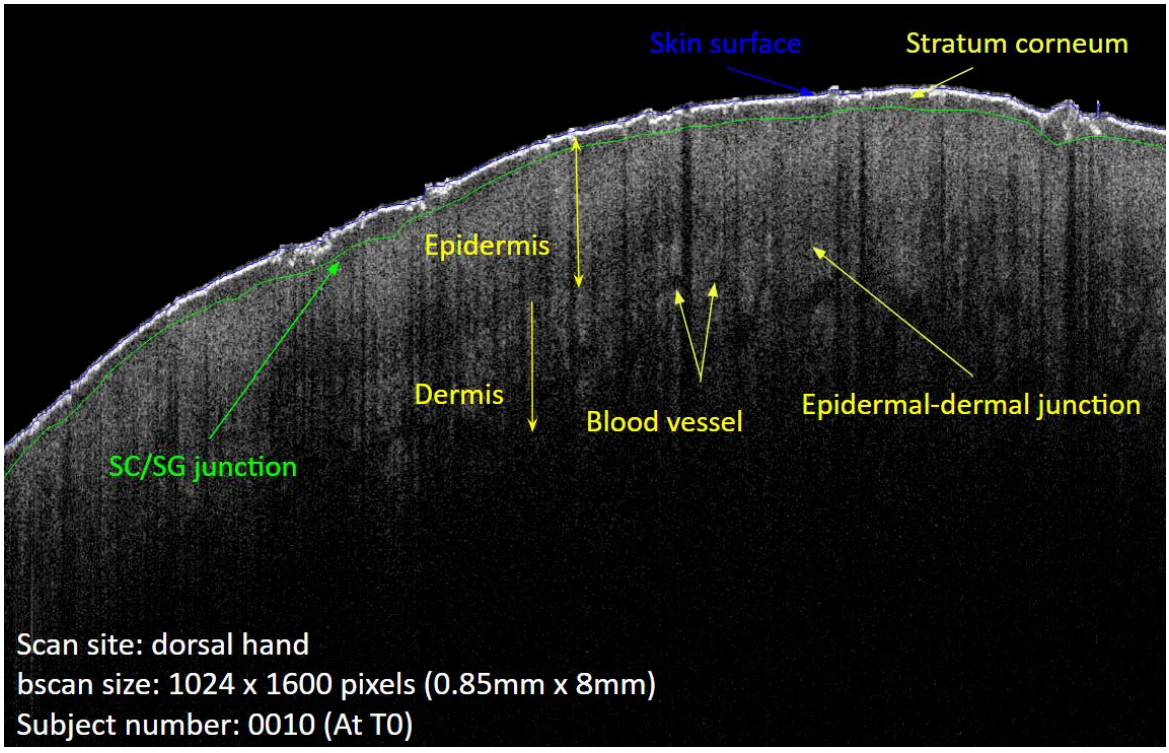

Figure 15. A typical B-scan of the subject's dorsal hand before hydration (T0) with skin surface (smoothed) and SC/SG junction manually detected. SC/SG: stratum corneum/stratum granulosum junction

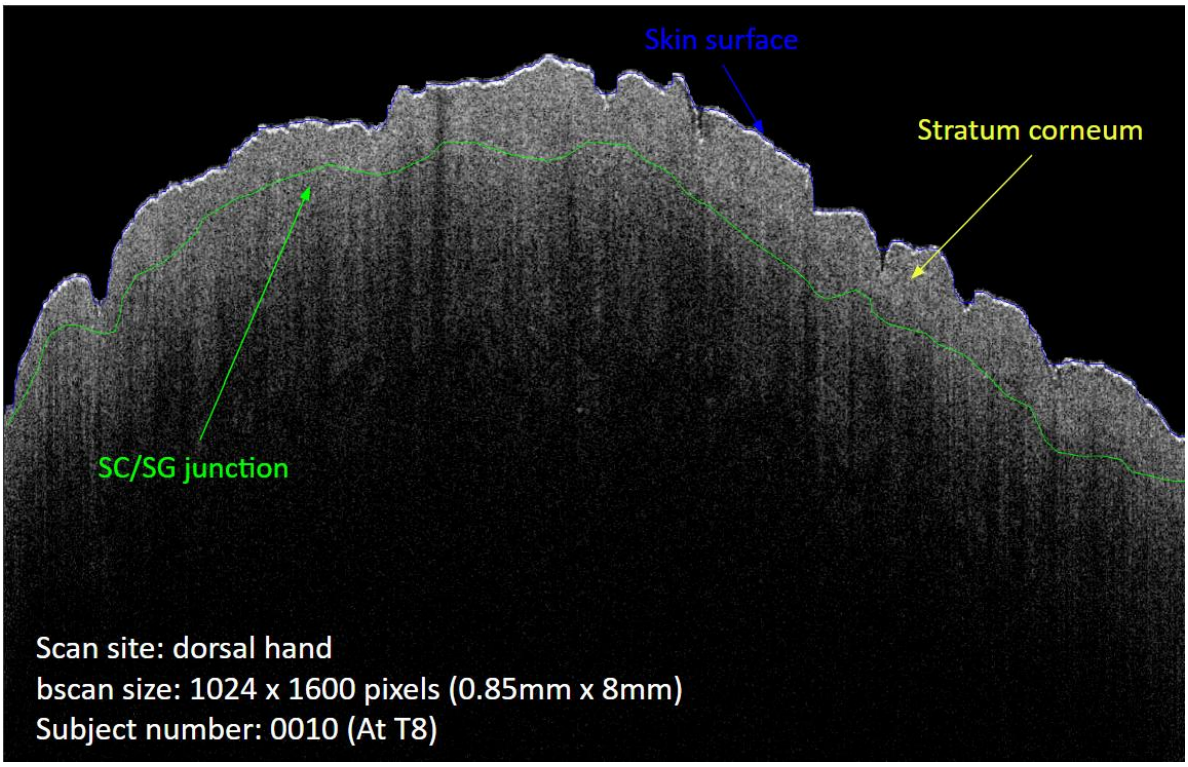

Figure 16. A typical B-scan of the subject's dorsal hand after hydration for 40 minutes (T8) with skin surface (smoothed) and SC/SG junction manually detected. SC/SG: stratum corneum/stratum granulosum junction

It is worth noting that for subjects with significantly thicker SC, after hydration in water for 40 minutes, in their B-scan, it is hard to find the location of epidermal/dermal junction and blood vessels. This could be due to that the epidermis, including the SC, is so thickened that the dermis is not detectable with the system penetration depth, hence other skin components are not resolvable.

4.32 SC thickness and reflectance calculation

The SC thickness and reflectance calculation are based on the detected skin surface and SC/SG junction. Each B-scan's size is 1024 x 1600 pixels, which corresponds to 1600 A-scans, the detected skin surface and SC/SG junction is a curve composed of 1600 points in the lateral direction of the B-scan. For manual detection, the points that are clicked/defined by the researcher, which compose the curve, are interpolated with a vector of 1600 points, to match the B-scan size. During the SC thickness calculation, two methods were performed to compare for a good representation of the SC thickness. The first one, namely curve point to curve point distance, is the vertical distance between each point on two curves (skin surface and SC/SG junction), see figure 17a). The second method is to search the minimum distance between the points, as shown in figure 17b), each point on the skin surface curve is

compared with all the points on the SC/SG junction curve, the minimum distance is selected for each point (each A-scan).

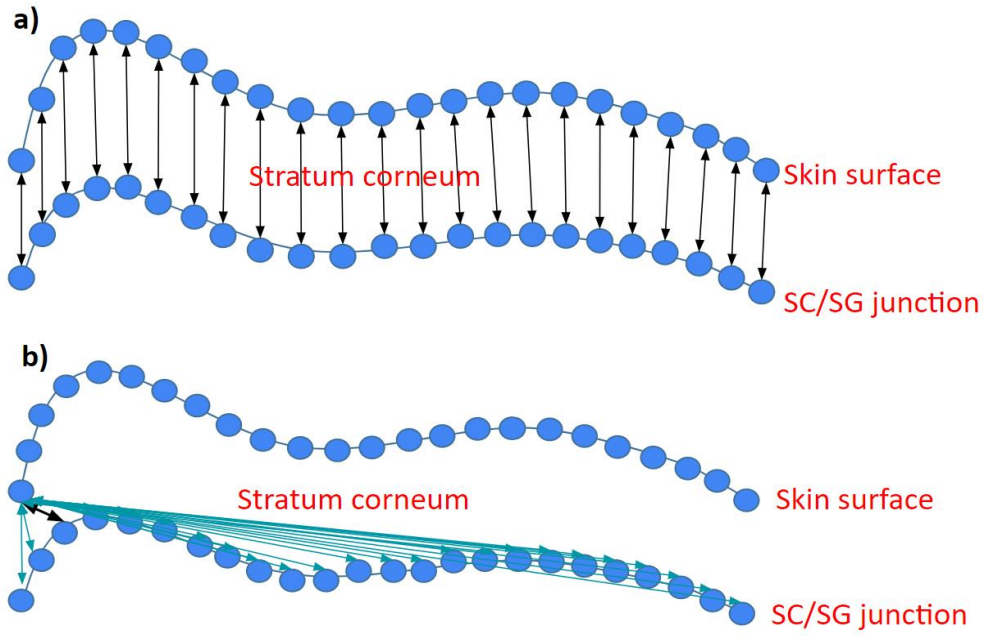

Figure 17. Schematic diagram of SC thickness calculation, a) namely curve point to curve point (Curve2Curve; b) minimum between curve points (Minimum).

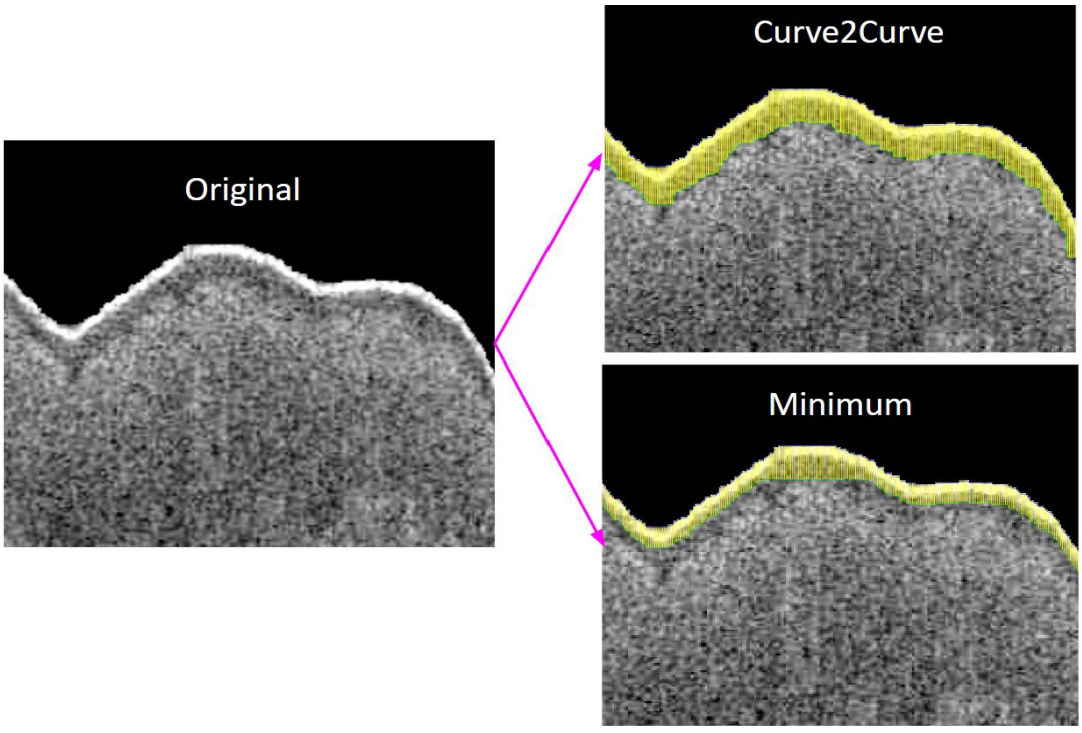

Figure 18. An example of SC thickness calculation from subject 001's B-scan at T0 (before hydration)

To determine the one which represents the SC thickness better, see figure 18 for an example of the results using two methods mentioned. As shown in figure 18, the yellow vertical lines represent the point-to-point distance calculated using curve point to curve point (Curve2Curve) and minimum between points methods. Based on the ‘coverage’ of the lines, using the Curve2Curve method, the lines cover the hypoechogenic area which we define as the SC better, the ‘coverage’ using the minimum distance method does not seem to cover all the SC. Thus, the SC thickness results are reported using the Curve2Curve method. Hence, the SC thickness is calculated as the vertical distance between the detected curve representing the skin surface and the SC/SG junction, multiplied by a factor of 0.85 (being pixel size in microns) and divided by the estimated refractive index of human SC, 1.5. The SC reflectance, obtained at each time interval for both hydration and dehydration phase, was defined as the reflectance averaged across the range of depth that define the SC at baseline. And the results were compared with the SC hydration measured with a Corneometer® CM 825 (Courage + Khazaka electronic GmbH).

In this chapter, how SC is being segmented in a visible-light OCT B-scan is listed, along with an explanation of the automatic segmentation for typical B-scans and manual segmentation for atypical B-scans. SC thickness and reflectance calculation are also described here, in later chapters, results of both parameters will be discussed, along with any factors that could have induced variations in the results are also stated.

References

[1]. D. G. Revin, R. A. Byers, M. Q. Duan, W. Li, and S. J. Matcher, “Visible-light optical coherence tomography platform for the characterization of the skin barrier,” Biomedical optics express, vol. 14, no. 8, pp. 3914–3923, 2023, doi: 10.1364/BOE.494356.
[2]. W. Drexler and J. G. Fujimoto, Optical Coherence Tomography: Technology and Applications (Springer International
Publishing, 2015).

5.0 Results

5.1 SC thickness

5.11 SC thickness at baseline, after hydrating in water for 40 minutes, and after drying in lab for 40 minutes

Previously mentioned, due to intermediate contrast of the SC/SG junction are indistinguishable from other layers in VIS-OCT B-scans during hydrating and dehydrating phase, SC thickness measurements were only obtained at 3 distinct times of: before hydration (T0), denote as baseline onwards, after hydrating in water for 40 minutes (T8) and after drying in lab for 40 minutes (T16). In this chapter, SC thickness results for 15 subjects are reported during seasons of spring/summer, autumn/winter and both seasons combined. Note here, there were 15 subjects who completed the experiment in either spring/summer or autumn/winter season, and there were 8 subjects who completed the experiments in both seasons. For subjects who completed the experiment in one out of two seasons, when calculating their SC thickness, their results are calculated from averaging across 16,000 A-scans (1,600 A-scans * 10 repeats); for subjects who completed the experiment in both seasons, their SC thickness are calculated from averaging across 32,000 A-scans (1,600 A-scans * 10 repeats * 2).

11 subjects completed the experiment in spring/summer seasons, and their SC thickness at 3 distinct times are plotted below. With an average SC thickness calculated from 16,000 A-scans per subject, it was found that for 11 subjects, their SC thickness [Mean & standard deviation (SD)] ranged from 6.1μm ± 0.1μm – 19.5μm ± 0.5μm with a population mean of 9.0μm ± 3. After hydrating in water for 40 minutes, their SC thickness increased to 20.7μm ± 0.2μm – 48.3μm ± 1.1μm, and the average thickness was found to be 24.7μm ± 8.3μm. After drying in the lab for 40 minutes, their SC thickness ranged between 5.5μm ± 0.1μm – 14.6μm ± 0.2μm, and the average thickness was found to be 7.3μm ± 2μm. As for 12 subjects who completed the experiment in autumn/winter season, their results are plotted below. Their baseline SC thickness [Mean & standard deviation (SD)] was calculated from averaging 16,000 A-scans per subject and is reported to be in a range of 5.7μm ± 0.2μm – 16.2μm ± 0.3μm, and the averaged SC thickness across population was calculated to be 8.9μm ± 3.0μm. After 40 minutes of hydrating in water, their SC thickness increased to 15.8μm ± 0.2μm – 26.7μm ± 0.9μm, and the population average SC thickness was found to be 19.5μm ± 3μm. After drying in the lab for 40 minutes, their SC thickness

decreased to 5.1μm ± 0.3μm – 15.3μm ± 0.6μm with a population mean of 8.2μm ± 3.0μm. For 15 subjects, their baseline SC thickness [Mean & standard deviation (SD)] calculated from averaging across 16,000 – 32,000 A-scans spans between 6.5μm ± 0.8μm – 16.4μm ± 3μm with an average of 9.0μm ± 3.1μm for population. After hydrating in water for 40 minutes, their SC thickness increased to a range of 16.1μm ± 0.4μm – 26.7μm ± 0.9μm with an average of 21.9μm ± 6.5μm for population. After drying in the lab for 40 minutes, their SC thickness decreased to a range of 3.5μm ± 0.1μm – 15.3μm ± 0.6μm with an average of 7.8μm ± 2.9μm.

The individual results for both seasons are listed in tables below, a figure with both seasons combined results is plotted below for each time interval. As shown in the figures, it is clear that subject 0010 and subject 0015's results are much larger than the rest of the groups, we consider them as 'outliers', therefore in later chapters where the possible factors which influence the results are being discussed, they are not included in the analysis.

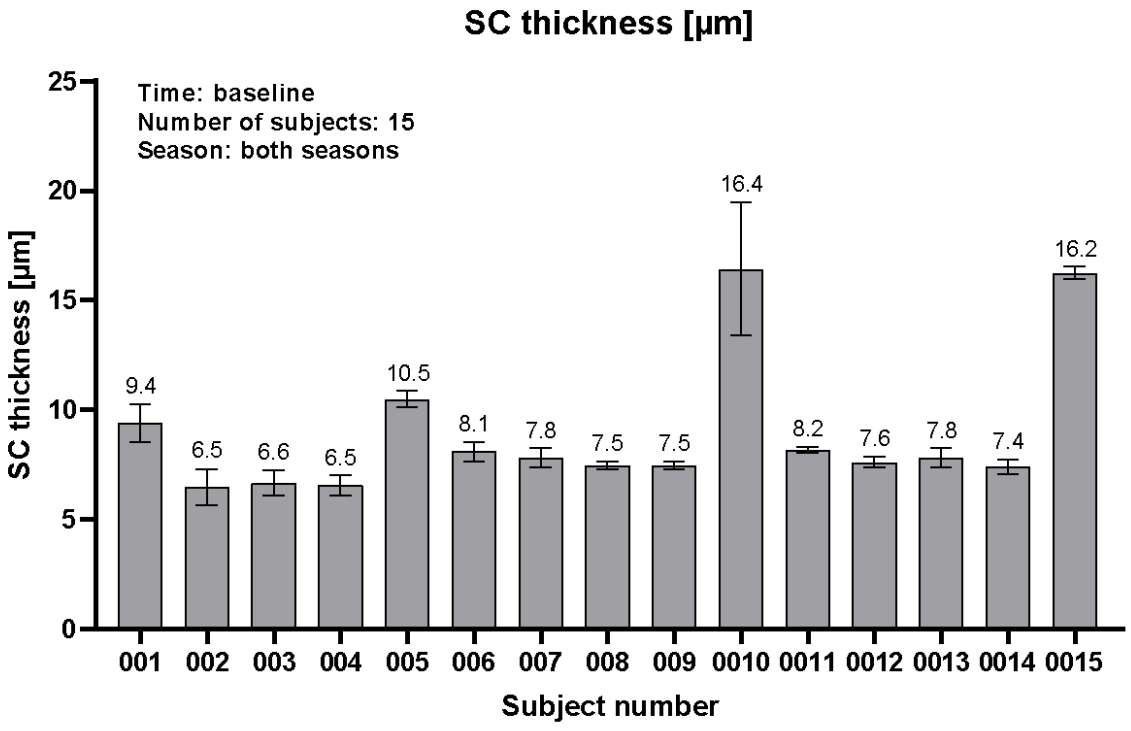

Figure 19. SC thickness (μm) [Mean & standard deviation (SD)] for 15 subjects average across 16,000 – 32,000 A-scans

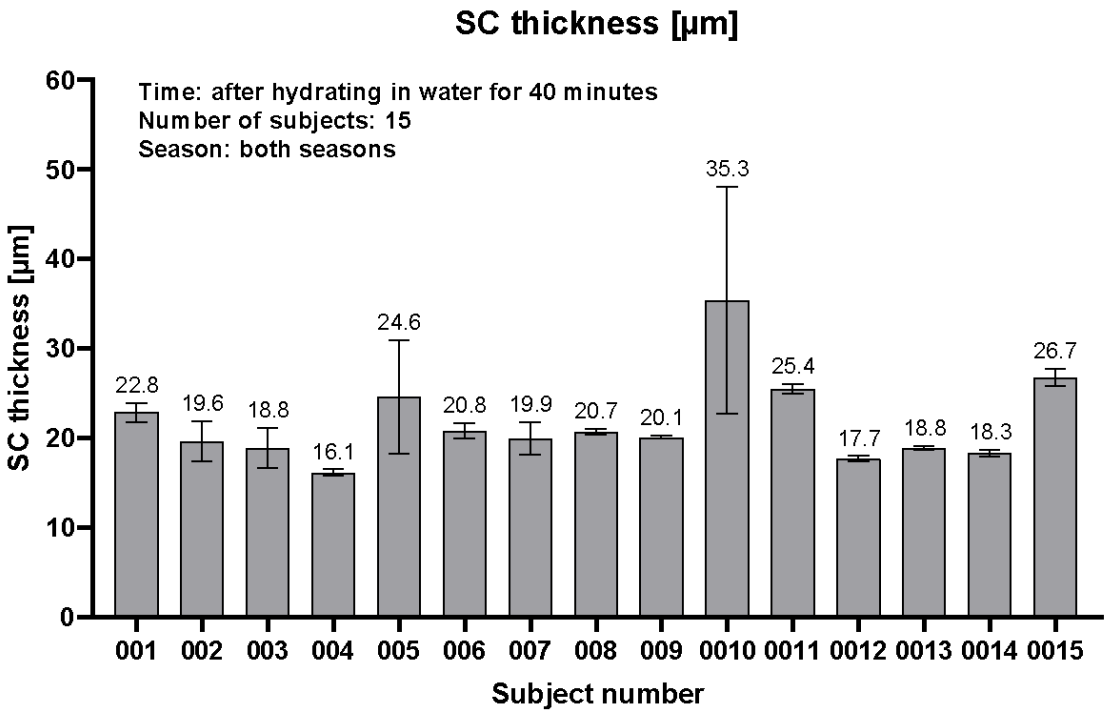

Figure 20. SC thickness (µm) [Mean & standard deviation (SD)] for 15 subjects average across 16,000 – 32,000 A-scans

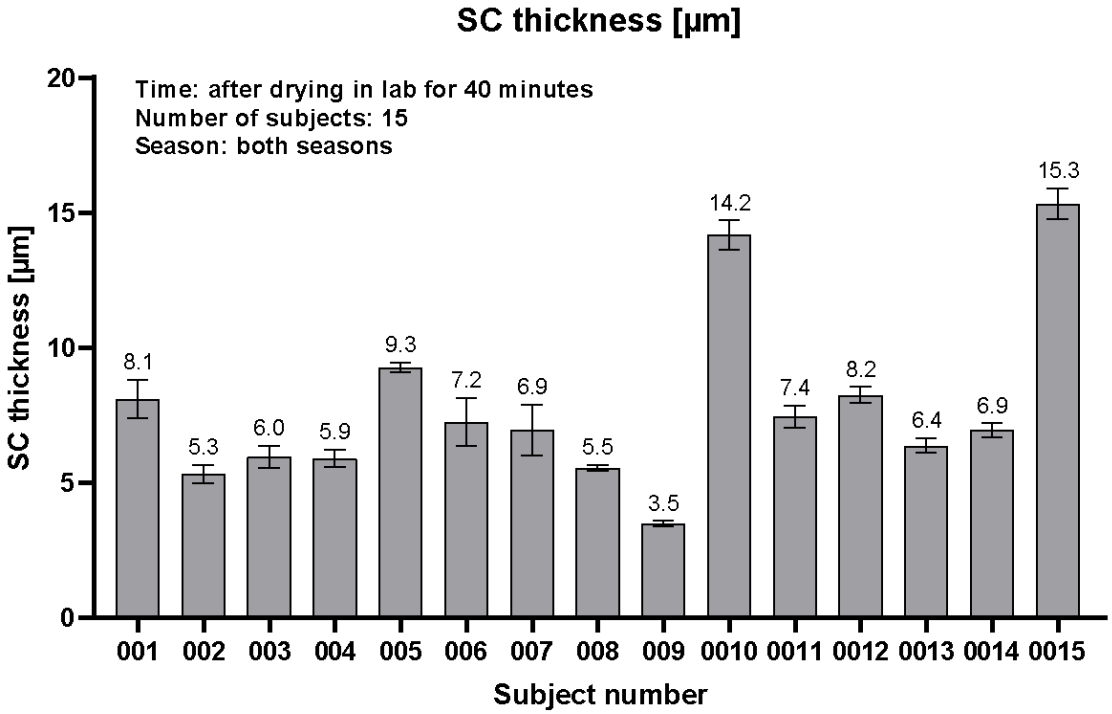

Figure 21. SC thickness (µm) [Mean & standard deviation (SD)] for 15 subjects average across 16,000 – 32,000 A-scans

SC thickness(μm) average across 16,000-32,000 A-scans for 15 subjects at baseline			
Subject number	Spring/summer	Autumn/winter	Both season combined
001	10.2μm ± 0.3μm	8.6μm ± 0.3μm	9.4μm ± 0.9μm
002	7.3μm ± 0.1μm	5.7μm ± 0.2μm	6.5μm ± 0.8μm
003	7.1μm ± 0.4μm	6.2μm ± 0.4μm	6.6μm ± 0.6μm
004	6.1μm ± 0.1μm	6.9μm ± 0.2μm	6.5μm ± 0.4μm
005	10.8μm ± 0.2μm	10.2μm ± 0.2μm	10.5μm ± 0.4μm
006	7.8μm ± 0.4μm	8.3μm ± 0.4μm	8.1μm ± 0.4μm
007	7.4μm ± 0.4μm	8.1μm ± 0.2μm	7.8μm ± 0.4μm
008	7.5μm ± 0.2μm		7.5μm ± 0.2μm
009	7.5μm ± 0.2μm		7.5μm ± 0.2μm
0010	19.5μm ± 0.5μm	13.6μm ± 0.3μm	16.4μm ± 3μm
0011	8.2μm ± 0.1μm		8.2μm ± 0.1μm
0012		7.6μm ± 0.2μm	7.6μm ± 0.2μm
0013		7.8μm ± 0.4μm	7.8μm ± 0.4μm
0014		7.4μm ± 0.3μm	7.4μm ± 0.3μm
0015		16.2μm ± 0.3μm	16.2μm ± 0.3μm

Table 1. Baseline SC thickness (μm) [Mean & standard deviation (SD)] for 15 subjects

SC thickness(μm) average across 16,000-32,000 A-scans for 15 subjects after hydrating in water for 40 minutes			
Subject number	Spring/summer	Autumn/winter	Both season combined
001	23.8μm ± 0.3μm	21.9μm ± 0.6μm	22.8μm ± 1.1μm
002	21.9μm ± 0.4μm	17.5μm ± 0.4μm	19.6μm ± 2.3μm
003	21.1μm ± 0.3μm	16.8μm ± 0.3μm	18.8μm ± 2.3μm
004	16.4μm ± 0.3μm	15.8μm ± 0.2μm	16.1μm ± 0.4μm
005	31.1μm ± 0.5μm	18.7μm ± 0.5μm	24.6μm ± 6.4μm
006	21.5μm ± 0.6μm	20.1μm ± 0.5μm	20.8μm ± 0.9μm
007	21.7μm ± 0.3μm	18.2μm ± 0.5μm	19.9μm ± 1.8μm
008	20.7μm ± 0.3μm		20.7μm ± 0.3μm

009	20.1μm ± 0.2μm		20.1μm ± 0.2μm
0010	40.3μm ± 1.1μm	23.7μm ± 1.1μm	35.3μm ± 1.2μm
0011	25.5μm ± 0.5μm		25.5μm ± 0.5μm
0012		17.6μm ± 0.3μm	17.6μm ± 0.3μm
0013		18.8μm ± 0.3μm	18.8μm ± 0.3μm
0014		18.3μm ± 0.4μm	18.3μm ± 0.4μm
0015		26.7μm ± 0.9μm	26.7μm ± 0.9μm

Table 2. SC thickness (μm) [Mean & standard deviation (SD)] for 15 subjects after hydrating in water for 40 minutes

SC thickness(μm) average across 16,000-32,000 A-scans for 15 subjects after drying in lab for 40 minutes			
Subject number	Spring/summer	Autumn/winter	Both season combined
001	8.8μm ± 0.3μm	7.5μm ± 0.2μm	8.1μm ± 0.7μm
002	5.5μm ± 0.1μm	5.1μm ± 0.3μm	5.3μm ± 0.3μm
003	5.6μm ± 0.2μm	6.3μm ± 0.1μm	5.9μm ± 0.4μm
004	5.7μm ± 0.2μm	6.1μm ± 0.3μm	9.3μm ± 0.2μm
005	9.3μm ± 0.2μm	9.3μm ± 0.1μm	9.3μm ± 0.2μm
006	8.1μm ± 0.2μm	6.4μm ± 0.2μm	7.2μm ± 0.9μm
007	6.0μm ± 0.5μm	7.7μm ± 0.3μm	6.9μm ± 0.9μm
008	5.5μm ± 0.1μm		5.5μm ± 0.1μm
009	3.5μm ± 0.1μm		3.5μm ± 0.1μm
0010	14.6μm ± 0.2μm	13.7μm ± 0.4μm	14.2μm ± 0.5μm
0011	7.4μm ± 0.4μm		7.4μm ± 0.4μm
0012		8.2μm ± 0.3μm	8.2μm ± 0.3μm
0013		6.4μm ± 0.3μm	6.4μm ± 0.3μm
0014		6.9μm ± 0.2μm	6.9μm ± 0.2μm
0015		15.3μm ± 0.6μm	15.3μm ± 0.6μm

Table 3. SC thickness (μm) [Mean & standard deviation (SD)] for 15 subjects after hydrating in water for 40 minutes

The group results are plotted below, where, to recollect, for 11 subjects, their SC thickness [Mean & standard deviation (SD)] at spring/summer season was found to be 9.0μm ± 3.6μm at baseline, after

hydrating in water for 40 minutes, it increased to 24.7µm ± 8.3µm, after drying in lab for 40 minutes, it decreased to 7.3µm ± 2.9µm. For 12 subjects, their SC thickness at autumn/winter season was found to be 8.9µm ± 3.0µm at baseline, after hydrating in water for 40 minutes, it increased to 19.5µm ± 3µm, after drying in lab for 40 minutes, it decreased to 8.2µm ± 3.0µm. For 15 subjects, their SC thickness with both seasons combined was found to be 9.0µm ± 3.1µm at baseline, after hydrating in water for 40 minutes, it increased to 21.9µm ± 6.5µm, after drying in lab for 40 minutes, it decreased to 7.8µm ± 2.9µm.

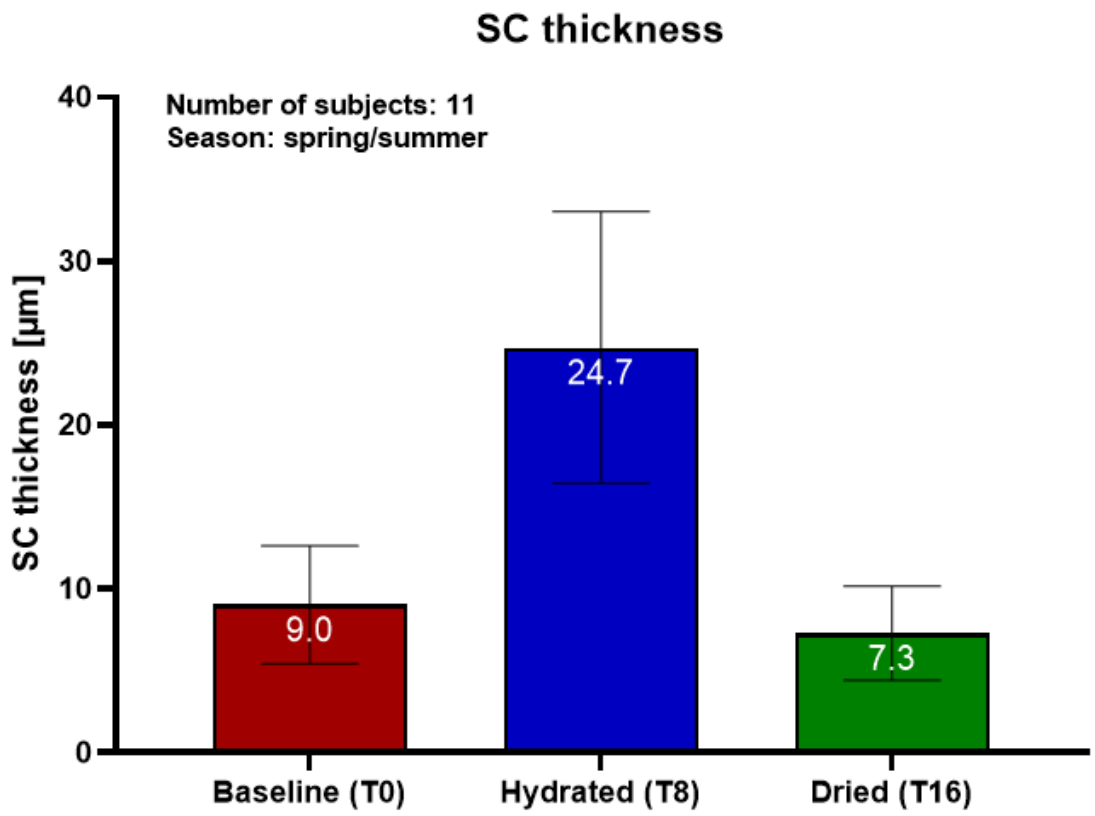

Figure 22. SC thickness (µm) [Mean & standard deviation (SD)] for 11 subjects average across 16,000 A-scans

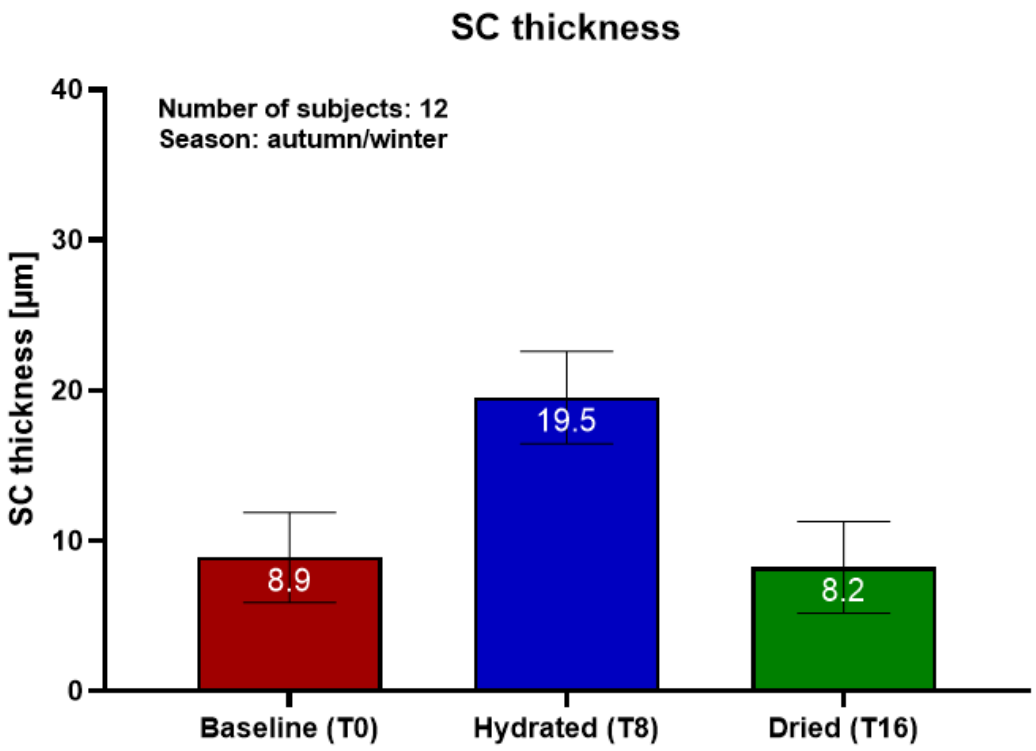

Figure 23. SC thickness (µm) [Mean & standard deviation (SD)] for 12 subjects average across 16,000 A-scans

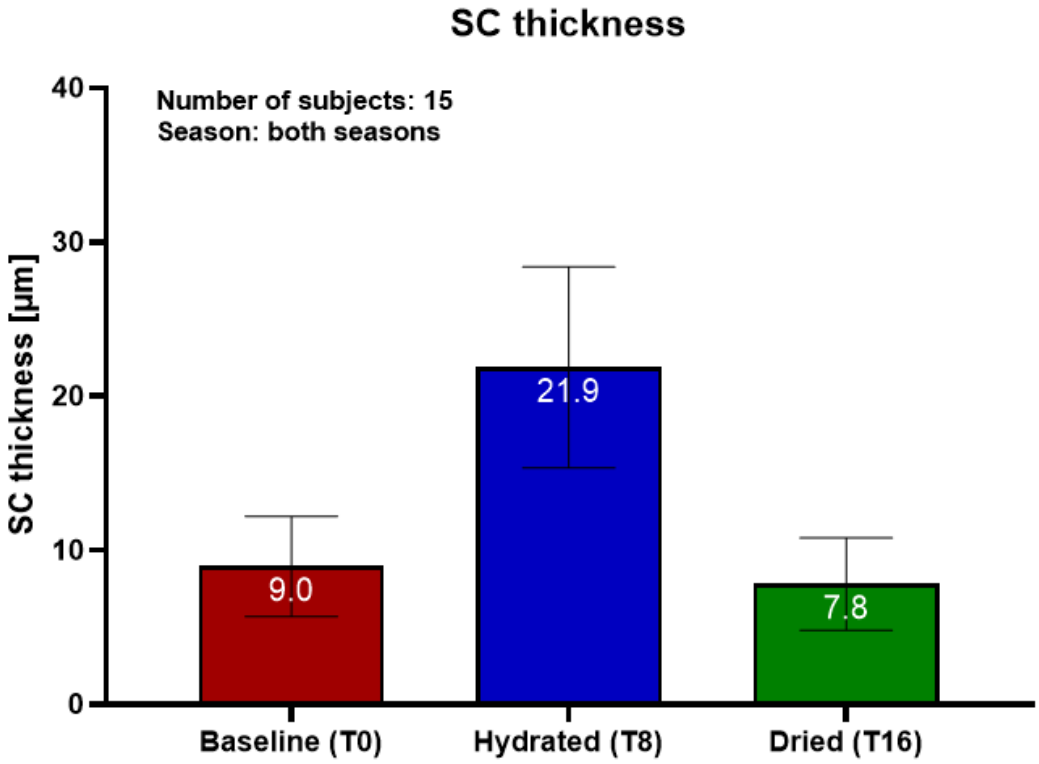

Figure 24. SC thickness (µm) [Mean & standard deviation (SD)] for 15 subjects average across 16,000 – 32,000 A-scans

5.12 SC thickness – Variability of results (individual, hydration state, season, age, gender)

To test the hypothesis that one's SC thickness is significantly different from another, a One-Way ANOVA test was used. For 11 subjects who completed their experiment in spring/summer season, their baseline SC thickness, after hydrating in water for 40 minutes, and after drying in lab for 40 minutes, all showed significant differences with each other with p values of $p < 0.0001$; $p < 0.0001$; and $p < 0.0001$ respectively (p value in statistics, is a probability value that describes how likely that the observed results happened by chance, and it was proposed by Ronald Fisher [1]. In general, $p < 0.05$ or lower is generally conferred statistically significant; $p = 0.05$ * means the observed result has a 5 % chance of being wrong, or happened by chance; $p = 0.01$ ** means the observed result has a 1 % chance of happening by chance; $p = 0.001$ means the observed result has a 0.01% chance of happening by chance; $p = 0.0001$ means the observed result has a 0.001% chance of happening by chance. And this applies to all of the statistical significance that appears in the results chapter). Similarly, the same test was used on 12 subjects who completed the experiment in autumn/winter season. Again, by performing One-Way ANOVA test, it was found that all of 12 subjects' SC thickness at baseline, after hydrating in water for 40 minutes and after drying in lab for 40 minutes, are significantly different from each other with p values of $p < 0.0001$; $p < 0.0001$; and $p < 0.0001$ respectively. When combing the SC thickness results for all 15 subjects, One-Way ANOVA test again showed significant differences in subjects' SC thickness at baseline, after hydrating in water for 40 minutes, and after drying in lab for 40 minutes with p values of $p < 0.0001$; $p < 0.0001$; and $p < 0.0001$.

To test the hypothesis that SC thickness at baseline is significantly different from after hydrating in water for 40 minutes and after drying in the lab for 40 minutes, student paired T-test was used, noted here, a normality test (D'Agostino-Pearson) was prior used to test whether the data points used come from a normal (Gaussian) distribution. For 11 subjects who completed the experiment in spring/summer season, 10 b-scans were gathered per subject, hence at each time interval, 110 B-scans were used in the normality test, results showed that B-scans gathered from 11 subjects for each time interval did not pass the normality test. Hence, when using paired T-test, normal distribution of the data points is not assumed. Nonparametric paired T-test shows that SC thickness at baseline, after hydrating in water for

40 minutes, and after drying in lab for 40 minutes are all significantly different from each other with p values of $p < 0.0001$; $p < 0.0001$; and $p < 0.0001$ respectively. Similarity, for 12 subjects who completed the experiment in autumn/winter season, 10 b-scans were gathered per subjects, hence at each time interval, 120 B-scans were used in the normality test, results showed that data points (B-scans) gathered from 12 subjects for each time interval did not pass the normality test. Hence, when using paired T-test, normal distribution of the data points is not assumed. Nonparametric paired T-test shows that SC thickness at baseline, after hydrating in water for 40 minutes, and after drying in lab for 40 minutes are all significantly different from each other with p values of $p < 0.0001$; $p < 0.0001$; and $p < 0.0001$ respectively. When 15 subjects are combined, 7 subjects have 10 B-scans from one of the seasons and 8 subjects have 20 B-scans from both seasons, and in total 15 subjects count up to 230 B-scans (7 subjects x 10 B-scans + 8 subjects x 10 B-scans x 2) per time interval, normality test was again used to see whether these data points are drawn from a normal distribution, and results showed that none of the time intervals' data points are drawn from a normal distribution. Hence, when using paired T-test, normal distribution of the data points is not assumed. Nonparametric paired T-test showed that SC thickness at baseline, after hydrating in water for 40 minutes, and after drying in lab for 40 minutes are all significantly different from each other with p values of $p < 0.0001$; $p < 0.0001$; and $p < 0.0001$, respectively.

As reported in previous chapters, inter-variations of the results among subjects were confirmed using ANOVA test. Variations of the results depending on hydrational state were also listed using T-test. In this chapter, other factors such as season, age and gender which could potentially induce variation in the results are discussed. To investigate the role of seasonal effect on the variability of results, 8 subjects who completed the experiment in both seasons, their SC thickness at baseline, after hydrating in water for 40 minutes, and after drying in lab for 40 minutes stated in the table 4. Like how it was reported in previous chapters, for 8 subjects, their baseline SC thickness [Mean & standard deviation (SD)] in spring/summer season span between a range of 6.1μm ± 0.1μm – 19.5μm ± 0.5μm with a population average of 9.5μm ± 0.1μm; after hydrating in water for 40 minutes, their SC thickness increased to 16.4μm ± 0.3μm – 48.3μm ± 1.1μm with a population average of 25.7μm ± 9.4μm; after drying in lab for 40 minutes, their SC thickness decreased to 5.5μm ± 0.1μm with a population average of 7.9μm ± 2.9μm. During autumn/winter season, the SC thickness [Mean & standard deviation (SD)]

for these 8 subjects at baseline, after hydrating in water for 40 minutes and after drying in the lab for 40 minutes are also stated in the table below. The baseline thickness for these 8 subjects in autumn/winter season spans between a range of 5.7μm ± 0.2μm – 13.6μm ± 0.7μm with a population average of 8.5μm ± 2.4μm; after hydrating in water for 40 minutes, their SC thickness increased to 15.8μm ± 0.2μm – 23.7μm ± 1.1μm with a population average of 19.1μm ± 2.6μm; after drying in lab for 40 minutes, their SC thickness decreased back to a range of 5.1μm ± 0.3μm – 13.8μm ± 0.4μm with a population average of 7.8μm ± 2.6μm. To test the hypothesis of SC thickness at spring/summer season is significantly different from at autumn/winter season, 7 subjects's result (excluding an outlier subject 0010) at each time interval were tested using standard paired non-parametric (assume no Gaussian distribution) T-test, the results at baseline, after hydrating in water for 40 minutes and after drying in lab for 40 minutes are plotted below. See figure below, nonparametric paired T-test shows that SC thickness quantified at baseline (T0) and after drying in the lab (T16) showed no significant difference, a significant difference ($p = 0.0156$ *) is detected after hydrating in water for 40 minutes (T8).

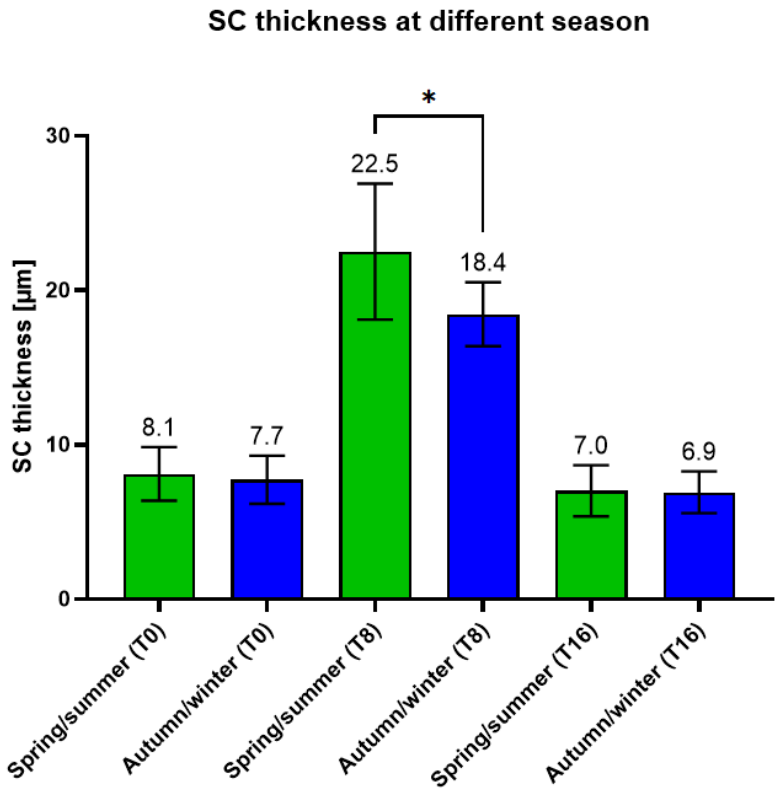

Figure 25. Paired T-test for SC thickness (μm) [Mean & standard deviation (SD)] during different season with outliers excluded

SC thickness(μm) average across 16,000- A-scans for 8 subjects at different season		
Season	Spring/summer	Autumn/winter
Before hydration	9.5μm ± 4.0μm	8.5μm ± 2.5μm
After hydrating in water for 40 minutes	25.7μm ± 9.9μm	19.1μm ± 2.7μm
After drying in lab for 40 minutes	7.9μm ± 3.1μm	7.8μm ± 2.7μm

Table 4. SC thickness (μm) [Mean & standard deviation (SD)] for 8 subjects at different season (including outliers)

To determine whether age factor played a role in the variability of the results, 15 subjects were sub-categorized into three age groups of 20-29 (6 subjects); 30-39 (5 subjects); and 40-60 (4 subjects). For the age group of 20-29, 6 subjects have 90 B-scans as 3 subjects completed the experiment in both seasons and 3 completed in one season; for the age group of 30-39, 5 subjects have in total 70 B-scans as 2 subjects completed the experiment in both season and 3 subjects completed the experiment in one season; for the age group of 40-60, 4 subjects have in total 70 B-scans as 3 subjects completed the experiment in both seasons and 1 subject completed the experiment in one season. Their SC thickness (with outliers) averaging from 16,000 – 32,000 A-scans are reported in table 5. As shown in figure 26, nonparametric unpaired T-test showed that (excluding the outliers in age group of 40-60, subject 0010 and subject 0015), all age groups' SC thickness are significant different from each other with significant p values $p < 0.0001$ **** (p value is a statistical measurement used to validate whether the observed results happened by chance. i.e., $p < 0.05$ or lower is generally conferred statistically significant; $p = 0.05$* means the observed result has a 5 % chance of being wrong, or happened by chance; $p = 0.01$** means the observed result has a 1 % chance of happening by chance; $p = 0.001$*** means the observed result has a 0.01% chance of happening by chance; $p = 0.0001$ means the observed result has a 0.001%**** chance of happening by chance).

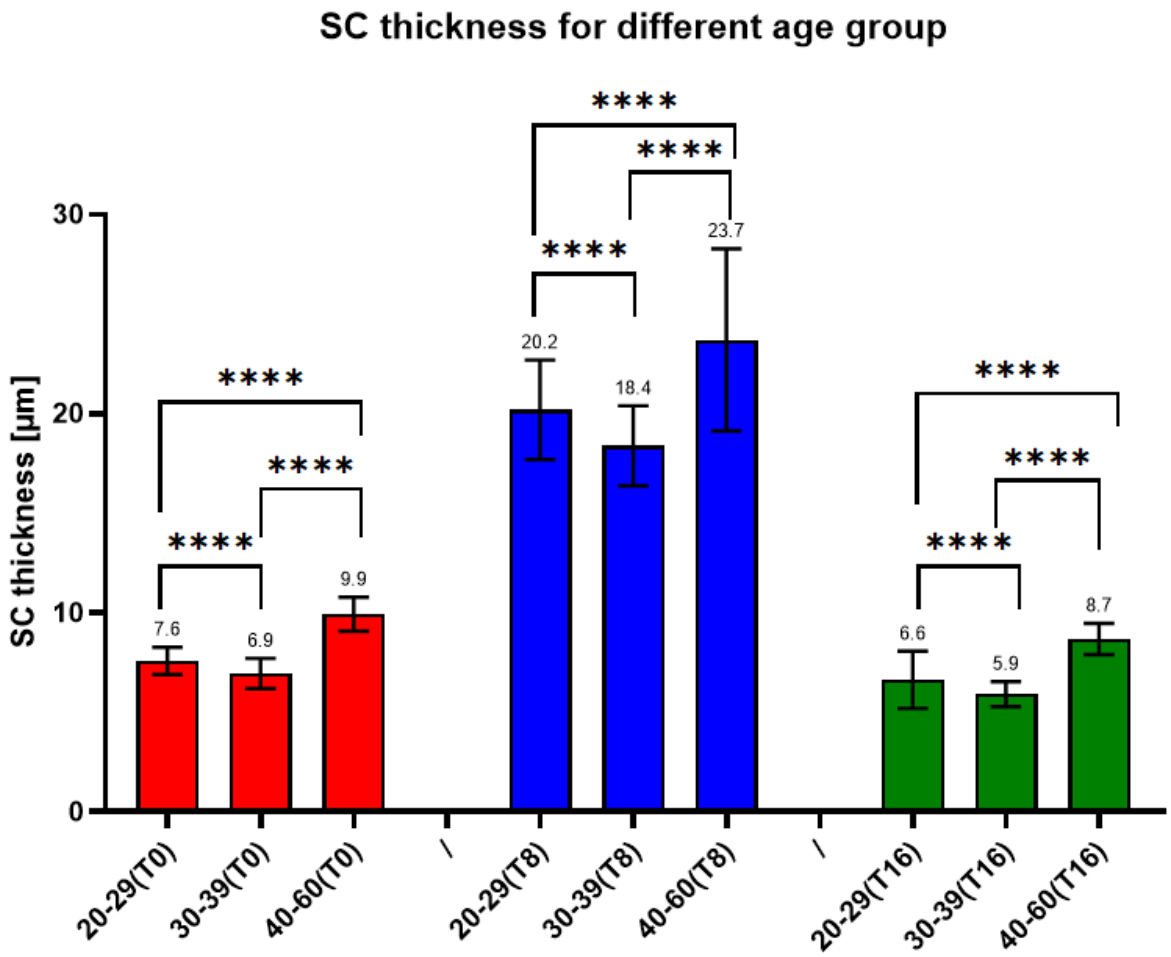

Figure 26. Unpaired T-test for SC thickness (µm) [Mean & standard deviation (SD)] for different age group with outliers excluded

SC thickness(µm) average across 16,000-32,000 A-scans for 15 subjects at various age groups and hydration states			
Hydration state/Age group	20-29 (yrs)	30-39(yrs)	40-60 (yrs)
Before hydration	7.6µm ± 0.6µm	7.1µm ± 0.6µm	13.1µm ± 3.7µm
After hydrating in water for 40 minutes	20.4µm ± 2.7µm	18.7µm ± 1.7µm	27.4µm ± 5.5µm
After drying in lab for 40 minutes	6.5µm ± 1.7µm	6.0µm ± 0.7µm	11.7µm ± 3.6µm

Table 5. SC thickness (µm) [Mean & standard deviation (SD)] for 15 subjects at various hydration states and age group (including outliers)

To determine whether gender played a role in the variability of the results, 15 subjects were sub-categorized into two groups of 10 males and 5 females. For male subject group, 160 B-scans were gathered as 6 subjects completed the experiment in both seasons and 4 subjects completed the experiment in one season; for the female subject group, 70 B-scans were gathered in total as 2 subjects

completed the experiment in both seasons and 3 subjects completed the experiment in one season. Their SC thickness (with outliers) averaging from 16,000 – 32,000 A-scans is reported in table 6. As shown in figure 27, nonparametric unpaired T-test showed that (excluding the outliers in male group subject 0010 and subject 0015), all gender groups' SC thickness are significant different from each other with at baseline and after drying in lab with significant p values of $p < 0.0001$**** and $p = 0.0006$***. No significant difference was detected at T8, i.e., after hydrating in water for 40 minutes.

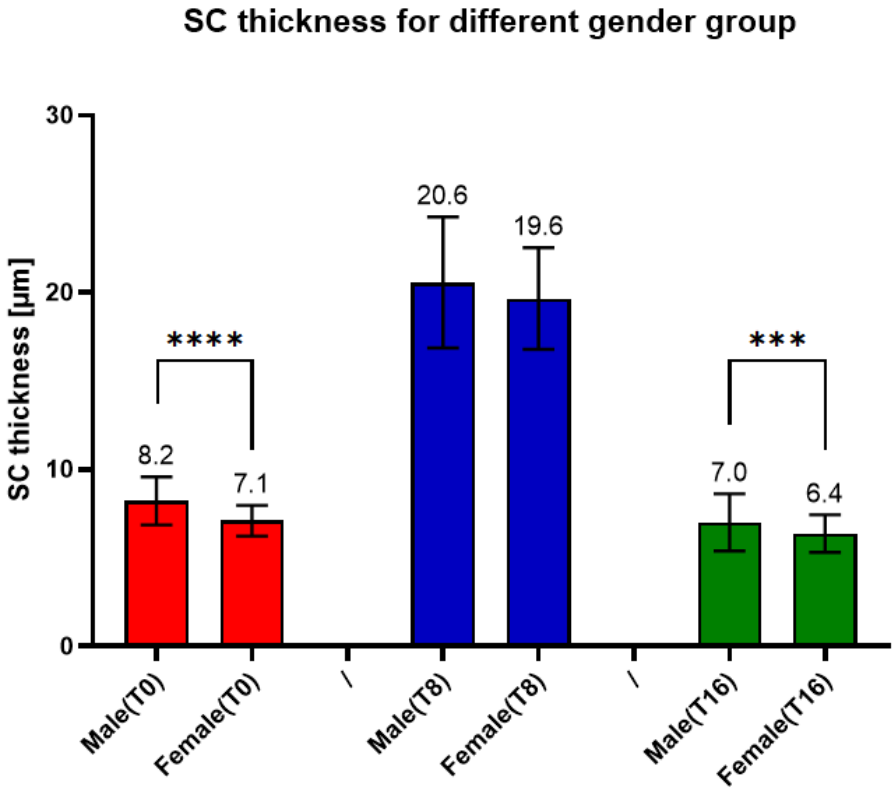

Figure 27. Unpaired T-test for SC thickness (µm) [Mean & standard deviation (SD)] for different gender group with outliers excluded

SC thickness(µm) average across 16,000-32,000 A-scans for 15 subjects in different gender groups		
Hydration state/Gender group	Male	Female
Before hydration	9.7µm ± 3.7µm	7.3µm ± 0.7µm
After hydrating in water for 40 minutes	22.5µm ± 5.4µm	20.1µm ± 3.1µm
After drying in lab for 40 minutes	8.3µm ± 3.7µm	6.7µm ± 0.5µm

Table 6. SC thickness (µm) [Mean & standard deviation (SD)] for 15 subjects at various hydration states and gender group (including outliers)

5.2 SC reflectance

5.21 SC reflectance at baseline, after hydrating in water for 40 minutes, and after drying in lab for 40 minutes

The second parameter that was quantified was the SC reflectance, which is defined as the average reflectance (average 'brightness') across the range of depth that defines the SC at baseline. As water enters the SC, scattering of the incident light signal increases as there is a greater density of the water molecule, thus resulting in a higher value in the back-scattered signal, reflected as a higher 'brightness' or higher reflectance. The reflectance value was calculated by averaging the pixel value excluding the surface pixels (skin surface signal is defined as the brightest 'entry signal', note here the melanocytes, i.e., the pigment substance present in the skin could reduce the skin surface signal due to absorption of light, however, subjects in the current subject pool mostly has 'bright' skin tone, hence the variation in skin surface signal intensity that could be influenced by this factor is neglected here), and it was obtained at each time interval during the hydration and dehydration phase.

To start, following the same reporting method as SC thickness, the value of SC reflectance for each subject at baseline, after hydrating in water for 40 minutes, and after drying in the lab for 40 minutes is reported. For 11 subjects who completed the experiment in spring/summer season, their SC reflectance at baseline, after hydrating in water for 40 minutes, and after drying in the lab for 40 minutes are plotted below. As shown in the figures below, at baseline, the SC reflectance Mean & standard deviation (SD)] results span across a range of 60.9dB ± 1.1dB – 66.0dB ± 0.7dB with a population average of 63.9dB ± 1.7dB; after hydrating in water for 40 minutes, their SC reflectance increased to a range of 65.9dB ± 1.1dB - 70.8dB ± 0.6dB with a population average of 68.0dB ± 1.6dB; after drying in lab for 40 minutes, their SC reflectance decreased to a range of 56.6dB ± 0.7dB - 66.5dB ± 0.7dB with a population mean of 63.9dB ± 2.9dB. For 12 subjects who completed the experiment in autumn/winter season, their SC reflectance [Mean & standard deviation (SD)]; at baseline, after hydrating in water for 40 minutes, and after drying in lab for 40 minutes are plotted below. As shown in the figures below, at baseline, the SC reflectance results span across a range of 59.8dB ± 1.2dB – 66.5dB ± 1.1dB with a population average of 63.8dB ± 2.3dB; after hydrating in water for 40 minutes, their SC reflectance increased to a range of 65.3dB ± 0.9dB - 73.9dB ± 0.9dB with a population average of 70.0dB ± 2.8dB; after drying in lab for 40 minutes, their SC reflectance decreased to a range of 59.6dB ± 0.8dB – 69.0dB ± 1.1dB with a

population mean of 64.7dB ± 2.9dB. When combining the results from both seasons for 15 subjects, by averaging across 16,000 – 32,000 A-scans, the SC reflectance results are plotted below. As shown in the figures below, the SC reflectance [Mean & standard deviation (SD)] for 15 subjects at baseline spans in a range of 59.8dB ± 1.2dB – 66.0dB ± 0.7dB with a population mean of 63.9dB ± 2.1dB; after hydrating in water for 40 minutes, their SC reflectance increased to a range of 65.3dB ± 0.9dB – 71.3dB ± 0.9dB with a population of 69.1dB ± 2.5dB; then again, after drying in lab for 40 minutes, their SC reflectance decreased to a range of 59.6dB ± 0.8dB – 67.1dB ± 1.5dB with a population average of 64.3dB ± 2.9dB. Individually, their results are reported in the tables below.

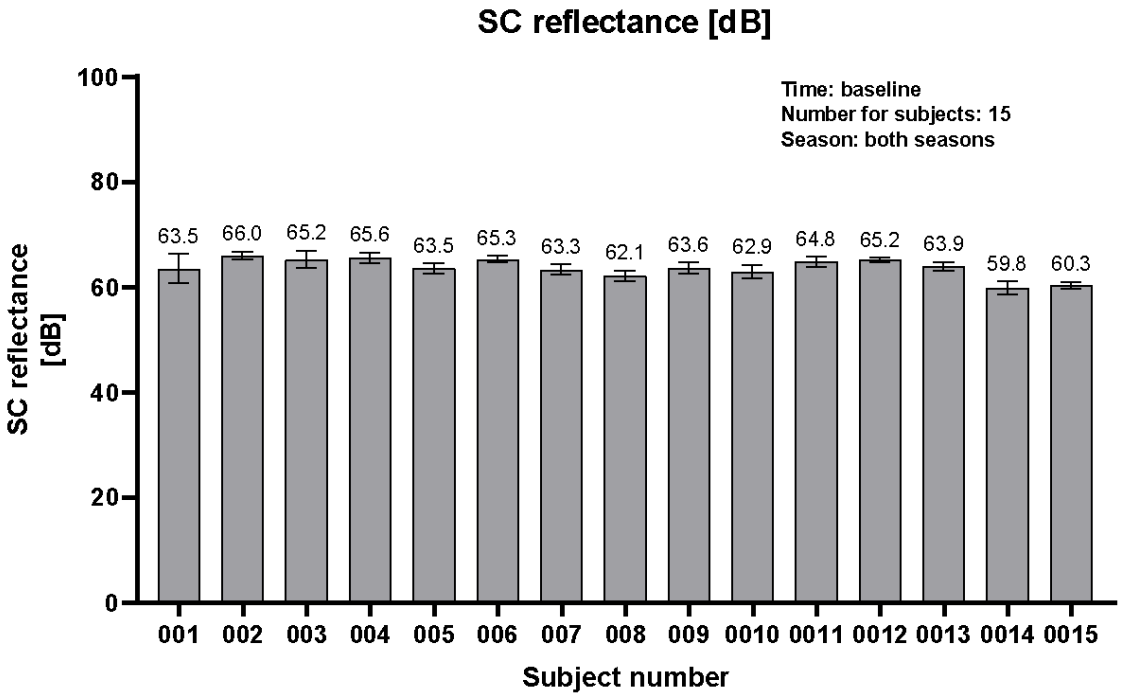

Figure 28. SC reflectance (dB) [Mean & standard deviation (SD)] for 15 subjects average across 16,000 -32,000 A-scans

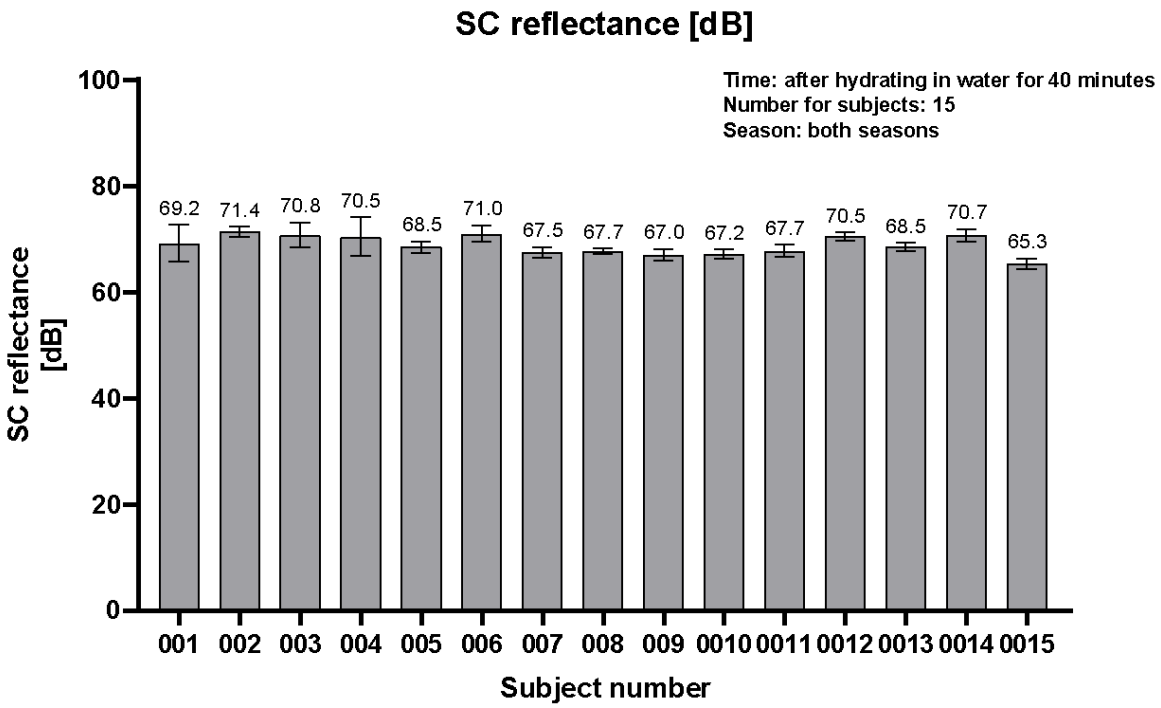

Figure 29. SC reflectance (dB) [Mean & standard deviation (SD)] for 15 subjects average across 16,000 -32,000 A-scans

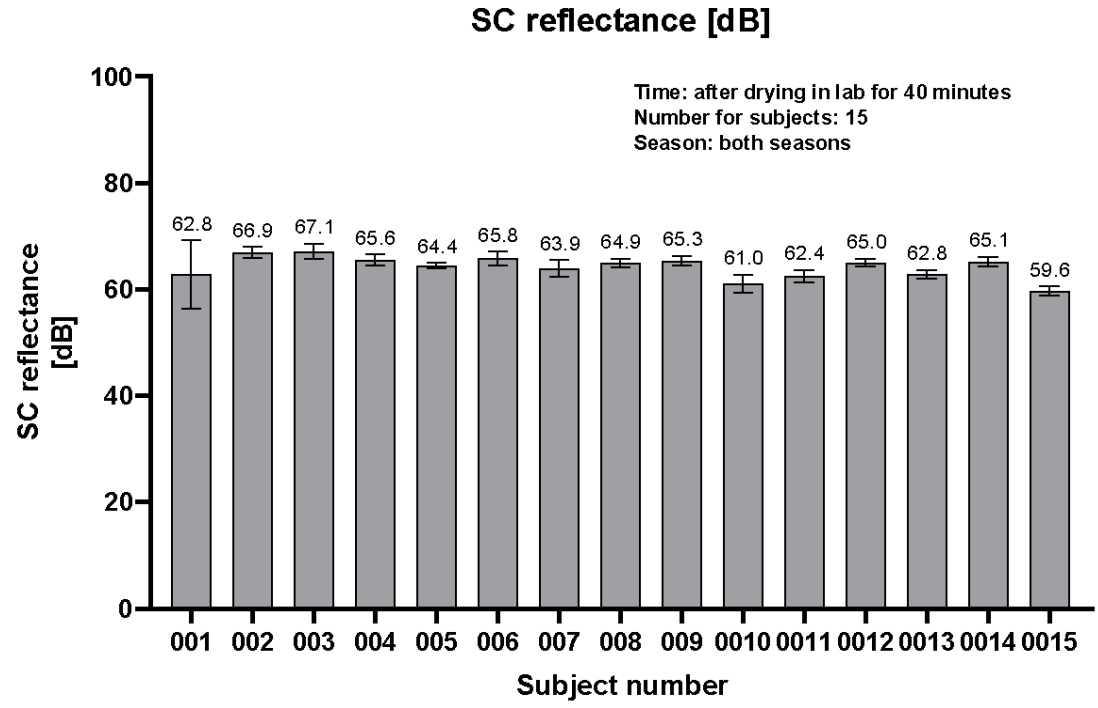

Figure 30. SC reflectance (dB) [Mean & standard deviation (SD)] for 15 subjects average across 16,000 -32,000 A-scans

SC reflectance(dB) average across 16,000-32,000 A-scans for 15 subjects in different seasons			
Subject number	Spring/summer	Autumn/winter	Combined SC reflectance
001	60.9dB ± 1.1dB	66.6dB ± 0.7dB	63.5dB ± 2.8dB
002	66.0dB ± 0.7dB	66.0dB ± 0.8dB	66.0dB ± 0.7dB
003	63.9dB ± 0.9dB	66.5dB ± 1.1dB	65.2dB ± 1.7dB
004	65.2dB ± 1.0dB	65.9dB ± 0.9dB	65.5dB ± 0.9dB
005	64.2dB ± 0.4dB	62.9dB ± 0.7dB	63.5dB ± 0.9dB
006	65.4dB ± 0.8dB	65.2dB ± 0.4dB	65.3dB ± 0.7dB
007	62.7dB ± 0.8dB	63.9dB ± 0.9dB	63.3dB ± 1.0dB
008	62.1dB ± 0.9dB		62.1dB ± 0.9dB
009	63.6dB ± 1.1dB		63.6dB ± 1.1dB
0010	63.8dB ± 1.0dB	62.0dB ± 0.9dB	62.9dB ± 1.3dB
0011	64.8dB ± 0.9dB		64.8dB ± 0.9dB
0012		65.2dB ± 0.4dB	65.2dB ± 0.4dB
0013		63.9dB ± 0.9dB	63.9dB ± 0.9dB
0014		59.8dB ± 1.2dB	59.8dB ± 1.2dB
0015		60.3dB ± 0.7dB	60.3dB ± 0.7dB

Table 7. Baseline reflectance (dB) [Mean & standard deviation (SD)] for 15 subjects

SC reflectance(dB) average across 16,000-32,000 A-scans for 15 subjects in different seasons			
Subject number	Spring/summer	Autumn/winter	Combined SC reflectance
001	65.9dB ± 1.1dB	72.4dB ± 0.5dB	69.1dB ± 3.4dB
002	70.8dB ± 0.6dB	71.9dB ± 0.9dB	71.3dB ± 0.9dB
003	68.6dB ± 0.8dB	72.9dB ± 0.9dB	70.7dB ± 2.4dB
004	67.0dB ± 0.9dB	73.9dB ± 1.0dB	70.5dB ± 3.7dB
005	69.0dB ± 1.0dB	68.8dB ± 0.9dB	68.5dB ± 1.1dB
006	69.8dB ± 1.1dB	72.1dB ± 0.9dB	70.9dB ± 1.5dB
007	67.5dB ± 1.1dB	67.4dB ± 1.1dB	67.5dB ± 1.1dB
008	67.7dB ± 0.5dB		67.7dB ± 0.5dB

009	67.0dB ± 1.1dB		67.0dB ± 1.1dB
0010	67.5dB ± 0.7dB	66.8dB ± 0.9dB	67.1dB ± 0.9dB
0011	67.7dB ± 1.2dB		67.7dB ± 1.2dB
0012		70.5dB ± 0.8dB	70.5dB ± 0.8dB
0013		68.5dB ± 0.8dB	68.5dB ± 0.8dB
0014		70.7dB ± 1.2dB	70.7dB ± 1.2dB
0015		65.3dB ± 0.9dB	65.3dB ± 0.9dB

Table 8. SC reflectance (dB) [Mean & standard deviation (SD)] for 15 subjects after hydrating in water for 40 minutes

SC reflectance(dB) average across 16,000-32,000 A-scans for 15 subjects in different seasons			
Subject number	Spring/summer	Autumn/winter	Combined SC reflectance
001	56.6dB ± 0.7dB	69.0dB ± 1.1dB	62.7dB ± 6.5dB
002	66.5dB ± 0.7dB	67.2dB ± 1.2dB	66.8dB ± 1.0dB
003	66.1dB ± 1.1dB	68.4dB ± 0.5dB	67.1dB ± 1.5dB
004	65.6dB ± 0.9dB	65.5dB ± 1.2dB	65.6dB ± 1.1dB
005	64.4dB ± 0.5dB	64.3dB ± 0.5dB	64.4dB ± 1.1dB
006	66.5dB ± 0.9dB	65.0dB ± 1.2dB	65.8dB ± 1.3dB
007	62.9dB ± 1.2dB	64.9dB ± 1.1dB	63.9dB ± 1.5dB
008	64.9dB ± 0.7dB		64.9dB ± 0.7dB
009	65.3dB ± 0.9dB		65.3dB ± 0.9dB
0010	62.4dB ± 1.2dB	59.6dB ± 0.8dB	61.0dB ± 1.7dB
0011	62.4dB ± 1.2dB		62.4dB ± 1.2dB
0012		65.0dB ± 0.7dB	65.0dB ± 0.7dB
0013		62.8dB ± 0.8dB	62.8dB ± 0.8dB
0014		65.1dB ± 0.9dB	65.1dB ± 0.9dB
0015		59.6dB ± 0.8dB	59.6dB ± 0.8dB

Table 9. SC reflectance (dB) [Mean & standard deviation (SD)] for 15 subjects after drying in lab for 40 minutes

The group results are plotted below, where, to recollect, for 11 subjects, their SC reflectance [Mean & standard deviation (SD)] at spring/summer season was found to be 63.9dB ± 1.7dB at baseline, after

hydrating in water for 40 minutes, it increased to 68.0dB ± 1.6dB, after drying in lab for 40 minutes, it decreased to 64.0dB ± 2.9dB. For 12 subjects, their SC reflectance at autumn/winter season was found to be 63.8dB ± 2.3dB at baseline, after hydrating in water for 40 minutes, it increased to 70.0dB ± 2.8dB, after drying in lab for 40 minutes, it decreased to 64.7dB ± 3.0dB. For 15 subjects, their SC reflectance with both seasons combined was found to be 63.9dB ± 2.1dB at baseline, after hydrating in water for 40 minutes, it increased to 69.1dB ± 2.5dB, after drying in lab for 40 minutes, it decreased to 64.3dB ± 2.9dB.

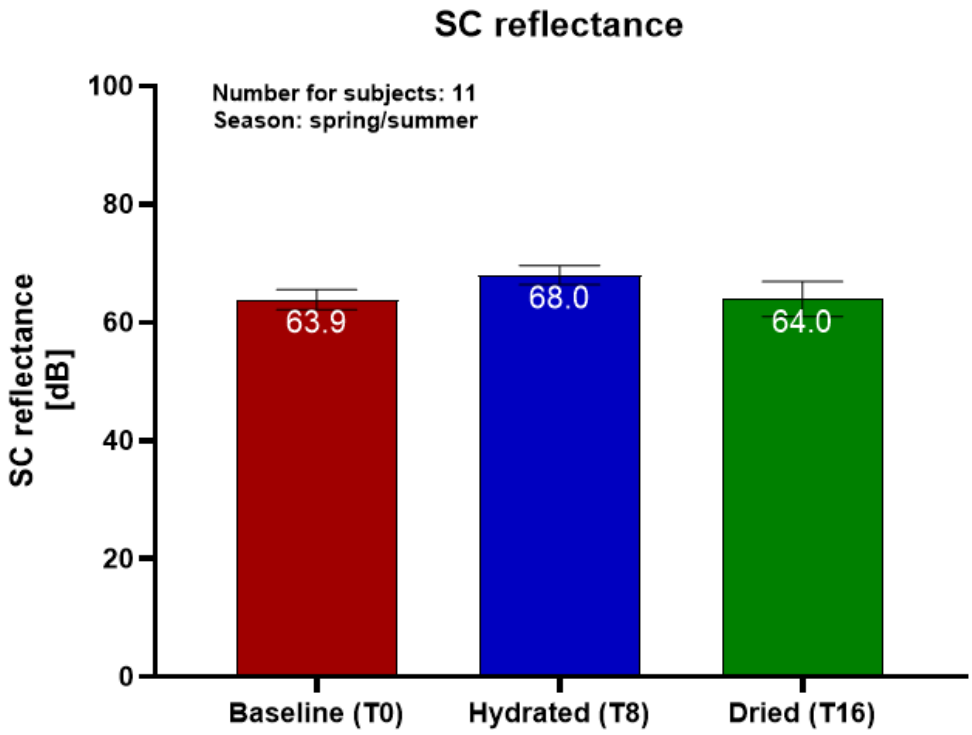

Figure 31. SC reflectance (dB) [Mean & standard deviation (SD)] for 11 subjects average across 16,000 A-scans

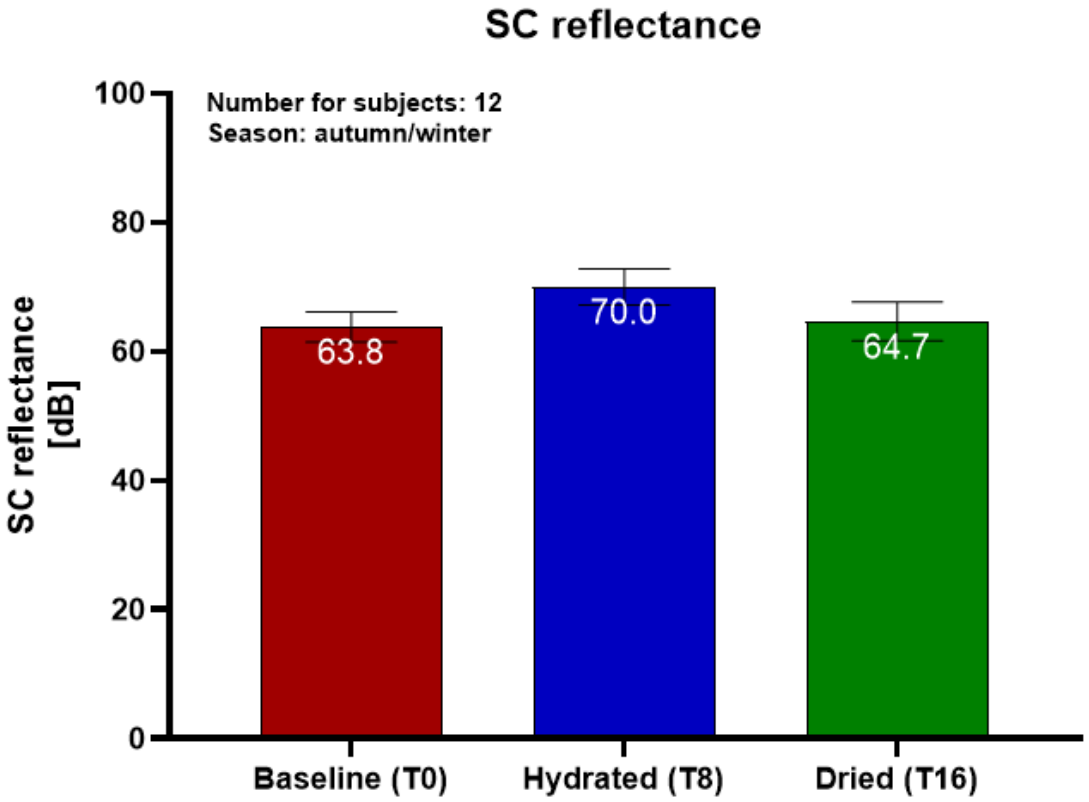

Figure 32. SC reflectance (dB) [Mean & standard deviation (SD)] for 12 subjects average across 16,000 A-scans

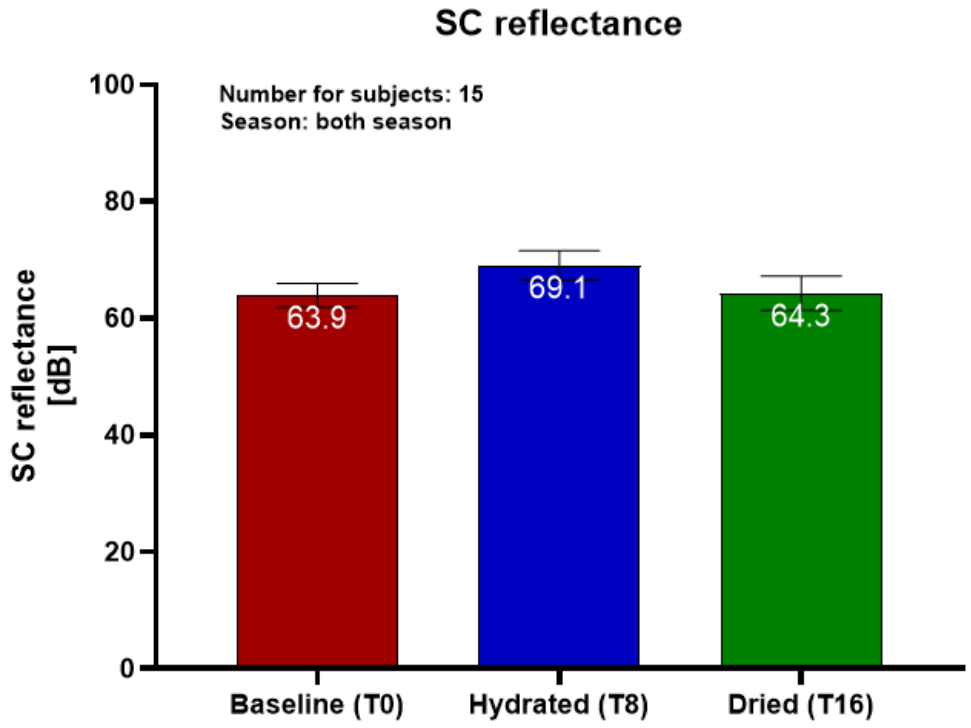

Figure 33. SC reflectance (dB) [Mean & standard deviation (SD)] for 15 subjects average across 16,000 A-scans

5.22 SC reflectance – Variability of results (individual, hydration state, season, age, gender)

Same as the analysis that was performed in previous chapters, to determine the inter-variability among subjects' results in SC reflectance, One-Way ANOVA test was used to investigate whether each subjects' SC reflectance significantly differ from each other. For 11 subjects who completed their experiment in spring/summer season, their SC reflectance at baseline, after hydrating in water for 40 minutes, and after drying in lab for 40 minutes, all showed statistical differences with each other with p values of $p < 0.0001$; $p < 0.0001$; and $p < 0.0001$ respectively, indicating the inter-variabilities among. Similarly, the same test was used on 12 subjects who completed the experiment in autumn/winter season. Again, by performing One-Way ANOVA, it was found that all of 12 subjects' SC reflectance in autumn/winter season before hydration, after hydrating in water for 40 minutes and after drying in lab for 40 minutes, are significantly different from each other with p values of $p < 0.0001$; $p < 0.0001$; and $p < 0.0001$ respectively. When combing the SC reflectance results for all 15 subjects, One-Way ANOVA test again showed significant differences in subjects' SC reflectance before hydration, after hydrating in water for 40 minutes, and after drying in lab for 40 minutes with p values of $p < 0.0001$; $p < 0.0001$; and $p = 0.0005$.

To test the hypothesis that SC reflectance at baseline is significantly different from after hydrating in water for 40 minutes and after drying in the lab for 40 minutes, standard paired T-test was used, and results are plotted below. Noted here, a normality test (D'Agostino-Pearson) was prior used to test whether the data points used come from a normal distribution. For 11 subjects who completed the experiment in spring/summer season, 10 b-scans were gathered per subjects, hence at each time interval, 110 B-scans were used in the normality test, results showed that data points (B-scans) gathered from 11 subjects for each time interval did not pass the normality test. Hence, when using standard paired T-test, normal distribution of the data points is not assumed. Standard paired T-test shows that apart from when comparing results at baseline with after drying in lab, SC reflectance at baseline, after hydrating in water for 40 minutes, and after drying in lab for 40 minutes are all significantly different from each other with p values of $p < 0.0001$ and $p < 0.0001$. Similarity, for 12 subjects who completed the experiment in autumn/winter season, 10 b-scans were gathered per subjects, hence at each time interval, 120 B-scans were used in the normality test, results showed that data points (B-

scans) gathered from 12 subjects for each time interval did not pass the normality test. Hence, when using standard paired T-test, normal distribution of the data points is not assumed. Standard paired T-test shows that SC reflectance s at baseline, after hydrating in water for 40 minutes, and after drying in lab for 40 minutes are all significantly different from each other with p values of $p < 0.0001$; $p < 0.0001$;and $p = 0.0009$ respectively. When 15 subjects are combined, 7 subjects have 10 B-scans from one of the seasons and 8 subjects have 20 B-scans from both seasons, and in total for 15 subjects count up to 230 B-scans (7 subjects x 10 B-scans + 8 subjects x 10 B-scans x 2) per time interval, normality test was again used to see whether these data points are drawn from a normal distribution, results showed that none of the time intervals' data points are drawn from a normal distribution. Hence, when using standard paired T-test, normal distribution of the data points is not assumed. Again, standard paired T-test shows that SC reflectance at baseline, after hydrating in water for 40 minutes, and after drying in lab for 40 minutes are all significantly different from each other with p values of $p < 0.0001$; $p < 0.0001$; and $p = 0.0079$, respectively.

As reported in previous paragraphs, inter-variations of the results among subjects were confirmed using ANOVA test. Variations of the results depending on hydrational state were also listed using T-test. In this chapter, other factors such as season, age and gender which could potentially induce variation in the results are discussed.

To determine the influence of seasonal factor on the variability of results, the SC reflectance [Mean & Standard deviation] results for 8 subjects who completed the experiment in both seasons at the time interval of: before hydration; after hydrating in water for 40 minutes; and after drying in lab for 40 minutes are stated in the table below. For 8 subjects, their baseline SC reflectance in spring/summer season span between a range of 60.9dB ± 1.1dB – 66.0dB ± 0.7dB with a population average of 64.0dB ± 1.8dBdB; after hydrating in water for 40 minutes, their SC reflectance increased to 65.9dB ± 1.1dB – 70.8dB ± 0.6dB with a population average of 68.2dB ± 1.8dB; after drying in lab for 40 minutes, their SC reflectance decreased to 56.5dB ± 0.7dB – 66.1dB ±1.1dB with a population average of 63.9dB ± 3.3dB. During autumn/winter season, their baseline SC reflectance in autumn/winter season span between a range of 59.8dB ± 1.2dB – 66.5dB ± 1.1dB with a population average of 64.3dB ± 2.3dB; after hydrating in water for 40 minutes, their SC reflectance increased to 67.4dB ± 1.1dB – 73.9dB ±

0.9dB with a population average of 71.2dB ± 2.4dB; after drying in lab for 40 minutes, their SC reflectance decreased to 64.4dB ± 0.5dB – 69.0dB ±1.1dB with a population average of 66.2dB ± 1.9dB. To test the hypothesis of SC reflectance at spring/summer season is significantly different from at autumn/winter season, 8 subjects' 80 B-scans at each time interval were tested using standard paired non-parametric (assume no Gaussian distribution) T-test, the results at baseline, after hydrating in water for 40 minutes and after drying in lab for 40 minutes are plotted below. See figures below, 8 subjects' results at each time interval were tested using standard paired non-parametric (assume no Gaussian distribution) T-test, the results at baseline (T0), after hydrating in water for 40 minutes (T8) and after drying in lab for 40 minutes (T16) are plotted below. As shown in the figure, nonparametric paired T-test shows that SC reflectance quantified at baseline (T0) and after drying in the lab (T16) showed no significant difference, a significant difference ($p = 0.0391$ *) is detected after hydrating in water for 40 minutes (T8).

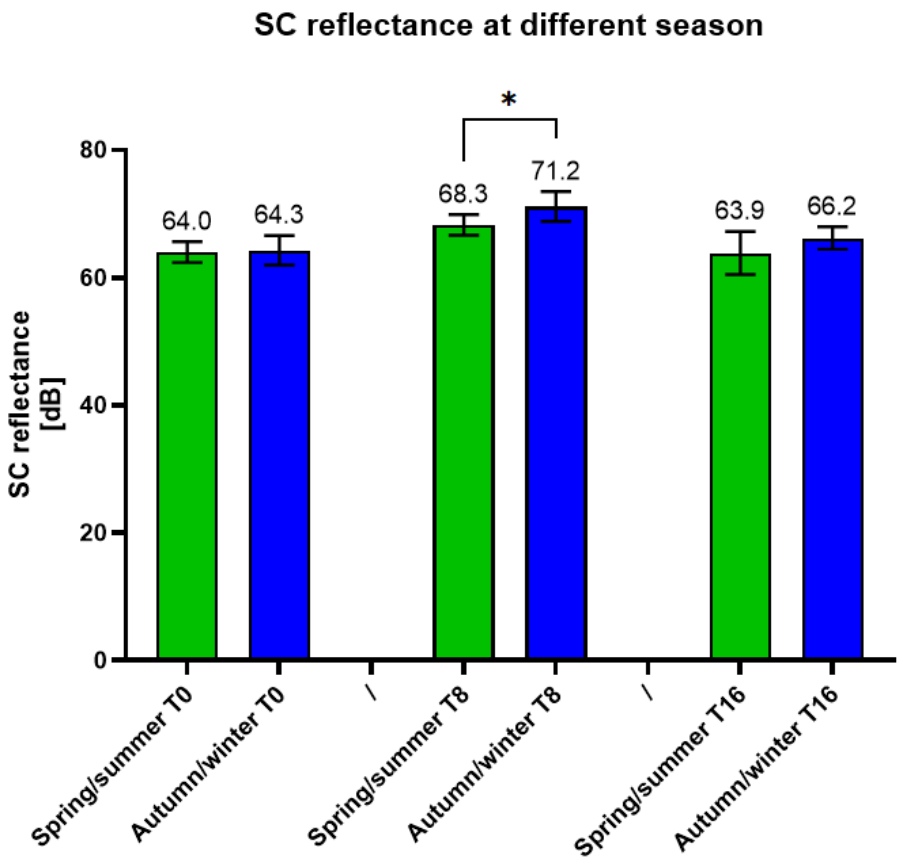

Figure 34. Paired T-test for SC reflectance (dB) [Mean & standard deviation (SD)] during different season

SC reflectance(dB) average across 16,000 A-scans for 8 subjects in different season		
Season	Spring/summer	Autumn/winter
Before hydration	64.0dB ± 1.8dBdB	64.3dB ± 2.3dB
After hydrating in water for 40 minutes	68.3dB ± 1.8dB	71.2dB ± 2.4dB
After drying in lab for 40 minutes	63.9dB ± 3.3dB	66.2dB ± 1.9dB

Table 10. SC reflectance (dB) [Mean & standard deviation (SD)] for 15 subjects at various hydration states at different season

To determine whether age factor played a role in the variability of the results, 15 subjects were sub-categorized into three age groups of 20-29 (6 subjects); 30-39 (5 subjects); and 40-60 (4 subjects). For the age group of 20-29, 6 subjects have 90 B-scans as 3 subjects completed the experiment in both seasons and 3 completed in one season; for the age group of 30-39, 5 subjects have in total 70 B-scans as 2 subjects completed the experiment in both season and 3 subjects completed the experiment in one season; for the age group of 40-60, 4 subjects have in total 70 B-scans as 3 subjects completed the experiment in both seasons and 1 subject completed the experiment in one season. Standard unpaired (non-parametric) T-test was used to detect whether subjects' SC reflectance of different age groups show differences significantly. As shown in figure 35, nonparametric unpaired T-test showed that all age groups' SC reflectance, expect the comparison between 20-29 and 30-30, are significant different from each other with significant p values of $p = 0.0003$***, and $p < 0.0001$ **** (p value is a statistical measurement used to validate whether the observed results happened by chance. i.e., $p < 0.05$ or lower is generally conferred statistically significant; $p = 0.05$* means the observed result has a 5 % chance of being wrong, or happened by chance; $p = 0.01$** means the observed result has a 1 % chance of happening by chance; $p = 0.001$*** means the observed result has a 0.01% chance of happening by chance; $p = 0.0001$ means the observed result has a 0.001%**** chance of happening by chance).

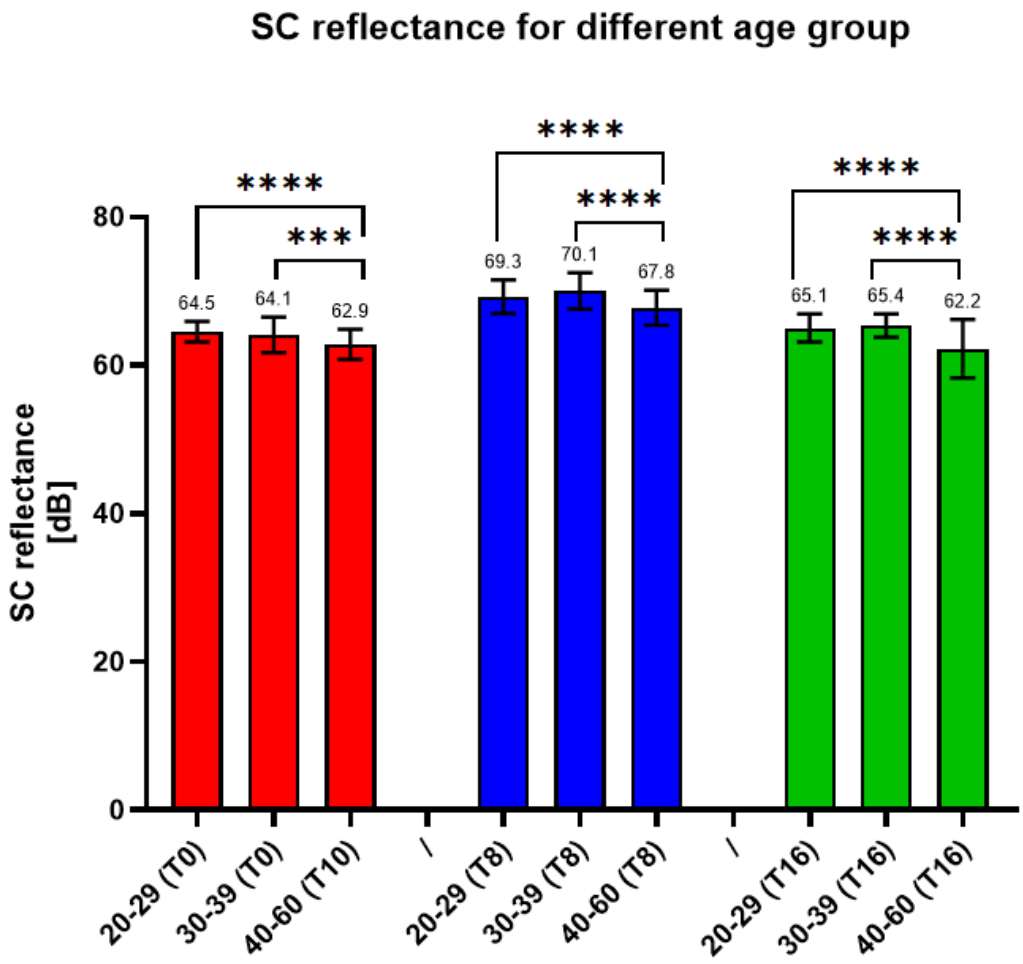

*Figure 35. Unpaired T-test for SC reflectance (*dB) [*Mean & standard deviation (SD)] for different age group*

SC reflectance(dB) average across 16,000-32,000 A-scans for 15 subjects at various age groups and hydration states			
Hydration state/Age group	20-29 (yrs)	30-39(yrs)	40-60 (yrs)
Before hydration	64.5dB ± 0.9dB	64.1dB ± 2.6dB	62.9dB ± 1.5dB
After hydrating in water for 40 minutes	69.3dB ± 1.9dB	70.1dB ± 1.6dB	67.8dB ± 1.7dB
After drying in lab for 40 minutes	65.1dB ± 1.6dB	65.4dB ± 1.5dB	62.2dB ± 2.1dB

Table 11. SC reflectance (dB) [Mean & standard deviation (SD)] for 15 subjects at various hydration states and age group

To determine whether gender played a role in the variability of the results, 15 subjects were sub-categorized into two groups of 10 males and 5 females. For male subject group, 160 B-scans were gathered as 6 subjects completed the experiment in both seasons and 4 subjects completed the experiment in one season; for the female subject group, 70 B-scans were gathered in total as 2 subjects completed the experiment in both seasons and 3 subjects completed the experiment in one season.

Standard unpaired (non-parametric) T-test was used to detect whether subjects' SC reflectance of different gender groups show differences significantly. As shown in figure 36, standard unpaired T-test shows that SC reflectance from different gender groups at baseline, after hydrating in water for 40 minutes are all significantly different from each other with p values of $p < 0.0001$ ****; $p < 0.0001$ **** ; $p = 0.0003$ *** respectively. Their SC reflectance averaging from 16,000 – 32,000 A-scans are also reported in table 12.

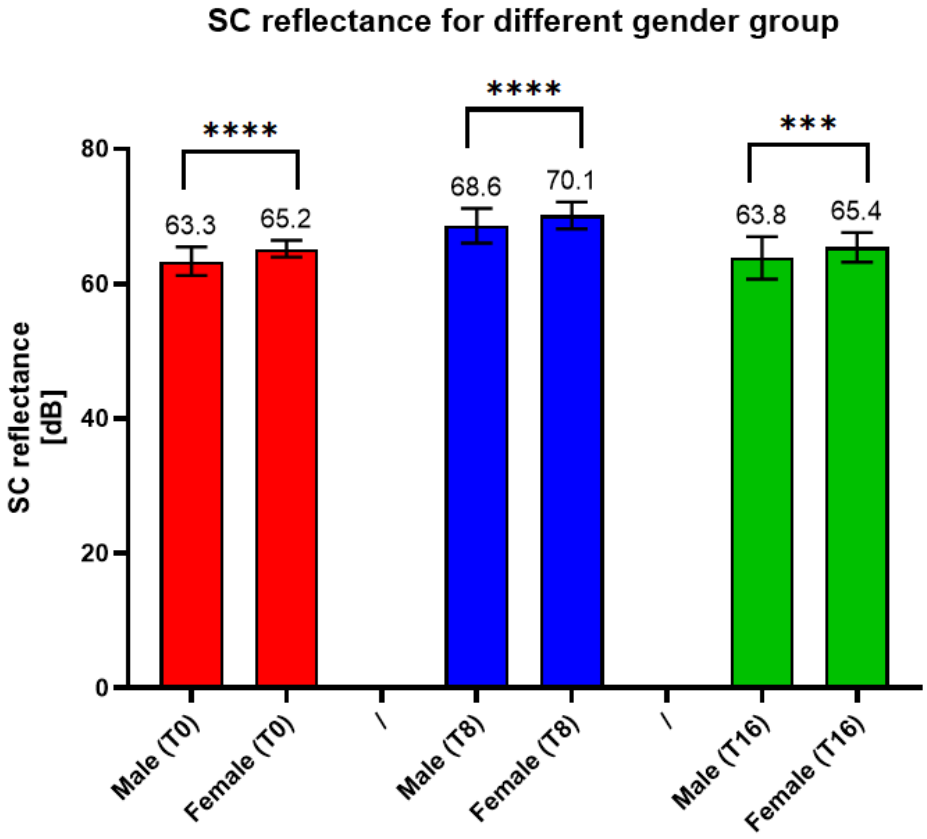

Figure 36. Unpaired T-test for SC reflectance (dB) [Mean & standard deviation (SD)] for different gender group

SC reflectance(dB) average across 16,000-32,000 A-scans for 15 subjects in different gender groups		
Hydration state/Gender group	Male	Female
Before hydration	63.3dB ± 1.8dB	65.2dB ± 0.8dB
After hydrating in water for 40 minutes	68.6dB ± 1.9dB	70.1dB ± 1.6dB
After drying in lab for 40 minutes	63.8dB ± 2.1dB	63.8dB ± 1.8dB

Table 12. SC reflectance (dB) [Mean & standard deviation (SD)] for 15 subjects at various hydration states and gender group

5.23 SC reflectance – hydrating and dehydrating phase

As SC reflectance measurements were gathered at every time interval during hydrating and dehydrating phases, for each subject, their results were separated at these phases. During hydrating phase (experiment time: 0 minutes → 40 minutes), water molecule diffuse into the SC as the water concentration in the bucket of water is higher than inside of SC. The initial stage of the diffusion process is expected to take place quickly, in later stages, as the water concentration increases in the SC, the diffusion speed is expected to slow down and then reach a steady state as it saturates. This physical principle is reflected in subjects' SC reflectance results, take subject 003 as an example, see figure 37a), subject 003's SC reflectance increases rapidly during the first 15-20 minutes, then the increase slows down and reaches a saturation point after 40 minutes. This non-linearly response can be fitted using nonlinear models. In Graphpad Prism, One-phase association was selected to fit the results for all subjects, see figure 37b) for the model of One-phase association, compared to subject 003's response during hydrating phase, the shape of the model matches the response of subject 003's SC reflectance result, and the fit of the model is quite good. The mathematical model of one phase association follows the equation of:

$$Y = Y0 + (Plateau - Y0) * (1 - exp\ (-K * x)\ ) \quad \textbf{(40)}$$

Where: $Y0$ is the Y value, here SC reflectance, when time is zero, i.e., at baseline, and it is expressed as the same unit as Y; $Plateau$ is the Y value at infinite times, and it is also expressed as the same unit as Y; K is the rate constant, and it is expressed in reciprocal of the time, here as $1/min$; Tau is the time constant, and it is computed as the reciprocal of K; $Span$ is the difference between $Y0$ and $Plateau$, and it is expressed in the same unit as the Y value.

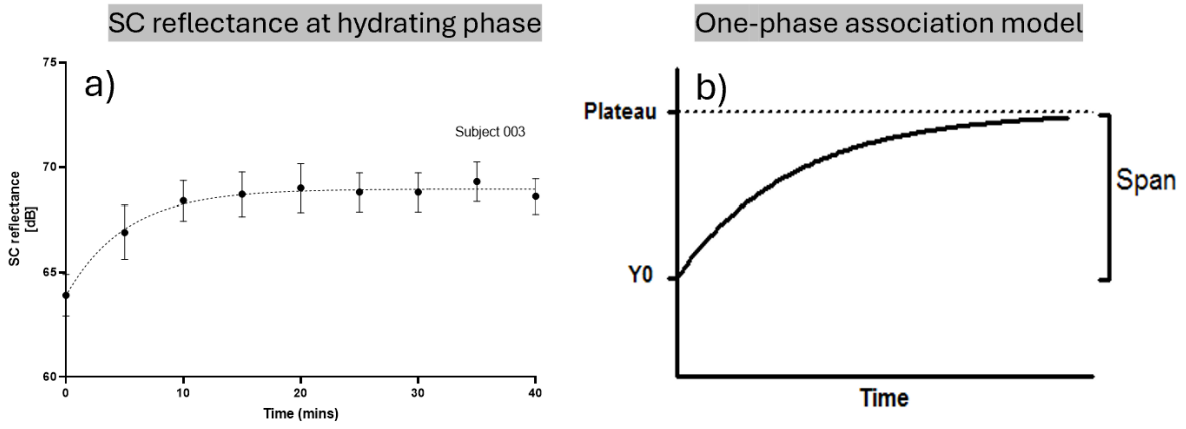

Figure 37. left - Subject 003's SC reflectance during hydrating phase with one phase association model fit. right - One phase association model from GraphPad Prism

For subjects who completed the experiment in spring/summer and autumn/winter seasons, along with combined both season measurements, their SC reflectance during hydrating phase along with its One-phase association model fit are plotted below. As shown in the figure 38 - 40, all subjects behave differently, the parameters that was chosen to help the author to understand subject's SC properties are: $Y0$, as in at what reflectance value they start with.; $Plateau$, as in what reflectance value the model indicates they finish; Tau is the time constant, and here, it provides some indications of 'how quickly' subject's SC reflectance value increase up to saturation; $span$, as in 'how much change is there for each subject during the same amount of hydration means applied.

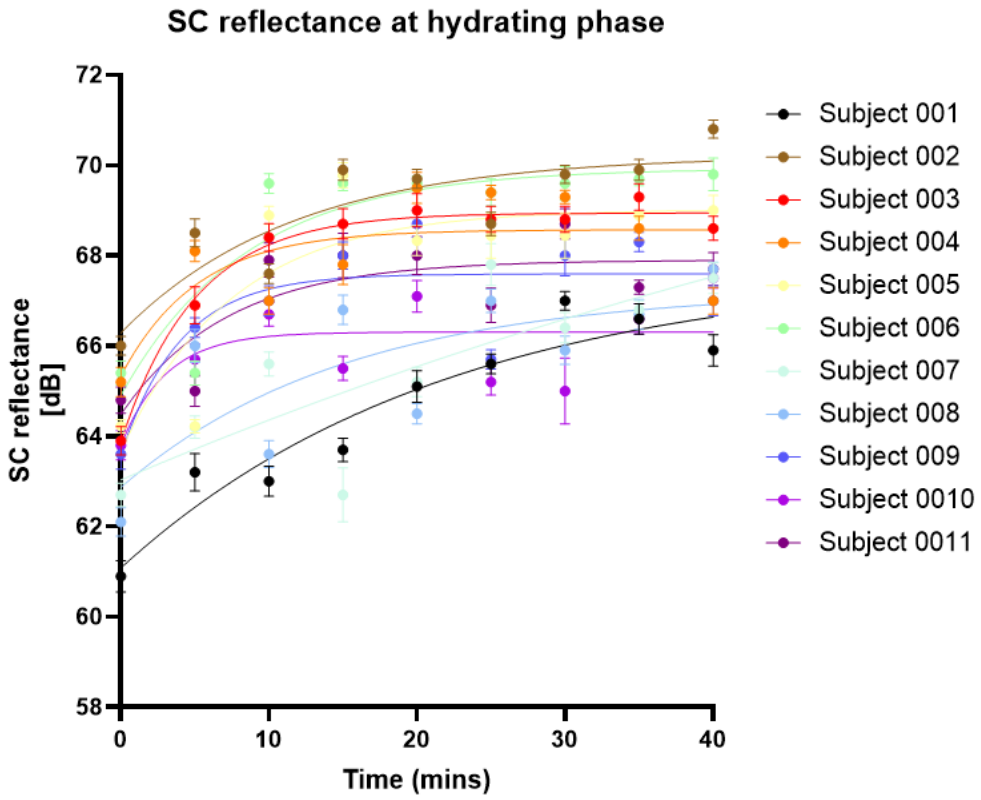

Figure 38. SC reflectance [Mean & standard error (SEM)] at hydrating phase during spring/summer season

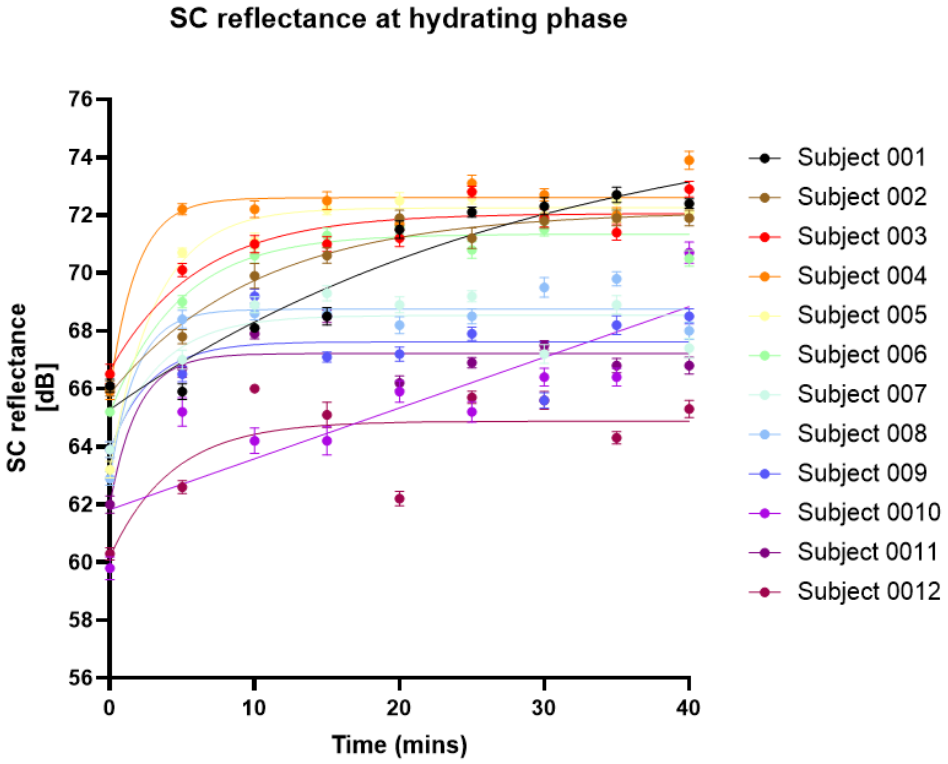

Figure 39. SC reflectance [Mean & standard error (SEM)] at hydrating phase during autumn/winter season

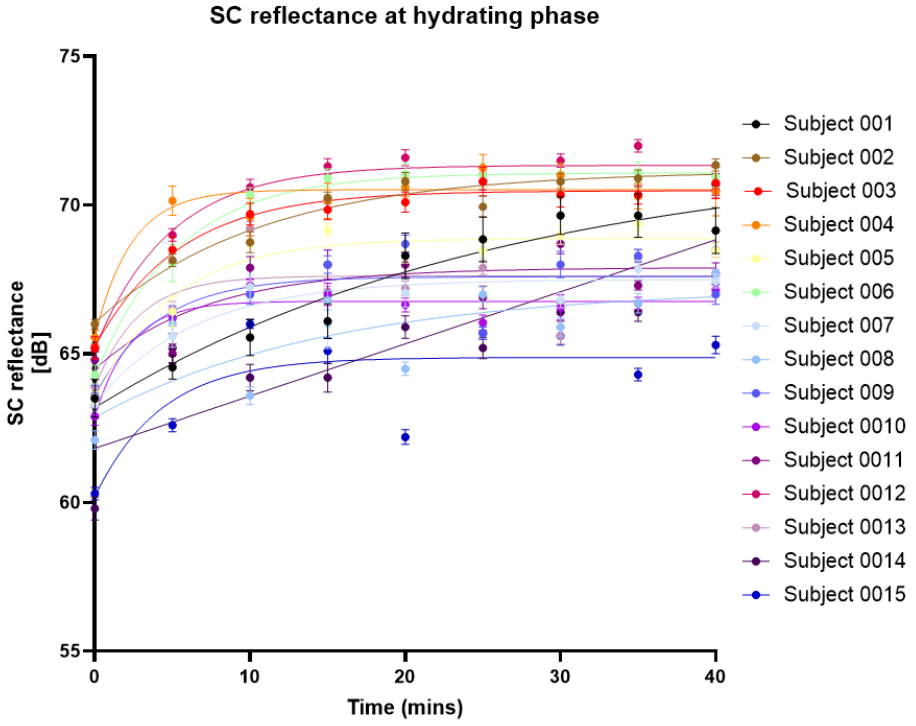

Figure 40. SC reflectance [Mean & standard error (SEM)] at hydrating phase during both spring/summer and autumn/winter season

11 subjects' SC reflectance results at hydrating phase & exponential fit model parameters					
Subject number	$Y0$(dB)	$Plateau$(dB)	Tau(mins)	$Span$(dB)	Rate constant
001	61.1	67.7	22.1	6.6	0.04
002	66.3	70.2	11.7	3.9	0.08
003	63.9	68.9	5.1	5.1	0.19
004	65.3	68.6	5.2	3.2	0.19
005	63.7	69.0	7.5	5.4	0.13
006	64.9	69.9	8.5	5.0	0.11
007	63.0	75.2	86.4	12.16	0.01
008	62.9	67.2	15.2	4.4	0.06
009	63.6	67.6	4.0	4.0	0.24
0010	63.8	66.3	3.1	2.5	0.32
0011	64.5	67.9	7.2	3.4	0.13

Table 13. 11 subjects' SC reflectance results with its' one phase model association fit parameters during hydrating phase at spring/summer season

12 subjects' SC reflectance results at hydrating phase & exponential fit model parameters					
Subject number	$Y0$(dB)	$Plateau$(dB)	Tau(mins)	$Span$(dB)	Rate constant
001	65.3	75.9	29.9	10.7	0.03
002	65.8	72.1	10.3	6.3	0.09
003	66.6	72.1	6.1	5.4	0.16
004	65.9	72.6	1.9	6.7	0.54
005	63.2	72.3	3.2	9.0	0.31
006	65.2	71.3	4.8	6.2	0.20
007	63.8	68.5	3.4	4.7	0.29
008	62.9	68.8	1.8	5.8	0.55
009	63.9	67.6	2.8	3.8	0.36
0010	61.8	NA	5.7	NA	NA
0011	62.0	67.2	1.3	5.2	0.51
0012	60.2	64.9	2.9	4.7	0.23

Table 14. 12 subjects' SC reflectance results with its' one phase model association fit parameters during hydrating phase at autumn/winter season

15 subjects' SC reflectance results at hydrating phase & exponential fit model parameters					
Subject number	$Y0$(dB)	$Plateau$(dB)	Tau(mins)	$Span$(dB)	Rate constant
001	63.2	71.8	26.4	8.6	0.03
002	66.0	71.2	10.7	5.1	0.09
003	65.2	70.5	5.5	5.2	0.18
004	65.6	70.5	2.3	4.9	0.42
005	63.4	68.9	4.9	5.4	0.20
006	64.2	71.1	5.3	6.9	0.18
007	63.3	67.5	6.5	4.2	0.15
008	62.9	67.2	15.2	4.4	0.06
009	63.6	67.6	4.0	4.0	0.24
0010	62.9	66.8	2.3	3.9	0.43
0011	64.5	67.9	7.2	3.4	0.13
0012	65.2	71.3	4.8	6.2	0.20
0013	63.9	67.6	2.8	3.8	0.36
0014	61.8	NA	5.7	NA	NA
0015	60.2	64.5	4.3	4.7	0.23

Table 15. 15 subjects' SC reflectance results with its' one phase model association fit parameters during hydrating phase at both season

For dehydrating phase (experiment time: 40 minutes □ 80 minutes), different from the hydrating phase, most of subjects' SC reflectance behaves linearly, hence a simple linear regression is used to fit all subjects' results. The linear regression model follows the mathematical representation of:

$$Y = slope * (X - Xintercept) \quad \textbf{(41)}$$

Here the $slope$ defines how steep is the line, and the time constant of this model is usually defined by $1/slope$ (mins); the $Y\ Intercept$ is the Y value when time(x) is zero, here is the SC reflectance value at the beginning of the dehydrating phase. When associating these model parameters with SC' properties, $1/slope$ was chosen to give indications of 'how quickly' SC reflectance decreases under the lab drying conditions. For subjects who completed the experiment in spring/summer and autumn/winter season, and combined both seasons, their SC reflectance during dehydrating phase along with its' linear regression model fit are plotted below.

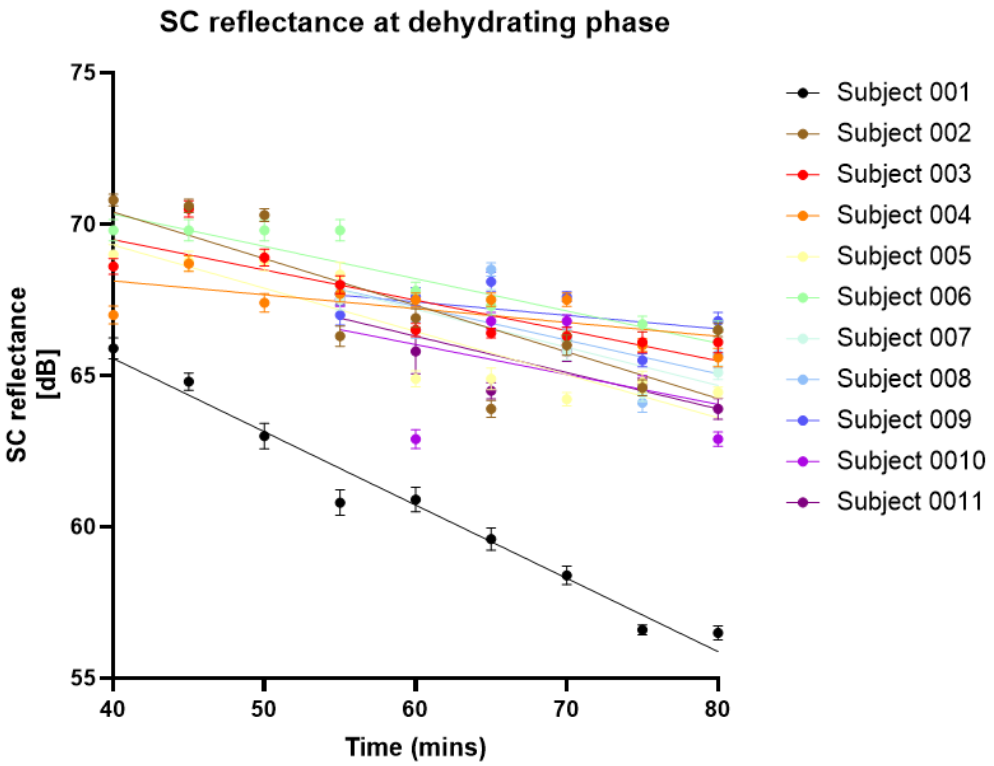

Figure 41. SC reflectance [Mean & standard error (SEM)] at dehydrating phase during spring/summer season

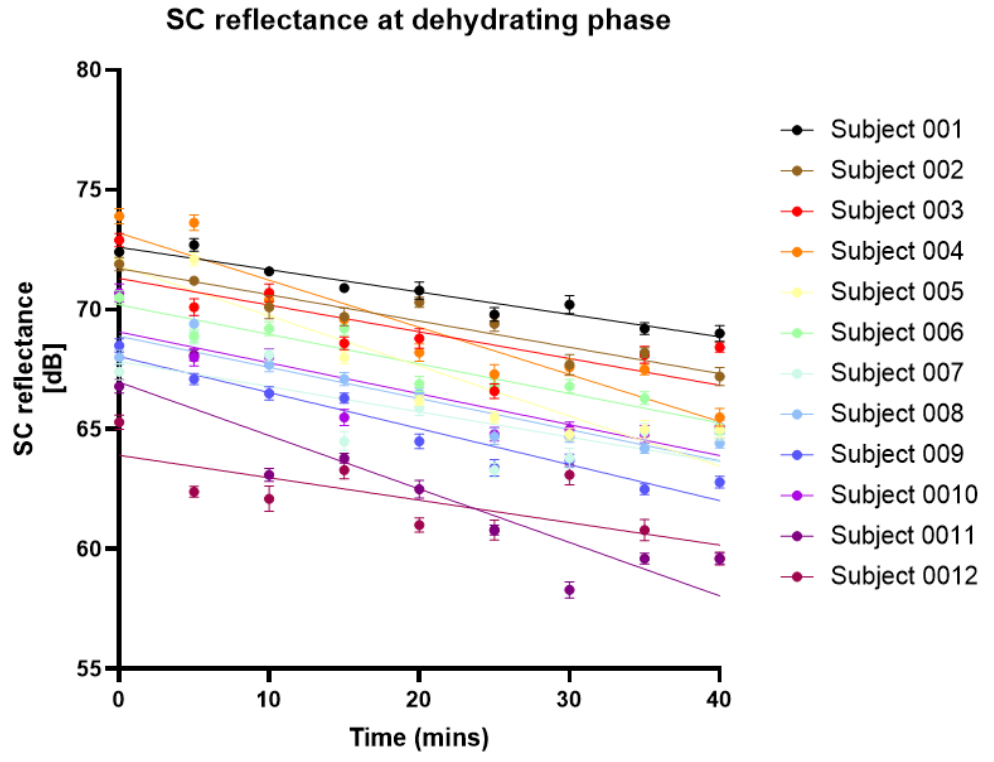

Figure 42. SC reflectance [Mean & standard error (SEM)] at dehydrating phase during autumn/winter season

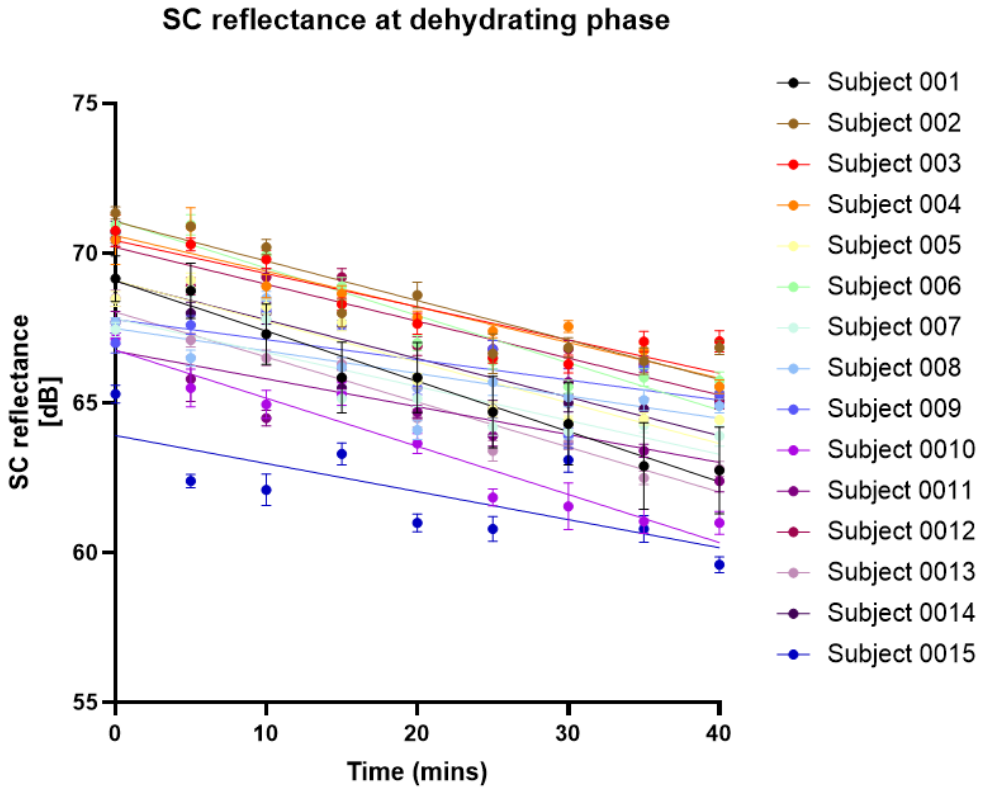

Figure 43. SC reflectance [Mean & standard error (SEM)] at dehydrating phase during both spring/summer and autumn/winter season

11 subjects' SC reflectance results at dehydrating phase & linear model fit parameters			
Subject number	Tau(mins)	$Y0$(dB)	Rate constant
001	4.1	75.2	-0.24
002	6.5	76.6	-0.15
003	10	73.5	-0.10
004	21.9	69.9	-0.04
005	7.0	75.0	-0.14
006	9.4	74.6	-0.10
007	7.9	74.8	-0.12
008	8.9	73.9	-0.11
009	22.4	70.1	-0.04
0010	10.1	71.9	-0.09
0011	8.3	73.5	-0.12

Table 17. 11 subjects' SC reflectance results with its' linear regression model parameters during dehydrating phase at spring/summer season

12 subjects' SC reflectance results at dehydrating phase & linear model fit parameters			
Subject number	Tau(mins)	$Y0$(dB)	Rate constant
001	10.7	72.6	-0.09
002	9.1	71.7	-0.10
003	8.9	71.3	-0.11
004	5.1	73.2	-0.19
005	4.8	71.8	-0.20
006	8.1	70.2	-0.12
007	9.5	67.8	-0.10
008	7.7	68.9	-0.12
009	6.7	68.0	-0.15
0010	7.8	69.1	-0.12
0011	4.5	66.9	-0.22
0012	10.7	63.9	-0.09

Table 18. 12 subjects' SC reflectance results with its' one phase model association fit parameters during dehydrating phase at autumn/winter season

15 subjects' SC reflectance results at dehydrating phase & linear model fit parameters			
Subject number	Tau(mins)	$Y0$(dB)	Rate constant
001	5.9	69.1	-0.16
002	7.6	71.1	-0.13
003	9.0	70.4	-0.11
004	8.4	70.6	-0.11
005	7.4	69.1	-0.13
006	6.3	71.1	-0.15
007	8.8	67.8	-0.11
008	13.3	67.5	-0.07
009	14.9	67.8	-0.06
0010	6.2	66.8	-0.16
0011	10.8	66.7	-0.09

0012	8.1	70.2	-0.12
0013	6.7	68.0	-0.15
0014	7.8	69.1	-0.12
0015	10.7	63.9	-0.09

Table 19. 15 subjects' SC reflectance results with its' one phase model association fit parameters during hydrating phase at both season

5.3 SC hydration (Corneometer)

5.31 SC hydration (Corneometer) at baseline, after hydrating in water for 40 minutes, after drying in lab for 40 minutes

Corneometer® CM 825 (Courage-Khazaka) is a fast, non-invasive, capacitance-based, commercially available equipment which measures the hydration level of the stratum corneum. Since it was introduced, for more than 35 years, Corneometer has been the most used method worldwide when investigating the skin hydration at its surface level (stratum corneum), the device itself is a hand-held probe which can provide repetitive measurements of stratum corneum hydration level promptly (1s), and the results given by the Corneometer is expressed in a numerous scale of [0-120]. Corneometer has been frequently used to validate other skin hydration measurements, in this research, since SC reflectance measured by the visible-light OCT system is associated with changes in the hydration state of stratum corneum, Corneometer measurements were obtained as validation data. As this device only became available to the author during autumn/winter 2023, Corneometer measurements were only obtained on subjects who completed the experiment in autumn/winter season. Note here the subject labelling refers to the same subject labelling for SC thickness and reflectance in autumn/winter season.

For 12 subjects who completed the experiment in autumn/winter season, Corneometer measurements were obtained for each subject per time interval with 5 repeats, the results are expressed in arbitrary units (AU) in a scale of 0-120, where 0 indicates the lowest hydration level and 120 indicate the highest hydration level that can be measured by such a device. For these subjects, their Corneometer measurements at the hydration state of before hydration, after hydrating in water for 40 minutes and after drying in the lab for 40 minutes are plotted below. As shown in the figures, for 12 subjects who completed the experiment in autumn/winter season, their SC hydration [Mean & Standard deviation (SD)] measured by Corneometer at baseline spans across 22±2 to 53±3 with a population mean of 36±11; after hydrating in water for 40 minutes, their SC hydration increased to 51±4 to 91±1 with a

population mean of 74±12; and after drying in lab for 40 minutes, their SC hydration decreased to 17±0 to 50±1 with a population mean of 40±9. The increase from baseline to hydrated state expressed in percentage span across 12% to 228% with a population mean of 102%; and the decrease from hydrated state to dried state expressed in percentage span across 24% to 74% with a population mean of 46%; and the changes from baseline to dried state span across 3% to 59% with a population mean of 10%. The individual results for these subjects are reported in the table below.

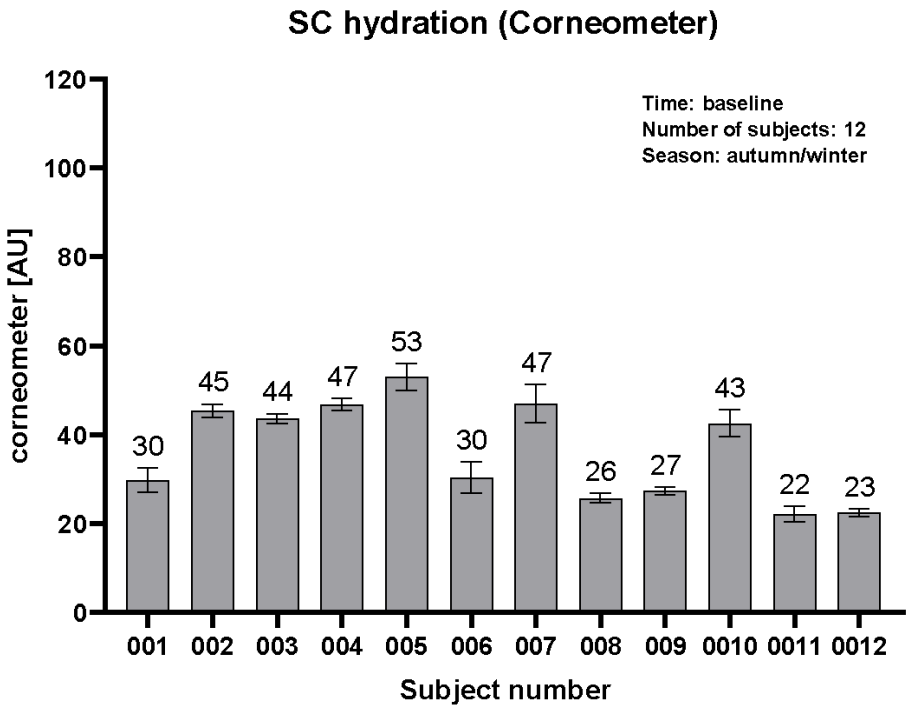

Figure 44. SC hydration [Mean & standard deviation (SD)] measured by Corneometer for 12 subjects average across 5 repeats

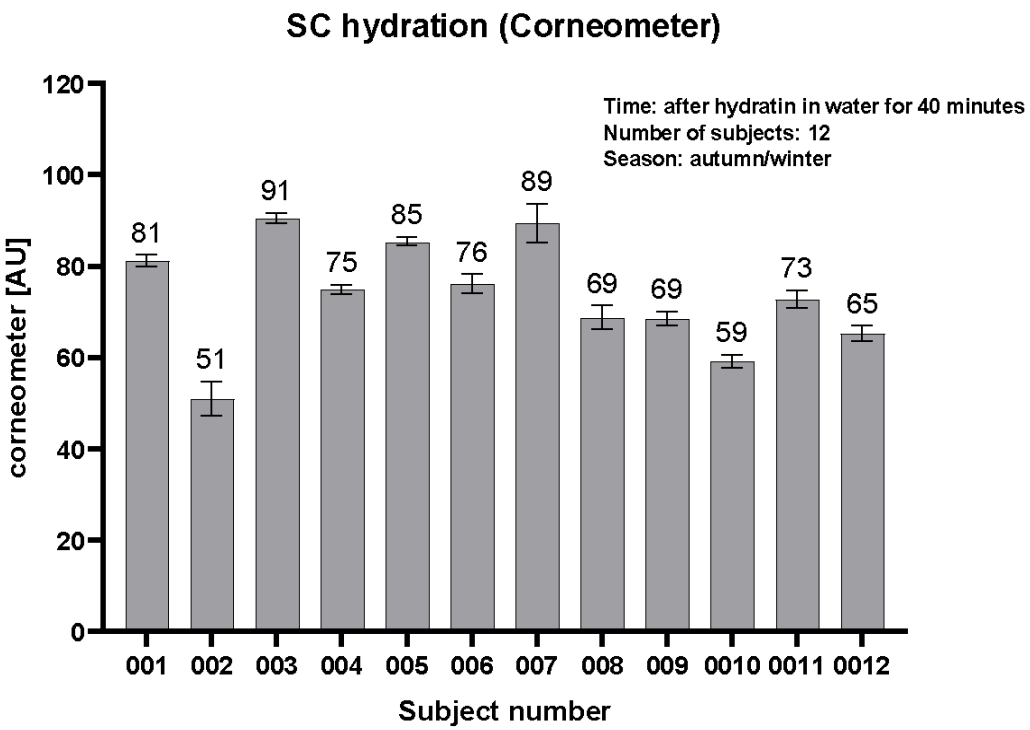

Figure 45. SC hydration [Mean & standard deviation (SD)] measured by Corneometer for 12 subjects average across 5 repeats

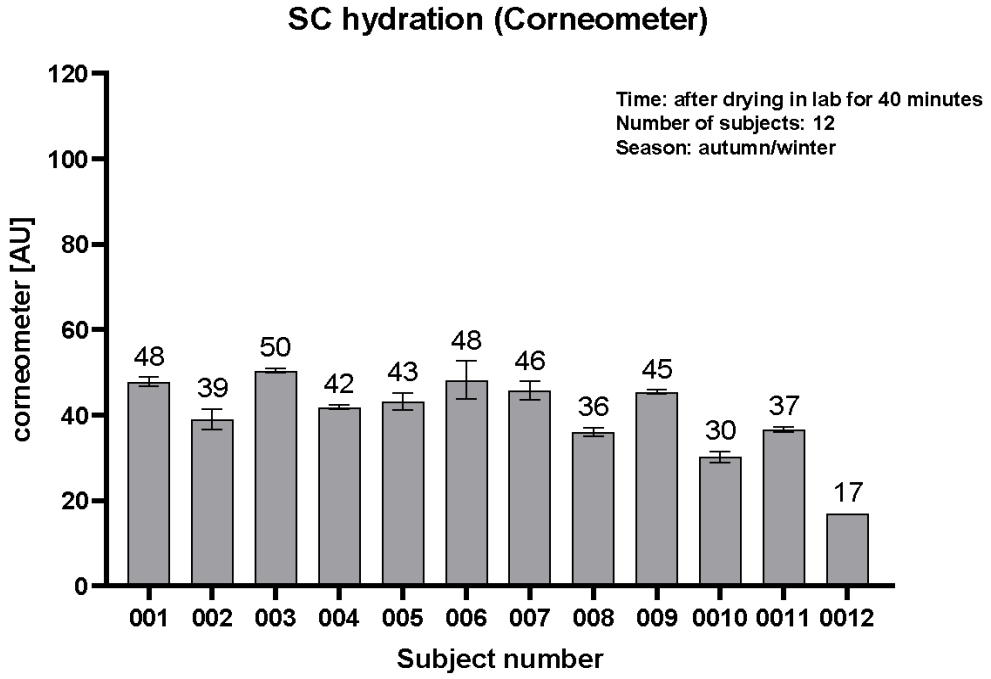

Figure 46. SC hydration [Mean & standard deviation (SD)] measured by Corneometer for 12 subjects average across 5 repeats

SC hydration (AU) average across 5 repeats for 12 subjects in autumn/winter seasons			
Subject number	Before hydration	After hydrating in water for 40 minutes	After drying in lab for 40 minutes
001	30±3	81±1	48±1
002	45±2	51±4	39±2
003	44±1	91±1	50±1
004	47±1	75±1	42±0
005	53±3	85±1	43±2
006	30±3	76±2	48±4
007	47±4	89±4	46±2
008	26±2	69±3	36±1
009	27±1	69±2	45±1
0010	43±3	59±1	30±1
0011	22±2	73±2	37±1
0012	23±1	65±2	17±0

Table 20. SC hydration measured by Corneometer (AU) [Mean & standard deviation (SD)] for 12 subjects at autumn/winter season at baseline, after hydrating in water for 40 minutes and after drying in lab for 40 minutes

5.32 SC hydration (Corneometer) - Variability of results (individual, hydration states, age, gender)

Same as the analysis that was performed in previous chapters for SC thickness and SC reflectance; to determine the inter-variability among subjects' results in SC hydration measured by Corneometer, a One-way ANOVA test was used to determine whether subjects' results differ significantly. For 12 subjects who completed their experiment in autumn/winter season, their SC hydration at baseline, after hydrating in water for 40 minutes, and after drying in lab for 40 minutes, all showed statistical differences with each other with p values of $p < 0.0001$; $p < 0.0001$; and $p < 0.0001$ respectively (p value is a statistical measurement used to validate whether the observed results happened by chance. i.e., $p < 0.05$ or lower is generally conferred statistically significant; $p = 0.05$* means the observed result has a 5 % chance of being wrong, or happened by chance; $p = 0.01$** means the observed result has a 1 % chance of happening by chance; $p = 0.001$*** means the observed result has a 0.01% chance of happening by chance; $p = 0.0001$ means the observed result has a 0.001%**** chance of happening by chance), indicating the inter-variabilities among subjects are significant. To test the hypothesis that

SC hydration at baseline is significantly different from after hydrating in water for 40 minutes and after drying in the lab for 40 minutes, standard paired T-test was used, and results are plotted below. Noted here, a normality test (D'Agostino-Pearson) was prior used to test whether the data points used come from a normal distribution. For 12 subjects who completed the experiment in autumn/winter season, 5 repeats were gathered per subject, hence at each time interval, 60 measurements were used in the normality test, results showed that measurements gathered from 12 subjects for each time interval did not pass the normality test. Hence, when using standard paired T-test, normal distribution of the data points is not assumed. Standard paired T-test shows that SC reflectance at baseline, after hydrating in water for 40 minutes, and after drying in lab for 40 minutes are all significantly different from each other with p values of $p < 0.0001$ and $p < 0.0001; p = 0.011$.

To investigate the role of age factor in the variability of results, 12 subjects were divided into different age group of 20-29 (4 subjects); 30-39 (4 subjects); 40-60 (4 subjects), hence, each age group has 20 measurement points, and standard unpaired non-parametric (assume no Gaussian distribution) T-test were used to determine whether their results differ significantly based on the separation of age groups. Standard unpaired T-test shows that SC hydration at baseline, when comparing the age group of 20-29 with 30-39, a significant difference was detected ($p < 0.0001$), when comparing the age group of 30-39 with 40-60, a significant difference was also detected ($p < 0.0001$), when comparing the age group of 20-29 with 40-60, no significant difference was detected. After hydrating in water for 40 minutes, all age group showed significant differences with each other ($p < 0.0001, p = 0.0123, p < 0.0001$). After drying in lab for 40 minutes, apart from when comparing the age group of 30-39 with 40-60, other age groups showed significant differences ($p < 0.0001, p < 0.0001$) in SC hydration measured by Corneometer.

SC hydration (AU) measured by Corneometer at various age groups and hydration states			
Hydration state/Age group	20-29 (yrs)	30-39(yrs)	40-60 (yrs)
Before hydration	43.5 ± 9.0	40.6 ± 8.1	25.1 ± 3.5
After hydrating in water for 40 minutes	85.4 ± 6.2	63.5 ± 9.6	72.1 ± 6.3
After drying in lab for 40 minutes	46.9 ± 3.7	39.1 ± 5.9	34.4 ± 11.4

Table 21. SC hydration (AU) [Mean & standard deviation (SD)] for 12 subjects at various hydration states and age group

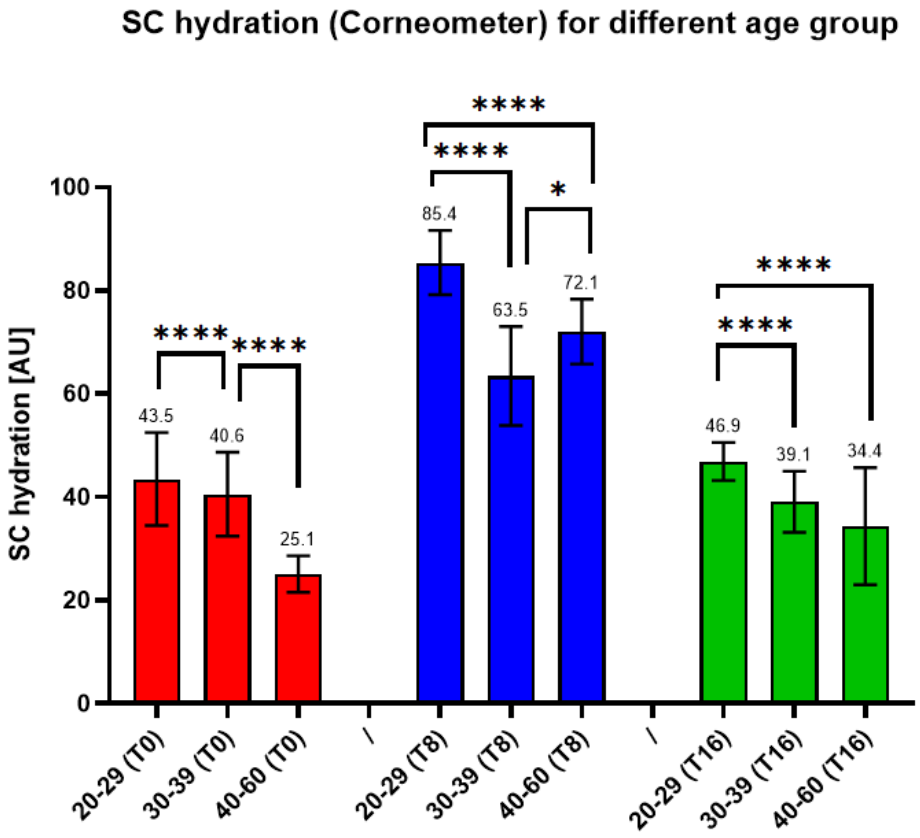

*Figure 47. Unpaired T-test for SC hydration (*AU) [*Mean & standard deviation (SD)] for different age group*

To investigate the role gender factor in the variability of results, 12 subjects were separated into two gender groups of males (8 subjects) and females (4 subjects), and standard unpaired T-test was used to assess whether their SC hydration (Corneometer) significantly differ from each other. As 5 Corneometer repeats were taken per subject, and there are 8 males and 4 females, there are 40 measurements from the male subjects' group and 20 from the female subjects' group for comparison, results are plotted below. As shown in the figures below, no significant differences were detected at baseline and after hydrating in water for 40 minutes, a significant difference was detected after drying in lab for 40 minutes ($p = 0.0002$). The group results are reported below.

SC hydration (AU) measured by Corneometer at various age groups and hydration states		
Hydration state/Gender group	Male	Female
Before hydration	36.2 ± 12.0	36.7 ± 8.3
After hydrating in water for 40 minutes	74.7 ± 9.9	71.6 ± 14.8
After drying in lab for 40 minutes	37.3 ± 9.6	45.8 ± 5.0

Table 22. SC hydration (AU) [Mean & standard deviation (SD)] for 12 subjects at various hydration states and gender group

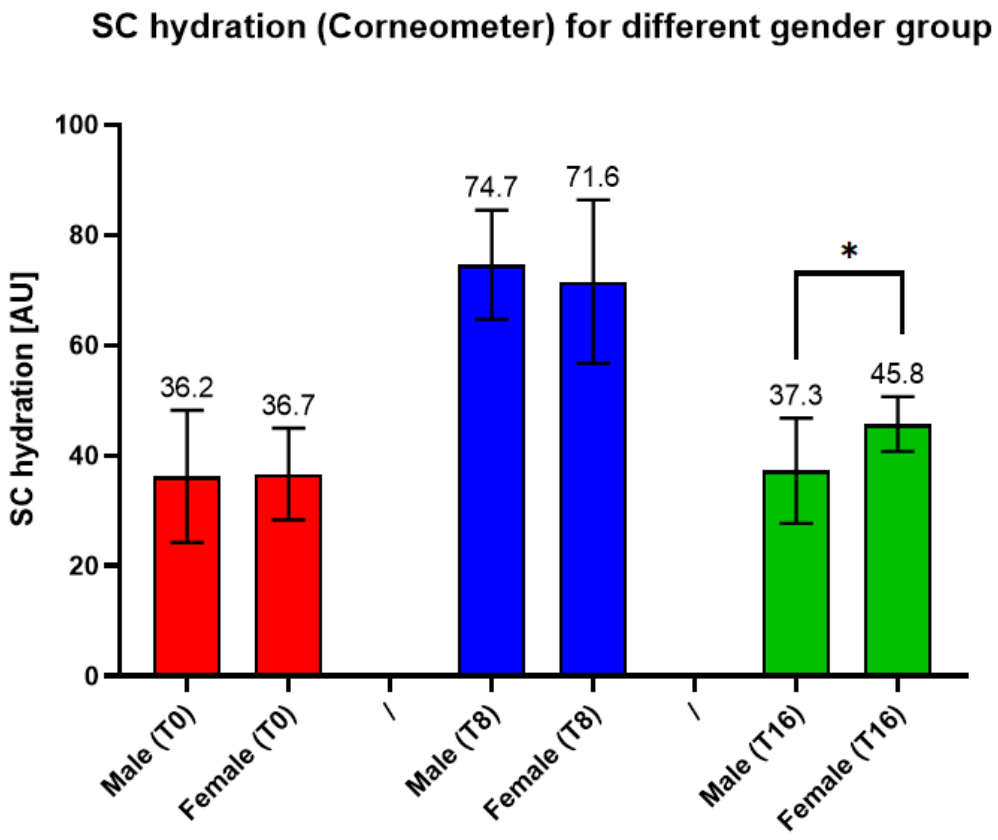

Figure 48. Unpaired T-test for SC hydration (AU) [Mean & standard deviation (SD)] for different gender group

5.33 SC hydration (Corneometer) – hydrating and dehydrating phase

Same as SC reflectance, SC hydration measured by Corneometer measurements was also gathered at every time interval during hydrating and dehydrating phase, and for 12 subjects who completed their experiment in autumn/winter season, their SC hydration at hydrating (experiment time: 0 minutes □ 40 minutes) and dehydrating (experiment time: 40 minutes □ 80 minutes) phase are plotted below with non-linear models of One-phase association for hydrating phase and One-phase decay for dehydrating phase. To recall, the mathematical model for One-phase association follows the equation of:

$$Y = Y0 + (Plateau - Y0) * (1 - exp\ (-K * x)\ ) \quad \textbf{(40)}$$

Where: $Y0$ is the Y value, here SC hydration, when time is zero, i.e., at baseline, and it is expressed as the same unit as Y; $Plateau$ is the Y value at infinite times, and it is also expressed as the same unit as Y; K is the rate constant, and it is expressed in reciprocal of the time, here as $1/min$; Tau is the time constant, and it is computed as the reciprocal of K; $Span$ is the difference between $Y0$ and $Plateau$, and it is expressed in the same unit as the Y value. And the mathematical model of One-phase decay for dehydrating phase is very similar to One-phase association and it follows the equation of:

$$Y = (Y0 - Plateau) * exp\ (-K * x) + Plateau \qquad \textbf{(42)}$$

And the notation for the parameters is the same as One-phase association. The models graphically are plotted below, and for 12 subjects, their SC hydration with corresponding nonlinear exponential models is also plotted below. The parameters of the model for each subject during both phases are reported in the tables below.

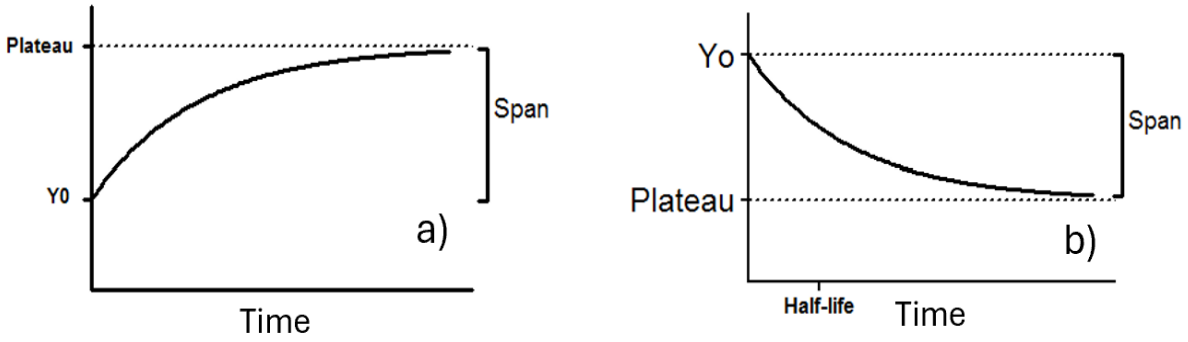

Figure 49. a) Exponential model – One-phase association; b) exponential mode – One-phase decay

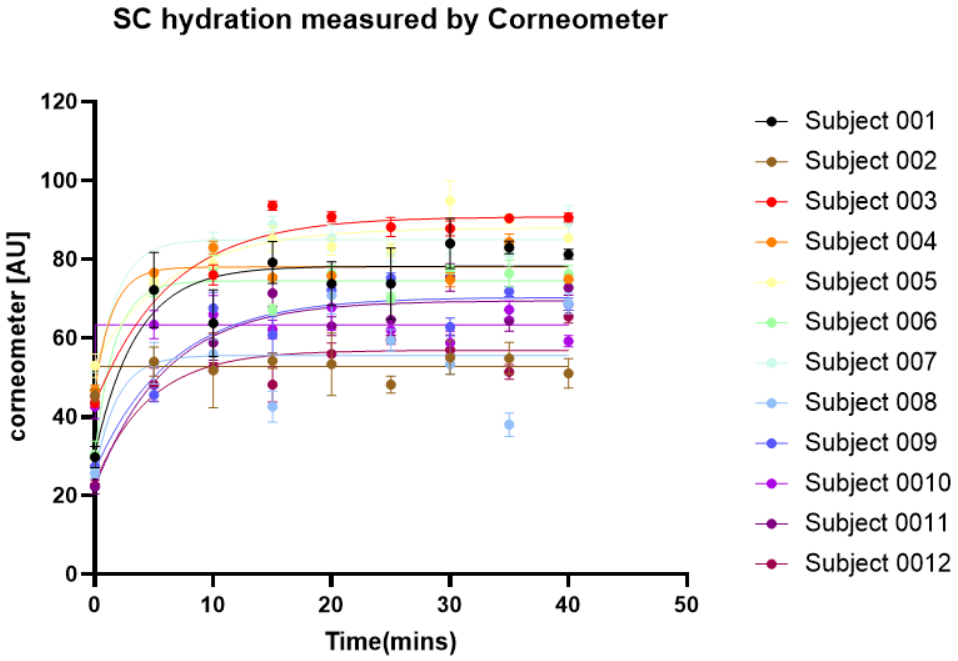

Figure 50. SC hydration [Mean & standard deviation (SD)] at hydrating phase during autumn/winter season

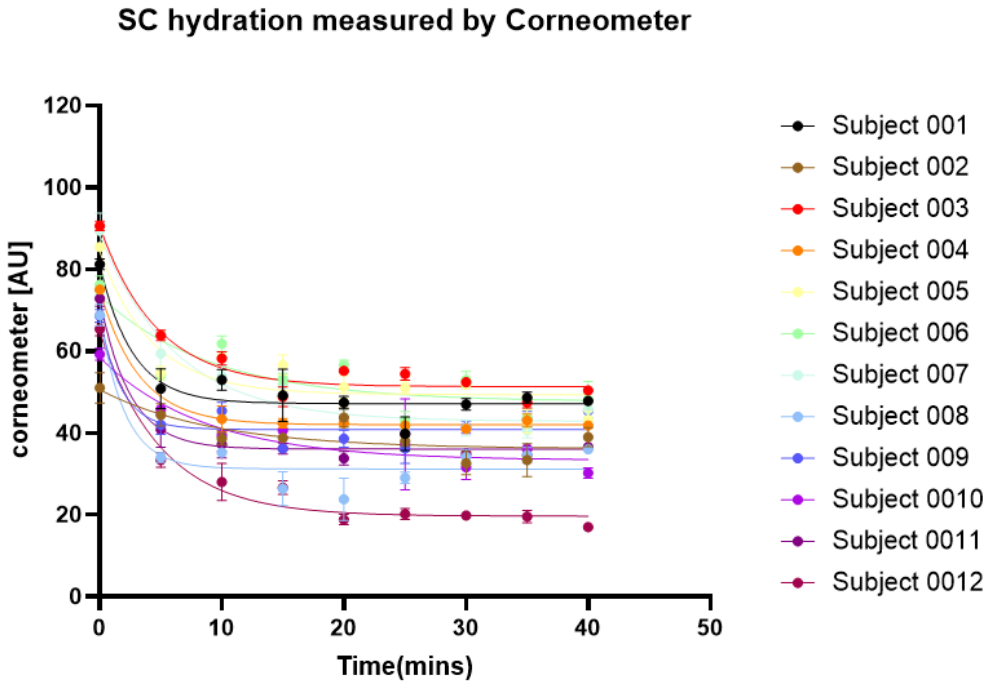

Figure 51. SC hydration [Mean & standard deviation (SD)] at dehydrating phase during autumn/winter season

12 subjects' SC hydration results at hydrating phase & exponential fit model parameters					
Subject number	$Y0$(AU)	$Plateau$(AU)	Tau(mins)	$Span$(AU)	Rate constant
001	30.5	78.2	3.8	47.7	0.28
002	50.3	NA	11.9	NA	NA
003	43.3	70.8	6.3	47.5	0.15
004	46.8	78.0	1.5	31.2	0.67
005	53.7	88.0	6.6	34.3	0.15
006	30.4	74.5	1.7	44.1	0.59
007	47.0	85.0	1.9	38.0	0.53
008	25.7	55.6	1.9	29.9	0.53
009	26.4	70.4	6.4	43.9	0.15
0010	56.8	NA	4.7	NA	NA
0011	22.2	69.5	6.0	47.3	0.16
0012	23.2	56.9	4.6	33.7	0.21

Table 23. 12 subjects' SC hydration results with its' one phase model association fit parameters during hydrating phase at autumn/winter season

12 subjects' SC hydration results at dehydrating phase & exponential fit model parameters					
Subject number	$Y0$(AU)	$Plateau$(AU)	Tau(mins)	$Span$(AU)	Rate constant
001	81.1	47.2	2.7	33.9	0.37
002	50.6	36.1	9.4	14.5	0.10
003	90.5	51.3	4.7	39.2	0.21
004	75.0	42.0	3.2	33.0	0.31
005	84.4	49.4	4.3	35.0	0.23
006	73.5	47.6	9.3	25.9	0.10
007	88.5	42.8	6.2	45.6	0.16
008	68.8	31.2	2.1	37.6	0.48
009	68.6	40.9	1.8	27.7	0.57
0010	58.5	33.3	8.5	25.2	0.11
0011	72.3	36.1	2.5	36.7	0.40
0012	64.7	19.6	5.1	45.1	0.19

Table 24. 12 subjects' SC hydration results with its' one phase model association fit parameters during dehydrating phase at autumn/winter season

5.4 Correlation between results

5.41 SC thickness Vs SC reflectance at baseline, after hydrating in water for 40 minutes and after drying in lab for 40 minutes

As we believe that SC reflectance measurements quantified by the VIS-OCT system may indicate information about subjects' SC hydration, as the back-scattered intensity of this layer increases as we hydrate it. In addition, literature has stated one's SC thickness is associated with its hydrational state, for 15 subjects, their SC thickness and SC reflectance measurements are investigated in this chapter to explore whether they correlate with each other. The results of this chapter are discussed in the later discussion chapters. For 15 subjects, Nonparametric Spearman's correlation test was performed on 15 subjects' SC thickness and reflectance at time intervals of baseline (T0), after hydrating in water for 40 minutes (T8) and after drying in lab for 40 minutes (T16), and results are plotted in figure 53,54,and 55. As shown in the figures, where each dot represents a comparison of 16,000 - 32,000 A-scan averages, results show that at baseline, no significant correlation was detected between subjects' SC thickness

and SC reflectance measurements. After hydrating in water for 40 minutes, a negative correlation was detected with a corresponding Spearman's correlation coefficient $r = -0.5827, p = 0.0248(*)$. After drying in lab for 40 minutes, a significant negative correlation was again detected between subjects' SC thickness and SC reflectance measurements with a corresponding Spearman's correlation coefficient $r = -0.6750, p = 0.0072(**)$.

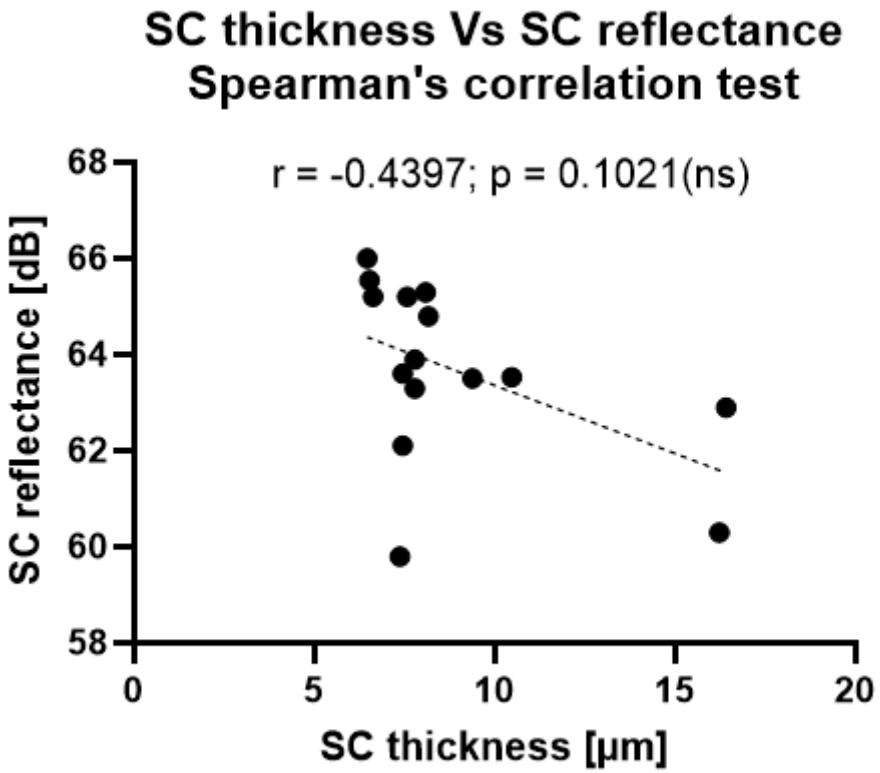

Figure 52. SC thickness Vs SC reflectance (Spearman's correlation test) at baseline

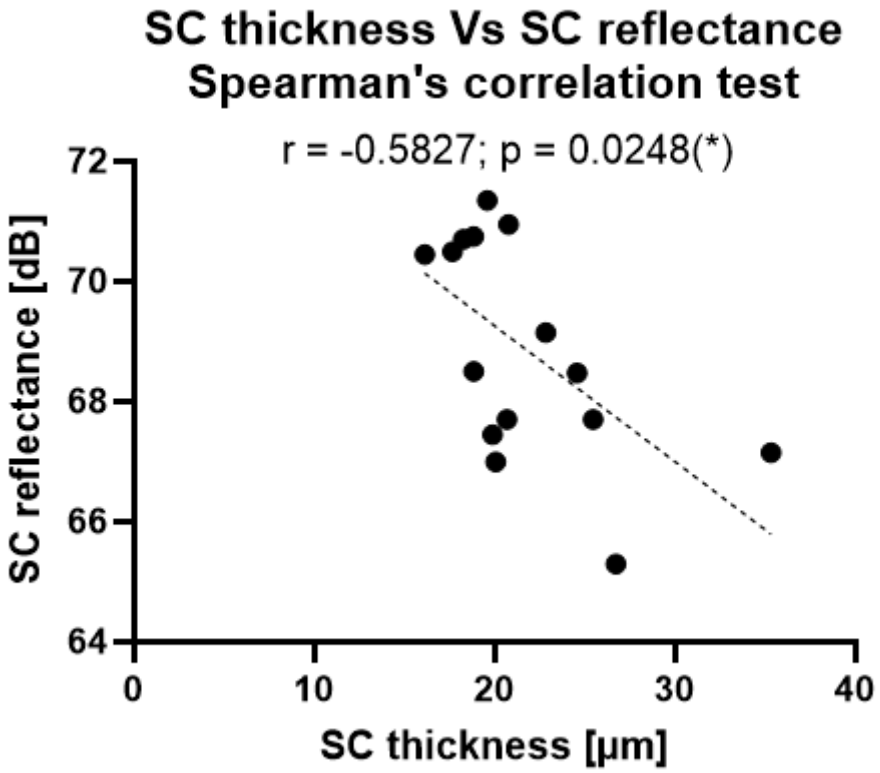

Figure 53. SC thickness Vs SC reflectance (Spearman's correlation test) after hydrating in water for 40 minutes

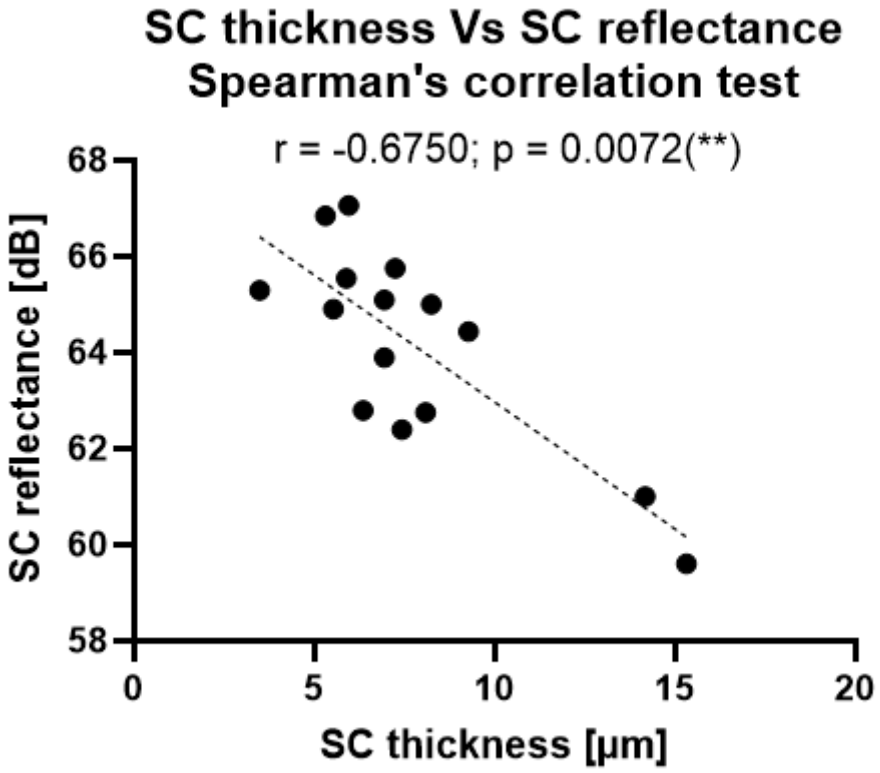

Figure 54. SC thickness Vs SC reflectance (Pearson's correlation test) after drying in lab for 40 minutes

Although a significant negative correlation is found between 15 subjects' SC thickness and reflectance at T8 and T16, looking at the plots, their results seems to be dominated by two particular points (outliers), hence, a new analysis with these two outliers (subject 0010 and subject 0015) removed is plotted below. As shown in figure 56, 57 and 58, although a negative correlation is detected between 13 subjects' SC thickness and reflectance, the correlation is not statistically significant.

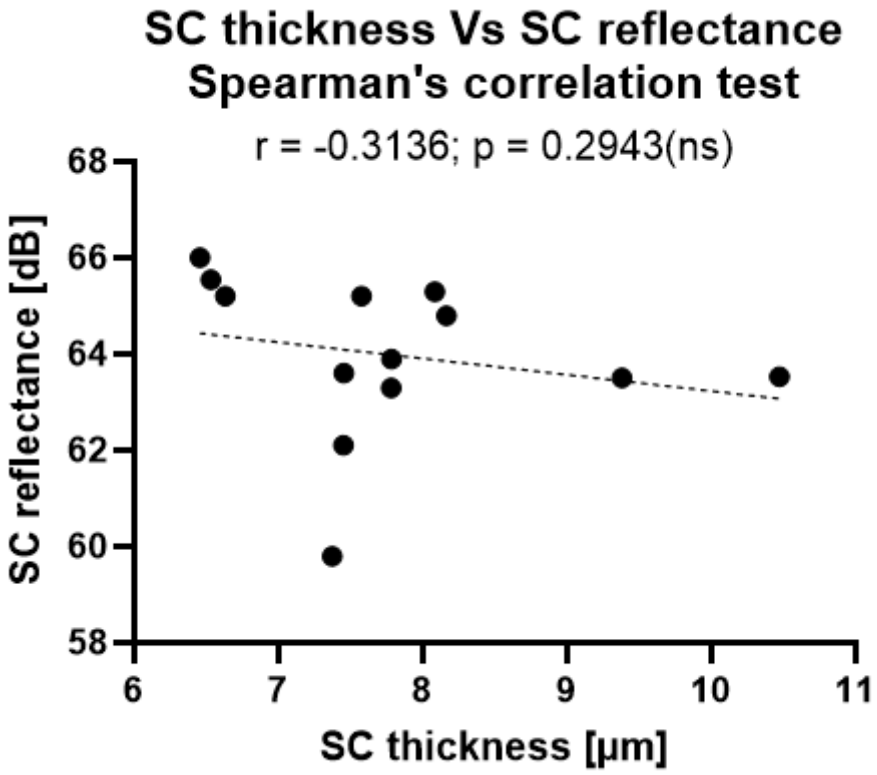

Figure 55. SC thickness Vs SC reflectance (Spearman's correlation test) at baseline with outliers removed

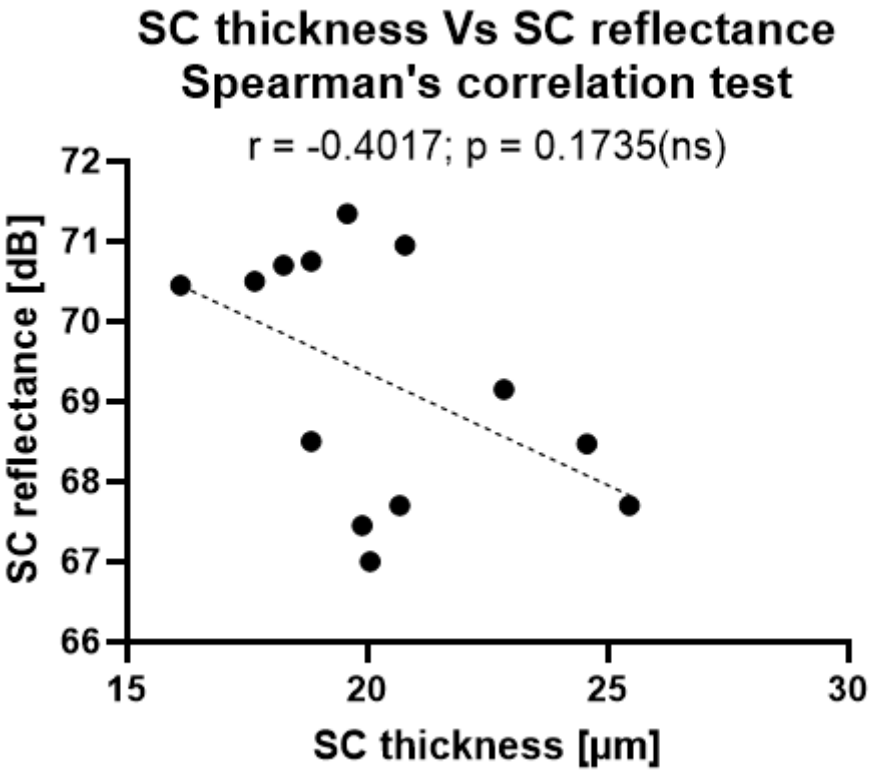

Figure 56. SC thickness Vs SC reflectance (Spearman's correlation test) after hydrating in water for 40 minutes with outliers removed

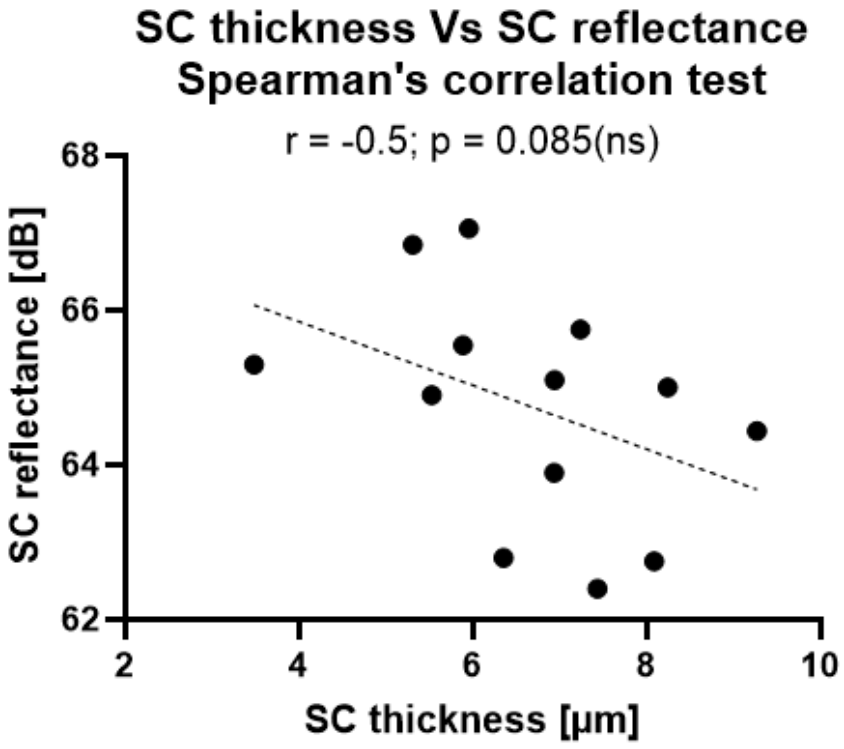

Figure 57. SC thickness Vs SC reflectance (Spearman's correlation test) after drying in lab for 40 minutes with outliers removed

5.42 SC thickness Vs SC hydration (Corneometer) at baseline, after hydrating in water for 40 minutes and after drying in lab for 40 minutes

Same as the previous chapter where subjects' SC thickness was investigated with their SC reflectance measurements, in this chapter, SC thickness results quantified from VIS-OCT system are compared with SC hydration measured by Corneometer for correlation analysis. As Corneometer only became available to the author during autumn/winter season, the comparison was only done for subjects who completed the experiment in autumn/winter season. For 12 subjects who completed the experiment in autumn/winter season, their SC thicknesses and SC hydrations measured by Corneometer with associated Spearman's correlation analysis are plotted below. As shown in the figures, where each dot represents a comparison between 16,000 A-scans' average of SC thickness with 5 Corneometer measurements' average, at baseline, using nonparametric Spearman's correlation test, a significant negative correlation was detected between subjects' SC thickness and SC hydration with a corresponding Pearson's correlation coefficient $r = -0.6084, p = 0.0399(*)$. After hydrating in water for 40 minutes, no significant correlation was detected and after drying in the lab for 40 minutes, no significant correlation was detected.

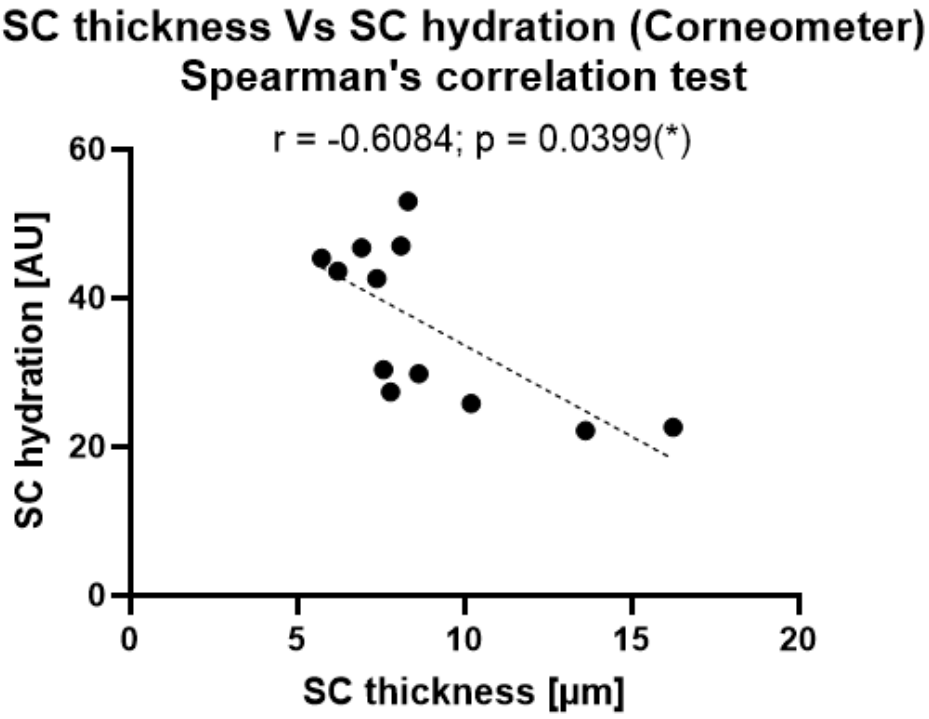

Figure 58. SC thickness Vs SC hydration measured by Corneometer (Spearman's correlation test) at baseline

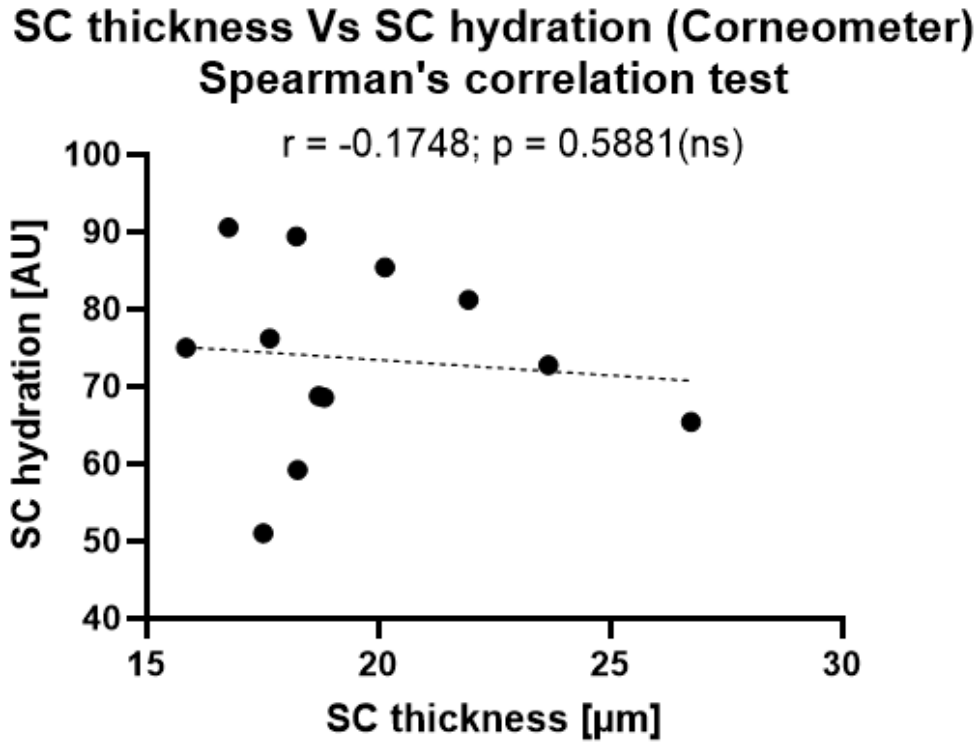

Figure 59. SC thickness Vs SC hydration measured by Corneometer (Spearman's correlation test) after hydrating in water for 40 minutes

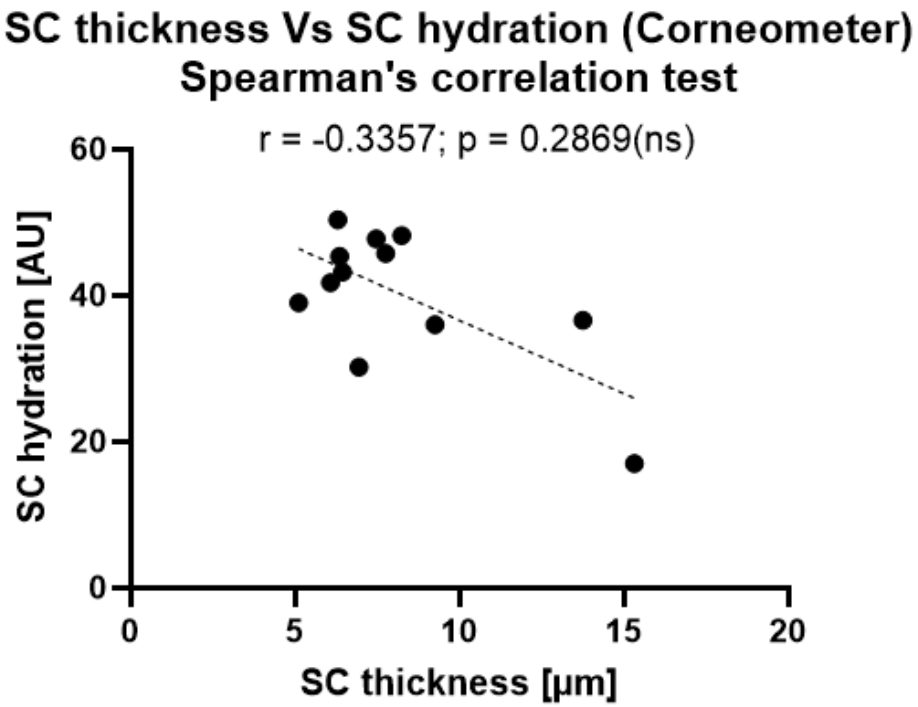

Figure 60. SC thickness Vs SC hydration measured by Corneometer (Spearman's correlation test) after drying in lab for 40 minutes

Similar to the previous analysis where SC thickness was investigated with SC reflectance, looking at the plots, the results of these correlations seem to be dominated by two particular points of outliers. Hence, a new analysis with these outliers removed is performed and plotted in figure 63, 64 and 65. As shown in these figures, a non-significant negative correlation was found between SC thickness and SC hydration measured by Corneometer at baseline, however, no correlation was detected after hydrating in water for 40 minutes and after drying in the lab for 40 minutes.

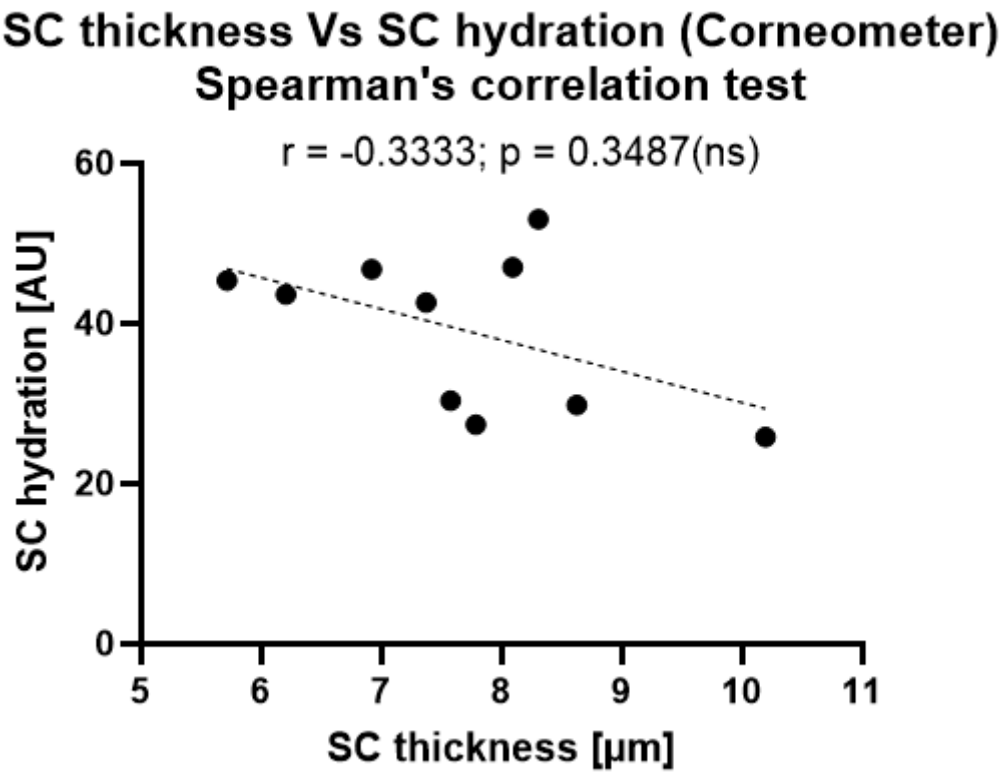

Figure 61. SC thickness Vs SC hydration measured by Corneometer (Spearman's correlation test) at baseline with outliers removed

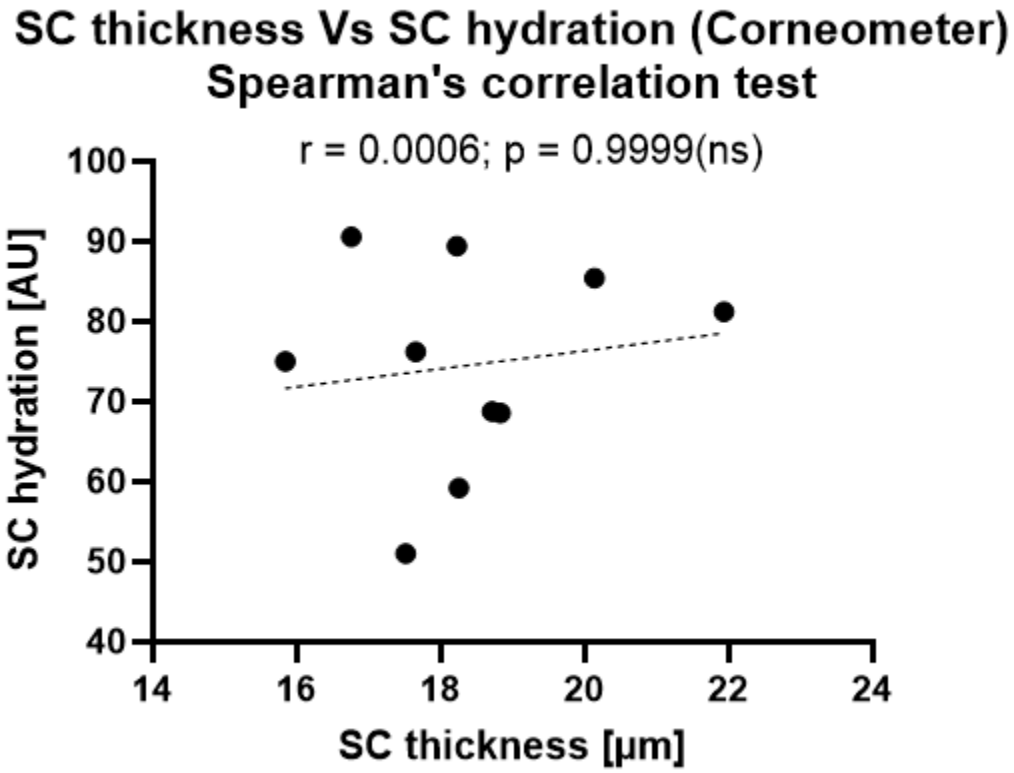

Figure 62. SC thickness Vs SC hydration measured by Corneometer (Spearman's correlation test) after hydrating in water for 40 minutes with outliers removed

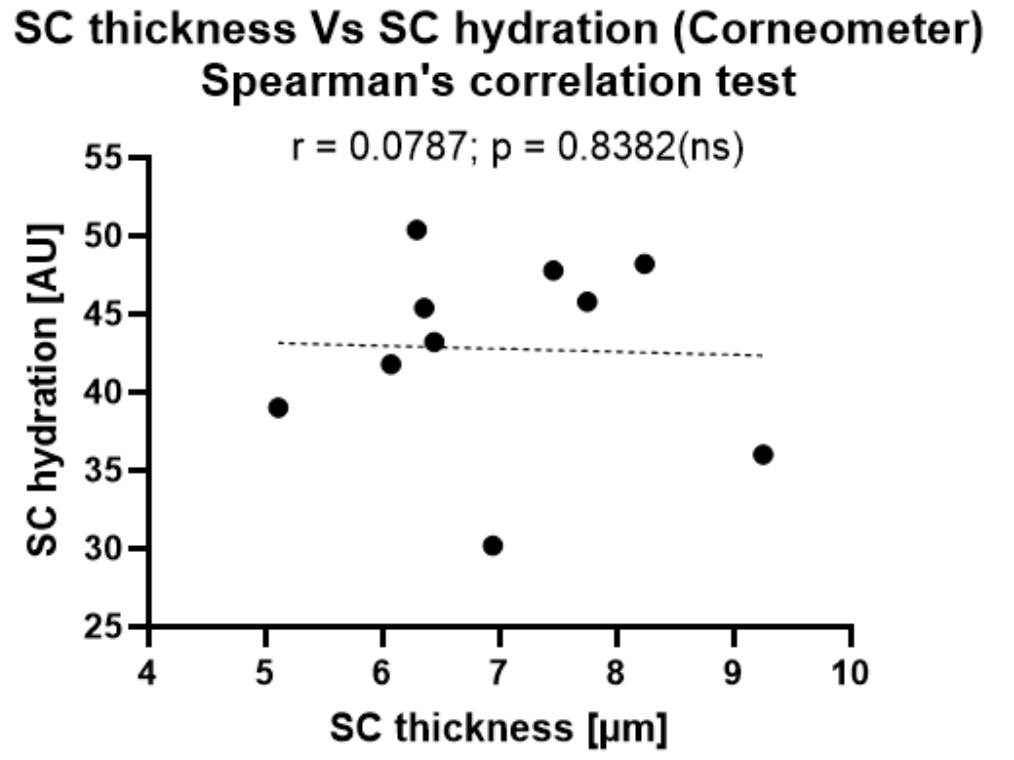

Figure 63. SC thickness Vs SC hydration measured by Corneometer (Spearman's correlation test) after drying in lab for 40 minutes with outliers removed

5.43 SC reflectance Vs SC hydration (Corneometer) at baseline, after hydrating in water for 40 minutes and after drying in lab for 40 minutes

As SC reflectance measurements and SC hydration measurements measured by Corneometer were obtained at each time interval during the hydrating and dehydrating phases, the correlations which take all time intervals into account will be explained in later chapters. In this chapter, SC reflectance and SC hydration measure by Corneometer at 3 distinct time intervals of: at baseline, after hydrating in water for 40 minutes and after drying in lab for 40 minutes assessed. See figures plotted below, where each dot represents a comparison between 16,000 A-scans' average of SC reflectance with 5 Corneometer measurements' average, at baseline, after hydrating in water for 40 minutes and after hydrating in water for 40 minutes, no significant correlations were observed.

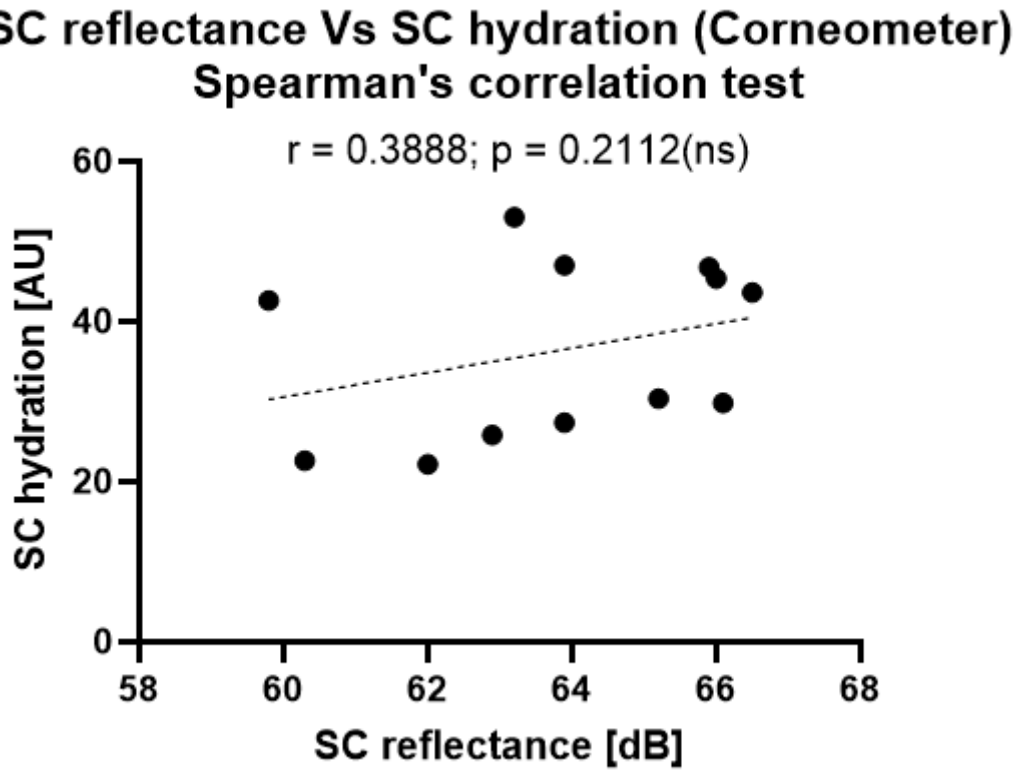

Figure 64. SC reflectance Vs SC hydration measured by Corneometer (Spearman's correlation test) at baseline

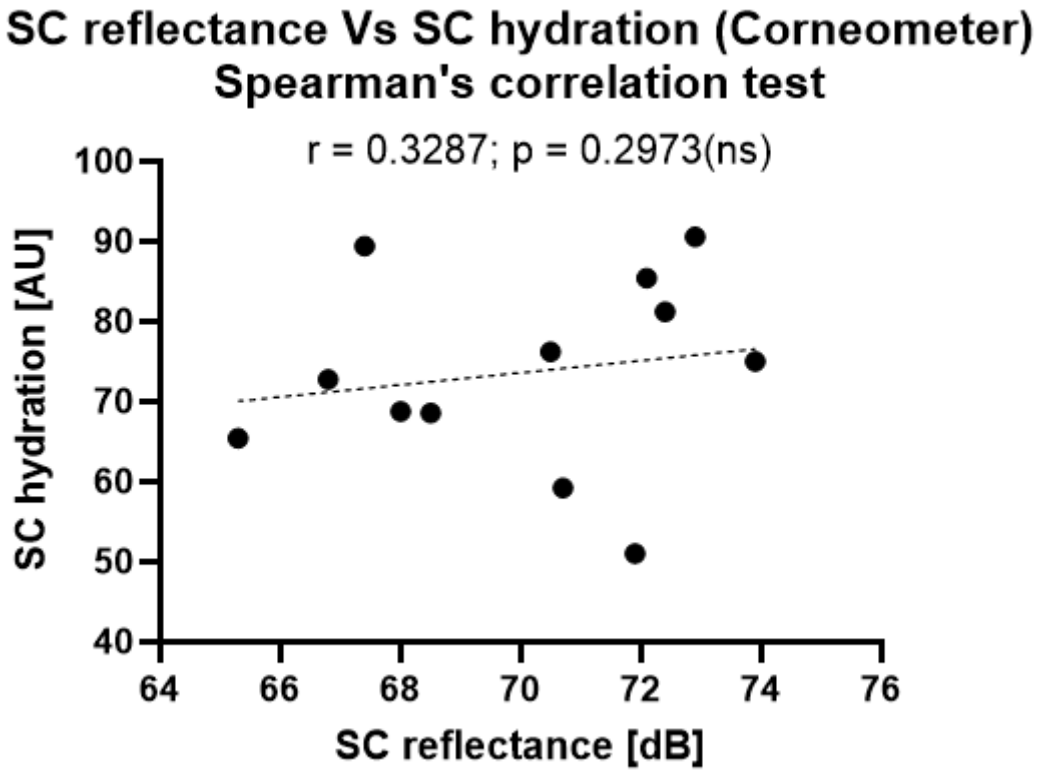

Figure 65. SC reflectance Vs SC hydration measured by Corneometer (Spearman's correlation test) after hydrating in water for 40 minutes

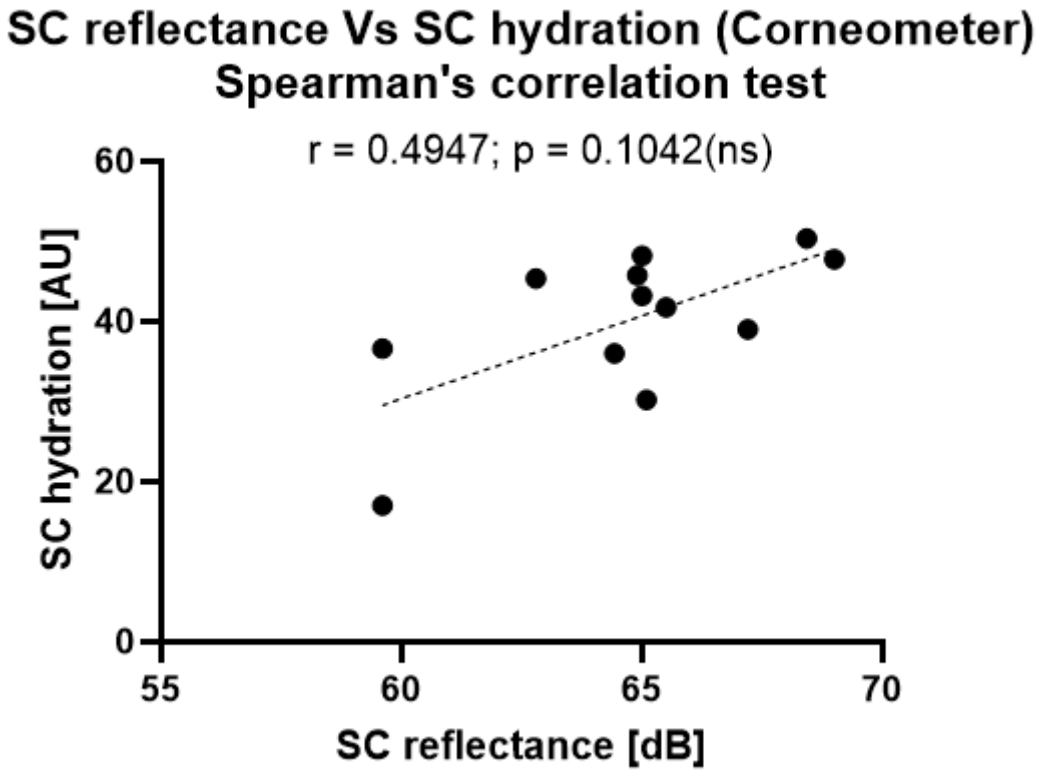

Figure 66. SC reflectance Vs SC hydration measured by Corneometer (Spearman's correlation test) after drying in lab for 40 minutes

5.44 SC reflectance Vs SC hydration (Corneometer) at hydrating phase and dehydrating phase

Previously described, SC reflectance and SC hydration (Corneometer) measurements were gathered at every time interval throughout the experiment in autumn/winter season, and individual results of how they change with time during hydrating and dehydrating phases are reported in previous chapters, in this chapter, group results of how they correlate with each other are investigated.

To start, SC reflectance and SC hydration (Corneometer) group results during hydrating phase are plotted below with a fitted exponential model (One-phase association), in the figure of SC reflectance, each dot represents 192,000 A-scans' average (16,000 A-scans * 12 subjects); and in the figure of SC hydration (Corneometer), each dot represents 60 Corneometer measurements' average (5 measurements * 12 subjects). The shape of these curve can be traced back to the explanation of the diffusion process of water molecule entering SC previously, where, during the hydrating phase (experiment time: 0 minutes 40 minutes), water molecule is diffused into the SC as the water concentration in the bucket of water is higher than the inside of SC. The initial stage of the diffusion process is expected to take place quickly, in later stages, as the water concentration increases in the SC, the diffusion speed is expected to slow down and then reach a steady state as it becomes saturated. This response will be reflected as a nonlinear curve which resembles the model of One phase association model.

Based on this model, it was found that the time constant Tau for SC reflectance is ~ 3.9 mins, in other words, the time where SC reflectance for 12 subjects to reach its' saturation state is ~ 3.9 mins. Likewise, the time constant Tau SC hydration (Corneometer) is ~ 2.4 mins, hence, the time that it takes for 12 subjects' SC to reach their fully hydrated state is ~2.4 mins.

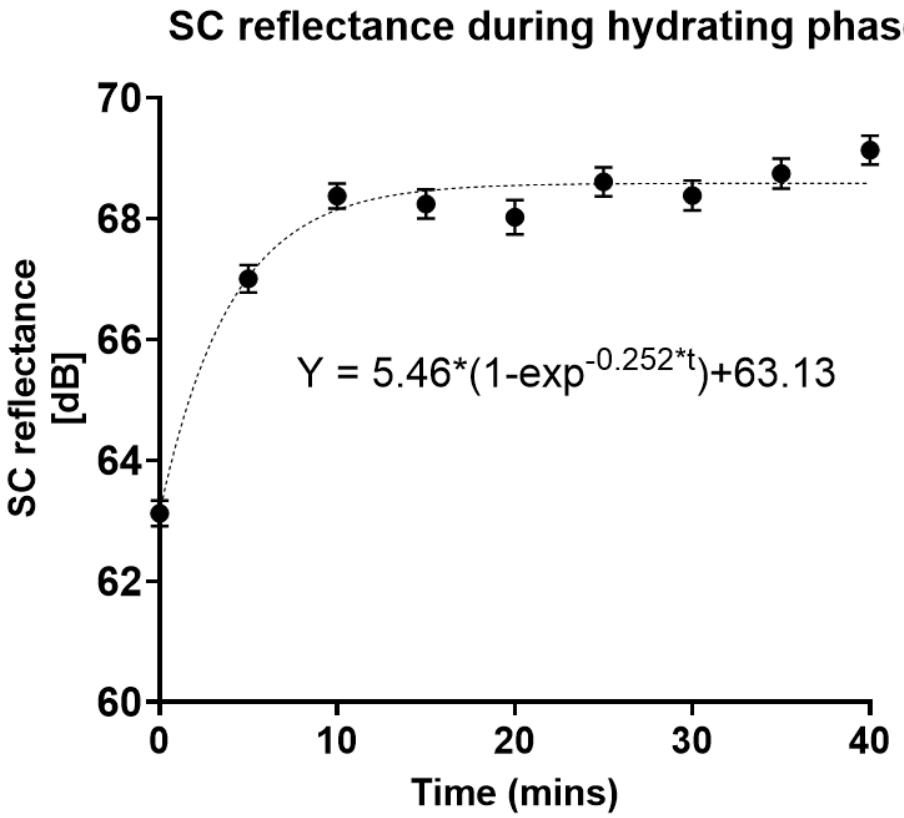

Figure 67. SC reflectance [Mean & standard error (SEM)] at hydrating phase

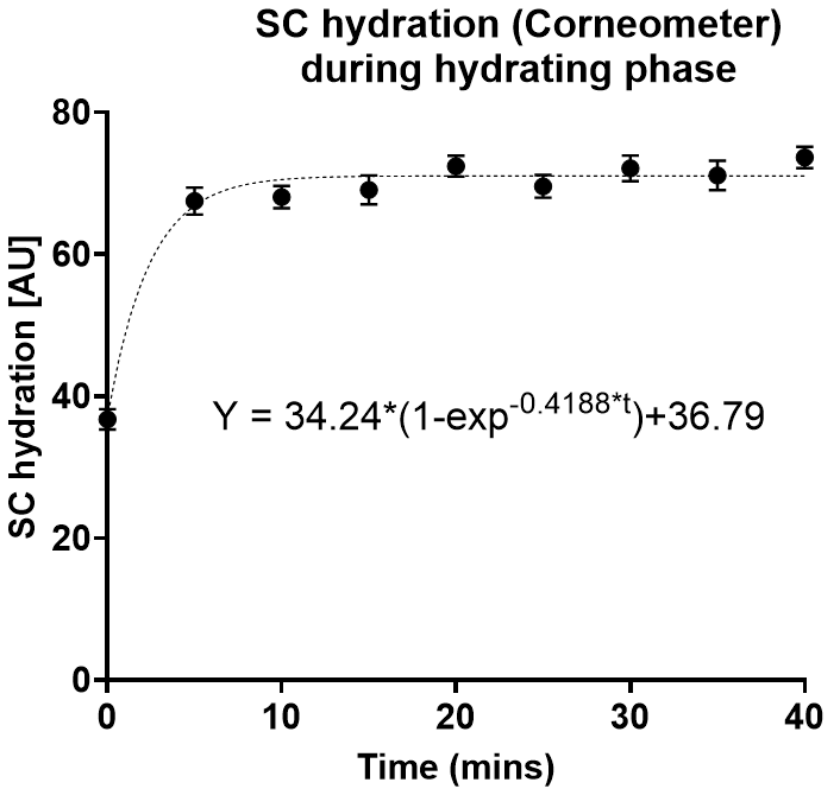

Figure 68. SC hydration measured by Corneometer [Mean & standard error (SEM)] at hydrating phase

To assess for these 12 subjects, whether their SC reflectance correlate with their SC hydration (Corneometer) at all 9-time intervals during hydrating phase (0 mins – T0, 5 mins – T1, 10 mins – T2, …, 40 mins - T9). See figure 71, where each dot represents a comparison between 192,000 A-scans' average with 60 Corneometer measurements' average at each time interval, Spearman's correlation test results showed that a non-significant positive correlation was detected with a corresponding correlation coefficient $r = 0.6833, p = 0.0503$.

As shown in this figure, it is clear that the correlation seems to be dominated by a comparison at T0, in order to get a vision whether this correlation still stands without this 'outlier's domination, a new analysis is performed with T0's comparison removed, and it is plotted in figure 72. Interestingly, with the outlier value at T0 removed, a significant positive correlation is detected between SC reflectance and SC hydration measured by Corneometry with a corresponding correlation coefficient $r = 0.7857, p = 0.0279(*)$.

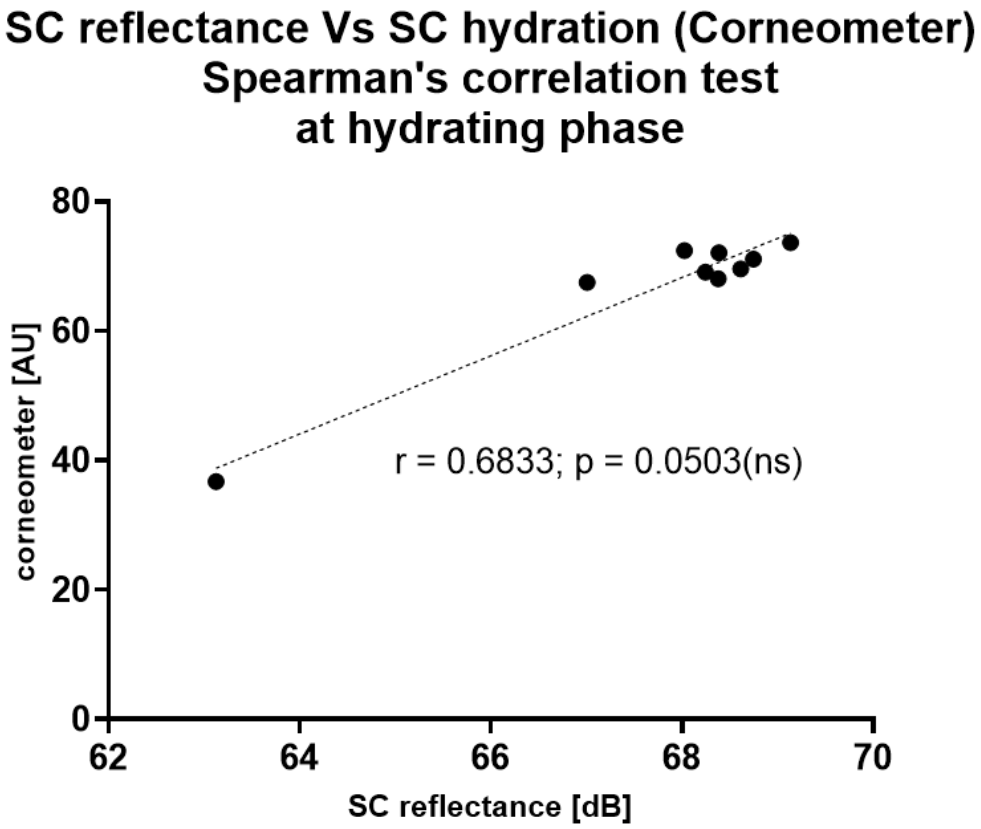

Figure 69. Spearman's correlation test for SC reflectance vs SC hydration measured by Corneometer at hydrating phase

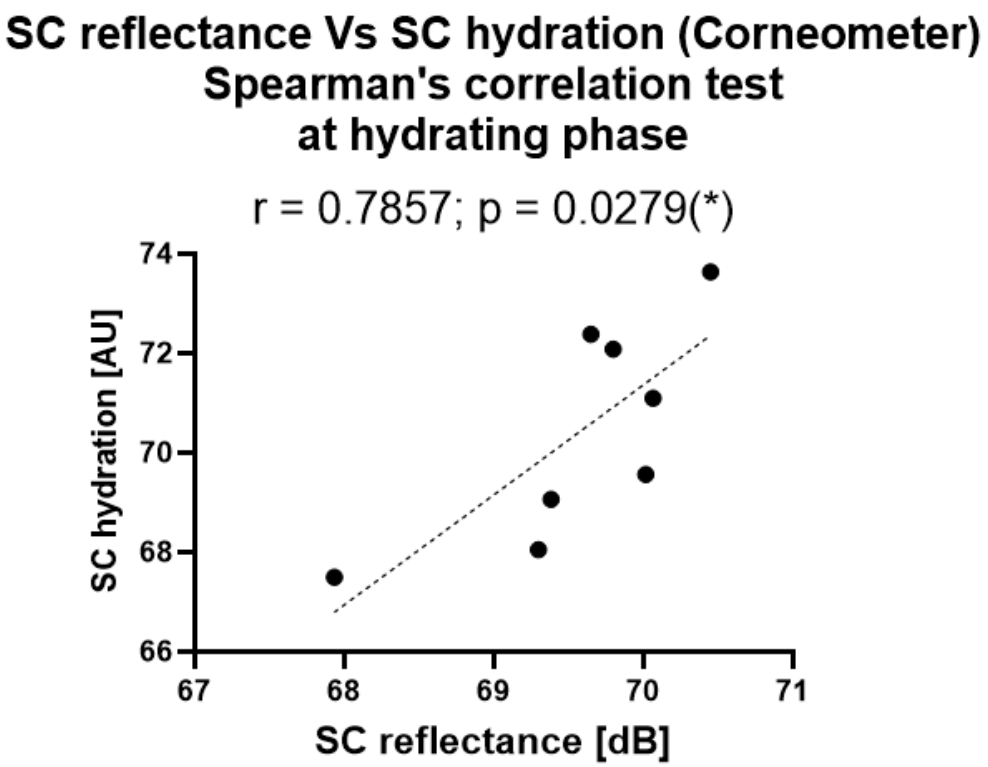

Figure 70. Spearman's correlation test for SC reflectance vs SC hydration measured by Corneometer at hydrating phase with 'outlier' removed.

When breaking down to each time interval and using 5 B-scans to compare with 5 Corneometer measurements for 12 subjects (n = 60), for each time interval from 0 mins to 40 mins (T0 – T8), The results are plotted in figure 73-81. As shown in these figures, 60 comparisons are plotted using 5 B-scans and 5 Corneometer readings from 12 subjects, then, a correlation test is performed with its corresponding correlation coefficient and significance value stated in these plots, and this is done for each time interval during hydrating phase. As shown, Spearman's correlation test showed expect at T8 (40 minutes of hydrating in water), SC reflectance and SC hydration (Corneometer) for 12 subjects showed significant positive correlations with each other, indicating when there is an increase in the SC reflectance value, there is an increase in the SC hydration value measure by Corneometer.

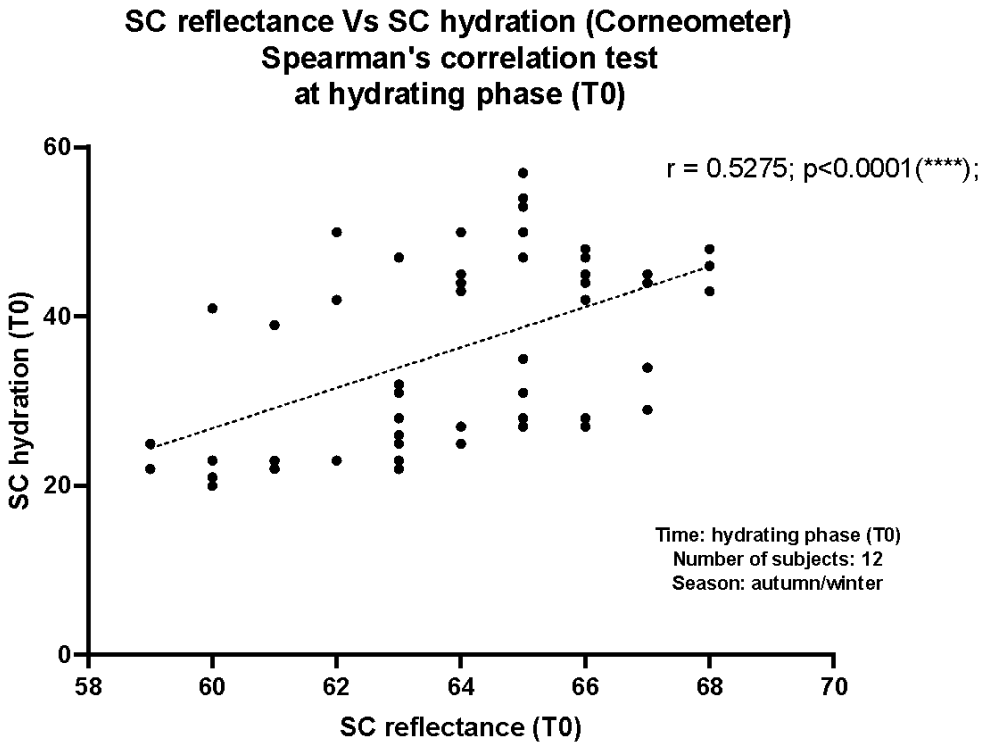

Figure 71. Spearman's correlation test for SC reflectance vs SC hydration measured by Corneometer at hydrating phase (T0)

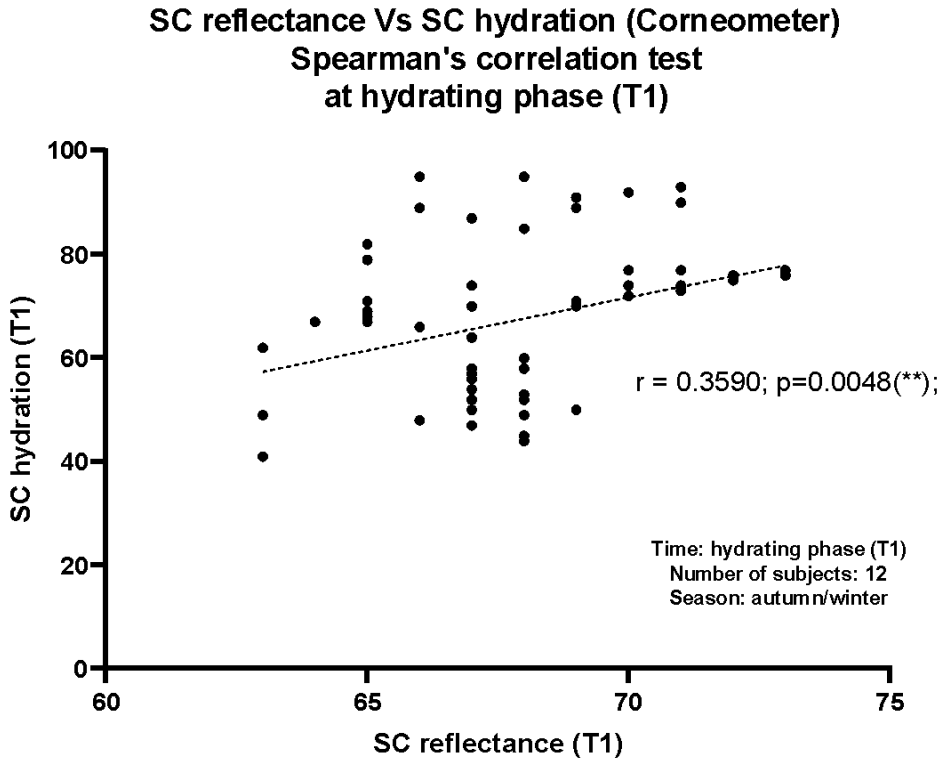

Figure 72. Spearman's correlation test for SC reflectance vs SC hydration measured by Corneometer at hydrating phase (T1)

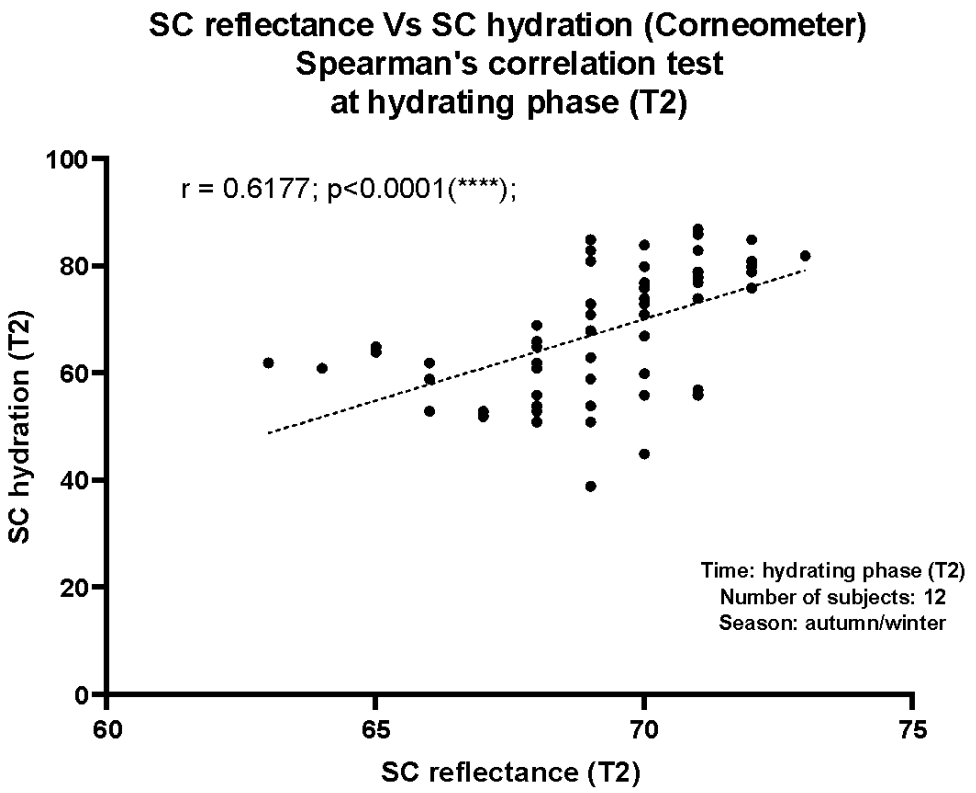

Figure 73. Spearman's correlation test for SC reflectance vs SC hydration measured by Corneometer at hydrating phase (T2)

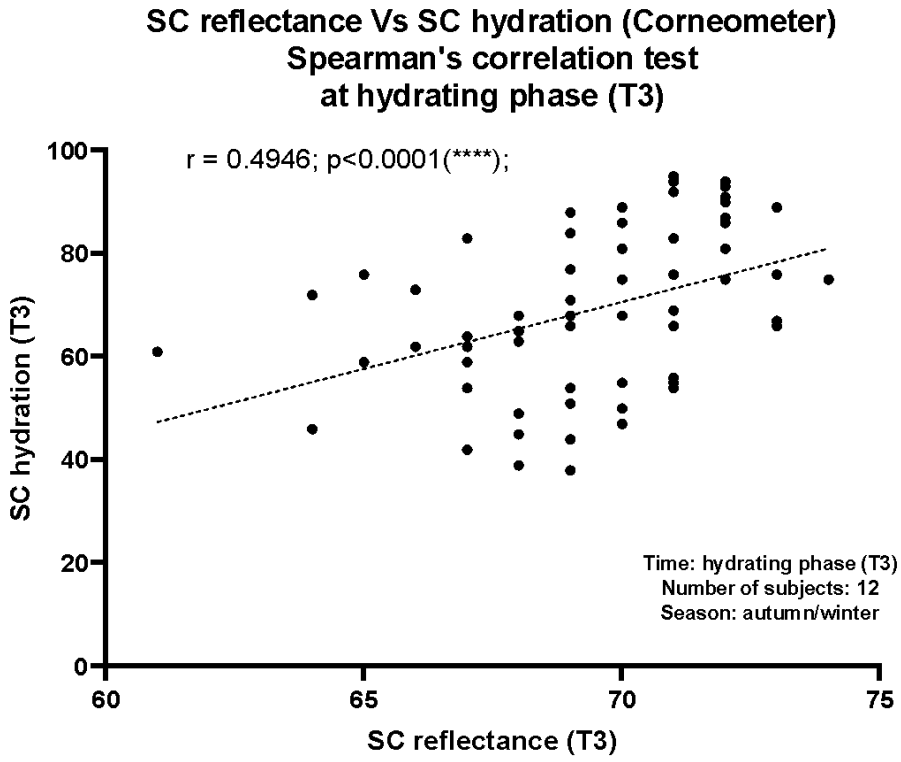

Figure 74. Spearman's correlation test for SC reflectance vs SC hydration measured by Corneometer at hydrating phase (T3)

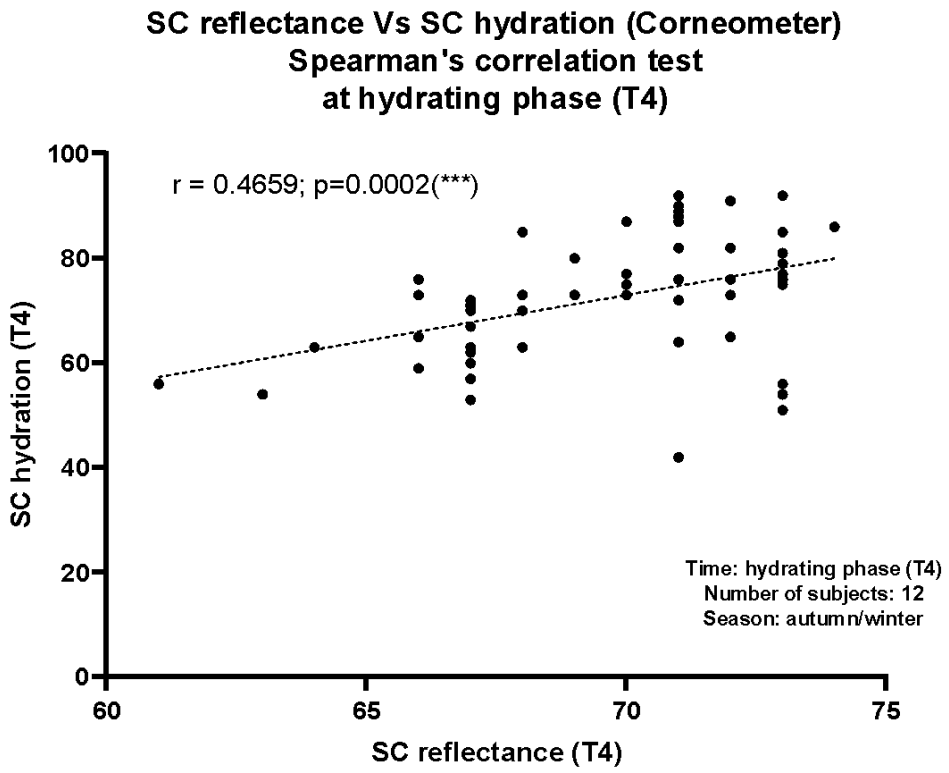

Figure 75. Spearman's correlation test for SC reflectance vs SC hydration measured by Corneometer at hydrating phase (T4)

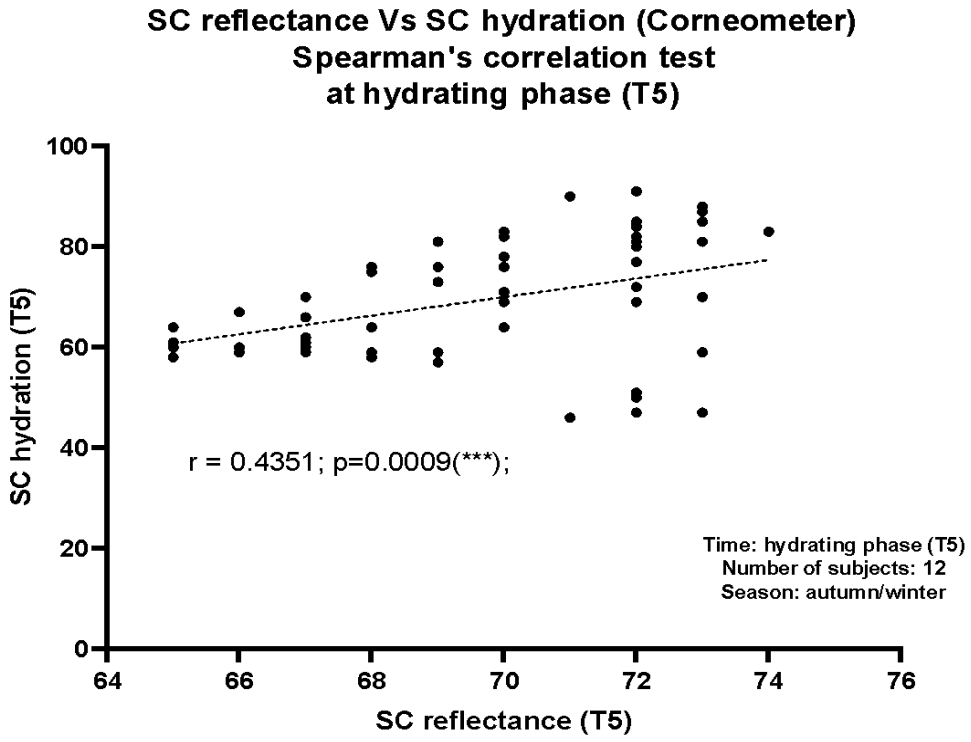

Figure 76. Spearman's correlation test for SC reflectance vs SC hydration measured by Corneometer at hydrating phase (T5)

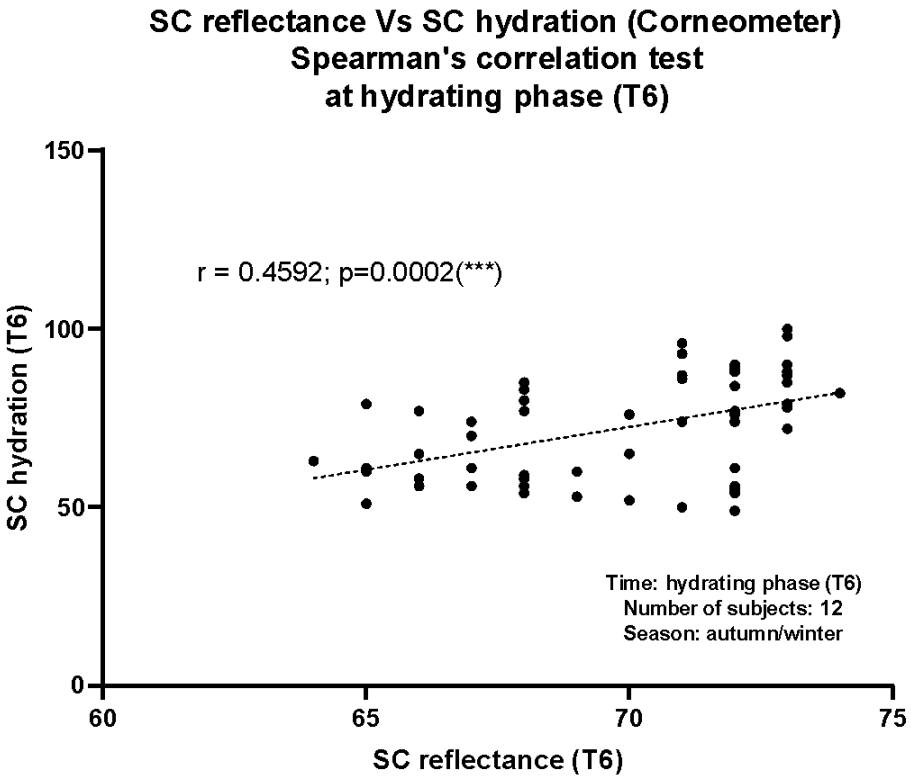

Figure 77. Spearman's correlation test for SC reflectance vs SC hydration measured by Corneometer at hydrating phase (T6)

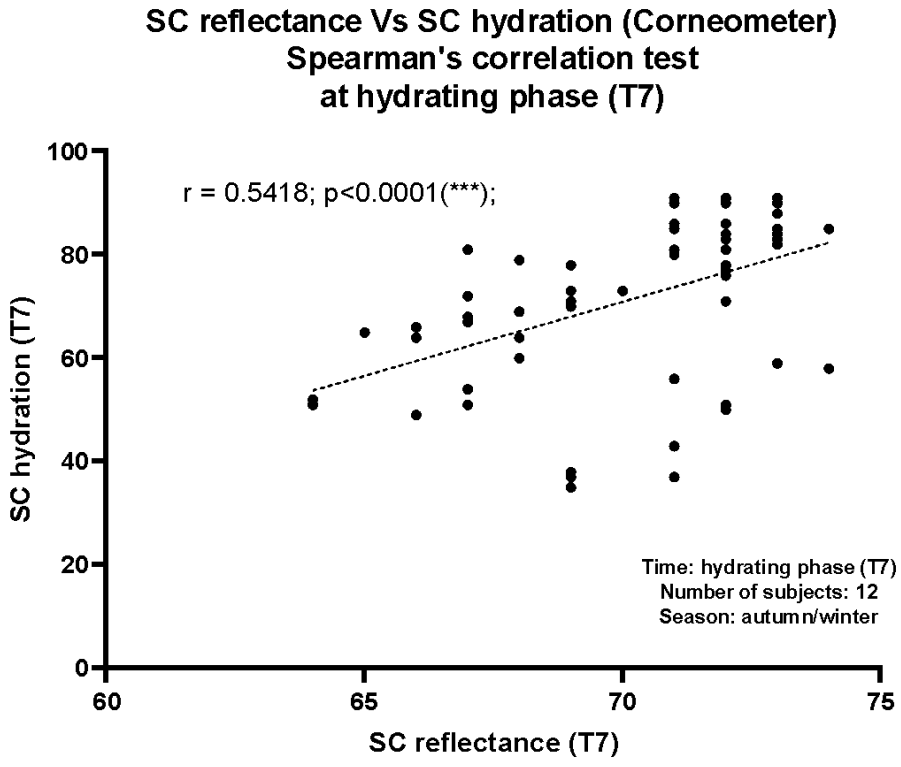

Figure 78. Pearson's correlation test for SC reflectance vs SC hydration measured by Corneometer at hydrating phase (T7)

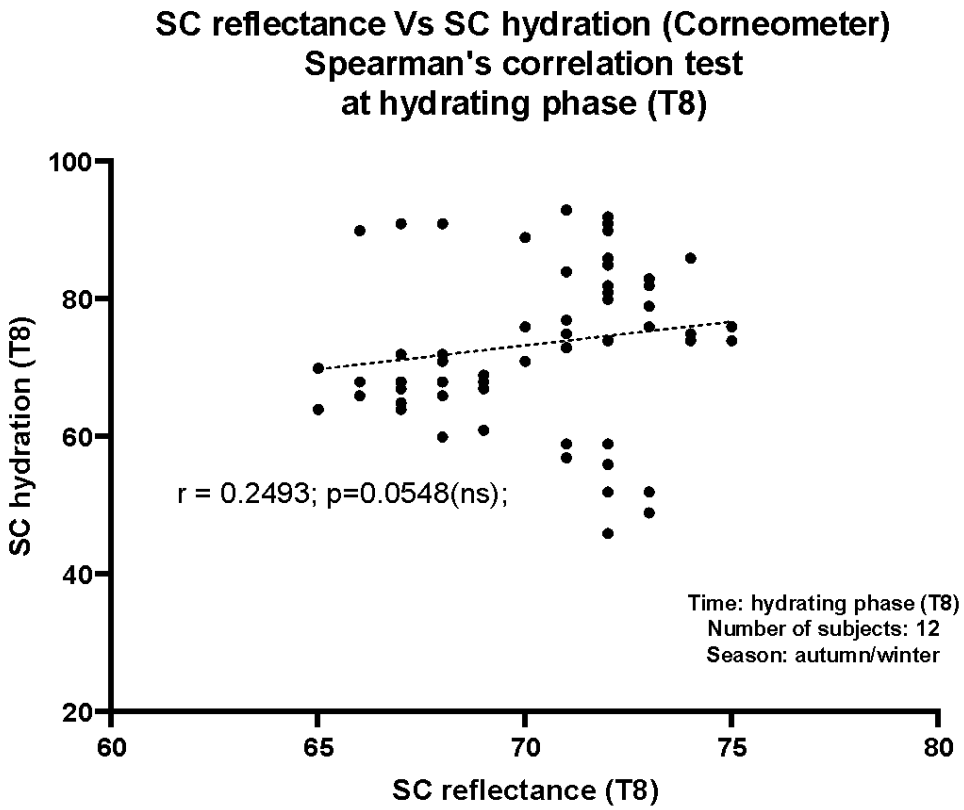

Figure 79. Spearman's correlation test for SC reflectance vs SC hydration measured by Corneometer at hydrating phase (T8)

During dehydrating phase (45 mins – T9, 50 mins – T10, 55 mins – T11, …, 80 mins; in graph denote as 0 mins – T8, 5 mins – T9, …., 80 mins - T16), SC reflectance and SC hydration (Corneometer) group results during dehydrating phase are plotted below with a fitted exponential model (One-phase decay), likewise, in the figure of SC reflectance, each dot represents 192,000 A-scans' average (16,000 A-scans * 12 subjects); and in the figure of SC hydration (Corneometer), each dot represents 60 Corneometer measurements' average (5 measurements * 12 subjects). Based on the one phase decay model fit, it was found that the time constant Tau for SC reflectance is ~ 28.6 mins, in other words, the time where SC reflectance for 12 subjects return to its original state is ~ 28.6 mins. Likewise, the time constant Tau SC hydration (Corneometer) is ~ 3.7 mins, hence, the time that it takes for 12 subjects' SC to return to its dehydrated state is ~3.7 mins.

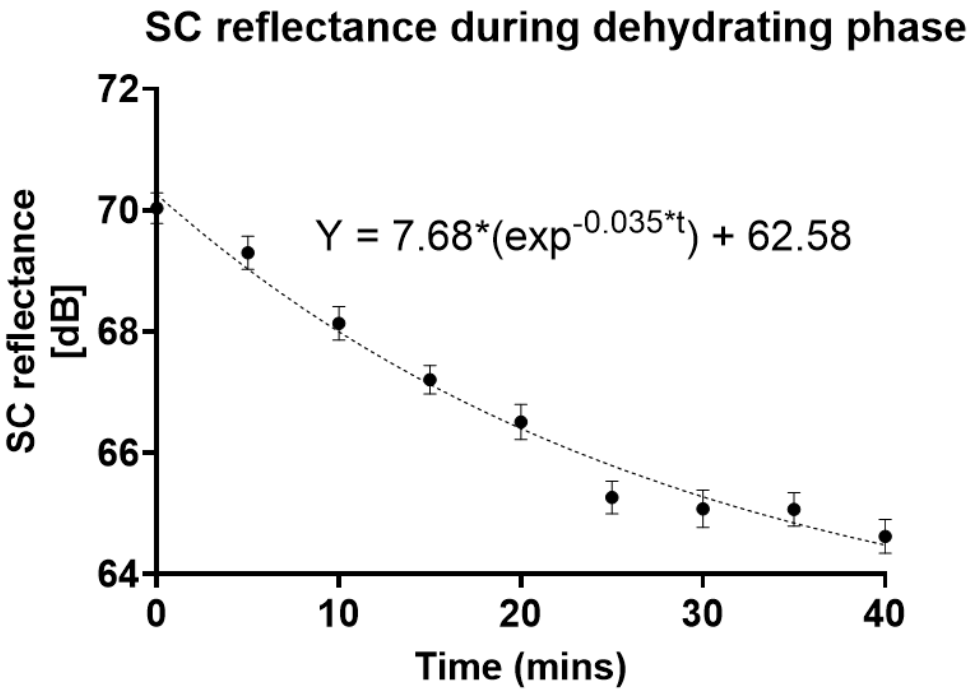

Figure 80. SC reflectance [Mean & standard error (SEM)] at dehydrating phase

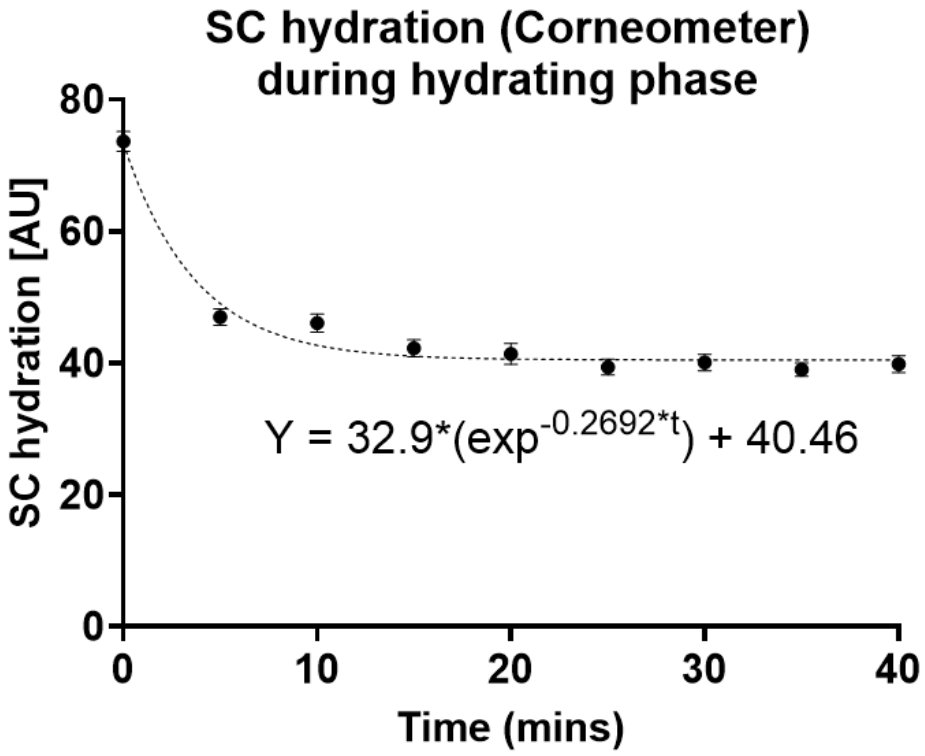

Figure 81. SC hydration measured by Corneometer [Mean & standard error (SEM)] at dehydrating phase

And, to assess for these 12 subjects, whether their SC reflectance correlate with their SC hydration (Corneometer) at all 9-time intervals during dehydrating phase (0 mins – T8, 5 mins – T9, 10 mins – T10, …, 40 mins – T16). As shown in figure 84, where each dot represents a comparison between 192,000 A-scans' average with 60 Corneometer measurements' average at each time interval during dehydrating phase, Spearman's correlation results showed that a significant positive correlation was detected with a corresponding Spearman's correlation coefficient $r = 0.9167, p = 0.0013(**)$.

Again, as shown in figure 84, it is clear that the correlation seems to be dominated by a comparison at T8, in order to get a vision whether this correlation still stands without this 'outlier's domination, a new analysis is performed with T8's comparison removed, and it is plotted in figure 85. Interestingly, with the outlier value at T8 removed, a significant positive correlation is still detected between SC reflectance and SC hydration measured by Corneometer with a corresponding correlation coefficient $r = 0.8810, p = 0.0072(*)$.

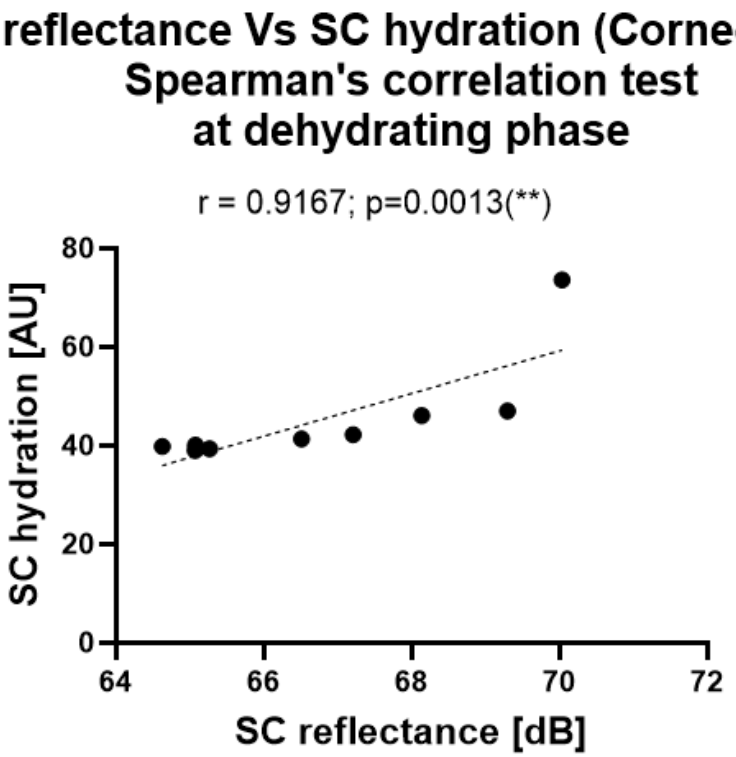

Figure 82. Spearman's correlation test for SC reflectance vs SC hydration measured by Corneometer at dehydrating phase

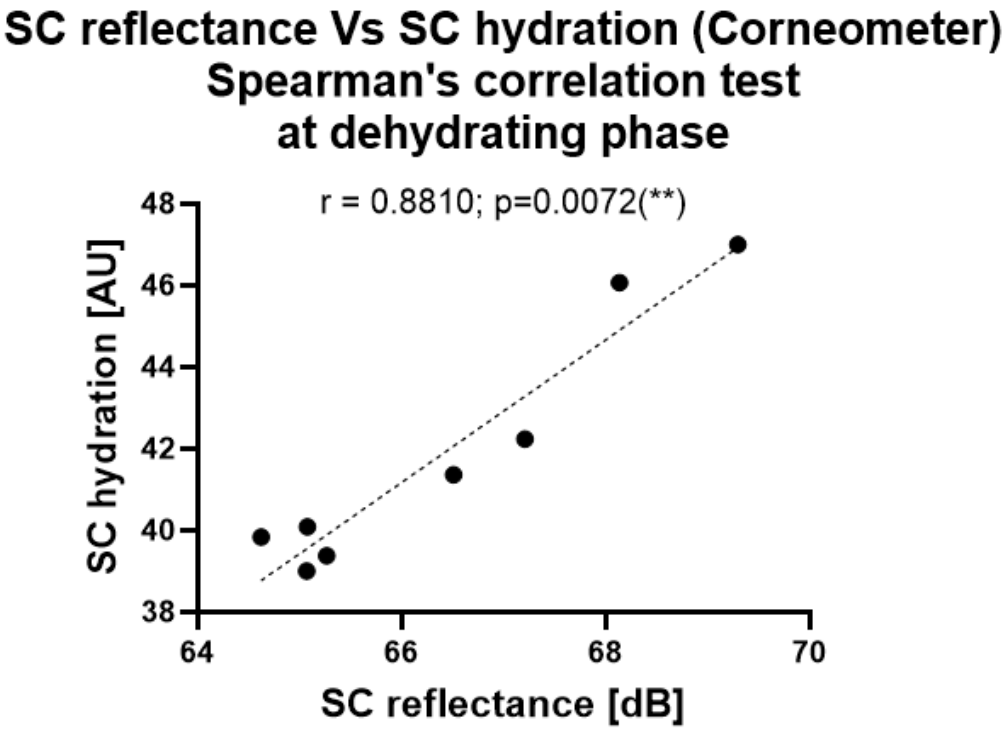

Figure 83. Spearman's correlation test for SC reflectance vs SC hydration measured by Corneometer at dehydrating phase with 'outliers' removed

Same as how it was reported during hydration phase, when breaking down to each time interval and using 5 B-scans to compare with 5 Corneometer measurements for 12 subjects (n = 60), for each time interval from 40 mins to 80 mins (T9 – T16), The results are plotted in figure 86-93. As shown in these figures, 60 comparisons are plotted using 5 B-scans and 5 Corneometer readings from 12 subjects, then, a correlation test is performed with its corresponding correlation coefficient and significance value stated in these plots, and this is done for each time interval during hydrating phase. As shown in the figures, at all-time interval during dehydrating phase (T9 – T16), SC reflectance and SC hydration (Corneometer) show significant positive correlations with each other, indicating when there is an increase in the SC reflectance value, there is an increase in the SC hydration value measure by Corneometer.

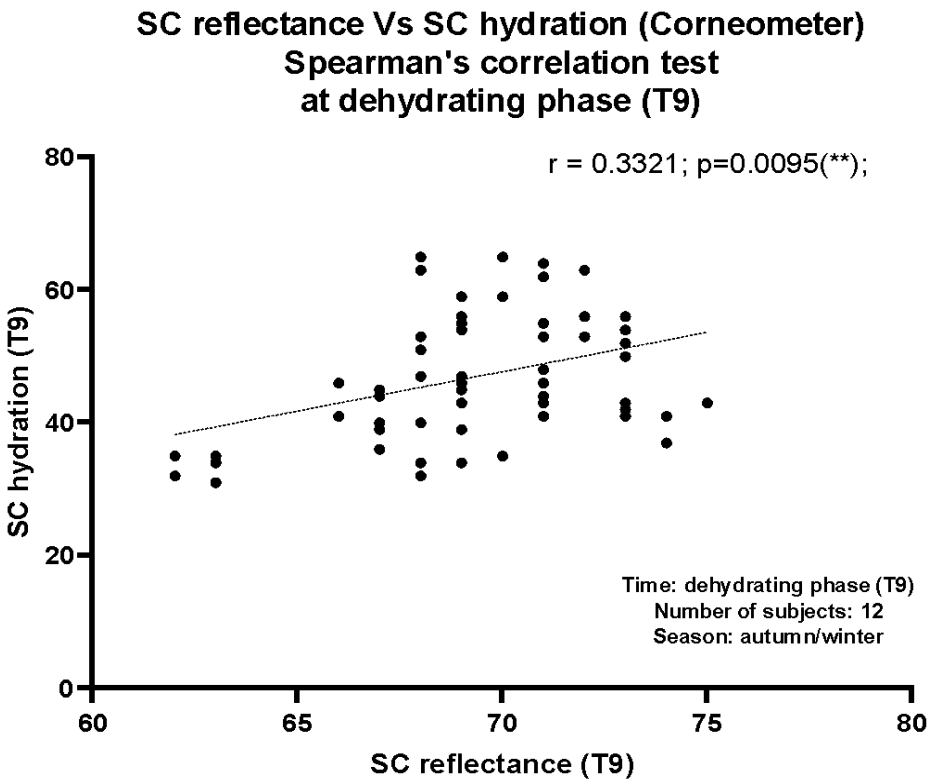

Figure 84. Spearman's correlation test for SC reflectance vs SC hydration measured by Corneometer at dehydrating phase (T9)

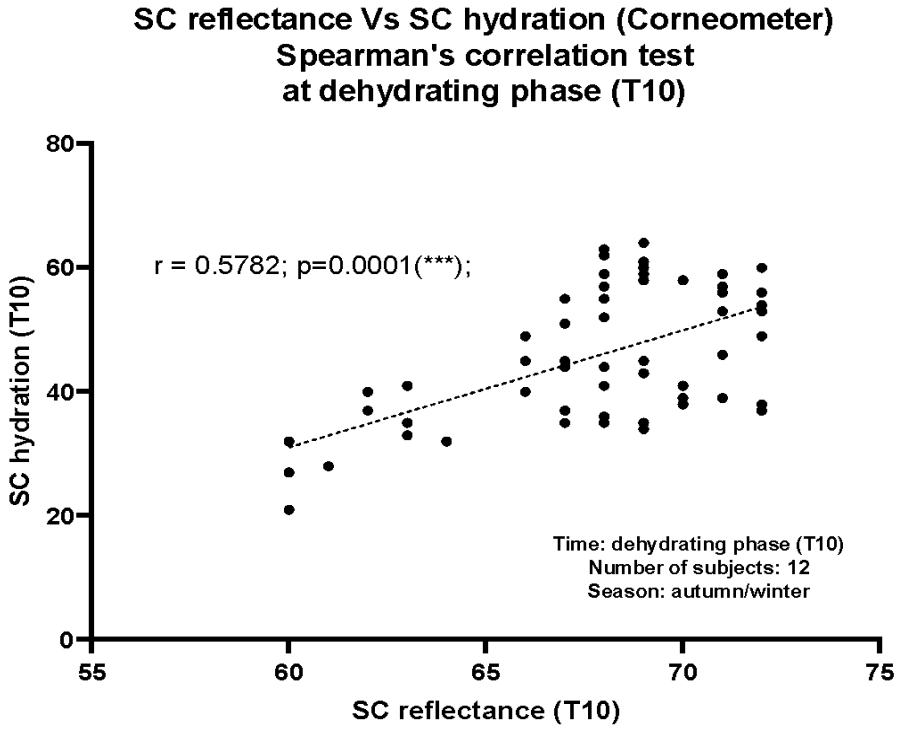

Figure 85. Spearman's correlation test for SC reflectance vs SC hydration measured by Corneometer at dehydrating phase (T10)

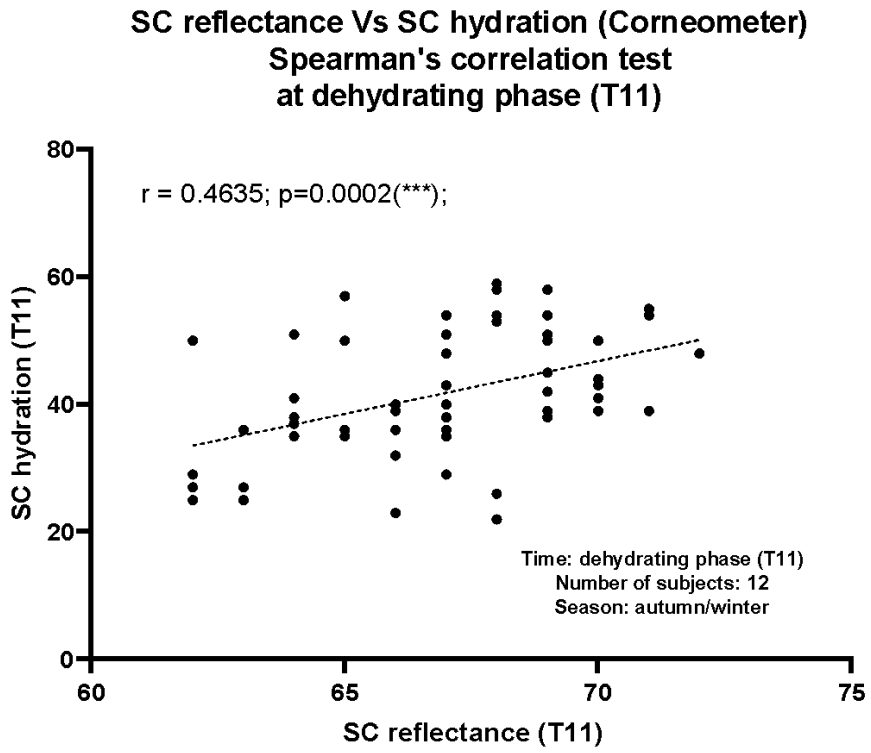

Figure 86. Spearman's correlation test for SC reflectance vs SC hydration measured by Corneometer at dehydrating phase (T11)

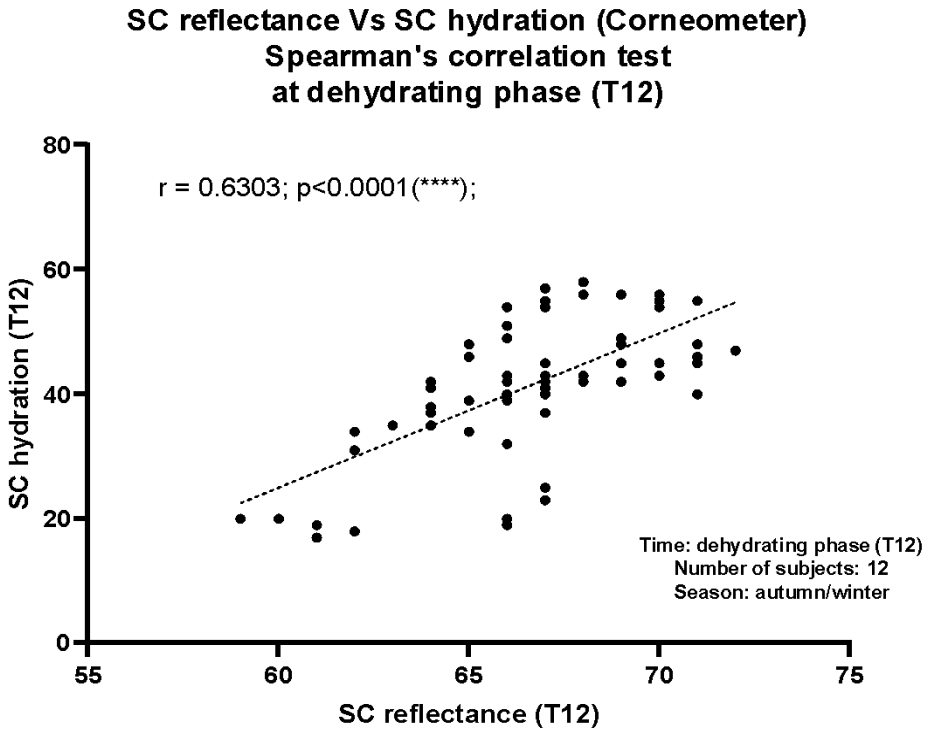

Figure 87. Spearman's correlation test for SC reflectance vs SC hydration measured by Corneometer at dehydrating phase (T12)

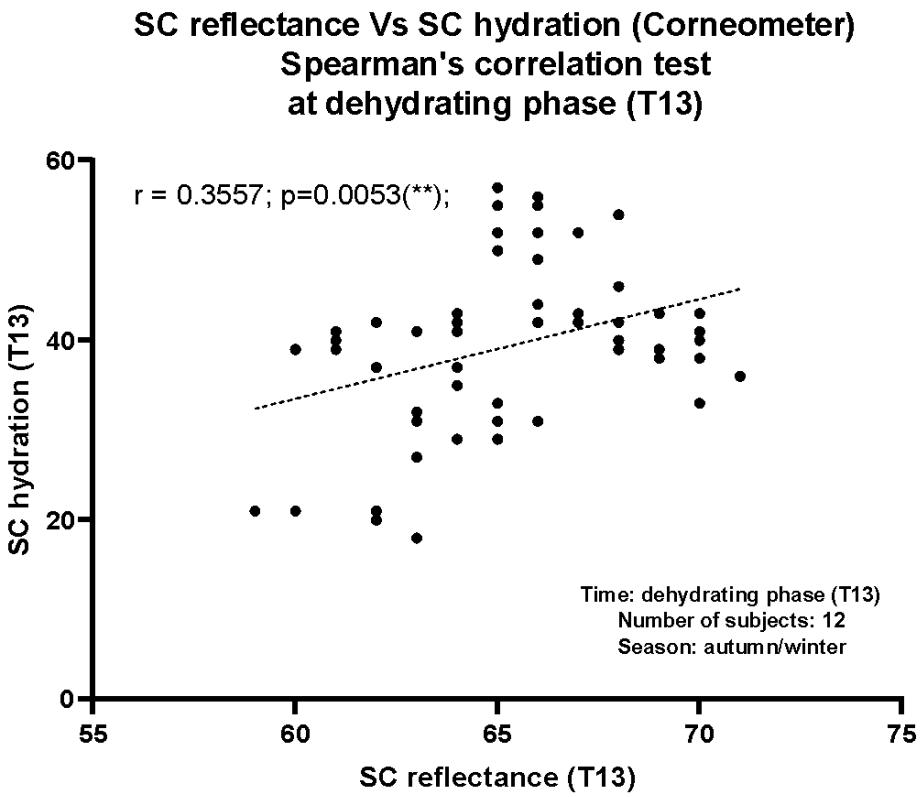

Figure 88. Spearman's correlation test for SC reflectance vs SC hydration measured by Corneometer at dehydrating phase (T13)

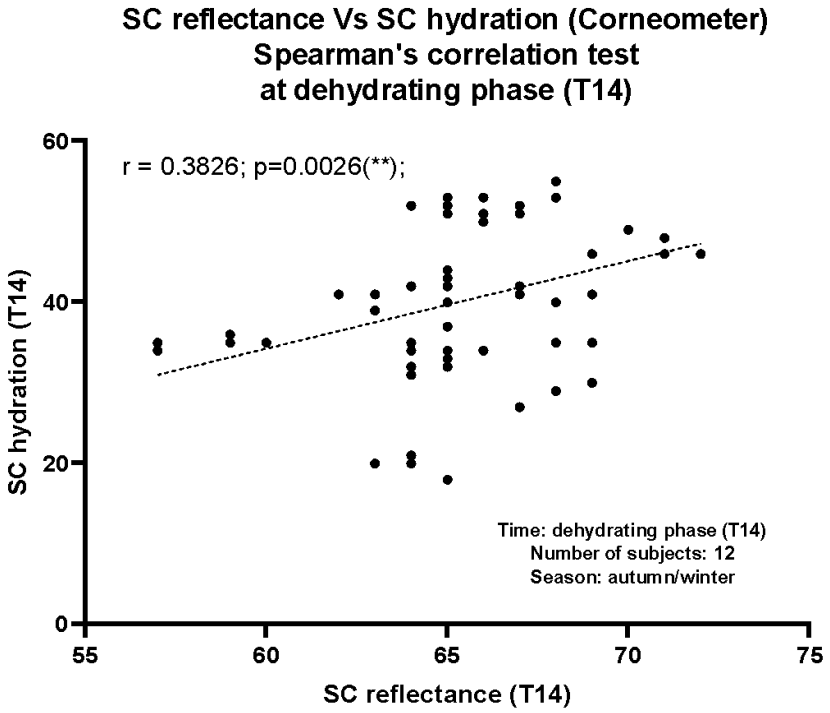

Figure 89. Spearman's correlation test for SC reflectance vs SC hydration measured by Corneometer at dehydrating phase (T14)

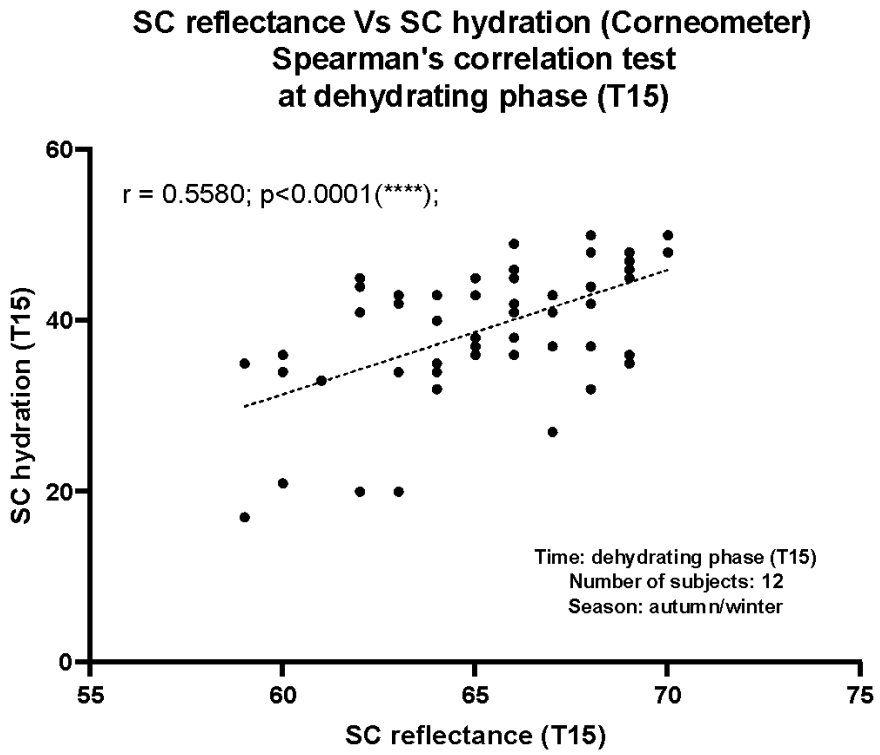

Figure 90. Spearman's correlation test for SC reflectance vs SC hydration measured by Corneometer at dehydrating phase (T15)

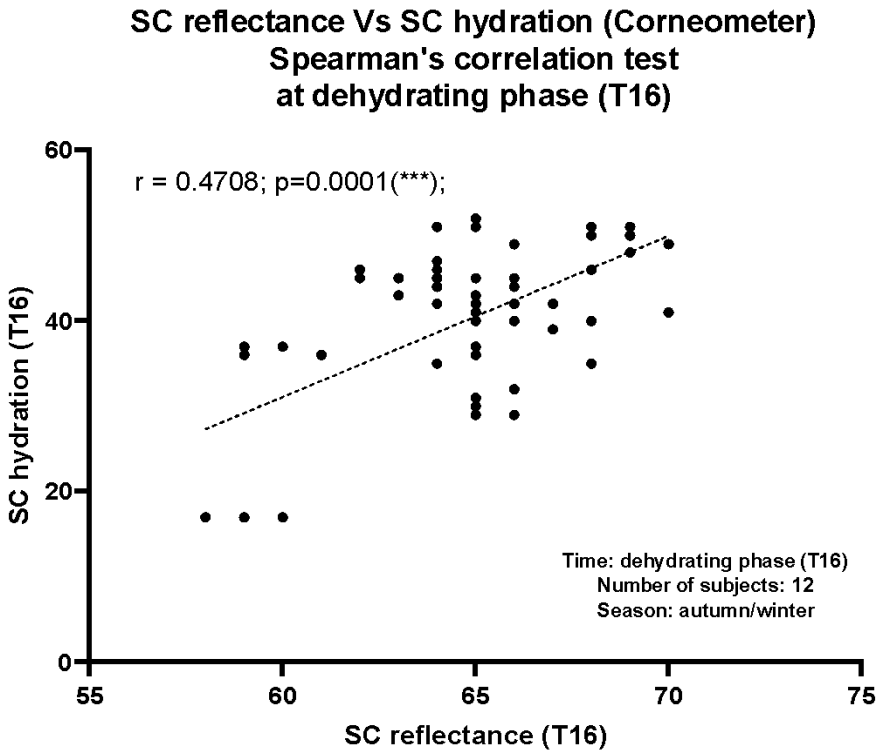

Figure 91. Spearman's correlation test for SC reflectance vs SC hydration measured by Corneometer at dehydrating phase (T16)

In this chapter, individual and group results of SC thickness, reflectance and Corneometer for 12-15 subjects were reported, along with its hydrational, seasonal, gender and age influences. How SC reflectance and Corneometer change in response to hydrating and dehydrating phase were also reported. How these parameters correlate with each other were also analysed with correlation tests, and the result of these findings, and its relevance to literature is discussed in later chapters.

Reference

[1]. Fisher RA (1925). Statistical Methods for Research Workers. Edinburgh, Scotland: Oliver & Boyd. ISBN 978-0-05-002170-5.

6.0 Discussion and conclusion

6.1 SC thickness

In literature, in vivo quantification of SC thickness remains as an ongoing research exploration due to an increased interest in skin barrier research. Confocal Raman microscopy (CRM) and optical coherence tomography (OCT) and its functional extension such as line-confocal OCT (LC-OCT) are two of the main imaging modalities when probing SC thickness at non-palmer skin sites, and results are reported largely at facial area, body flexure and extremities, SC thickness at these body sites are reported to be within the range of 10μm – 30μm. It is agreed in these studies, low SC thickness value is often found at facial area and forearms, while body sites like the trunk, chest and the leg tend to have higher SC thickness. The NIR-OCT system is often used to quantify SC thickness on load-bearing skin sites such as the heel, fingertip or the palm, and results are reported to be on a scale of hundreds of microns. In this study, SC thickness at dorsal hand of 15 healthy human subjects are quantified in vivo using VIS-OCT system, where a population mean of 9.0μm ± 3.1μm with a range across 6.5μm ± 0.8μm – 16.4μm ± 3μm was quantified at baseline. Such results appear to be smaller when compared with few studies in literature where the dorsal hand's SC thickness is quantified, Egawa et. al reported a result of 29.3μm ±6.8μm (n=15) using CRS; Monnier et. al reported a result of 29.5μm ± 5.7μm (n=29) using LC-OCT; Chaeuvel-Picard et. al also reported a result of 24.1μm ± 4.6μm (n=8) using LC-OCT and Koehler et. al reported a result of 32.3μm ± 5.5μm (n=30) using multiphoton laser tomography (MLT). The fact that current studies' results are lower than literature can be explained with several aspects. Firstly, the data used in this study did not pass the D'Agostino - Pearson normality test suggesting that from a statistical point of view, the results of this study are unlikely to represent the true population. Furthermore, the inter-variability across these 15 subjects is relatively high, as in, the difference between subjects with the smallest SC thickness and subjects with the highest SC thickness are on a scale of ~10 micrometres across all seasons, indicating that true population mean may be higher than the current results. Secondly, when subjects were taking B-scans, due to the probe of the current VIS-OCT system is fixated at a position which the subjects are often required to bend their hand or hold a fist to make a clean scan, knowing that body position (relaxed or overextended) greatly impacts their skin thickness where, epidermal thickness measured when body sites are overextended are ~20% lower than when relaxed [1], suggests that if subjects' dorsal hand are measured at a rest position, their SC thickness value shall be higher. Interestingly, the reason that current studies' results calculated from

VIS-OCT are around 3 times lower than the results calculated from LC-OCT, this can be explained by a slight different SC identification, see figure 94a) below, the author's research team believed that the 'dark band' with a clear junction from dark to bright transition is the SC (highlighted in yellow), this is based on empirical knowledge of OCT B-scans of palmer skin, where the thickened SC appear to be a 'dark band' and thickness of SC at palmer skin sites such as the fingertip is quantified based on this segmentation, see figure 94c). However, LC-OCT B-scans of the subject's dorsal hand obtained by Monnier et. al (figure 94b) drew a slightly different identification, their OCT system has an isotropic resolution of ~1μm which enables them to visualise nuclei of SC cells, and, based on histological knowledge of that SC consists enucleated corneocyte, and the layer below SC, stratum granulosum(SG)'s corneocyte has a stretched nuclei, below stratum granulosum, stratum spinosum's corneocytes has a round-ish nuclei, Monnier et. al's identification of SC/SG junction are drawn where they start to see a stretched nucleus. This identification spans beyond the 'dark band' identification of the current study, and by rough estimation, Monnier's SC identification consists of a 'dark band' and a hyper-reflective band below the 'dark band' and above stretched nuclei, and the hyper-reflective band is around 2X thicker than the 'dark band', this may explain their results are 3X higher than the current study. Similarly, LC-OCT results on SC thickness reported by Chaeuvel-Picard et. al are also based on this identification. One could claim that the hyper-reflective band does not have nuclei which makes them a part of SC, however, the author could argue that the intensity of the signal at this area is high enough to cover the potential presence of really stretched nuclei which would make them a part of SG. With above said, current study quantified human SC thickness at dorsal hand in vivo for 15 healthy subjects, these results agree with most of the literature where human SC thickness are reported to be on a scale of 10-30μm, however, it appear to be smaller than the results reported by LC-OCT and other imaging system such as multiphoton laser tomography and confocal Raman spectroscopy. This could be due to the limited number of subjects enrolled in study, the skin sites' position when measured as well as a different identification of SC, the gap between current studies' results and the limited results reported in literature emphasis the paucity of human SC thickness in vivo data, nevertheless, current study's results shall offer an explorative opportunity for a more comprehensive study.

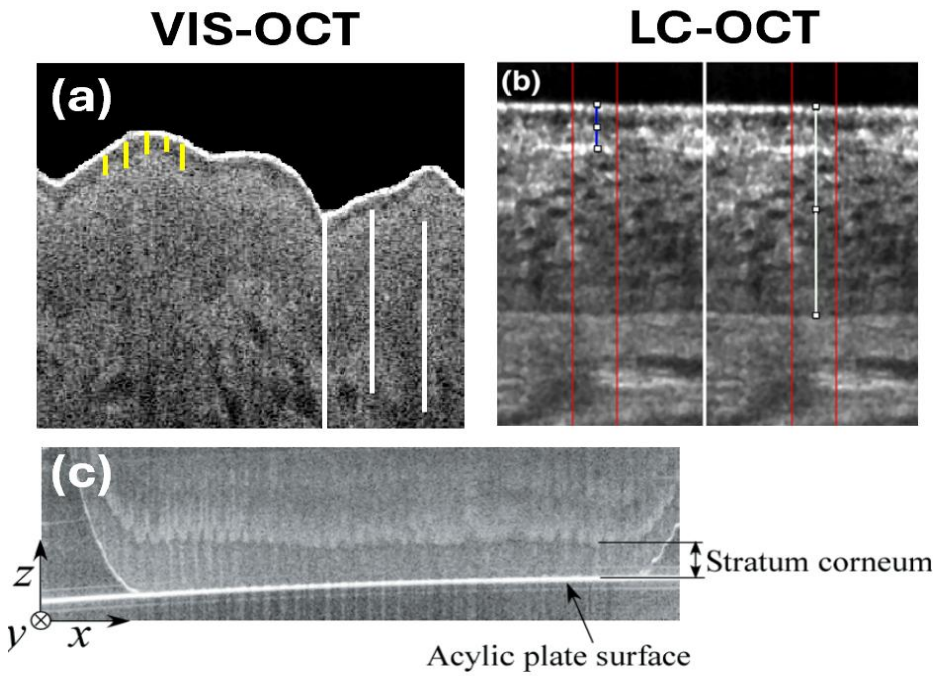

Figure 92. a) VIS-OCT B-scan of a 43 male subject's dorsal hand, SC identification (yellow) and epidermis identification (white); b) LC-OCT B-scan of a 33 female subject's dorsal hand, SC identification (blue) and epidermis identification (white); 3) OCT B-scan of a male subject's fingertip against acrylic plate [2].

The interaction between water and SC is an interesting direction as it can reflect skin barrier function, as in, how SC responds to water exposure may reveal insights on SC permeability, which is stated to be associated with SC hydration and intercellular lipid organisation within the layer. It is illustrated that prolonged water exposure disrupts the architecture of the intercellular lipids in SC, which increases the SC permeability. Warner et. al reported that using electron microscopy, after 4 hours of water exposure, SC thickness of 2 male subjects increased 3 times and after 24 hours of water exposure, their SC thickness increased 4 times. The thickness change can be explained with the uptake of water that happens in corneocytes and across the intercellular space where cisternae form, and the size and number of cisternae increases with time of exposure. The swelling of corneocytes is suggested by water molecules moving into the cells due to osmotic gradients, also stated, the existence of intercellular cisternae may be a result of a reduction of the corneodesmosomes as a function of water exposure time, leading to a dilation of the intercellular space for cisternae formation [3]. Using cryo-scanning electron microscopy, Bouwstra et. al reported that the mean SC cell thickness of isolated human abdomen skin increased by a factor of 2 after hydrating using saturated sodium carbonate (360nm ± 27nm 750nm ± 100nm), and the swelling of corneocytes mainly happens in the perpendicular direction to skin surface which shows that SC swelling by water increases its thickness [4]. Another ex

vivo study done by Norlen et. al obtained isolated breast SC from 20 healthy female subjects and incubated them in distilled water for 90 minutes and 24 hours, reported, using confocal laser scanning microscopy, the average SC thickness increased around 26%, from 13.6μm ± 3.5μm to 17.2μm ± 3.6μm, and there was no significant difference in SC thickness increase between 90 minutes and 24 hours of incubation [5]. Like Bouwstra's study on single corneocytes cell level, Richter et. al acquired one male subject's SC near the inside of his wrist and investigated corneocytes swelling under incubation of distilled water, where an increase of cell volume and 50% of its height (221nm ± 3nm → 330nm ± 6nm) was recorded using scanning force microscopy, this study also affirmed that SC swelling causes an increase in its' thickness [6]. Egawa et. al reported that using water-soaked cotton wool on subjects' forearms for 90 seconds, an increase by a factor of 2 in SC thickness was observed using confocal Raman spectroscopy [7]. A recent ex vivo study done by Evora et. al collected corneocytes from 3 healthy female subjects at their forearm and the heel, using atomic force microscopy (AFM), it is stated that SC swelling was observed in subjects' forearm corneocytes with a thickness increase of ~52% after incubating in distilled water, and a thickness increase of ~20% was observed at heel corneocytes [8]. In current study, 15 subjects' SC thickness increased 144% on average (individual: 65% - 212%) after immersing in water for 40 minutes, this result appear to be higher than what has been reported in ex vivo studies where single corneocyte's height after incubating in water can increase up to 50%, however, it complies with in vivo literature of SC thickness increased by a factor of 2 under application of water-soaked cotton. The finding of this study also affirms the fact that SC swelling under water incubation occurs in the axial direction which directly can be measured as an increase in SC thickness.

The effect of ageing on SC thickness based on ex vivo or in vivo studies in literature are inconsistent, an early autopsy study done by Shuster et. al reported that for 90 Caucasian men, there is a negative correlation between their skin thickness and age, whereas for 107 women, no change in their SC thickness until they reach their 50s, and a thinning of SC thickness was observed [9]. The results of Shuster et. al's study matches with Zhen et. al's study where a decrease in SC thickness is observed in male subject's ex vivo [10]. A review study done by Russell-Goldman states that although SC undergo structural changes during ageing, where it becomes less resistant to environmental triggers, and the cellular cohesion of this layer increases due to a decrease in the intercellular lipids thus results in

stiffening of the layer, the thickness of this layer remains unchanged [11]. Shirata et. al obtained in vivo SC thickness measurements using reflectance confocal microscopy (RCM) on 44 healthy female subjects' malar region and reported that younger age group (18-35)'s results show no significant difference with older age group (40-60) [12]. In vivo measurements that demonstrate no age variations on SC thickness were also reported by Maria Pene et. al using multiphoton 3D imaging, where, although a thinning on epidermis thickness because of epidermal-dermal junction flattening was observed, SC thickness of two age groups of 18-25 years and 70-75 years showed no significant differences [13]. Another in vivo study done by Koehler et. al quantified SC thickness for 30 subjects with three age groups of (mean age = 23 years; 47 years; 72 years) at their forearm and dorsal hand using multiphoton laser topography (MLT) and reported that, a significantly thinner SC was found for all age groups at their forearm than dorsal hand, but no significant difference was observed for different age groups, however, an increase of 7μm was observed [14]. Furthermore, In vivo measurements reported by Bonnier et al's using LC-OCT on 100 healthy Caucasian female subjects stated a 7.6% increase in SC thickness when comparing the age group of 20-30 with 61-70 across their facial area [15]. Similar studies were done on 109 Asian female subjects where LC-OCT was used to quantify age related change on subjects' skin, it was reported that Asian female subjects' facial SC increased 3.8% with advanced age (20-30 years to 51-60) [16]. Rigal et. al reported that using Raman confocal microscopy (RCM) in vivo, SC thickness of subjects under the age of 24 has significantly thinner SC than subjects who's older than 70, Rigal et. al suggested the reasons behind an increase in the SC thickness with advanced age is due to a lower epidermal proliferation rate associated with a lower desquamation rate, an increased corneocytes size and an increased cohesiveness within the SC as subjects grow older [17]. Another prevalence angle to assess skin ageing in relation to its thickness is through cumulative UV exposure, and Olsen et. al measured 249 healthy subjects' epidermal thickness using dynamic-OCT, where a significant negative correlation between epidermal thickness and age was observed on facial area. Olsen et.al stated that this can be explained by a decrease in cellular count and epidermal layers with increasing age. However, it was reported that epidermal thickness at the dorsal hand increased with cumulative work-related UV exposure [18]. Lopez et.al reported an increase in epidermal-dermal thickness after UV exposure using High-frequency ultrasound, and in general, the result of age related, cumulative UV-exposed in skin thickening has been mainly reported in the epidermal and dermal area, not in SC, and it is expected to be related to the inflammation response

upon exposure to UV [19]. In this study, the age factor on SC thickness is investigated via separating 15 subjects into age groups of 20-29 (6 subjects); 30-39 (5 subjects); 40-60 (4 subjects). Using unpaired T-test, a significant difference was found between all age groups, interestingly, after removing potential outliers which could lead to biased results, a significant difference was still detected among all age groups. Where, for each group, including the outliers, before hydrating in water, the average SC thickness for these age groups is 7.6μm ± 0.6μm, 7.1μm ± 0.6μm and 13.1μm ± 3.7μm; after hydrating in water for 40 minutes, their SC thickness increased to 20.4μm ± 2.7μm, 18.7μm ± 1.7μm and 27.4μm ± 5.5μm; after drying in lab for 40 minutes, their SC thickness returned to 6.5μm ± 1.7μm, 6.0μm ± 0.7μm and 11.7μm ± 3.6μm. Although a significant difference is detected between the age group of 20-29 and 30-39, the difference in mean is smaller than the standard deviation of the results, as in, at baseline, the difference in mean between two age groups is 0.5μm, which is smaller than the standard deviation of 0.6μm; same trends are observed at time interval of after hydrating in water for 40 minutes (mean difference = 1.7μm, standard deviation = 1.7μm – 2.7μm), and after drying in lab for 40 minutes (mean difference = 0.5μm, standard deviation = 0.7μm – 1.7μm). Hence, the decrease in SC thickness when comparing subjects in their 20s with subjects in their 30s is arguably questionable. However, when comparing with the age group of 40-60 with younger groups, where the differences in mean when comparing the age group of 20-29 and 30-39 with 40-60 are greater than the standard deviation, and there is an increase of roughly 5μm – 7μm in SC thickness of the age group of 40-60 when comparing with age groups of 20-29 and 30-39. The finding of the current study complies with Bonnier's and Rigal's study, where an increase in SC thickness is reported when SC thickness of younger group (20-40) with SC thickness of elder group (40-60).

Seasonal variation is known to impact skin barrier function as it alters biophysical parameters of SC such as TEWL and SC hydration. Seo et. al carried out a longitudinal study where 10 healthy Korean female subjects were recruited and their TEWL, SC hydration (Corneometry) over the course of 1 year were monitored and measured at facial areas. Reported, subjects' TEWL is significantly higher in winter than summer, and no significant difference was observed on SC hydration [20]. Similarly, 10 healthy male subjects' SC hydration (Corneometry) and TEWL were measured across different seasons by Ishikawa et. al, where TEWL on the cheek, buttock and the palm were found significantly higher in autumn/winter than in spring/summer, at skin sites of forehead, lip, upper arm and the palm, SC

hydration measurements were found to be significantly higher in spring/summer than in autumn/winter [21]. A comprehensive review study done by Engebretsen et. al concluded that change of climatic condition negatively impacts skin barrier function, where low humidity and low temperature during winter season results in a reduction in SC lipid, SC hydration (Corneometry) and NMFs, thus causing SC to be more permeable and more susceptible to irritants [22]. An in vivo study done by Uchegbulam el al. conducted SC hydration (Corneometry), epidermal thickness (OCT) and TEWL measurements on 14 male subjects' lower arm and upper arm and reported that, TEWL at lower arm and upper arm showed a reduction of 14.7% - 22.2% from winter to summer, SC hydration showed an increase of 25.5% - 26.3% at both lower arm and upper arm, and results of epidermal thickness showed that there is an increase of 22.7% - 22.6% from winter to summer. Uchegbulam et. al suggested that the increase in TEWL in winter is linked with lower relative humidity in winter, and the increase in epidermal thickness from winter to summer is likely to be associated with swelling of corneocytes because of higher relative humidity in summer [23]. In current study, SC thickness for 8 subjects showed a significant increase from winter to summer at hydrated state with outliers excluded, no significant difference was detected at baseline and after drying, this finding complies with Uchegbulam et al's study where there is an increase in the epidermal thickness for 14 subjects from winter to summer, likewise, the increase in SC thickness is likely to be caused by SC swelling due to a higher relative humidity in summer season.

The influence of gender on SC thickness in literature is also lacking and often under-reported, Zhen et. al stated that cell layers of SC for female and male subjects do not differ [24]. Sandby-Moller et. al reported that SC thickness biopsy of 71 subjects show no significant differences between two gender groups [25]. Firooz et. al claimed that using ultrasound scanning, epidermal thickness of male subjects' necks is significantly higher (15%) than female subjects [26]. Using OCT, Gambichler reported that in a population pool of 83 subjects, epidermal thickness of male and female showed no significant difference [27]. Meng et. al measures facial epidermal thickness of 118 subjects using high-frequency ultrasound and reported that male subjects had a significantly higher epidermal thickness (~10%) than female subjects [28]. In the current study, at baseline and after drying, it was found that male subjects' SC thickness is significantly higher than female subjects' with outliers excluded, this finding partially with Firooz et. al's study and Meng et al's in vivo study where a thickener epidermal thickness is

detected in men than women, however, it does not comply with ex vivo studies done by zhen et. al and Sandby-Moller et. al.

Having described above, human SC thickness in vivo results of the current study mostly agree with what has been stated in literature, the influence of hydration on SC swelling is confirmed with an increased SC thickness. It was found that SC thickness for older subjects group is higher than younger subjects group, this is explained by a lower proliferation rate of the epidermis accompanied by an increase in corneocytes size and cohesiveness as subjects grow older. In addition, the accumulation of UV exposure during the aging process has been reported to increase the epidermal and dermal thickness due to the inflammation response upon UV exposure, although its effect on SC thickness has not been studied, this could add to the observation of the thickening of SC thickness during ageing. The SC thickness in this study was reported to be higher in male subjects, this partially agree with some literatures where male subjects SC thickness was reported to be higher than female subjects at certain body sites, this may be associated with personal life habit rather than genetic reasons, where, male subjects are more likely to engage in outdoor activities where SC may thicken due to UV exposure, and, female subjects are more likely to use personal wash product which may thinner their SC thickness. Seasonal effect on SC thickness was confirmed in the current study, where SC thickness was found to be higher in spring/summer season, this agrees with literature where a higher humidity rate in spring/summer season leads to SC swelling.

6.2 SC hydration (Reflectance and Corneometer)

As stated in literature, until now, Corneometer still remains as the ‘gold standard’ electric sensing method to measure SC hydration based on its advantages of prompt and easy measurements. However, the device itself is quite sensitive to pressure, if the probe is pushed down too hard, the device will give a higher reading as it is measuring ‘deeper’ tissue. To calibrate this, when taking the measurements, the operator takes multiple measurements until a consistent reading is achieved, then the operator will record 5 repeats during the experiment. Although the device is the most widely used tool to record SC hydration, it does not provide subsurface information of the layered tissue, OCT, on the other hand, under the ‘seeing is believing’ idea, can give a cross-sectional scan of the skin. As the OCT reflectance value changes during hydrating and dehydrating phase, it was hypothesized that SC

reflectance measured by VIS-OCT can reflect hydration information on subjects' SC. Chapter 5.44 illustrated that, via conducting correlation test on 12 subjects' reflectance and Corneometer results, it was confirmed that at all time intervals except T8 (T0, T1,….T16) during the experiment, there is a significantly positive correlation between subjects' SC reflectance and Corneometer results. Moreover, how SC reflectance behave during hydrating phase (T0-T8) resembles how Corneometer results behave, where they both increase rapidly from T0-T4, then gradually stabilize and reach 'steady state' from T4-T8, and the time constant of Corneometer (~2.4 mins) and SC reflectance (~3.9 mins) is very close. During dehydrating/drying phase, SC reflectance and Corneometer results both decay non-linearly, except, Corneometer decays more rapidly with a smaller time constant of ~3.7 mins, and SC reflectance has a larger time constant of ~28.6 mins. These correlations demonstrate that SC reflectance measured by VIS-OCT can be used to indicate subjects' SC hydration to a certain extent.

Looking at the descriptive statistics of SC reflectance and Corneometer in chapter 5.21 and 5.31, where, for 12 subjects, from baseline to 40 minutes of hydrating in water, SC reflectance increased from 63.8dB ± 2.3dB to 70.0dB ± 2.8dB, the increase in SC reflectance indicating that the back-scattered signal is increased due to more scattering in this layer by capture more water molecule, and the increase is ~6dB (4x brighter) and for Corneometer, their results increased from a baseline value of 36±11 to 74±12. Both increase in SC reflectance and Corneometer results under the same hydrating condition are significant, and the same trend applies to the dehydrating/drying phase. After drying in the lab for 40 minutes, SC reflectance for 12 subjects decreased from 70.0dB ± 2.8dB to 64.7dB ± 3.0dB, and their Corneometer decreased from 74±12 to 40±9, significances in these decreases under the same drying condition were also detected. Interestingly, a significant difference was also detected between these two parameters at baseline and after dried in lab, combing the time constant results, as in, both for SC reflectance and Corneometer, the time constant for hydrating phase is smaller than the drying phase, indicating that the physiological process of SC's uptake of water during hydrating phase is faster than losing of water during drying phase.

When considering the age factor in the variability of results, at T0, T8 and T16, no significant difference in SC reflectance was detected between the age group of 20-29 and 30-39, a significant difference was detected between the age group of 20-29 and 40-60, as well as the age group of 30-39 and 40-60 at

these times. Corneometer results yields slightly different results where a significant difference was detected between all age group at T8; at T0, no significant difference was detected between the age group of 20-29 and 40-60, but a significant difference was detected between the age group of 30-39 and 40-60, as well as 20-29 and 30-39; at T16, no significant difference was detected between the age group of 30-39 and 40-60, a significant difference was detected between the age group of 20-29 and 30-39, as well as 20-29 and 40-60. Despite slight differences in these significant differences in detection, it was observed that SC reflectance value and Corneometer results decrease with age at baseline, such an observation can be explained by there being less 'free' water molecule in SC with advanced age, ChunSik et. al reported that older subject's group has higher amount of water molecule that is bonded with surrounding intercellular lipid (ICL), natural moisturizing factor (NMF) and keratin, hence less 'free' water molecule presence in SC results in a drier skin [29]. Biniek et. al also reported that the kinetic of water movement through tissue decreases with age [30]. Interestingly, Lubberding et. al reported that only male subjects' SC decreases with age, while female subjects' SC show opposite trend [31], similarly, Sator et. al reported that at the dorsal hand, male subjects' SC hydration decreases with age [32]. It is generally agreed that SC hydration decreases with age due to a reduction in NMF and sebum secretion, and lipid bilayer lateral packing increases which results in less water diffusion into SC, current study illustrated this via demonstrating a decreasing trend in SC reflectance and Corneometer values with age.

When considering the gender factor, unpaired T-test on SC reflectance showed significant difference when separating 15 subjects into a male group (n=10) and female group (n=5) at T0, T8, T16; while Corneometer results showed significant difference between male group (n=8) and female group (n=4) at T16, but no significant difference was detected at T0 and T8 and It was found that female subject group had a higher value in SC reflectance (at T0, T8, T16) and Corneometer results (at T0 and T16). Although the current study reported a higher SC hydration in female subjects, it only agrees with literature partially. A recent study done by Chicharr-Luna et. al recruited 504 subjects (female: 191; male: 313) and measured their SC hydration at foot area using Corneometer, it was stated that when exceeding the age of 60, female subjects' SC hydration was found to be higher than male subjects', they also affirmed the inverse correlation between SC hydration and age [33]. Liu et. al conducted a SC hydration study on 168 subjects (female: 84; male: 84) and reported that, gender difference in SC

hydration measured by Corneometer was detected at subjects' dorsal hands where female subjects with age above 50 had a lower SC hydration than male subjects. Liu et. al suggested that the fact that female subjects had a lower SC hydration in aged population is caused by a lower hormone secretion (estrogen), as estrogen plays a key role in SC hydration regulation and women who experience menopause is reported to have a lower estrogen production, hence leading to a lower SC hydration [34]. Luebberding et. al conducted a study on 300 subjects (female: 150; male: 150) and reported that male subjects' SC hydration is higher than female subjects' at their cheek, forehead and neck, however, at dorsal hand, female subjects had a higher SC hydration than male subjects [35]. Another study done by Mayrovitz et. al measured 30 subjects' (female: 16; male: 14) SC hydration at their forearm and reported that male subjects had a higher reading than female subjects, they suggest that this gender diversity in SC hydration could be caused by a different sebum secretion [36]. Current study's result complies with Chicharr-Luna et. al's and Lubberding et al's finding where a higher SC hydration reflected as Corneometer and SC reflectance value is detected in female subjects, however, it does not comply with studies which reported contradictory results due to hormonal secretion. This mismatch could be due to a limited study subjects and methodology variation. It is generally accepted that SC hydration decays with ageing due to a lower secretion and density of intercellular lipids, NMFs and corneodesmosomes which weakens the barrier function. The gender variation has several argument aspects in literature, some may claim that female subjects' SC hydration is linked with hormonal regulation where, a lower SC hydration can occur during the take-off of menopause; however, different personal washing habit may result in a higher SC hydration for female subjects in skin sites where moisturizing product is frequently applied, such as facial area and hands.

Seasonal influence on SC hydration is not demonstrated with Corneometer as such a device was only available in autumn/winter season, however, interestingly, SC reflectance was found to be significantly higher in autumn/winter at T8 and T16 with a rather equal baseline (T0) value. One possible explanation for this is that during autumn/winter season, subjects are more likely to apply moisturizing product which increased the NMFs and lipid in their SC, thus, under the same hydrating condition, subjects' SC can absorb more water which is reflected as a higher SC reflectance value; at T16, SC reflectance value is higher in autumn/winter also can be explained by the application of moisturizing product results in SC with a higher hygroscopic component density which enables SC to retain water longer. This finding is

partially supported when looking at the time constant of SC reflectance for 8 subjects who completed the experiment in both season, mentioned before, the time constant of SC reflectance during both hydrating and dehydrating phases can be used to indicate 'how quickly' subjects' SC uptake water and 'how slowly' it loses water, illustrated in the table below, the average time for subjects' SC uptake water in spring/summer season is greater than in autumn/winter, again, this could be due to a higher density of the hygroscopic substance in SC in autumn/winter. The time constant for the dehydrating phase does not differ much and in fact, it is slightly higher in spring/summer. This observation again emphasises that the physiological process behind the uptake of water in SC is different from loss of water.

Time constant (minutes) of SC reflectance in different season for 8 subjects				
Subject number	Spring/summer hydrating	Autumn/winter Hydrating	Spring/summer Dehydrating	Autumn/winter Dehydrating
001	22.1	29.9	4.1	10.7
002	11.7	10.3	6.5	9.1
003	5.1	6.1	10	8.9
004	5.2	1.9	21.9	5.1
005	7.5	3.2	7.0	4.8
006	8.5	4.8	9.4	8.1
007	86.4	3.4	7.9	9.5
0010	3.1	5.7	10.1	7.8
Average	**18.7**	**8.2**	**9.6**	**8**

Table 25. time constant of SC reflectance during hydrating and dehydrating phase in both seasons.

Having described above, SC hydration remains as an active research topic due to its key role in skin barrier function, as in, a well-regulated SC hydration in SC is important for a normal desquamation rate due to its participation in many enzymatic processes. If SC hydration drops below a critical value, the skin becomes very dry and flaky which makes SC more susceptible to environmental triggers. Current study demonstrated that, when breaking down to each time interval, SC reflectance results measured by VIS-OCT show significant correlations with Corneometer results during autumn/winter season, this finding affirmed that VIS-OCT not only can be used quantify SC thickness, it also can be used to investigate SC hydration, which is particularly useful for clinical and non-clinical investigations. SC hydration reflected by SC reflectance and Corneometer results both show age and gender variations,

which is fractionally supported by literature. Mentioned before, it is agreed that ageing causes a reduction in NMF and lipid production, which causes SC hydration to be found lower in the aged population, this is demonstrated in current study where SC reflectance and Corneometer measurement decrease with age. Gender variation is shown in SC reflectance and Corneometer results in current study, however, it is only supported by some of the literature reviewed. The time constant quantified for both parameters show individual variation, and hydrating or dehydrating phase independence, indicating SC's uptake of water is likely to be independent from its' loss of water. This is backed by physiological explanation where SC's water intake path is different from the water evaporating path, where water molecules diffuse into the SC is partially preserved within corneocytes and bounded with intracellular keratin, another fraction of water molecule is bounded with hygroscopic molecules such as NMFs, lipid and keratin in the lipid matrix and is depended on the osmotic gradient between SC and external humidity. The water molecule which evaporates out of SC is depended on the lipid organization, and the intercellular lipid is organized tightly with water molecule into a parallel lamellar membrane, and this lipid organization is described as orthorhombic which helps SC to retain water effectively [37].

To conclude, SC hydration quantified by the VIS-OCT reflectance value agrees with what has been stated in literature, a significant correlation was also detected between SC hydration quantified by Corneometer and VIS-OCT reflectance value. Hence, the findings of the current study doubtlessly offer insights and potentials of using the VIS-OCT system in skin barrier research. The ability of assessing uptake water rate and water loss rate using this system will be particularly useful in assessing effectiveness of treatment for xerosis skin, and this, to be explained in future work.

References

[1]. R. Maiti, M. Duan, S. G. Danby, R. Lewis, S. J. Matcher, and M. J. Carré, "Morphological parametric mapping of 21 skin sites throughout the body using optical coherence tomography," Journal of the mechanical behavior of biomedical materials, vol. 102, pp. 103501–103501, 2020, doi: 10.1016/j.jmbbm.2019.103501.
[2].T. OKUYAMA, R. NIWATA, and M. TANAKA, "Measurement of Young's Modulus of Stratum Corneum in Finger by Optical Coherence Tomography," Journal of the Japan Society of Applied Electromagnetics and Mechanics, vol. 29, no. 1, pp. 137–142, 2021, doi: 10.14243/jsaem.29.137.
[3]. R. R. Warner, K. J. Stone, and Y. L. Boissy, "Hydration Disrupts Human Stratum Corneum Ultrastructure," Journal of investigative dermatology, vol. 120, no. 2, pp. 275–284, 2003, doi: 10.1046/j.1523-1747.2003.12046.x.
[4]. J. A. Bouwstra, A. de Graaff, G. S. Gooris, J. Nijsse, J. W. Wiechers, and A. C. van Aelst, "Water Distribution and Related Morphology in Human Stratum Corneum at Different Hydration Levels," Journal of investigative dermatology, vol. 120, no. 5, pp. 750–758, 2003, doi: 10.1046/j.1523-1747.2003.12128.x.
[5]. L. Norlén, A. Emilson, and B. Forslind, "Stratum corneum swelling. Biophysical and computer assisted quantitative assessments," Archives of Dermatological Research, vol. 289, no. 9, pp. 506–513, 1997, doi: 10.1007/s004030050231.

[6]. T. Richter, J. H. Müller, U. D. Schwarz, R. Wepf, and R. Wiesendanger, “Investigation of the swelling of human skin cells in liquid media by tapping mode scanning force microscopy,” Applied physics. A, Materials science & processing, vol. 72, no. 7, pp. S125–S128, 2001, doi: 10.1007/s003390100750.
[7]. M. Egawa, T. Hirao, and M. Takahashi, “In vivo estimation of stratum corneum thickness from water concentration profiles obtained with raman spectroscopy,” Acta dermato-venereologica, vol. 87, no. 1, pp. 4–8, 2007, doi: 10.2340/00015555-0183.
[8]. A. S. Évora, Z. Zhang, S. A. Johnson, and M. J. Adams, “The effects of hydration on the topographical and mechanical properties of corneocytes,” Journal of the mechanical behavior of biomedical materials, vol. 150, p. 106296, 2024, doi: 10.1016/j.jmbbm.2023.106296.
[9].Z. Ya-Xian, T. Suetake, and H. Tagami, “Number of cell layers of the stratum corneum in normal skin relationship to the anatomical location an the body, age, sex and physical parameters,” Archives of Dermatological Research, vol. 291, no. 10, pp. 555–559, 1999, doi: 10.1007/s004030050453.
[10]. S. Shuster, M. M. Black, and E. McVITIE, “The influence of age and sex on skin thickness, skin collagen and density,” British journal of dermatology (1951), vol. 93, no. 6, pp. 639–643, 1975, doi: 10.1111/j.1365-2133.1975.tb05113.x.
[11]. E. Russell-Goldman and G. F. Murphy, “The Pathobiology of Skin Aging: New Insights into an Old Dilemma,” The American journal of pathology, vol. 190, no. 7, pp. 1356–1369, 2020, doi: 10.1016/j.ajpath.2020.03.007.
[12]. M. M. Fossa Shirata, G. A. D. Alves, and P. M. B. G. Maia Campos, “Photoageing-related skin changes in different age groups: a clinical evaluation by biophysical and imaging techniques,” International journal of cosmetic science, vol. 41, no. 3, pp. 265–273, 2019, doi: 10.1111/ics.12531.
[13]. A. M. Pena et. al, “In vivo multiphoton multiparametric 3D quantification of human skin aging on forearm and face,” Scientific reports, vol. 12, no. 1, pp. 14863–14863, 2022, doi: 10.1038/s41598-022-18657-z.
[14]. M. J. Koehler, T. Vogel, P. Elsner, K. König, R. Bückle, and M. Kaatz, “In vivo measurement of the human epidermal thickness in different localizations by multiphoton laser tomography,” Skin research and technology, vol. 16, no. 3, pp. 259–264, 2010, doi: 10.1111/j.1600-0846.2010.00437.x.
[15]. F. Bonnier et. al, “Line-field confocal optical coherence tomography coupled with artificial intelligence algorithms to identify quantitative biomarkers of facial skin ageing,” Scientific reports, vol. 13, no. 1, pp. 13881–13881, 2023, doi: 10.1038/s41598-023-40340-0.
[16]. A. Ali et. al, “Comparison of facial skin ageing in healthy Asian and Caucasian females quantified by in vivo line-field confocal optical coherence tomography 3D imaging,” Skin research and technology, vol. 30, no. 9, p. e13643, 2024, doi: 10.1111/srt.13643.
[17]. A. Rigal, R. Michael-Jubeli, A. Nkengne, A. Baillet-Guffroy, A. Bigouret, and A. Tfayli, “Raman confocal microscopy and biophysics multiparametric characterization of the skin barrier evolution with age,” Journal of biophotonics, vol. 14, no. 9, pp. e202100107-n/a, 2021, doi: 10.1002/jbio.202100107.
[18]. J. Olsen, G. Gaetti, K. Grandahl, and G. B. E. Jemec, “Optical coherence tomography quantifying photo aging: skin microvasculature depth, epidermal thickness and UV exposure,” Archives of dermatological research, vol. 314, no. 5, pp. 469–476, 2022, doi: 10.1007/s00403-021-02245-8.
[19]. H. Lopez, J. Z. Beer, S. A. Miller, and B. Z. Zmudzka, “Ultrasound measurements of skin thickness after UV exposure: a feasibility study,” Journal of photochemistry and photobiology. B, Biology, vol. 73, no. 3, pp. 123–132, 2004, doi: 10.1016/j.jphotobiol.2003.11.004.
[20]. J. Y. Seo et. al, “Longitudinal study of the interplay between the skin barrier and facial microbiome over 1 year,” Frontiers in microbiology, vol. 14, pp. 1298632–1298632, 2023, doi: 10.3389/fmicb.2023.1298632.
[21]. J. Ishikawa et. al, “Variations in the ceramide profile in different seasons and regions of the body contribute to stratum corneum functions,” Archives of Dermatological Research, vol. 305, no. 2, pp. 151–162, 2013, doi: 10.1007/s00403-012-1286-5.
[22]. K. A. Engebretsen, J. D. Johansen, S. Kezic, A. Linneberg, and J. P. Thyssen, “The effect of environmental humidity and temperature on skin barrier function and dermatitis,” Journal of the European Academy of Dermatology and Venereology, vol. 30, no. 2, pp. 223–249, 2016, doi: 10.1111/jdv.13301.
[23]. I. Uchegbulam, S. G. Danby, R. Lewis, M. J. Carré, and R. Maiti, “Effect of seasonal change on the biomechanical and physical properties of the human skin,” 2022.
[24].Z. Ya-Xian, T. Suetake, and H. Tagami, “Number of cell layers of the stratum corneum in normal skin relationship to the anatomical location an the body, age, sex and physical parameters,” Archives of Dermatological Research, vol. 291, no. 10, pp. 555–559, 1999, doi: 10.1007/s004030050453.
[25]. J. Sandby-Møller, T. Poulsen, and H. C. Wulf, “Epidermal Thickness at Different Body Sites: Relationship to Age, Gender, Pigmentation, Blood Content, Skin Type and Smoking Habits,” Acta dermato-venereologica, vol. 83, no. 6, pp. 410–413, 2003, doi: 10.1080/00015550310015419.
[26]. A. Firooz, A. Rajabi-Estarabadi, H. Zartab, N. Pazhohi, F. Fanian, and L. Janani, “The influence of gender and age on the thickness and echo-density of skin,” Skin research and technology, vol. 23, no. 1, pp. 13–20, 2017, doi: 10.1111/srt.12294.
[27]. T. Gambichler, R. Matip, G. Moussa, P. Altmeyer, and K. Hoffmann, “In vivo data of epidermal thickness evaluated by optical coherence tomography: Effects of age, gender, skin type, and anatomic site,” Journal of dermatological science, vol. 44, no. 3, pp. 145–152, 2006, doi: 10.1016/j.jdermsci.2006.09.008.
[28]. Y. Meng, L. Feng, J. Shan, Z. Yuan, and L. Jin, “Application of high-frequency ultrasound to assess facial skin thickness in association with gender, age, and BMI in healthy adults,” BMC medical imaging, vol. 22, no. 1, pp. 1–113, 2022, doi: 10.1186/s12880-022-00839-w.

[29]. C. Choe, J. Schleusener, J. Lademann, and M. E. Darvin, “Age related depth profiles of human Stratum Corneum barrier-related molecular parameters by confocal Raman microscopy in vivo,” Mechanisms of ageing and development, vol. 172, pp. 6–12, 2018, doi: 10.1016/j.mad.2017.08.011.
[30]. K. Biniek, J. Kaczvinsky, P. Matts, and R. H. Dauskardt, “Understanding age-induced alterations to the biomechanical barrier function of human stratum corneum,” Journal of dermatological science, vol. 80, no. 2, pp. 94–101, 2015, doi: 10.1016/j.jdermsci.2015.07.016.
[31]. S. Luebberding, N. Krueger, and M. Kerscher, “Skin physiology in men and women: in vivo evaluation of 300 people including TEWL, SC hydration, sebum content and skin surface pH,” International journal of cosmetic science, vol. 35, no. 5, pp. 477–483, 2013, doi: 10.1111/ics.12068.
[32]. P.-G. Sator, J. B. Schmidt, and H. Hönigsmann, “Comparison of epidermal hydration and skin surface lipids in healthy individuals and in patients with atopic dermatitis,” Journal of the American Academy of Dermatology, vol. 48, no. 3, pp. 352–358, 2003, doi: 10.1067/mjd.2003.105.
[33]. E. Chicharro-Luna, S. Zúnica-García, C. Martinez-Algarra, and A. Gracia-Sánchez, “Age-related variations in stratum corneum hydration in the foot,” Maturitas, vol. 189, p. 108104, 2024, doi: 10.1016/j.maturitas.2024.108104.
[34]. Z. Liu, S. Song, W. Luo, P. M. Elias, and M.-Q. Man, “Sun-induced changes of stratum corneum hydration vary with age and gender in a normal Chinese population,” Skin research and technology, vol. 18, no. 1, pp. 22–28, 2012, doi: 10.1111/j.1600-0846.2011.00536.x.
[35]. S. Luebberding, N. Krueger, and M. Kerscher, “Skin physiology in men and women: in vivo evaluation of 300 people including TEWL, SC hydration, sebum content and skin surface pH,” International journal of cosmetic science, vol. 35, no. 5, pp. 477–483, 2013, doi: 10.1111/ics.12068.
[36]. H. N. Mayrovitz, K. Aoki, E. Deehan, and M. Ruppe, “Epidermal and dermal hydration in relation to skin color parameters,” Skin research and technology, vol. 30, no. 8, pp. e70028-n/a, 2024, doi: 10.1111/srt.70028.
[37]. Verdier-Sévrain S, Bonté F. Skin hydration: a review on its molecular mechanisms. J Cosmet Dermatol. 2007 Jun;6(2):75-82. doi: 10.1111/j.1473-2165.2007.00300.x. PMID: 17524122.

7.0 Other explorative work

7.1 The use of VIS-OCT in a glycerine based moisturising cream testing (pilot study – preliminary findings)

7.11 Study background

As demonstrated by the main study, VIS-OCT system developed by the author's research group established its capability in quantifying human SC thickness and hydration in vivo. SC thickness and hydration results of the main study showed individual, seasonal, age and gender variations, how SC reflectance change under the same hydration and drying condition also indicates that VIS-OCT system can be used to determine the 'how quickly' and 'how slowly' subjects' SC can uptake and lose water. Based on this, during the last couple of months of this PhD study, the author decided to perform an extended pilot study to explore the possibility of using the VIS-OCT system in testing the effect of a commercialised moisturising cream.

5 subjects from the current subject's pool (2 females, 3 males, age between 25-60) were given an over-the-counter moisturising cream (L'Occitane Hand Creams) where the main ingredients include: water; glycerin (humectant); cetostearyl alcohol (emulsion stabilizer); sunflower seed oil, shea butter and some other emulsifier carrying agent and scent extract. Such cream claims to moisturise and smooth the skin. Subjects were instructed to apply such cream twice per day on their dorsal hand (the skin site they used for the main experiment) for roughly 1 month, VIS-OCT scans were acquired after 1 month's application and compared with the previous results acquired in winter/2023. As this study is an extended study of the main experiment, the experiment setup, materials and methods, experimental procedures and protocols were the same as the main study.

7.12 Preliminary findings

Using the same SC thickness quantification described in chapter 4.3, SC thickness of 5 subjects before and after the cream application is plotted in figure 95. As shown in the figure, for 5 subjects, their SC thickness [Mean ± Standard deviation] at baseline was 8.2μm ± 2.9μm, and it increased to 10.0μm ± 4.5μm after 1 month of tested cream application, nonparametric paired T-test showed that the difference before and after the tested cream application is significant ($p < 0.0001$); after hydrating in water for 40

minutes, their SC thickness before cream application was 19.1μm ± 3.2μm, and it increased to 22.8μm ± 9.6μm, nonparametric paired T-test also showed significance ($p = 0.0157$) in this increase; after drying in lab for 40 minutes, their SC thickness before cream testing was 7.7μm ± 3.1μm, and it increased to 9.5μm ± 4.3μm after the application of tested cream, and again, nonparametric paired T-test showed significance ($p < 0.0001$) in this increase. However, it is worth noticing the increase in these results appear to be smaller than the standard deviation of the group. Using the same SC reflectance quantification, SC reflectance of 5 subjects before and after the cream application is plotted in figure 96. As shown in the figure, for 5 subjects, their SC reflectance [Mean± Standard deviation] at baseline was 65.3dB ± 1.9dB, and it increased to 67.8dB ± 2.0dB after 1 month of cream application, nonparametric paired T-test showed significance ($p < 0.0001$) in this increase; after 40 minute of hydrating in water, their SC reflectance increased from 71.6.3dB ± 2.6dB to 73.5dB ± 2.6dB, and nonparametric paired T-test also showed significance in this increase; after drying in lab for 40 minutes, their SC reflectance again increased from 65.8dB ± 3.6dB to 70.3dB ± 2.7dB, nonparametric paired T-test also demonstrated this increase is significant.

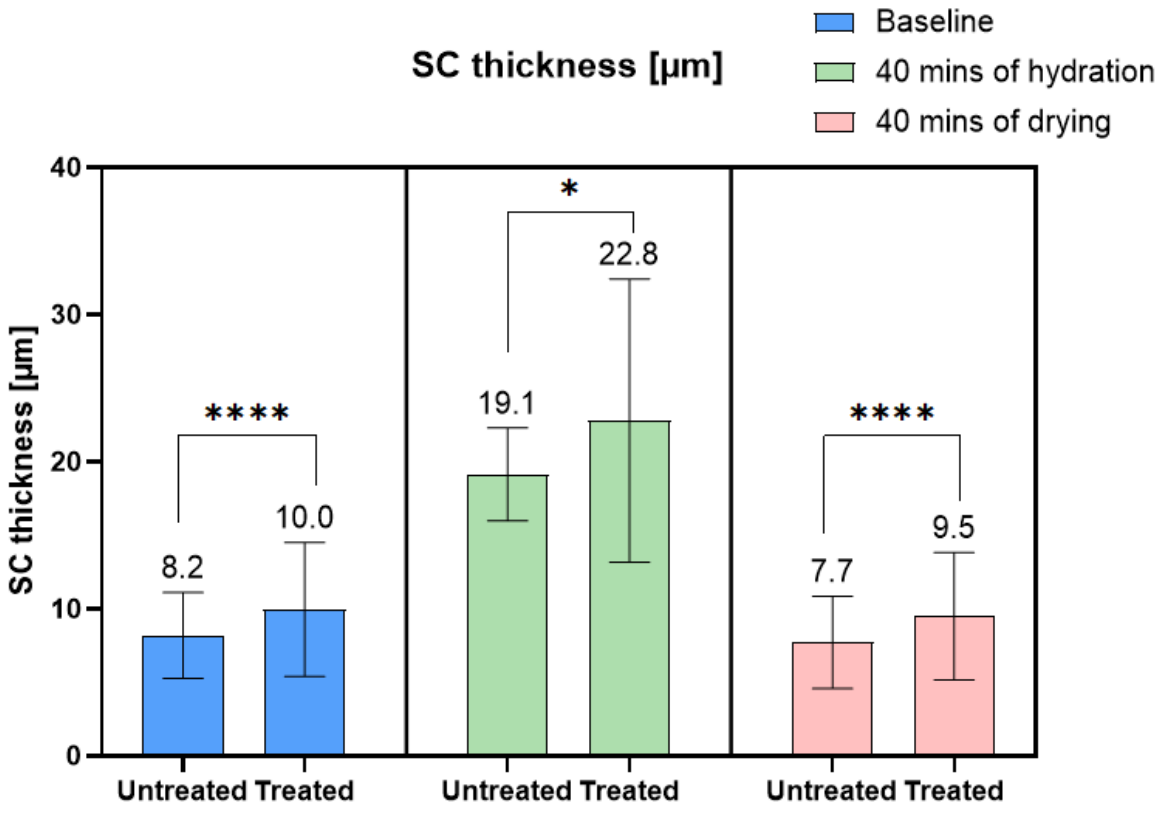

Figure 93. SC thickness (Mean± Standard deviation) [μm] of 5 subjects before and after the cream application

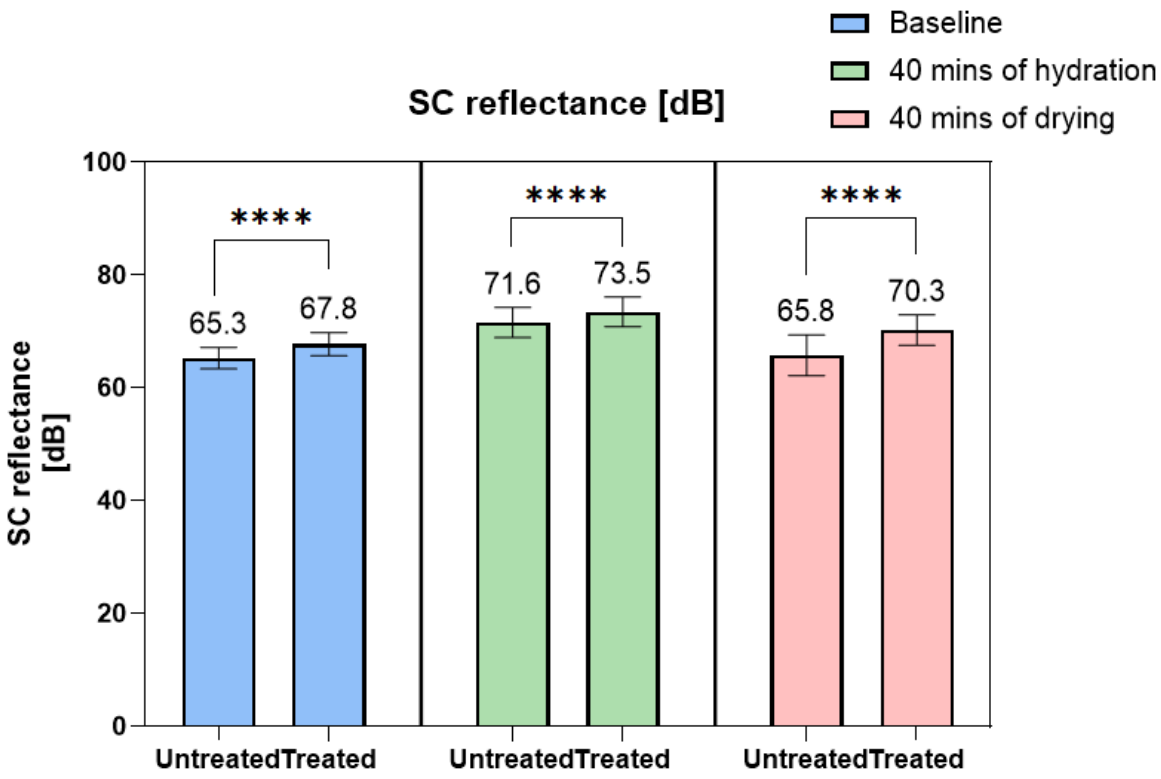

Figure 94. SC reflectance (Mean± Standard deviation) [dB] of 5 subjects before and after the cream application

Regarding how SC reflectance behaves during the hydrating and dehydrating phase, see figure 97. As shown in the figure, for 5 subjects, during hydrating phase (T0 - baseline, T1 – 5 minutes of hydrating,…T8 – 40 minutes of hydrating), both treated and untreated SC's reflectance behaves non-linearly, using the same nonlinear exponential model (One-phase association) to fit the results, it was found that the time constant for untreated hand is ~7.3 minutes, as for treated hand, the time constant is ~6.5 minutes. Two curves resemble each other with very similar span (changes in SC reflectance from baseline to the end of hydrating phase) except, the treated curve has a higher value of ~2dB at the start, as well as at the steady state end. These results indicate that after 1 month of cream application, subjects' SC reflectance increased by ~2dB, and the time for subjects' SC to reach saturation under 40 minutes of hydration in water has increased by ~1 minute. During the dehydrating phase (T8 – 0 minutes of drying, T9 – 5 minutes of drying, …T16 – 40 minutes of drying), subjects treated and untreated SC's reflectance decay differently. Using the linear exponential model (One-phase decay) to fit the results, it is clear to see the untreated curve decays rapidly whereas for treated results, it decays slowly and even after 40 minutes of drying, it is still far from the 'steady state' end. The non-linear exponential model results show that the time constant for the untreated curve is ~28.6

minutes, whereas for the treated curve, the time constant in which the model is formulated is ~85.5 minutes. And after 40 minutes of drying, the treated skin's SC reflectance is much higher than the untreated one.

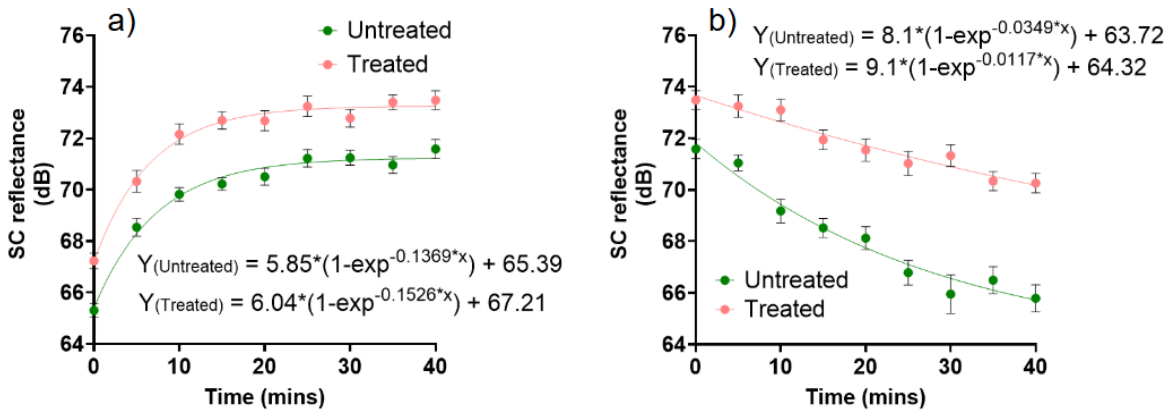

Figure 95. left - SC reflectance [dB] for both treated and untreated hand during hydrating phase for 5 subjects; right – SC reflectance [dB] for both treated and untreated hand during dehydrating phase for 5 subjects

When looking at the changes from baseline to fully hydrated state, for untreated skin, 5 subjects' SC reflectance increased ~6dB, as for treated skin, their SC reflectance also increased ~6dB except, the treated skin had a higher starting value as well as higher ending value. This suggests that the cream application increased subjects' SC hydration reflected by a higher SC reflectance value, this could be due to the humectant within the cream increasing SC' ability to attract water from the environment. The more interesting finding hinders in the dehydrating phase, as in, when we look at how SC reflectance behaves during dehydrating phase, treated skin's SC reflectance only decreased ~3dB after 40 minutes of drying in lab, whereas untreated skin's SC reflectance decreased ~6dB. This indicates that the water retention ability of SC after 1 month of the tested cream application has increased, as the time which the model predicts SC to lose the water has increased from ~29 minutes to ~86 minutes also suggests that the cream application increased subjects' SC's ability in retaining water, hence, the skin is 'more hydrated'.

7.13 Discussion and conclusion

In the current study, we observed a significant increase in SC thickness after 4 weeks of application of a glycerine-water based moisturising cream on 5 subjects' dorsal hand imaged by VIS-OCT, at baseline, after hydrating in water for 40 minutes and after drying in lab for 40 minutes, the increase in SC thickness falls within a range of 20%-25%, this is in agreement with Crowther et al.'s finding where,

after 2 weeks of applying a glycerine-water based cream on 14 subjects' forearm, a significant increase of 10% was observed in subjects' SC thickness measured by confocal Raman spectroscopy [1]. However, the increase in SC thickness in the current study is smaller than the group standard deviation, this yields the need of a larger population for further study to enhance the reliability of results. An in vivo study done by Loden et al. reported that after 10 days application of a cream containing 20% glycerine on 17 healthy subjects' forearm, a significant increase in SC hydration reflected as an increase in Corneometer value was found, the finding of this study agrees with current study's results on an increase in SC hydration reflected as a significant increase in SC reflectance, as there are more water molecules being captured in this layer, thus leads to more scattering of the interference signal [2]. Using a dynamic vapour sorption chamber, glycerine has shown its ability in terms of water retaining, as in, compared to distilled water, in an evaporation test, a sample which contains 20% of glycerine in distilled water has a lower evaporation rate. This finding can be related to current study's result of that, the time constant of SC reflectance during dehydrating phase on treated hand is larger than untreated hands, hence affirming that application of humectant containing cream can increase SC's ability in retaining water, and thus, being assessed by VIS-OCT system [3].

To summarize, studies on the effect of different moisturising cream remain as an active and ongoing topic as xerosis skin is the most common symptoms in many dermatological diseases, skin barrier biomarkers such as SC hydration and SC thickness can be quantified by some well-established methods such as Corneometer and confocal Raman microscopy, however, literatures on skin barrier biomarkers quantification show variations and limitations on these methods. Hence, new modalities which allows a tomographic view onto the subsurface information on skin is needed, VIS-OCT system thus pose as a novel, non-invasive, fast at acquiring imaging technique for skin barrier investigations. The main study of this part of research has demonstrated that VIS-OCT system can be used to quantify skin barrier biomarkers, this extended pilot study strengthens its' ability in skin barrier treatment evaluation, although, the subjects pool for this research is relatively small, the findings of this research offer new aspects and new methods in skin barrier research.

.

7.2 SC Elasticity as a function of corneodesmosomes cohesion

7.21 Objectives

During the early months of this 3-year PhD project, the primary stratum corneum biomarker targeted for this research was SC corneodesmosomes cohesion, described in chapter 1.2, corneodesmosome is an adhesive protein complex which links the corneocytes together to ensure SC is equipped with a fine tensile strength against external stimuli, and it is reported that AD patients' corneocytes are more weakly bound as their corneodesmosome cohesion is degraded. Inspired by a study done by T.Okuyama et. al, where a compressive force was applied onto human subjects' fingertip via a contacting acrylic plate, by probing the SC thickness change using OCT, Young's modulus of SC among 5 male subjects were obtained, the result of their study reported a value of 0.18Mpa – 1.84Mpa, which is an acceptable range of human SC Young's modulus in vivo [1]. Hence, it was speculated by the author that SC elastic modulus (Young's modulus), which can be used as an indicator to evaluate one's corneodesmosome cohesion, can be calculated as a function of SC thickness change under an induced force. To achieve this objective, also stated in the author's confirmation review report, the initial step is to affirm that the VIS-OCT system developed by the author's research group is capable of quantifying human SC thickness in vivo, and, through conducting the experiment done on 15 human subjects, the VIS-OCT system has validated itself in quantifying human SC thickness and reflectance in vivo. The next step would be to design and build an actuation module which can be embedded with the VIS-OCT system to induce tensile force on skin models to explore the possibility of quantifying Young's modulus of human SC in vivo, and an active project of this idea is currently under investigation. Listed below is a comprehensive literature review done by the author to help list requirements and conditions for future FEM model or real design of this idea.

7.22 Literature review on skin/stratum corneum elasticity

When surveying skin elasticity quantifications during literature research, one of the most referenced classifications when concluding results is based on the measurement method, which can be categorized into suction, indentation, compression, tension and torsion. Among these various approaches, suction method appears to be the most widely reported, this is due to the development and commercialisation of a particular device, Cutometer® (Courage Khazaka electronic GmbH), see figure 124 below, Cutometer is a non-invasive device invented to determine skin elasticity in vivo. The principle of

Cutometer is straightforward, negative pressure is applied onto skin sites via a vacuum tube, parts of skin that gets sucked into the aperture with a changeable diameter is detected via a non-contact optic module, depending on the selected mode, the suction process is repeated with a relaxation time interval. The ratio between the skin that gets elevated into the aperture and the applied pressure yields information on skin stiffness, the time-related data as a function of applied pressure also adds knowledge on the viscoelastic feature of the tested skin [2]. Reported, Cutometer has been used extensively to study the inter- and intra- differences of skin elasticity, Lubberding et. al recruited 300 volunteers at an equal gender ratio and assessed their elastic parameter via Cutometer, results showed that intra-variation was presented at skin sites of the facial, forearm and the hand. Apart from body sites variation, gender factor also influenced the elastic constant, it was noted that during natural aging, the elastic index for male subjects dropped steadily while for female subjects, it decreased in a stepwise manner, it was suggested that the stepwise decrease for female subjects may be correlated with hormonal changes, i.e., when perimenopause takes place [3]. Similarly, a study done by Ruy et. al recruited 96 volunteers from Korea to study their elastic features using Cutometer, results showed that the viscoelastic parameter (R3 – fatigue, or 'tiring effect of skin') showed significant difference at upper arm, lower back and lower cheek, which ascertained the intra- variation in human skin elasticity [4]. Furthermore, Nedelec et. al also demonstrated that regional factor does contribute to the presence of intra-variation in skin elasticity using Cutometer, measurements were obtained from 241 healthy subjects at different age group across 16 body sites, ageing influence was verified by parameter R0, i.e., maximum skin deformation, regional differences were also confirmed [5]. Besides gender and regional factors, the influence of aging also appears to be one of the common aspects to look at when assessing skin elasticity, Kim et. al categorized 21 healthy female subjects into a 'young' group in their 20s and an 'old' group in their 50s and took their elasticity measurement via Cutometer. Skin sites chosen to be assessed were the cheek, eye, and their volar forearm. The results confirmed that all the chosen parameters showed significant differences between two age groups primarily, additionally, their results also stated that all 3 anatomical skin sites had significant differences between each other [6]. A study done by Ahn et. al reported equivalent findings with 44 healthy female subjects aged between 20-61 years old, Cutometer was used on the facial area, and the results of gross elasticity and skin firmness index matched Kim's finding that the younger age group had a higher elastic value [7]. Furthermore, focusing only on the cheek, a study done by Ohshima et. al recruited 32 healthy subjects

between the ages of 29-55 and measured their cheek elastic properties using Cutometer, their results additionally ascertained that age factor has a negative influence on skin elasticity [8]. Till now, Cutometer still remains as a widely used tool to quantify skin elasticity in dermocosmetic and clinical areas, however, in literature, a paucity of information regarding the limitations, reliability and accuracy of this device is acknowledged. According to the user instruction, during usage, it is said to apply 'gentle' pressure when holding the probe at 90 degrees from the testing site, however, quantitative specification of this pressure is not provided. Although when taking measurements using Cutometer, it is often that the repeated measurements are recorded, however, consistent measurements are difficult to obtain, this 'error' unquestionably adds inter- and intra- variations to the results and this aspect is often under-stated. A study done by Bonaparte stated that even a small contact pressure change between the probe and the skin sites would result in a rather significant variation in the elastic measurement, which highlights the limitation of this method. In addition, information related to the sub-surface of skin is not detected. Although some have argued that at a small pressure, the elastic value indicates the superficial layer of skin and at a large pressure, the results are associated with a deeper layer, such argument has no validation yet [9].

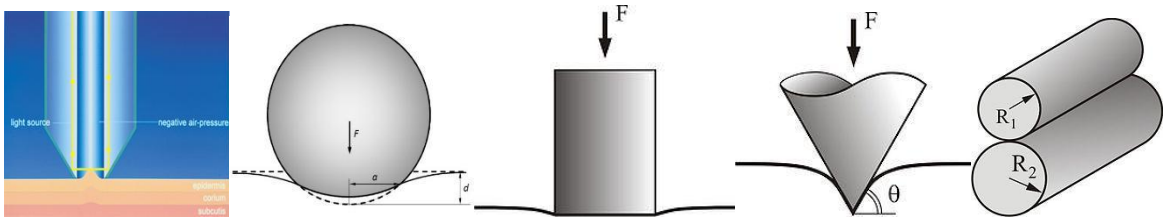

Figure 96. (left – Cutometer [10]; Hertz contact mechanics: second left – elastic sphere indentor in contact with elastic half space; middle – cylinder indentor in contact with elastic half space; second right – conical tip indenter in contact with elastic half space; right -two cylinder in contact [11]).

Indentation method is another division that claims to measure the mechanical properties of skin in vivo without inducing pre-stress to disrupt the natural stress state of skin, its clinical motivation mostly correlates with microneedle drug delivery and tactile sensation. Back in the 1990s, Flange et. al used a durometer to assess the induration of 12 patients with sclerodermatous skin, durometer is a device that is used in industrialization to measure material's hardness, its principle is based on that material's harness is a function of the penetration depth of the device at given force. Their results showed that durometer measurements for scleroderma patients highly correlated with the scores of skin severity standard for cutaneous disease at that time. Such finding then suggested an indentation method could be used to investigate the elastic property of human skin [12]. Inspired by this approach combined with Hertz contact mechanics, see figure 96, a decent amount of research has been carried out to evaluate

skin elasticity via estimating Young's modulus. Hertz's contact mechanics is usually used to study the deformation when one solid object is in contact with another where a perpendicular direction's stress is applied between two surfaces. The surface friction should be theoretically considered but it is neglected in some cases for simplicity reasons, due to the involvement of elastic modulus when determining relevant parameters with specific geometry of the objects, it was adapted by researchers to study the skin elasticity. For example, shown in figure 96, when an elastic sphere is in contact with an elastic half place, i.e., an elastic material defined to extended infinitely in all directions when the top surface is the boundary, the theory states that the force F induced is a function of the Young's modulus E^* of the material, contact radius R as a function of the deformation d itself, see equation below.

$$F = \left(\frac{3}{4}\right) * E^* * R^{\frac{1}{2}} * d^{\frac{3}{2}}; a = \sqrt{Rd}; \frac{1}{E^*} = \frac{1-v1^2}{E_1} + \frac{1-v2^2}{E_2}; d = \frac{a^2}{R} = \left(\frac{9F^2}{16E^{*2}R}\right)^{\frac{1}{3}} \textbf{(43)}$$

Here E_1 and E_2, $v1$ and $v2$ are the Young's modulus and Poisson ratio of the two contacting objects, in the case of a study done by Dai et. al a steel indenter is in contact with human facial skin perpendicularly, assuming the contact is frictionless and the skin's response to indentation is linear, the deformation is assumed as a function of the penetration depth, Young's modulus of the skin via:

$$\frac{1}{E^*} = \frac{1-v2^2}{E_2} \qquad \textbf{(44)}$$

Where E^* is the Young's modulus of steel and E_2 is the Young's modulus of the skin, the experimental results obtained here were compared with theoretical calculations, although the exact value did not match, the trend of each results set where the penetration depth is a function of the induced force and contact radius coherently matched, suggesting that this method could be used to estimate one's skin elasticity. Numerically, Young's modulus of subjects' facial skin ranged between 0.3Mpa – 1.1Mpa [13]. Using the same physical principle, Geerligs et. al carried-out research to calculate the Young's modulus of SC and viable epidermis via a micro-indentation device ex vivo, where, isolated SC sample were derived from volunteers, using a sphere tip with a radius of 500μm, micro loads were applied onto the isolated samples, validation experiments were initially performed on silicone samples, FEM model where numerical estimations were also calculated. Their results showed for a 20μm thick SC and an 80μm thick viable epidermis, Young's modulus derived from a load-displacement curve are both to be 0.6Mpa [14]. Note that Hertz's contact mechanics theory does not only apply to a spherical indenter getting in contact with an elastic half place, it is also valid for other geometry such as conical tip or cylinder indenter, see figure 96 for different contact geometry, hence, the mathematical estimation for

Young's modulus also varies. Continue with the direction of micro-indentation, Yuan et. al measured SC's Young's modulus of isolated porcine samples using a nano-indenter in atomic force microscopy, and the indenter geometry varied from a sphere probe to a spherical tip, by taking measurement at a wet and dry condition, the resulting Young's modulus varied from 10 Mpa – 100 Mpa [15]. Similarly, Jee et. al carried out a study to measure Young's modulus of isolated porcine SC with micro-indenter of changing radius via atomic force microscopy and obtained results of 0.87Gpa. The choice of porcine skin for both mentioned experiments is based on the morphology of porcine skin that resembles human skin even after a few days of harvesting [16]. Another piece of research done by Asencio used isolated human skin and applied indentation via a novel hair nano/micro indenter, although the actual geometry of hair indenter resembles a conical tip, the mathematical derivation of Young's modulus were based on a spherical end gets in contact with an elastic half space, and the results of human SC's Young's modulus were found to be 0.43Gpa at a 40% relative humidity [17]. Stating the importance of measuring SC properties in vivo, Iravanimanesh et. al sued a micro tip indenter from atomic force microscopy on 4 human subjects' fingertip, and by measuring the contact force as well as penetration depth, with a modified Hertz's model for conical tip, human SC Young's modulus at fingertip were reported to be 107.4Mpa [18]. Among all of the reviewed literature on quantifying skin elasticity via indentation method, often seen, results reported noticeably have a big range based on skin's hydration state, measured via in vivo or ex vivo and indentor's geometry.

Tensile test is another approach to quantify skin elasticity via assessing the strain-stress response, i.e., when a stress is applied directional, the strain or the deformation is measured, assuming a linear response at micro pressure level, Young's modulus of the skin can be estimated. In dermatology, it has been used to study the elastic modulus and Poisson ratios. Different from the suction and indentation method, which applies 'pressing' or 'pulling' along normal direction of skin, claimed by Lim et. al, uniaxial tensile test is used to apply force that is parallel to skin's Langer line, and it can be used to study the anisotropy of human skin based on strain-stress response [19]. Although it is broadly believed that uniaxial tensile test is insufficient to gather skin elasticity value due to the simplicity of single directional force, as in, in real life, no force is singular due to skin's complicated structure, studies were still done ex vivo to obtain an estimation on skin elasticity [20]. Liu et. al collected an isolated human SC sample from a 36-year-old female subject and measured the elasticity using a uniaxial tensometer, with a

modified relative humidity of 7%, 40% and 100%, they reported a Young's modulus value of 20 Mpa – 200 Mpa. It was also noticed that, at low humidity conditions of 7% and 40%, the strain-stress curve had a linear response and when the relative humidity was increased to 100%, the strain-stress curve showed non-linear response [21]. Likewise, a study done by Levi et. al used a uniaxial and biaxial tensile apparatus on isolated human SC and calculated the Young's modulus, their results corresponded with Liu's finding where an increase in relative humidity results in a decrease in the Young's modulus of sample. Numerically, the Young's modulus of isolated sample dropped from 272 Mpa – 28 Mpa when relative humidity increased from 20% to 100% [22]. Another study done by Wu et. al used in-plane and out-of-plane tensile tests on isolated human SC and obtained a Young's modulus value of 2Mpa and 0.8Mpa with a relative humidity of 100%, their results coherently matched the trend of increasing relative humidity decreasing Young's modulus as well [23]. Another direction of estimating Young's modulus of skin is via the torsion method, Sanders et. al calculated the elastic modulus for 19 healthy subjects using an angular deformation torsion device [24]. Galarrage et. al carried out a pilot study to project the potential aspect of a torsion device in assessing skin elasticity for patients with systemic sclerosis, by using a torsion device on the forearm and the hand for patients and subjects from a control group, it was stated that their torsion test can be used to distinguish healthy subjects from patients with systemic sclerosis based on their elastic parameter [25]. Based on this method, commercially available devices such as dermal torque meter and Twistometer were developed for skin elasticity measurements, the principle of such devices is based on inducing stress on the skin surface via a rotating disc, the angular displacement can be used to estimate Young's modulus [26].

When skin elasticity is being studied, without specifying which layer, many efforts have been made towards quantification of elastic or viscoelastic value of skin. Although it is commonly acknowledged that skin behaves in a way that is heterogeneous, anisotropic and non-linear in response to distortion, research has been done with assumptions such as linear response. For example, when quantifying Young's modulus of SC or epidermis via indentation, as such a method is based on Hertz's contact mechanics, assumptions for this theory are the strain/deformation are small enough to be within the elastic phase of response (assume linearity) and the contact surface is frictionless. It has come across to the author's attention that, when skin elasticity is being quantified, big variation in results arise based on the assumption of how skin behaves, whether it is assumed to behave linearly elastic, non-linearly

elastic, or viscoelastically. When using Cutometer to quantify skin elasticity, skin is assumed to behave viscoelastic; when using indentation method, skin is assumed to behave linearly in response to a small, induced force, and the contact is assumed to be frictionless; when using torsion or tensile method, skin is assumed to behave heterogeneously, and a stress-strain curve is commonly used to represent results. In addition, variation of results also emerges based on how skin is modelled, as in, whether skin is modelled as a single layer or multilayer material. Furthermore, variation of results also rises from whether skin is being assessed in vivo, ex vivo or in vitro. To the author's interest, when narrowing down from skin elasticity to SC elasticity, variation of results also appears based on these factors. Geerligs et. al used a micro-indenter on isolated human SC and obtained a Young's modulus of 0.6Mpa. Asenyio et. al used a novel nano hair indenter on isolated human SC and found the Young's modulus to be 0.43Gpa. Yuan et. al used a nano-indenter on isolated porcine SC and retrieved a Young's modulus value of 10 Mpa – 100 Map at wet and dry conditions. Jee et. al also obtained Young's modulus for isolated porcine SC to be 15.6Mpa. Crichton et. al used a nano-indenter on an isolated murine sample and gathered a Young's modulus of 0.75Mpa – 1.62Mpa [27]. Iravanimanesh et. al reported a human SC Young's modulus in vivo of 107.4Mpa, interesting, a case study done by Pailler-Mattei used a micro-indenter on isolated human SC and on subjects in vivo, and obtained a Young's modulus value 1Gpa for isolated sample, and 0.7Mpa – 0.8Mpa for subjects in vivo and stated that SC itself, does not contribute to the global mechanical properties of skin [28]. Another PhD thesis study done by Groves also used a small indentor on human subjects' forearm and reported a Young's modulus of 0.039Mpa – 0.065Mpa (spherical indenter and cylindrical indenter) [39]. Liu et. al quantified Young's modulus of isolated human SC via uniaxial tensile method and obtained a value of roughly 200 Mpa – 20 Mpa when the relative humidity increased from 7% to 100%. A study done by Levi et. al also quantified Young's modulus for human SC and obtained a result of 272 Mpa – 28 Mpa when relative humidity increased from 20% - 100%. Wu et. al used a tensile test on isolated human SC and obtained results of 2 Mpa – 0.8Mpa with a rise in the humidity level. Hara et. al used Cutometer on 78 female subjects' cheeks and obtained a Young's modulus value for human SC to be 1.993Mpa [29]. When Leveque et. al tried to assess the influence of SC within the skin using a computation model, a value of 0.05Mpa was used as the human SC Young's modulus in vivo, which was taken from a handbook of non-invasive methods of skin investigation [30,31]. Computational skin model was also developed by Leyva-Mendival et. al which used a human SC Young's modulus value of 0.6Mpa – 370 Mpa and reported that even with a relatively

small thickness, SC played a significant role over the entire skin layer under simulated compression and tensile force [32]. Some early human SC Young's modulus of 1.6Mpa – 6.4Mpa was also obtained by Panisset et. al via suction method [33]. By using a compression method on human finger pad skin, a Young's modulus value of human SC was reported to be 0.1Gpa by Dzidek et al [34]. Optical coherence elastography (OCE) has also been used to detect tissue elasticity, for example, dynamic Harmonic OCE has been utilized to quantify skin elasticity, Liang et. al introduced mechanical waves onto human skin and skin phantom, surface wave propagation was detected and used to compute skin elasticity. In their study, Young's modulus of human SC was estimated to be 0.023Mpa – 0.1Mpa depends on the hydration state [35]. Du et. al carried out a study where a non-contact OCE was used to quantify Young's modulus of healthy and diseased (systemic sclerosis) murine skin in vivo and in vitro, interestingly noted that PS-OCT has also been used to aid the diagnosis of systemic sclerosis. Young's modulus of murine skin was quantified by the wave velocity under an induction of small air pulses by a pneumatic value embedded in the system, and results showed that such method was able to identify fibrotic skin from healthy skin in an objective, non-invasive and rapid manner [36]. Li et. al carried out a study where surface acoustic wave was applied onto human skin, by using phase-sensitive OCT to detect the wave propagation and phase velocity, stratified skin's Young's modulus with a numerical value of 0.5Mpa, 0.15Mpa and 0.05Mpa was obtained for epidermis, dermis and hypodermis [37]. Apart from using compression, harmonic and transient waves to induce force, Lu et. al combined the suction method from Cutometer with OCT and built a hand-held probe to image human skin in vivo, by quantifying the skin deformation, mechanical features of dermis were obtained [38].

In summary, when quantifying skin elasticity, wide variation of results emerges from different approaches; skin model; assumptions related to physical theories of elasticity; hydration states; in vivo or ex vivo; species; skin sites; clinical interest; a similar situation also applies to SC elasticity. Although the range of reported values spans widely, some observations of trends can be made. For example, human SC Young's modulus in vivo measurements usually falls under a few Mpa, when taking an isolated sample, the value increases sharply. This could be due to the fact that most of the isolated samples are tested for fraction purposes. Whereas for in vivo testing, small stress level is usually induced, and damages of skin avoided. Another clear observation is that the hydration state of SC plays a big role in results, mostly stated, when relative humidity increases, Young's modulus of SC decreases.

Some less obvious observations such as in vivo indentation testing tend to provide small, valued Young's modulus is also useful to note when designing experiments for our interest. Hence, although the reported value spans greatly, insightfully information is still taken during the literature surveying.

SC'S Young's modulus (Mpa)	Measurement method	In vivo/Ex vivo	Species
0.023 – 0.1 **[35]**	OCE	In vivo	Human
0.039 - 0.065 **[39]**	Indentation	In vivo	Human
0.05 **[30, 31]**	FEM model	-	Human
0.18 - 1.84 **[1]**	OCE	In vivo	Human
0.5 **[37]**	OCE	In vivo	Human
0.6 **[32]**	FEM model	-	Human
0.6 **[14]**	Indentation	Ex vivo	Human
0.7 - 0.8 **[28]**	Indentation	In vivo	Human
0.75 - 1.62 **[27]**	Indentation	Ex vivo	Murine
0.8 - 2 **[23]**	Tensile	Ex vivo	Human
1.6 - 6.4 **[33]**	Suction	In vivo	Human
1.993 **[29]**	Suction	In vivo	Human
10 - 100 **[15]**	Indentation	Ex vivo	Porcine
15.6 **[16]**	Indentation	Ex vivo	Porcine
20 -200 **[21]**	Tensile	Ex vivo	Human
28 - 272 **[22]**	Tensile	Ex vivo	Human
107.4 **[18]**	Indentation	In vivo	Human
430 **[17]**	Indentation	Ex vivo	Human
870 **[16]**	Indentation	Ex vivo	Porcine

Table 26. Young's modulus of stratum corneum reported in literature

Reference

[1]. T. OKUYAMA, R. NIWATA, and M. TANAKA, “Measurement of Young’s Modulus of Stratum Corneum in Finger by Optical Coherence Tomography,” Journal of the Japan Society of Applied Electromagnetics and Mechanics, vol. 29, no. 1, pp. 137–142, 2021, doi: 10.14243/jsaem.29.137.

[2]. M. S. Woo et. al, “Comparison of skin elasticity test results from the Ballistometer® and Cutometer,” Skin research and technology, vol. 20, no. 4, pp. 422–428, 2014, doi: 10.1111/srt.12134.

[3]. S. Luebberding, N. Krueger, and M. Kerscher, “Mechanical properties of human skin in vivo: a comparative evaluation in 300 men and women,” Skin research and technology, vol. 20, no. 2, pp. 127–135, 2014, doi: 10.1111/srt.12094.

[4]. H. S. Ryu, Y. H. Joo, S. O. Kim, K. C. Park, and S. W. Youn, “Influence of age and regional differences on skin elasticity as measured by the Cutometer,” Skin research and technology, vol. 14, no. 3, pp. 354–358, 2008, doi: 10.1111/j.1600-0846.2008.00302.x.

[5]. B. Nedelec et. al, “Skin characteristics: normative data for elasticity, erythema, melanin, and thickness at 16 different anatomical locations,” Skin research and technology, vol. 22, no. 3, pp. 263–275, 2016, doi: 10.1111/srt.12256.

[6]. M. A. Kim, E. J. Kim, and H. K. Lee, “Use of SkinFibrometer® to measure skin elasticity and its correlation with Cutometer® and DUB® Skinscanner,” Skin research and technology, vol. 24, no. 3, pp. 466–471, 2018, doi: 10.1111/srt.12455.

[7]. S. Ahn, S. Kim, H. Lee, S. Moon, and I. Chang, “Correlation between a Cutometer® and quantitative evaluation using Moire topography in age-related skin elasticity,” Skin research and technology, vol. 13, no. 3, pp. 280–284, 2007, doi: 10.1111/j.1600-0846.2007.00224.x.

[8]. H. Ohshima et. al, “Use of Cutometer area parameters in evaluating age-related changes in the skin elasticity of the cheek,” Skin research and technology, vol. 19, no. 1, pp. e238–e242, 2013, doi: 10.1111/j.1600-0846.2012.00634.x.

[9] P. Bonaparte, D. Ellis, and J. Chung, “The effect of probe to skin contact force on Cutometer MPA 580 measurements,” Journal of medical engineering & technology, vol. 37, no. 3, pp. 208–212, 2013, doi: 10.3109/03091902.2013.779325.

[10]. V. Falanga and B. Bucalo, “Use of a durometer to assess skin hardness,” Journal of the American Academy of Dermatology, vol. 29, no. 1, pp. 47–51, 1993, doi: 10.1016/0190-9622(93)70150-R.

[11]. A. Dai, S. Wang, L. Zhou, H. Wei, Z. Wang, and W. He, “In vivo mechanical characterization of human facial skin combining curved surface imaging and indentation techniques,” Skin research and technology, vol. 25, no. 2, pp. 142–149, 2019, doi: 10.1111/srt.12623.

[12]. M. Geerligs, L. van Breemen, G. Peters, P. Ackermans, F. Baaijens, and C. Oomens, “In vitro indentation to determine the mechanical properties of epidermis,” Journal of biomechanics, vol. 44, no. 6, pp. 1176–1181, 2011, doi: 10.1016/j.jbiomech.2011.01.015.

[13]. Y. Yuan and R. Verma, “Measuring microelastic properties of stratum corneum,” Colloids and surfaces, B, Biointerfaces, vol. 48, no. 1, pp. 6–12, 2006, doi: 10.1016/j.colsurfb.2005.12.013.

[14]. T. Jee and K. Komvopoulos, “In vitro measurement of the mechanical properties of skin by nano/microindentation methods,” Journal of biomechanics, vol. 47, no. 5, pp. 1186–1192, 2014, doi: 10.1016/j.jbiomech.2013.10.020.

[15]. R. Álvarez-Asencio et. al, “Nanomechanical properties of human skin and introduction of a novel hair indenter,” Journal of the mechanical behavior of biomedical materials, vol. 54, pp. 185–193, 2016, doi: 10.1016/j.jmbbm.2015.09.014.

[16]. S. Iravanimanesh, M. A. Nazari, F. Jafarbeglou, M. Mahjoob, and M. Azadi, “Extracting the elasticity of the human skin in microscale and in-vivo from atomic force microscopy experiments using viscoelastic models,” Computer methods in biomechanics and biomedical engineering, vol. 24, no. 2, pp. 188–202, 2021, doi: 10.1080/10255842.2020.1821000.

[17]. K. H. Lim et. al, “New extensometer to measure in vivo uniaxial mechanical properties of human skin,” Journal of biomechanics, vol. 41, no. 5, pp. 931–936, 2008, doi: 10.1016/j.jbiomech.2008.01.004.

[18]. N. Kumaraswamy, H. Khatam, G. P. Reece, M. C. Fingeret, M. K. Markey, and K. Ravi-Chandar, “Mechanical response of human female breast skin under uniaxial stretching,” Journal of the mechanical behavior of biomedical materials, vol. 74, pp. 164–175, 2017, doi: 10.1016/j.jmbbm.2017.05.027.

[19]. X. Liu, J. Cleary, and G. K. German, “The global mechanical properties and multi-scale failure mechanics of heterogeneous human stratum corneum,” Acta biomaterialia, vol. 43, pp. 78–87, 2016, doi: 10.1016/j.actbio.2016.07.028.

[20]. K. Levi, R. J. Weber, J. Q. Do, and R. H. Dauskardt, “Drying stress and damage processes in human stratum corneum,” International journal of cosmetic science, vol. 32, no. 4, pp. 276–293, 2010, doi: 10.1111/j.1468-2494.2009.00557.x.
[21]. K. S. Wu, W. W. van Osdol, and R. H. Dauskardt, “Mechanical properties of human stratum corneum: Effects of temperature, hydration, and chemical treatment,” Biomaterials, vol. 27, no. 5, pp. 785–795, 2006, doi: 10.1016/j.biomaterials.2005.06.019.
[22]. R. Sanders, “Torsional elasticity of human skin in vivo,” Pflügers Archiv, vol. 342, no. 3, pp. 255–260, 1973, doi: 10.1007/BF00591373.
[23]. B. Galarraga et. al, “A novel approach to measuring skin elasticity in systemic sclerosis: results from a pilot study,” Scandinavian journal of rheumatology, vol. 40, no. 3, pp. 211–216, 2011, doi: 10.3109/03009742.2010.530610.
[24]. M. Qassem and P. Kyriacou, “Review of Modern Techniques for the Assessment of Skin Hydration,” Cosmetics (Basel), vol. 6, no. 1, p. 19, 2019, doi: 10.3390/cosmetics6010019.
[25]. M. L. Crichton, B. C. Donose, X. Chen, A. P. Raphael, H. Huang, and M. A. F. Kendall, “The viscoelastic, hyperelastic and scale dependent behaviour of freshly excised individual skin layers,” Biomaterials, vol. 32, no. 20, pp. 4670–4681, 2011, doi: 10.1016/j.biomaterials.2011.03.012.
[26]. C. Pailler-Mattei, S. Pavan, R. Vargiolu, F. Pirot, F. Falson, and H. Zahouani, “Contribution of stratum corneum in determining bio-tribological properties of the human skin,” Wear, vol. 263, no. 7, pp. 1038–1043, 2007, doi: 10.1016/j.wear.2007.01.128.
[27]. J. L. Lévêque and B. Audoly, “Influence of Stratum Corneum on the entire skin mechanical properties, as predicted by a computational skin model,” Skin research and technology, vol. 19, no. 1, pp. 42–46, 2013, doi: 10.1111/j.1600-0846.2012.00664.x.
[28]. J. Serup, G. B. E. Jemec, and G. L. Grove, Handbook of non-invasive methods and the skin, 2nd ed. Boca Raton, Fla. ; London: CRC/Taylor & Francis, 2006.
[29]. M. F. Leyva-Mendivil, A. Page, N. W. Bressloff, and G. Limbert, “A mechanistic insight into the mechanical role of the stratum corneum during stretching and compression of the skin,” Journal of the mechanical behavior of biomedical materials, vol. 49, pp. 197–219, 2015, doi: 10.1016/j.jmbbm.2015.05.010.
[30]. M. F. Leyva-Mendivil, A. Page, N. W. Bressloff, and G. Limbert, “A mechanistic insight into the mechanical role of the stratum corneum during stretching and compression of the skin,” Journal of the mechanical behavior of biomedical materials, vol. 49, pp. 197–219, 2015, doi: 10.1016/j.jmbbm.2015.05.010.
[31]. F. Panisset, D. Varchon, and P. Agache, “Non invasive assessment of stratum corneum young’s modulus in vivo,” Journal of biomechanics, vol. 27, no. 6, pp. 844–844, 1994, doi: 10.1016/0021-9290(94)91453-2.
[32]. B. M. Dzidek, M. J. Adams, J. W. Andrews, Z. Zhang, and S. A. Johnson, “Contact mechanics of the human finger pad under compressive loads,” Journal of the Royal Society interface, vol. 14, no. 127, pp. 20160935–20160935, 2017, doi: 10.1098/rsif.2016.0935.
[33]. X. Liang and S. A. Boppart, “Biomechanical Properties of In Vivo Human Skin From Dynamic Optical Coherence Elastography,” IEEE transactions on biomedical engineering, vol. 57, no. 4, pp. 953–959, 2010, doi: 10.1109/TBME.2009.2033464.
[34]. Y. Du et. al, “Rapid, noninvasive quantitation of skin disease in systemic sclerosis using optical coherence elastography,” Journal of biomedical optics, vol. 21, no. 4, pp. 046002–046002, 2016, doi: 10.1117/1.JBO.21.4.046002.
[35]. Li, C, Guan, G, Huang, Z, Wang, RK & Nabi, G 2015, Full skin quantitative optical coherence elastography achieved by combining vibration and surface acoustic wave methods. in VV Tuchin, KV Larin, MJ Leahy & RK Wang (eds), Proceedings Volume 9322: Dynamics and Fluctuations in Biomedical Photonics XII. vol. 9322, 93220O, SPIE-International Society for Optical Engineering, SPIE Photonics West 2015, San Francisco, United States, 7/02/15. https://doi.org/10.1117/12.2075666
[36]. L. Bartolini et. al, “Toward clinical elastography of dermal tissues: A medical device to probe skin’s elasticity through suction, with subsurface imaging via optical coherence tomography,” Review of scientific instruments, vol. 91, no. 7, pp. 074101–074101, 2020, doi: 10.1063/5.0009639.

8.0 Limitations and future work

The main objective of this research is to investigate quantified skin barrier biomarkers using novel visible-light OCT systems, the main study quantified stratum corneum thickness and hydration for 15 healthy human subjects, and the results mostly agree with literature. One limitation of this research is that the number of subjects is relatively small, which makes the evaluation of results confined when seasonal, gender and age factors are involved. However, the results of this study still offer valuable information in skin barrier research, and, in a foreseeable future, to represent the true population better, a larger subject pool should be gathered where anatomical, gender, age, skin type, ethnicity characteristics are considered. The methodology of this research can be improved in several aspects, first, the methodology of the main study did not consider the influence of the position of the subjects' hands, where a stretched or relaxed position could lead to different results, hence, following experiment should also presuppose this aspect. The hydration means of this study was immersing subjects' hands in a bucket of water for 40 minutes, such a method was relatively time-consuming and uncomfortable to an extent, although all subjects were willingly to participate in full studies, a simpler hydration approach such as using wet cotton pads is advised. The VIS-OCT scan processing can be advanced as well, currently, the processing algorithm of finding skin surface and stratum corneum/stratum granulosum junction for typical B-scans is optimised and fast, however, for atypical B-scans where the contrast of junction is not easily defined require manual segmentation. Manual segmentation can be time consuming and difficult, the current volumetric scan consists of 10 B-scans which makes the manual segmentation time acceptable, however, when volumetric scans of skin become large, an improved algorithm should be developed to replace manual segmentation.

The desirable outcome of this research would be to translate this VIS-OCT system into clinics to assess skin barrier biomarkers for healthy or Atopic dermatitis (AD) patients. Knowing that the system developer of this system is actively working on a software approach to improve the axial resolution, via conducting more studies on a larger subject pool with an advanced VIS-OCT system, the author is convinced that such an outcome is achievable. In parallel, another ongoing project in the author's research group is to build an actuation module on the system to induce tensile force on skin, hence, another skin barrier biomarker, corneodesmosome cohesion shall be examined in the future.

9.0 Supplement

9.1 VIS-OCT image processing code

```
%% Surface calculation
%  Load B-scans and display B-scans
imds = imageDatastore('C:\Users\lstad\OneDrive\Tayclyn
desktop\Spring\001\T0\*.jpg');
imgs = readall(imds);
for i = 1: length(imgs)
   images(:,:,i) = imgs{i};
end
% calculate sum of every 5 pixels
bscan10pixelmax = zeros(size(images));
for i = 1:(size(images,1)-9)
   for j = 1:size(images,2)
       for m = 1:size(images,3)
           bscan10pixelmax(i,j,m) = sum(images(i:i+4,j,m));
       end
   end
end
% find the maximum as the entry signal
bscan10pixelmaxx = zeros(size(bscan10pixelmax,2),size(bscan10pixelmax,3));
bscan10pixelmaxy = zeros(size(bscan10pixelmax,2),size(bscan10pixelmax,3));
for m = 1:size(bscan10pixelmax,3)
   [bscan10pixelmaxx(:,m),bscan10pixelmaxy(:,m)] =
max(bscan10pixelmax(20:size(bscan10pixelmax,1),:,m));
end
yreal = bscan10pixelmaxy+20;
yrealfilter25 = medfilt1(yreal,25);
%% Visually inspect surface calculation
for x = 1: size(images,3)
   imshow(images(:,:,x));
   hold on;
   plot(yrealfilter25(:,x));
   pause(0.5);
end
%% Calculate SC thickness
darkband_thickness = zeros(10,1600);
darkband_thickness_mean = zeros(1,10);
darkband_thickness_um = zeros(1,10);
curve_sc = zeros(1600,10);
vector = 1:1:1600;
for n = 1:size(images,3)
   image1 = images(:,:,n);
   y1 = yrealfilter25(:,n);
   newimage1 = zeros(size(image1),'double');
   newimage1gra_dark = zeros(size(newimage1),'double');
   newimage1gra_bright = zeros(size(newimage1),'double');
   newimage1gramax = zeros(1600,1);
   for j = 1:1600-4
       for i = 1:1024-20
       newimage1(y1(j):1024,j) = image1(y1(j):1024,j);
```

```
        %newimage1gra_dark(i,j) =
mean(newimage1(y1(j):y1(j)+4,j))/(newimage1(i:i+4,j));
        newimage1gra_dark(i,j) =
mean(newimage1(y1(j):y1(j)+4,j))/(newimage1(i,j));
        end
    end
    x = newimage1gra_dark;
    x(isinf(x)|isnan(x)) = 0;
    maxvectorx = zeros(1600,1);
    maxvectory = zeros(1600,1);
    for i = 1:1600-1
    [maxvectorx(i),maxvectory(i)] = max(x(y1(i):(y1(i)+20),i));
    % for hydrated segementation [maxvectorx(i),maxvectory(i)] =
max(x(y1(i):(y1(i)+50),i));
    maxvectory(maxvectory == 1) = NaN;
    maxvectory(i) = maxvectory(i)+y1(i);
    end

    maxvectoryfilter25 = medfilt1(maxvectory,25,'omitnan');
    darkband_thickness(n,:) = maxvectoryfilter25' - yrealfilter25(:,n)';
    curve_sc(:,n) = maxvectoryfilter25';
    darkband_thickness_mean= mean(darkband_thickness');
    darkband_thickness_um = darkband_thickness_mean*0.85/1.5;
end
%% Visual inspect SC thickness calculation
for x = 1: size(images,3)
    imshow(images(:,:,x));
    hold on;
    plot(yrealfilter25(:,x),'r');
    hold on;
    plot(curve_sc(:,x),'y');
    pause(0.5);
end
%% Manual segementation in Imagelabeller
vector = 1:1:1600;
skinsurface1 = gTruth.LabelData.skinsurface{1,1};
sc1 = gTruth.LabelData.sc{1,1};
curve_skinsurface1 = interp1(skinsurface1(:,1),skinsurface1(:,2),vector);
curve_sc1 = interp1(sc1(:,1),sc1(:,2),vector);
darkband_thickness1 = curve_sc1 - curve_skinsurface1;
darkband_thickness_mean1 =
mean(darkband_thickness1(~isnan(darkband_thickness1)))*0.85/1.5;
darkband_thickness_sd1 =
std(darkband_thickness1(~isnan(darkband_thickness1)))*0.85/1.5;
%% Visual inpect Manual segementation
imshow(images(:,:,1),[45 90]);
hold on;
plot(curve_skinsurface1,'r');
plot(curve_sc1,'y');
```

Part 2. Investigating anti-inflammatory skin treatment using polarisation-sensitive optical coherence tomography

1. Study background

During this 3-year PhD study, the author has primarily focused on exploring the possibility of quantifying human SC biomarkers in vivo for the main clinical interest of the author's research group, atopic dermatitis (AD). The main experiment carried out successfully demonstrated the ability of VIS-OCT system in human SC thickness quantification in vivo, in addition, it was also affirmed that human SC thickness change under different hydration state can be detected, furthermore, based on the strong correlation between SC reflectance and Corneometer measurements, it was established that VIS-OCT system can be used to study human SC hydration. With such findings, the author believes that VIS-OCT system can be used to study another skin barrier biomarker, corneodesmosome cohesion via probing human SC Young's modulus under an induced force, and future study shall be conducted. In parallel, the author has devoted herself to another large clinical trial study called SMART (Skin biomarkers for atopic eczema Therapy evaluation), this study is led by M.J.Cork et. al, where novel skin biomarkers are evaluated to assess the treatment for AD, in specific, to study the changes in skin induced by topical anti-inflammatory treatment, corticosteroids betamethasone valerate and non-steroidal crisaborole were applied onto subjects' forearm, their skin images were scanned by OCT to study the effects of these treatments. One of the primary goals of this clinical trial is to assess whether any treatment cause skin atrophy, which is one of the common side effects of topical corticosteroids application, other explorative objectives include using Mexameter to assess skin erythema/redness and evaluate skin barrier integrity via taking transepidermal water loss (TEWL) measurement through tape-stripping. The author's role in such a study is mainly involved with processing OCT scans, creating tools via MATLAB to effectively visualise the results, analysing part of the results and writing conference papers and refereed journals with relevant findings. The findings of this research which involves the author's work has been published in Biomedical optic express as 'Potential application of PS-OCT in the safety assessment of non-steroidal topical creams for atopic dermatitis treatment. Biomedical Optics Express Vol. 14, Issue 8, pp. 4126-4136 (2023).', in this chapter, the second part of this PhD research is reported below in a published journal paper format.

2. Introduction

Atopic dermatitis (AD), or atopic eczema, described in details in previous chapter, shortly, is a chronic inflammatory disease with common symptoms of itch and dried skin, the causes of AD can be explained by genetic and environmental factors and the severity of AD is associated with IgE levels, the prevalence of AD has increased remarkably over the past 7 decades and now affecting up to 10-20% of the population. Patients with mild-moderate AD are often treated with topical corticosteroids (TCS), this is due TCS has been popular since the 1950's based on its good cost to efficacy ratio. As AD is a chronic and recurring disease, TCS is often prescribed and used by patients over long periods of time, however, it is widely accepted that TCS can induce skin atrophy and striae [1]. Skin barrier function can also be negatively impacted by TCS when skin becomes more fragile over time, and TCS-induced skin atrophy can also accelerate skin ageing. Hence, AD therapies which can mimic the side effects of treatments are under active development. Crisaborole, a non-steroidal phosphodiesterase 4 (PDE4) inhibitor, has been approved by FDA in 2016 to treatment AD patients over the age of 2 years old, its principle is based on the blockage of the hydrolysis of cyclic adenosine monophosphate (cAMP), and thereby deactivate the inflammatory cytokines that causes pruritus. A review study done by Barnes et. al stated that when assessing TCS-induced skin atrophy, whole-skin thickness and epidermal thickness are the most studied parameters, and, across 14 clinical studies, after 2-8 weeks of TCS application, whole skin thickness decreased 5% - 20% via ultrasound sonography and x-ray radiology assessments. In another 10 clinical studies, after 2-6 weeks of TCS application, epidermal thickness decreased 5% - 40% via OCT and histometry assessments. Hence, TCS-induced skin atrophy is commonly associated with epidermis. OCT is a non-invasive tomographic imaging tool that has been applied to assess TCS-induced epidermal atrophy [3], and its principle has been illustrated in previous chapters. Since healthy human dermal collagen is organized in a basket wave-like structure, and TCS has been reported to decrease the collagen intensity and alter the collagen metabolism in dermis, which may also be linked with skin atrophy, an OCT variant, PS-OCT is used here to study the dermal collagen properties. PS-OCT, i.e., polarization sensitive OCT, is a function extension of OCT here in addition to detecting back-scattered light intensity, polarization state of light is also detected [4]. PS-OCT is equipped with common OCT advantages of high-speed scanning, good penetration depth and fine resolution, it can also measure phase retardance, diattenuation and tissue depolarization. The added knowledge grants PS-OCT the ability to different birefringent tissue such as muscle, ligament, tendon and scar tissue from

other tissue, in dermatology, PS-OCT has been used to image striae, identify basal cel carcinoma (BCC) and assess disease progression of systemic sclerosis [5].

3. Materials and method

In this study, PS-OCT is used to study the dermal collagen birefringence under the administration of TCS and Crisaborole. 37 AD patients were recruited in this study, with an age range of 18-65 years old (24 female, 13 male), 32 subjects completed the study. Crisaborole 2% ointment and betamethasone valerate 0.1% cream (BMV) were applied to subjects' inner forearms twice per day over the course of 4 weeks. PS-OCT images were gathered on day 1 and day 29. The study was approved by East Midlands – Derby Research Ethics Committee (REC Reference 20/EM/0006), with NCT number – NCT04194814.

Mentioned earlier, PS-OCT's principle relies on the polarisation of light. As an electromagnetic wave, light is defined as a transverse wave propagating in the Z direction, its electric field (E field) and magnetic field (B field) are perpendicular to each other while also being perpendicular to the propagation Z axis. To describe the polarisation states, few field components are needed to be listed in order to explain the field's oscillation state, which brings out the Jones vector, complex value where ex and ey corresponds to the amplitude of electric and magnetic field, and field phase information is denoted as δ. Polarisation states are commonly divided into 3 types, linear polarisation occurs when there are only oscillation propagates in E- or B- field, i.e., x or y direction, in which vertical linear state occurs when oscillation only propagates in x direction with same amplitude; and horizontal linear state occurs when oscillation only propagates in y- direction with equal amplitude. When two fields have the same amplitude and a phase delay of a quarter of a wave, i.e., $\delta = \pm 90^{o}$, it is defined as a circular polarised state. When the field amplitude and phase delay are arbitrary, the light is called to be elliptical polarised. Another way of describing the polarisation of light is using the Stoke vector, with 4 field components [I Q U V] ^{T}. The component Q, U, V corresponds to the three-axis information, and I indicates the light intensity. The light intensity I is equal to √(V^2+U^2+Q^2) and degree of polarisation is equal to √(V^2+U^2+Q^2)/I. When the light is fully polarised, degree of polarisation equals to 1 or unity, when it is partially polarised, degree of polarisation is less than unity and for depolarised light, degree of

polarisation is nearly zero. The OCT system has many branches based on design, PS-OCT can also be time or spectral domain, the PS-OCT used in this piece of research is shown in figures below.

A swept source laser with a centre wavelength of 1315nm, full width half maximum of 128nm, duty cycle of 60%, i.e., ratio of pulse duration w.r.t total duration, and a wavelength scanning rate of 10kHz, its' output power to the system is 10mW. The light from the swept source is feed into a polarisation controller (PC) and then an in-line linear polariser (IL-PL) to ensure a linearly polarised light. Then, linearly polarised light travels to a 2x2 polarisation maintaining coupler (PMC1, OLCPLP-22-131-10-90-FA, Opto-link Corp, China) via a PMF, polarization maintaining fibre and gets split into two beams, 10% goes to reference path and 90% goes to sample arm via a 3-port polarization maintaining circulator (OLCIR-P-3-131-300-90-FA, Opto-link Corp, China). For the reference arm, the light beam goes through a linear polarizer that oriented at 45° to the PMF slow axis and gets reflected from the stationary reference mirror and goes through a circulator, then it enters the detection arm with a polarization state of 45° w.r.t. the slow axis of PMF. As for the sample arm, the light beam travels to the sample via a quarter wave plate (QWP, NT55-547, Edmund Optics, US) oriented at 45° w.r.t the PMF, which ensure a circular polarized light for sample scanning, then, the light beam travels to the sample via a galvanometer, i.e., an electromechanical tool for electric current measurements (6214, Cambridge Technology, US) and an objective lens (Thorlabs LSM03, US). Sample beam is thus scattered by the sample and interfere with the reference beam at a second PMC2 (OLCPL-P-22-131-50-90-FA, Opto link, China). The interference signal is split by the PMC2 equally into two polarization beam splitters (PBS, PBS-31-P-2-L-3-Q, NovaWave Techno, US), and interference beams are split into horizontally and vertically polarized light beams and detected by two balanced detectors (1817-FC, New Focus, US). This PS-OCT system has an axial resolution of roughly 10μm and a lateral resolution of roughly 20μm in air. For each acquired set of B-scans, the volumetric size of the data is 512x600x600 pixels, corresponds to 2x6x6mm with a voxel size of 4x10x10μm, and the scans were processed in MATLAB (2019a, MATLAB). The raw interferometric signals were initially processed using inverse Fast Fourier Transform (FFT) to produce complex amplitudes A_H & A_V in the horizontal and vertical polarization directions with depth information, where these complex amplitudes were used to generated backscattered intensity via $\left|A_H^2\right| + [A_V^2]$. PM fibre misalignment can cause B-scan to have artifacts such as ghost reflections and horizontal stripes, these were removed by a wavelet-FFT filtering

algorithm developed by the author's research group previously, details can be found here [6]. The skin surface and location of the dermal epidermal junction (DEJ) is essential to quantify dermal birefringence, and it is also computed via an algorithm developed previously by the author's research group, details can be found here [7].

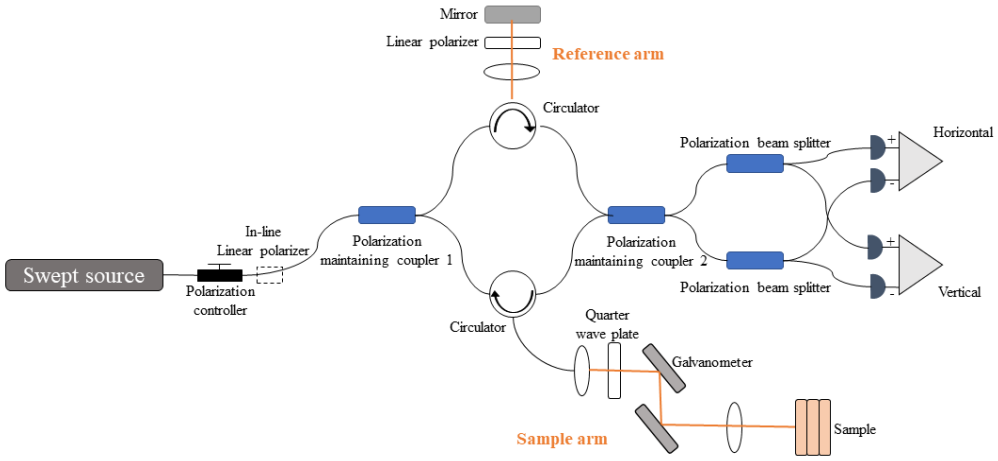

Figure 97. PS-OCT system configuration

Quantifying the birefringence of biological tissue via computation of Stokes vector has been established previously by Götzinger et. al, and the author's research group has previously used this method to investigate dermal birefringence for subjects with striae. To elucidate, A_H & A_V are used here to calculate the Stokes vector at each voxel using:

$$S = (I\ Q\ U\ V) = \left(\left|A_V^2\right| + \left[A_H^2\right].\ \left|A_V^2\right| - \left[A_H^2\right].\ 2A_V A_H cos\Delta\theta\ 2A_V A_H sin\Delta\theta\right) \quad \textbf{(45)}$$

Here, as mentioned above, 4 Stokes vectors elements are denoted as I, Q, U, V, the amplitude of signal in both directions are denoted as $\left|A_V^2\right|$and $\left|A_H^2\right|$, the phase difference between two channels $\Delta\theta = arg(A_V) - \arg(A_H)$, and the vector is further normalized by:

$$\hat{S} = \left(\hat{Q}\ \hat{U}\ \hat{V}\right) = (Q/I\ U/I\ V/I) \quad \textbf{(46)}$$

Following Lin et.al, by taking the dot product of Stokes vector at skin surface $(\hat{S}_{ref})$ and at a discrete depth z_i, the phase retardance at this depth $\phi_r z_i$ can be calculated via:

$$\hat{S}_{ref} \cdot \hat{S}_{z_i} = A(z_i)cos[(\phi_r(z_i)] \quad \textbf{(47)}$$

Here, $\phi_r(z_i)$ is an oscillatory term that describes the birefringence-induced periodic modulation of the polarisation state. $A(z_i)$ describes the gradual loss of polarisation due to scattering of light, noise and speckle fluctuations. This calculation assumes that orientation of the fast axis with the target dermal range does not vary strongly with depth. The phase retardance profile $\phi_r(z_i)$ that carries birefringence

information is extracted from computing the phase of LHS signals, and birefringence of the target area is quantified by estimating the slope of $\phi_r(z_i)$ with depth, and computing the linear regression over the depth range of ~200μm (~50 pixels) below the dermal epidermal junction.

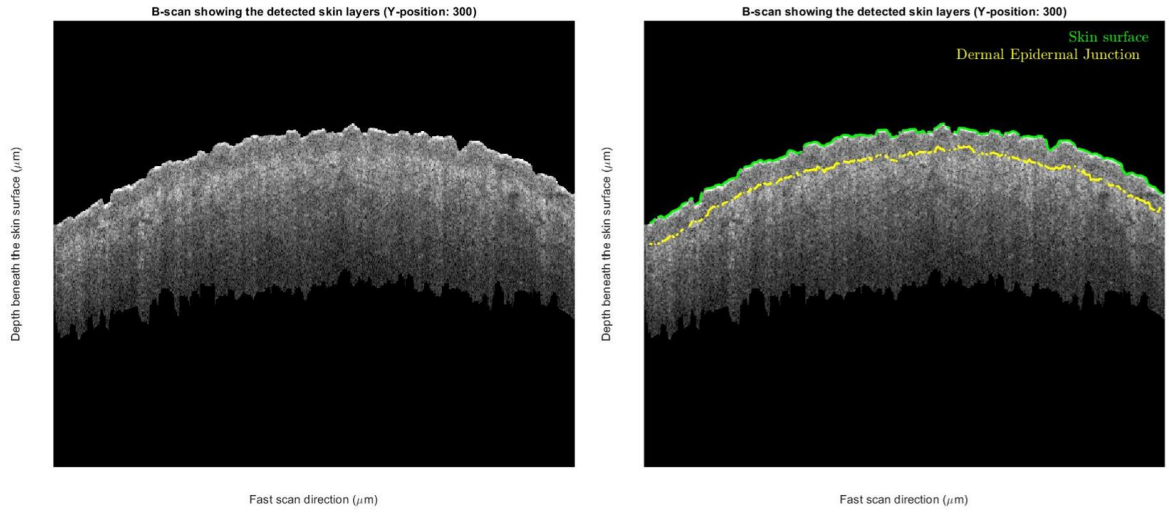

Figure 98. left: A raw B-scan (Y position of 300 refers to the 300th frame of a volumetric scan) from a volumetric scan of 600 frames before epidermis and dermis segmentation. Right: A B-scan (Y position of 300 refers to the 300th frame of a volumetric scan) from a volumetric scan of 600 frames after epidermis and dermis segmentation.

As $\phi_r(z_i)$ is wrapped into the primary interval of -π to +π radius, it must be unwrapped to get an accurate slope measurement, whenever there is a jump between two neighbouring axial pixel that exceeds the primary interval of ±π, multiples of ±2π are added until the jump falls under π, this is done using the MATLAB 'unwrap' command. And the slope m is converted into a local birefringence Δn by $\Delta n = m\lambda_0 RI/(4\pi\Delta z)$. And here λ_0 is the center wavelength of the PS-OCT system (1301nm), Δz is the pixel size in air (4μm), RI is the refractive index of tissue (1.4). One problem which may arise from this unwrapping is that error unwrapping can occur which results in an incorrected high birefringence value, to minimize this error detected, Lin et. al examined the histology and en-face plots of the birefringence value and found that any birefringence value exceeded 600 X 10^{-6} are most certainly be caused by noise-induced unwrapping, in such cases, the birefringence is taken using the original, wrapped phase profile [8].

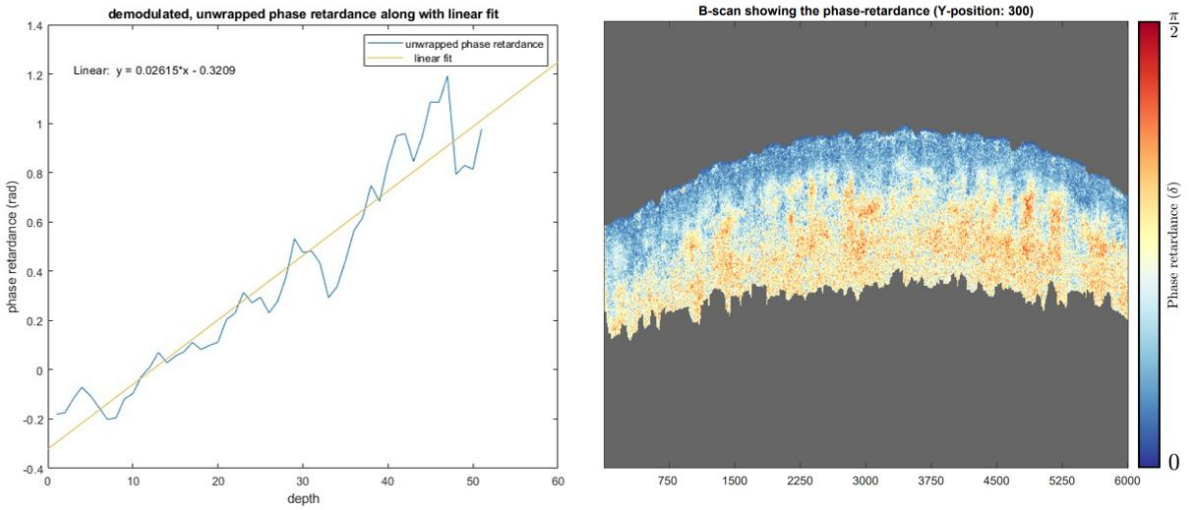

Figure 99. left: An example of average unwrapped phase retardance over 600 frames at a dermal position (marked in red in Fig. 4.) along with its linear fit. right: An example B-scan (Y position of 300 refers to the 300th frame of a volumetric scan) from a volumetric scan of 600 frames showing the phase-retardance.

4. Results, discussion and conclusions

32 out of 37 subjects completed the study and PS-OCT scans of them were obtained on day 1 and day 29 with 3 repeats for each subject in both arms. Descriptive results of dermal birefringence values are illustrated in tables below.

Metrics	Crisaborole(day 1)	BMV (day1)	Crisaborole(day29)	BMV (day29)
25% Percentile	469 X 10^{-6}	451 X 10^{-6}	466 X 10^{-6}	535 X 10^{-6}
Median	521 X 10^{-6}	536 X 10^{-6}	532 X 10^{-6}	626 X 10^{-6}
75% Percentile	612 X 10^{-6}	584 X 10^{-6}	607 X 10^{-6}	694 X 10^{-6}
Mean	540 X 10^{-6}	523 X 10^{-6}	536 X 10^{-6}	623 X 10^{-6}
Standard Deviation	100 X 10^{-6}	91 X 10^{-6}	89 X 10^{-6}	94 X 10^{-6}
Std. Error of mean	17 X 10^{-6}	16 X 10^{-6}	15 X 10^{-6}	16 X 10^{-6}

Table 27. Descriptive statistical table for dermal collagen birefringence for all 32 subjects who completed the study, before (day1) and after (day29) treatment.

Metrics	Crisaborole (day29 – day1)	BMV (day29 – day1)
Mean of differences	-3.99 X 10^{-6}	100.02 X 10^{-6}
Standard deviation of differences	74.82 X 10^{-6}	103.3 X 10^{-6}
95% confidence interval	(-32.32 to 24.44) X 10^{-6}	(63.21 to 136.84) X 10^{-6}
P-value (paried T-test)	0.7757	<0.0001

Table 28. Dermal collagen birefringence changes from baseline, for all 32 subjects who completed the study, before (day1) and after (day29) treatment.

As shown in the descriptive table, before crisaborole application, the average dermal birefringence was 540 X 10^{-6}, and it decreased to 536 X 10^{-6}; whereas for BMV, the average dermal birefringence before

application was 523 $X10^{-6}$, and it increased to 623 X 10^{-6}. Paired T-test showed that there is no significant difference between the dermal birefringence prior and after application of crisaborole, whereas for BMV, a significant difference was detected prior and after application. Such results indicate that after 4 weeks of daily application of BMV, an increase in dermal birefringence was detected, and crisaborole did not produce such a change. This finding broadly agrees with Jung et al., where 16 male subjects were treated with TCS on their volar arm, clobetasol propionate and betamethasone dipropionate for 4 weeks. In vivo multiphoton microscope and 'second harmonic-to-autofluorescence aging index of dermis' (SAAID) measurements were obtained on treated and control arms, their results showed that TCS significantly increases the SAAID index and another significant increase in the en-face multiphoton topography second harmonic generation (MPT-SHG) signal intensities was detected. Such results suggest that dermal collagen fibre density or alignment may be increased by TCS application, this can be explained by a reorientation of the dermal fibre, its' alignment is changed from a random network into a more aligned, even more compressed structure [9]. An earlier study done by Lehmann et al. also evaluated TCS-induced dermal changes using electron micron microscopy where, after 6 weeks of clobetasol propionate application, subjects' fibrous dermal collagen network reorganized into a more compact structure, which strengthens the possibility that such dermal structural change could lead to dermal thinning [10]. Since its introduction in 1952, TCS has been widely used in dermatology as an anti-inflammatory drug based on its characteristics of effectiveness and cost-efficient, however, adverse effects such as skin atrophy also have been reported. Many studies have devoted its focus in epidermal thinning when reporting skin atrophy and less have focused on the dermal aspect, it is believed that TCS negatively impact collagen synthesis which cause a loss of dermal extracellular matrix, and this aspect could also contribute to TCS-induced skin atrophy. The results of this study suggest that dermal collagen undergoes a structure change after TCS application, and crisaborole did not produce such a change. By assuming that birefringence fast axis does not vary much across dermal depth, this study presents a way to quantify dermal birefringence. In healthy human dermis, collagen and elastin fibres are organized in a woven mesh-like way, TCS application is reported to alter this structure by increasing the dermal birefringence. This study demonstrates a novel PS-OCT application in assessing AD treatment.

Reference

[1]. U. R. Hengge, T. Ruzicka, R. A. Schwartz, and M. J. Cork, “Adverse effects of topical glucocorticosteroids,” Journal of the American Academy of Dermatology, vol. 54, no. 1, pp. 1–15, 2006, doi: 10.1016/j.jaad.2005.01.010.
[2]. L. Barnes, G. Kaya, and V. Rollason, “Topical Corticosteroid-Induced Skin Atrophy: A Comprehensive Review,” Drug safety, vol. 38, no. 5, pp. 493–509, 2015, doi: 10.1007/s40264-015-0287-7.
[3]. M. Coßmann and J. Welzel, “Evaluation of the atrophogenic potential of different glucocorticoids using optical coherence tomography, 20-MHz ultrasound and profilometry; a double-blind, placebo-controlled trial,” British journal of dermatology (1951), vol. 155, no. 4, pp. 700–706, 2006, doi: 10.1111/j.1365-2133.2006.07369.x.
[4]. M. R. Hee, D. Huang, E. A. Swanson, and J. G. Fujimoto, “Polarization-sensitive low-coherence reflectometer for birefringence characterization and ranging,” Journal of the Optical Society of America. B, Optical physics, vol. 9, no. 6, pp. 903–908, 1992, doi: 10.1364/JOSAB.9.000903.
[5]. M. Q. Duan et. al, “Potential application of PS-OCT in the safety assessment of non-steroidal topical creams for atopic dermatitis treatment,” 2023.
[6]. R. Byers and S. Matcher, “Attenuation of stripe artifacts in optical coherence tomography images through wavelet-FFT filtering,” 2019.
[7]. M. Q. Duan et. al, “Potential application of PS-OCT in the safety assessment of non-steroidal topical creams for atopic dermatitis treatment,” 2023.
[8]. W. C. Lin, R. A. Byers, W. Li, S. G. Danby, M. J. Cork, and S. J. Matcher, “Imaging striae distensae : a comparison between PS-OCT and digital dermoscopy,” 2021.
[9]. S. Jung et al., “In vivo characterization of structural changes after topical application of glucocorticoids in healthy human skin,” Journal of biomedical optics, vol. 22, no. 7, pp. 076018–076018, 2017, doi: 10.1117/1.JBO.22.7.076018.
[10]. P. Lehmann, P. Zheng, R. M. Lavker, and A. M. Kligman, “Corticosteroid Atrophy in Human Skin. A Study by Light, Scanning, and Transmission Electron Microscopy,” Journal of investigative dermatology, vol. 81, no. 2, pp. 169–176, 1983, doi: 10.1111/1523-1747.ep12543603.